BIOMARKERS AND THERAPEUTIC TARGETS OF REPROGRAMMED TUMOR METABOLISM

EDITED BY: Wei Zhao, Zhe-Sheng Chen and Haishi Qiao

PUBLISHED IN: Frontiers in Molecular Biosciences

frontiers Research Topics

ISSN 1664-8714
ISBN 978-2-88976-167-8
DOI 10.3389/978-2-88976-167-8

About Frontiers

Frontiers is more than just an open-access publisher of scholarly articles: it is a pioneering approach to the world of academia, radically improving the way scholarly research is managed. The grand vision of Frontiers is a world where all people have an equal opportunity to seek, share and generate knowledge. Frontiers provides immediate and permanent online open access to all its publications, but this alone is not enough to realize our grand goals.

Frontiers Journal Series

The Frontiers Journal Series is a multi-tier and interdisciplinary set of open-access, online journals, promising a paradigm shift from the current review, selection and dissemination processes in academic publishing. All Frontiers journals are driven by researchers for researchers; therefore, they constitute a service to the scholarly community. At the same time, the Frontiers Journal Series operates on a revolutionary invention, the tiered publishing system, initially addressing specific communities of scholars, and gradually climbing up to broader public understanding, thus serving the interests of the lay society, too.

Dedication to Quality

Each Frontiers article is a landmark of the highest quality, thanks to genuinely collaborative interactions between authors and review editors, who include some of the world's best academicians. Research must be certified by peers before entering a stream of knowledge that may eventually reach the public - and shape society; therefore, Frontiers only applies the most rigorous and unbiased reviews.
Frontiers revolutionizes research publishing by freely delivering the most outstanding research, evaluated with no bias from both the academic and social point of view. By applying the most advanced information technologies, Frontiers is catapulting scholarly publishing into a new generation.

What are Frontiers Research Topics?

Frontiers Research Topics are very popular trademarks of the Frontiers Journals Series: they are collections of at least ten articles, all centered on a particular subject. With their unique mix of varied contributions from Original Research to Review Articles, Frontiers Research Topics unify the most influential researchers, the latest key findings and historical advances in a hot research area! Find out more on how to host your own Frontiers Research Topic or contribute to one as an author by contacting the Frontiers Editorial Office: frontiersin.org/about/contact

BIOMARKERS AND THERAPEUTIC TARGETS OF REPROGRAMMED TUMOR METABOLISM

Topic Editors:
Wei Zhao, City University of Hong Kong, SAR China
Zhe-Sheng Chen, St. John's University, United States
Haishi Qiao, China Pharmaceutical University, China

Citation: Zhao, W., Chen, Z.-S., Qiao, H., eds. (2022). Biomarkers and Therapeutic Targets of Reprogrammed Tumor Metabolism. Lausanne: Frontiers Media SA.
doi: 10.3389/978-2-88976-167-8

Table of Contents

frontiers in Molecular Biosciences

ORIGINAL RESEARCH
published: 22 April 2021
doi: 10.3389/fmolb.2021.598218

SphK2/S1P Promotes Metastasis of Triple-Negative Breast Cancer Through the PAK1/LIMK1/Cofilin1 Signaling Pathway

Weiwei Shi[1†], Ding Ma[1†], Yin Cao[1†], Lili Hu[1], Shuwen Liu[2], Dongliang Yan[1], Shan Zhang[1], Guang Zhang[1], Zhongxia Wang[1,2], Junhua Wu[2*] and Chunping Jiang[1,2*]*

[1] Department of Hepatobiliary Surgery, The Affiliated Drum Tower Hospital of Nanjing University Medical School, Nanjing, China, [2] Jiangsu Key Laboratory of Molecular Medicine, Medical School, Nanjing University, Nanjing, China

OPEN ACCESS

Edited by:
Zhe-Sheng Chen,
St. John's University, United States

Reviewed by:
Pranav Gupta,
Albert Einstein College of Medicine, United States
Haishi Qiao,
China Pharmaceutical University, China

***Correspondence:**
Chunping Jiang
chunpingjiang@163.com
Junhua Wu
wujunhua@nju.edu.cn
Zhongxia Wang
freud_t@126.com

[†] These authors have contributed equally to this work

Specialty section:
This article was submitted to Molecular Diagnostics and Therapeutics, a section of the journal Frontiers in Molecular Biosciences

Received: 26 February 2021
Accepted: 23 March 2021
Published: 22 April 2021

Citation:
Shi W, Ma D, Cao Y, Hu L, Liu S, Yan D, Zhang S, Zhang G, Wang Z, Wu J and Jiang C (2021) SphK2/S1P Promotes Metastasis of Triple-Negative Breast Cancer Through the PAK1/LIMK1/Cofilin1 Signaling Pathway. Front. Mol. Biosci. 8:598218. doi: 10.3389/fmolb.2021.598218

Background: Triple-negative breast cancer (TNBC) features a poor prognosis, which is partially attributed to its high metastatic rate. However, there is no effective target for systemic TNBC therapy due to the absence of estrogen, progesterone, and human epidermal growth factor 2 receptors (ER, PR, and HER-2, respectively) in cancer. In the present study, we evaluated the role of sphingosine kinase 2 (SphK2) and its catalyst sphingosine-1-phosphate (S1P) in TNBC metastasis and the effect of the SphK2-specific inhibitor ABC294640 on TNBC metastasis.

Methods: The function of SphK2 and S1P in TNBC cell metastasis was evaluated using transwell migration and wound-healing assays. The molecular mechanism of SphK2/S1P mediating TNBC metastasis was investigated using Western blot, histological examination, and immunohistochemistry assays. The antitumor activity of ABC294640 was examined in an *in vivo* TNBC lung metastatic model.

Results: Sphingosine kinase 2 promoted TNBC cell migration through the generation of S1P. Targeting SphK2 with ABC294640 inhibited TNBC lung metastasis *in vivo*. p21-activated kinase 1 (PAK1), p-Lin-11/Isl-1/Mec-3 kinase 1 (LIMK1), and Cofilin1 were the downstream signaling molecules of SphK2/S1P. Inhibition of PAK1 suppressed SphK2/S1P-induced TNBC cell migration.

Conclusion: Sphingosine kinase 2/sphingosine-1-phosphate promotes TNBC metastasis through the activation of the PAK1/LIMK1/Cofilin1 signaling pathway. ABC294640 inhibits TNBC metastasis *in vivo* and could be developed as a novel agent for the clinical treatment of TNBC.

Keywords: sphingosine kinase 2, sphingosine-1-phosphate, ABC294640, metastasis, triple-negative breast cancer

INTRODUCTION

Breast cancer is the most common malignant tumor and the leading cause of cancer-related death among women worldwide (Bray et al., 2018). Triple-negative breast cancer (TNBC) is a unique subtype of breast cancer in which the estrogen receptor (ER), progesterone receptor (PR), and human epidermal growth factor receptor 2 (HER-2) are not expressed (Perou et al., 2000).

Although TNBC accounts for only 15–20% of breast cancers, it is characterized by profound invasion, poor prognosis, and short survival time. Moreover, patients with TNBC cannot receive endocrine and targeted therapies due to the lack of ER, PR, and HER-2 (Hwang et al., 2019). Finding new targets for TNBC treatment is of great clinical significance for patients with TNBC.

Accumulating evidence suggests that sphingosine-1-phosphate (S1P) is a potent bioactive lipid mediator that is involved in cancer development and progression by regulating tumor proliferation, migration, and angiogenesis (Hla and Brinkmann, 2011). Sphingosine kinase (SphK) is the key regulatory enzyme, catalyzing the formation of S1P. To date, two isoforms of SphK have been identified: SphK1 and SphK2 (Hait et al., 2006). The cancer-promoting functions of SphK1/S1P in TNBC are well-defined by compelling evidence. Previous studies have reported that SphK1/S1P promotes TNBC metastasis through the Notch signaling pathway (Wang et al., 2018) and that the inhibition of SphK1 reduces TNBC cell growth through the ERK1/2 and AKT signaling pathways (Datta et al., 2014). However, the role of SphK2/S1P in these processes is not clearly recognized.

Although early studies proposed a possible proapoptotic/anticancer function of SphK2 (Liu et al., 2003), accumulating evidence suggests that SphK2/S1P has tumor-promoting activity similar to SphK1/S1P. Qiu et al. (2016) reported that SphK2 promotes cell growth, migration, and invasion in papillary thyroid carcinoma. Knockdown of SphK2 inhibits the growth of human osteosarcoma cells (Xu et al., 2017). Moreover, ABC294640, a selective inhibitor of SphK2, was shown to suppress the progression of many cancers (French et al., 2010). Importantly, ABC294640 is currently under evaluation in a phase II clinical trial as an agent for the treatment of advanced hepatocellular carcinoma. The role of SphK2 in breast cancer has also been explored in recent studies. Antoon et al. (2011) reported that the SphK2 expression is higher in TNBC cells than in human breast epithelial cells, and high level of SphK2/S1P improved TNBC cell growth. In addition, the pharmacological inhibition of SphK2 slowed TNBC cell proliferation *in vitro* and *in vivo* (Antoon et al., 2010). However, few studies have focused on the effect of SphK2 on TNBC cell migration. Only Gao and Smith (2011) reported that the ablation of SphK2 inhibited the migration of MDA-MB-231 TNBC cells, but the underlying mechanism and whether ABC294640 could reduce the metastasis of TNBC have not been well elucidated.

Sphingosine-1-phosphate can promote breast cancer metastasis by activating multiple signaling cascades. S1P has been reported to increase p21-activated kinase 1 (PAK1) activity (Egom et al., 2010, 2011) and even directly stimulate PAK1 (Maceyka et al., 2008). In the presence of active PAK1, the phosphorylation of both p-Lin-11/Isl-1/Mec-3 kinase 1 (LIMK1) and Cofilin1 is greatly enhanced, which leads to actin cytoskeleton formation and increase in cell motility (Jang et al., 2012). Given the importance of PAK1 (Shrestha et al., 2012) and LIMK1 (Li et al., 2014) in breast cancer metastasis, we examined whether the PAK1/LIMK1/Cofilin1 signaling pathway is the downstream signaling cascade of SphK2/S1P.

In the present study, we explored the role and potential molecular mechanism of SphK2/S1P in TNBC metastasis. Moreover, ABC294640 was used to examine the effect of targeting SphK2 on TNBC metastasis.

RESULTS

Knockdown of SphK2 Suppresses TNBC Cell Migration

To investigate the role of SphK2 in TNBC cell migration, SphK2 siRNAs were transfected into two TNBC cell lines: MDA-MB-231 and BT-549. The successful knockdown of SphK2 in MDA-MB-231 and BT-549 cells was verified by real-time quantitative PCR (RT-qPCR) and Western blot assays. SphK2 siRNA transfection resulted in significantly decreased expression of SphK2 at both the mRNA and protein levels in MDA-MB-231 and BT-549 cells, whereas SphK1 expression was not affected (**Figures 1A,B**). Wound-healing and transwell migration assays were used to observe cell migration. The cell migration in the SphK2 siRNA groups was markedly lower than that in the control groups (**Figures 1C,D**), indicating that SphK2 plays an important role in TNBC cell migration.

Pharmacological Inhibition of SphK2 Decreases TNBC Cell Migration

Sphingosine kinase 2 was inhibited with ABC294640, a selective SphK2 inhibitor, to assess the effect of SphK2 on TNBC cell migration. The CCK-8 assay was used to evaluate the effect of ABC294640 on TNBC cell viability, and a concentration of 12.5 μM was selected for the SphK2 inhibition experiment because no obvious inhibition of cell viability was observed at this concentration: relative cell viability was 91.62% for MDA-MB-231 cells and 90.76% for BT-549 cells (**Figure 2A**). The wound-healing and transwell migration assays showed that the migratory ability of both MDA-MB-231 and BT-549 cells was decreased after exposure to 12.5 μM ABC294640 for 24 h (**Figures 2B,C**).

Sphingosine Kinase 2 Overexpression Promotes TNBC Cell Migration

MDA-MB-231 and BT-549 TNBC cells were stably transfected with LV-SphK2 lentivirus to enhance SphK2 expression. SphK2 expression in MDA-MB-231 and BT-549 cells was significantly increased compared with that in control cells confirmed by Western blot and qRT-PCR assays (**Figures 3A,B**). The migratory ability of LV-SphK2 TNBC cells was significantly increased, further supporting the importance of SphK2 in TNBC cell migration (**Figures 3C,D**).

Sphingosine-1-Phosphate Production Positively Correlates With SphK2 Expression in TNBC Cells

Since the main biological function of SphK2 is to catalyze the generation of S1P, we further evaluated the role of S1P in SphK2-induced TNBC cell migration. The S1P level in TNBC cells

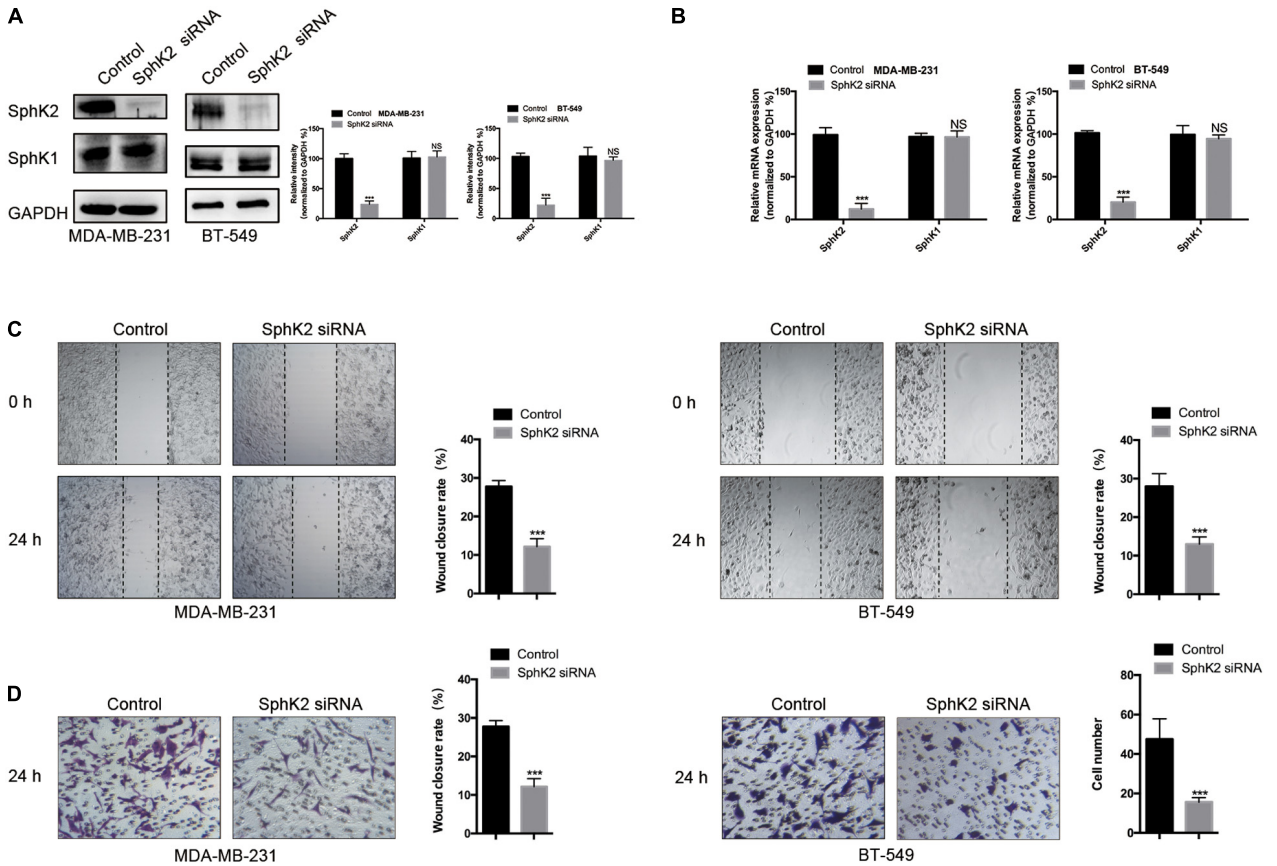

FIGURE 1 | Effects of SphK2 knockdown on TNBC cell migration. **(A)** SphK2 and SphK1 protein expression in TNBC cells transfected with SphK2 siRNA or control siRNA was determined by Western blot assay. **(B)** Relative SphK2 and SphK1 mRNA expression determined by RT-qPCR in TNBC cells transfected with SphK2 siRNA or control siRNA. **(C)** The migration of TNBC cells transfected with SphK2 siRNA or control siRNA was evaluated by a wound-healing assay. **(D)** The migration of TNBC cells transfected with SphK2 siRNA or control siRNA was evaluated by a transwell assay. The results of each assay are representative of three independent experiments. The bars represent the mean ± SD of three independent experiments. ***$p < 0.001$; NS, not significant.

after the inhibition or overexpression of SphK2 was measured by liquid chromatography-tandem mass spectrometry (LC-MS/MS). As expected, the pharmacological inhibition of SphK2 by ABC294640 decreased S1P production in MDA-MB-231 and BT-549 cells (**Figure 4A**; lowered by 0.49 and 0.5 compared with the control group, respectively). Meanwhile, overexpression of SphK2 increased the S1P level in these two cell lines (**Figure 4B**; 1.74-fold and 1.65-fold higher than control group, respectively). These data suggested that S1P production in TNBC cells was positively correlated with SphK2.

Exogenous S1P Promotes TNBC Cell Migration and Restores the Reduced Migratory Ability of SphK2-Knockdown TNBC Cells

Since the inhibition of SphK2 suppressed the S1P production, and SphK2 overexpression promoted S1P production in TNBC cells, we hypothesized that the effect of SphK2 on the migratory ability of TNBC cells was achieved by S1P. To determine whether S1P could promote the migration of TNBC cells, 4 μM exogenous S1P was added to the cell culture medium during transwell migration and wound-healing assays. Exogenous S1P stimulation markedly improved the migratory ability of TNBC cells (**Figures 5A,B**), suggesting that S1P promotes TNBC cell migration. Furthermore, when S1P was added to the medium of SphK2-knockdown TNBC cells, the impaired migratory ability was restored (**Figures 5C,D**). Collectively, the above results indicated that SphK2 promoted TNBC cell migration by catalyzing the production of S1P.

Pharmacological Inhibition of PAK1 Decreases TNBC Cell Migration and Reduces the Increased Migratory Ability of TNBC Cells Due to SphK2 Overexpression or Exogenous S1P Stimulation

Based on some research that S1P could promote cell migration through PAK1 activation, we questioned whether PAK1 was activated by SphK2/S1P in TNBC cells. To clarify the role of PAK1 in modulating TNBC metastasis, TNBC cells were exposed

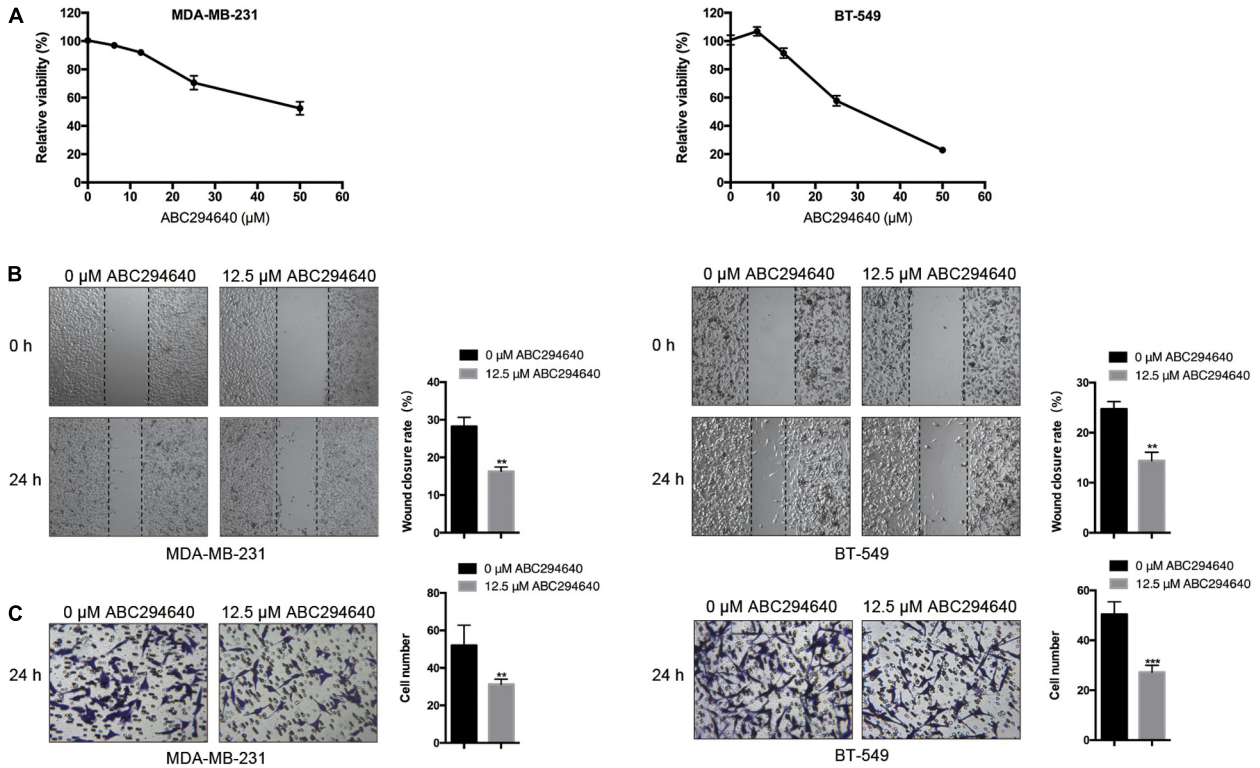

FIGURE 2 | Effects of SphK2 inhibition on TNBC cell migration. **(A)** The effect of ABC294640 on TNBC cell viability was evaluated by a CCK-8 assay. **(B)** Wound-healing assay on the migration of TNBC cells treated with the SphK2 inhibitor ABC294640 (12.5 μM). **(C)** Transwell assay on the migration of TNBC cells exposed to ABC294640 (12.5 μM). The results of each assay are representative of three independent experiments. The bars represent the mean ± SD of three independent experiments. $^{**}p < 0.01$, $^{***}p < 0.001$.

to the PAK1 inhibitor IPA-3, and a concentration of 5 μM was selected based on the PAK1 inhibition experiment, in which viability of cells exposed to 5 μM IPA-3 was 94.70% in MDA-MB-231 cells and 90.77% in BT-549 cells, showing no significant inhibition of cell viability (**Figure 6A**). After exposure to 5 μM IPA-3 for 24 h, PAK1 phosphorylation declined (**Figure 6B**), indicating that PAK1 activity was decreased. The results of the transwell migration and wound-healing assays showed that the inhibition of PAK1 activity by IPA-3 decreased the migration of TNBC cells (**Figures 6C,D**). In addition, the increased migration ability of TNBC cells due to SphK2 overexpression or exogenous S1P stimulation was reversed by IPA-3 treatment (**Figures 6E–H**). Therefore, PAK1 was confirmed to promote the migration of TNBC cells and could be a downstream molecule of SphK2/S1P.

Sphingosine Kinase 2/Sphingosine-1-Phosphate Regulates TNBC Cell Migration Through the Activation of PAK1/LIMK1/Cofilin1 Signaling

Currently, the molecular mechanisms of SphK2-mediated TNBC cell migration are unknown. Since PAK1 is a downstream molecule of SphK2/S1P, and PAK1 can promote cell motility through the activation of LIMK1/Cofilin1, we hypothesized that SphK2/S1P could regulate the migration of TNBC cells in a PAK1/LIMK1/Cofilin1 signaling-dependent manner. Therefore, we measured the phosphorylation level of PAK1, LIMK1, and Cofilin1 in TNBC cells subjected to different treatments. The Western blot assay results showed that the phosphorylation of PAK1, LIMK1, and Cofilin1 was decreased in TNBC cells with SphK2 knockdown or inhibition (**Figures 7A,B**) but increased in SphK2-overexpressed TNBC cells (**Figure 7C**). The exogenous S1P stimulation also increased the phosphorylation of PAK1, LIMK1, and Cofilin1 (**Figure 7D**). These results suggested that the PAK1/LIMK1/Cofilin1 signaling pathway participates in SphK2/S1P-mediated migration of MDA-MB-231 and BT-549 cells.

Sphingosine Kinase 2-Selective Inhibitor ABC294640 Reduces the Lung Metastasis of TNBC Cells *in vivo*

To determine the therapeutic potential of pharmacological inhibition of SphK2 in TNBC, the effect of ABC294640 on tumor metastasis was examined in a 4T1 xenograft mouse model. Mice with established, size-matched 4T1 tumors were divided into two groups and treated with ABC294640 or vehicle. Tumor weight showed no significant difference between groups at the end point

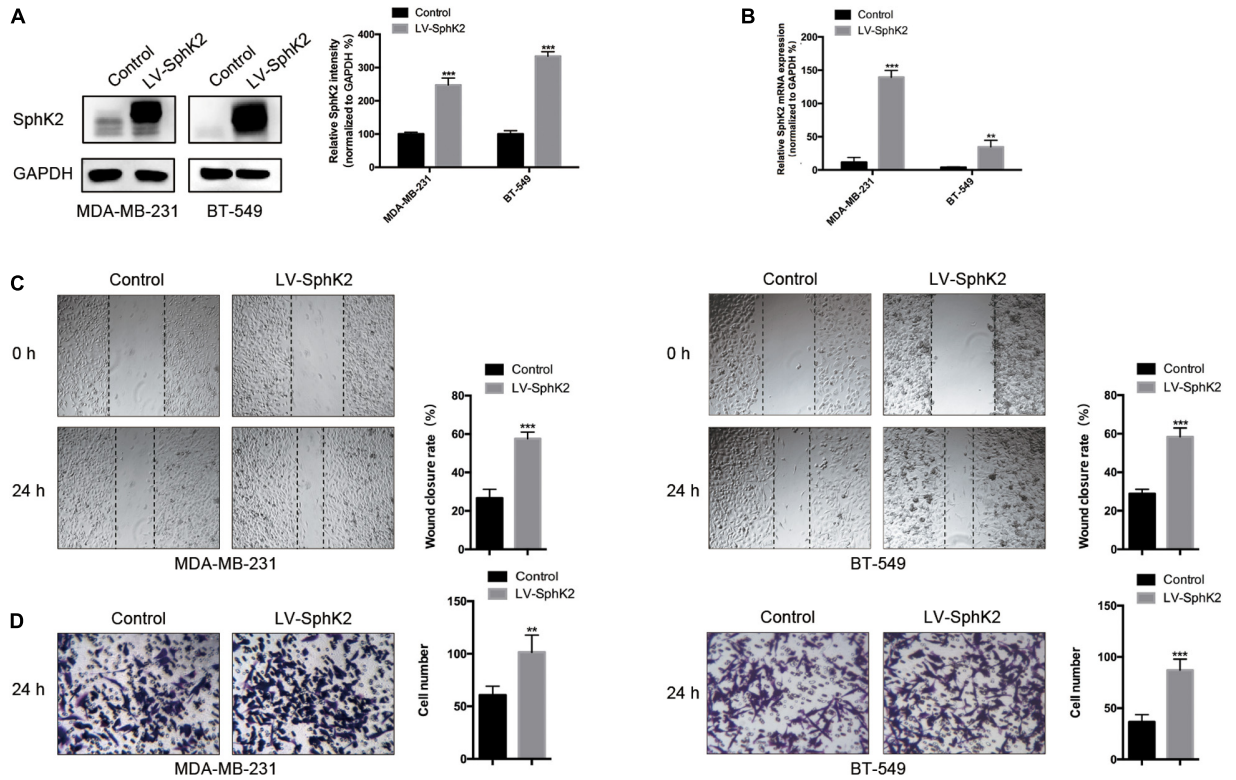

FIGURE 3 | Effects of SphK2 overexpression on TNBC cell migration. **(A)** SphK2 protein expression in TNBC cells transfected with LV-SphK2 lentivirus or control virus was measured by Western blot assay. **(B)** Relative SphK2 mRNA expression levels in TNBC cells transfected with LV-SphK2 lentivirus or control virus were measured by RT-qPCR. **(C,D)** The migration of TNBC cells transfected with LV-SphK2 lentivirus or control lentivirus was evaluated by wound-healing and transwell assays. The results of each assay are representative of three independent experiments. The bars represent the mean ± SD of three independent experiments. $^{**}p < 0.01$, $^{***}p < 0.001$.

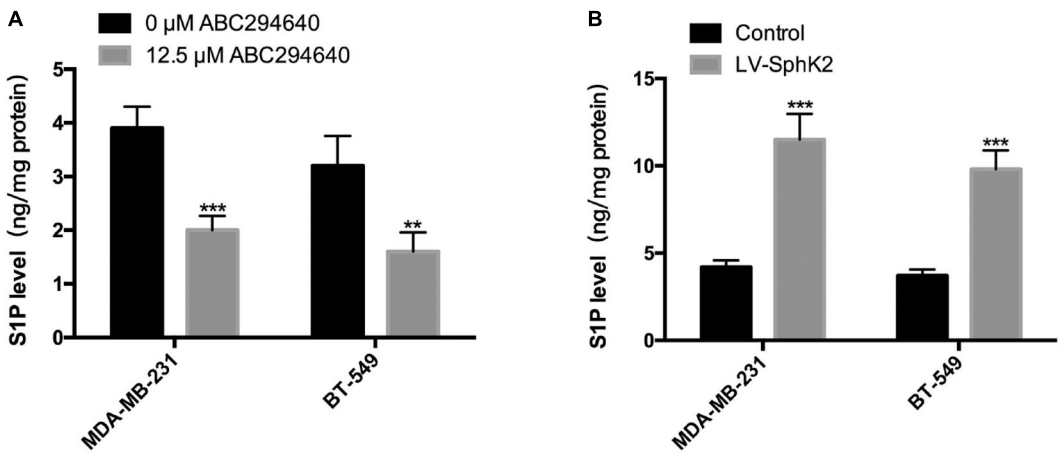

FIGURE 4 | Influence of SphK2 pharmacological inhibition and overexpression on S1P production in TNBC cells. **(A)** Intracellular S1P production measured via LC-MS/MS in TNBC cells exposed to ABC294640 (12.5 μM) for 24 h. **(B)** S1P analyses were conducted in SphK2-overexpressing and control TNBC cells via LC-MS/MS. The results of each assay are representative of three independent experiments. The bars represent the mean ± SD of three independent experiments. $^{**}p < 0.01$, $^{***}p < 0.001$.

of treatment (**Figure 8A**). There was also no distinct difference in the tumor volume between the two groups during 4 weeks of treatment (**Figure 8A**), while an obvious increase in the number and size of lung metastatic nodules was observed in the vehicle control group at the end of the treatment (**Figure 8B**), indicating that ABC294640 could decrease TNBC metastasis *in vivo*.

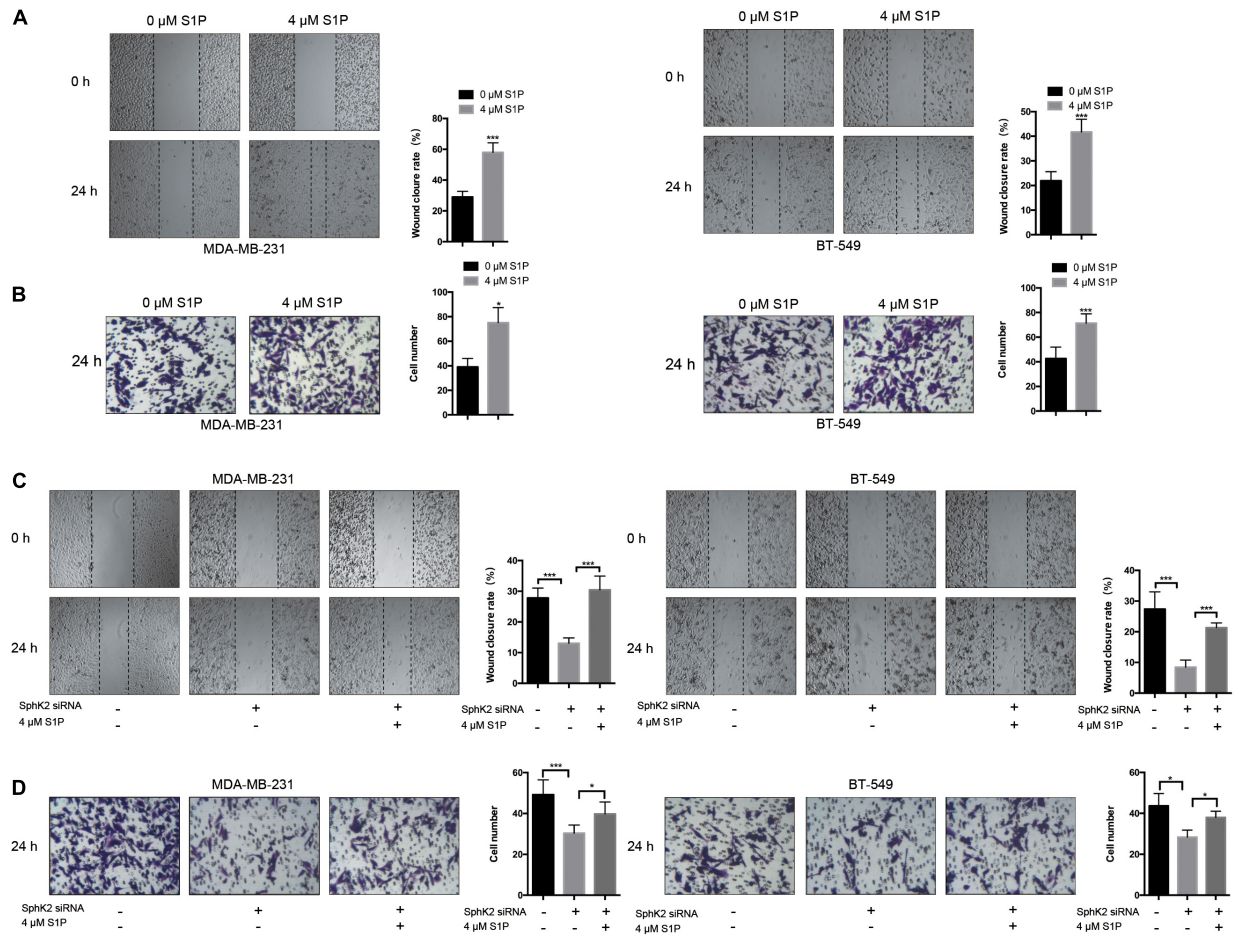

FIGURE 5 | Effects of exogenous S1P on TNBC cell migration. **(A,B)** TNBC cell migration was examined after treatment with 4 μM S1P by wound-healing and transwell assays. **(C,D)** TNBC cells transfected with SphK2 siRNA were exposed to 4 μM S1P. Cell migration was evaluated by wound-healing and transwell assays. The results of each assay are representative of three independent experiments. The bars represent the mean ± SD of three independent experiments. $^{*}p < 0.05$, $^{***}p < 0.001$.

Moreover, we performed a histological assessment on orthotopic tumors and lung metastatic nodules. No significant difference in TUNEL or Ki-67 staining was observed between tumors from ABC294640-treated mice and those from control mice, indicating that treatment with 40 mg/kg ABC294640 had minimal influence on tumor apoptosis or proliferation (**Figure 8C**). Similar to the results *in vitro*, orthotopic tumors and lung metastatic nodules from the control group exhibited stronger staining for p-PAK1, p-LIMK1, and p-Cofilin1 than that from ABC2945640-treated group (**Figure 8D**), further supporting the hypothesis that SphK2/S1P regulates the metastasis of TNBC through the activation of PAK1/LIMK1/Cofilin1 signaling pathway.

DISCUSSION

Triple-negative breast cancer is a highly aggressive cancer that lacks targeted therapy (De Laurentiis et al., 2010); therefore, the need to identify efficient targets for TNBC therapy is important. Our research showed that SphK2, a key enzyme that converts sphingosine to S1P, is involved in TNBC cell migration. Similar to the results observed in human renal cancer cells (Gao and Smith, 2011), the ablation of SphK2 decreased TNBC cell migration. In addition, the pharmacological inhibition of SphK2 with ABC294640 diminished TNBC cell migration in the present study. Another study reported that the inhibition of SphK2 activity by other inhibitors had an inhibitory effect on the migration in HeLa cells (Lee et al., 2017). Moreover, we found that the overexpression of SphK2 led to an increased migratory ability of TNBC cells. Our results were in consistent with a previous study that reported that upregulation of SphK2 partially increased the migration of papillary thyroid carcinoma cells (Qiu et al., 2016). The results from the present study and others suggest that SphK2 is involved in tumor metastasis and that SphK2 might be a therapeutic target in TNBC.

Accumulating evidence demonstrates that S1P is a critical second messenger that regulates the migration of various cells, including cancer cells (Sekine et al., 2011; Bao et al., 2012) myofibroblasts (Li et al., 2012), dendritic cells (Eigenbrod et al.,

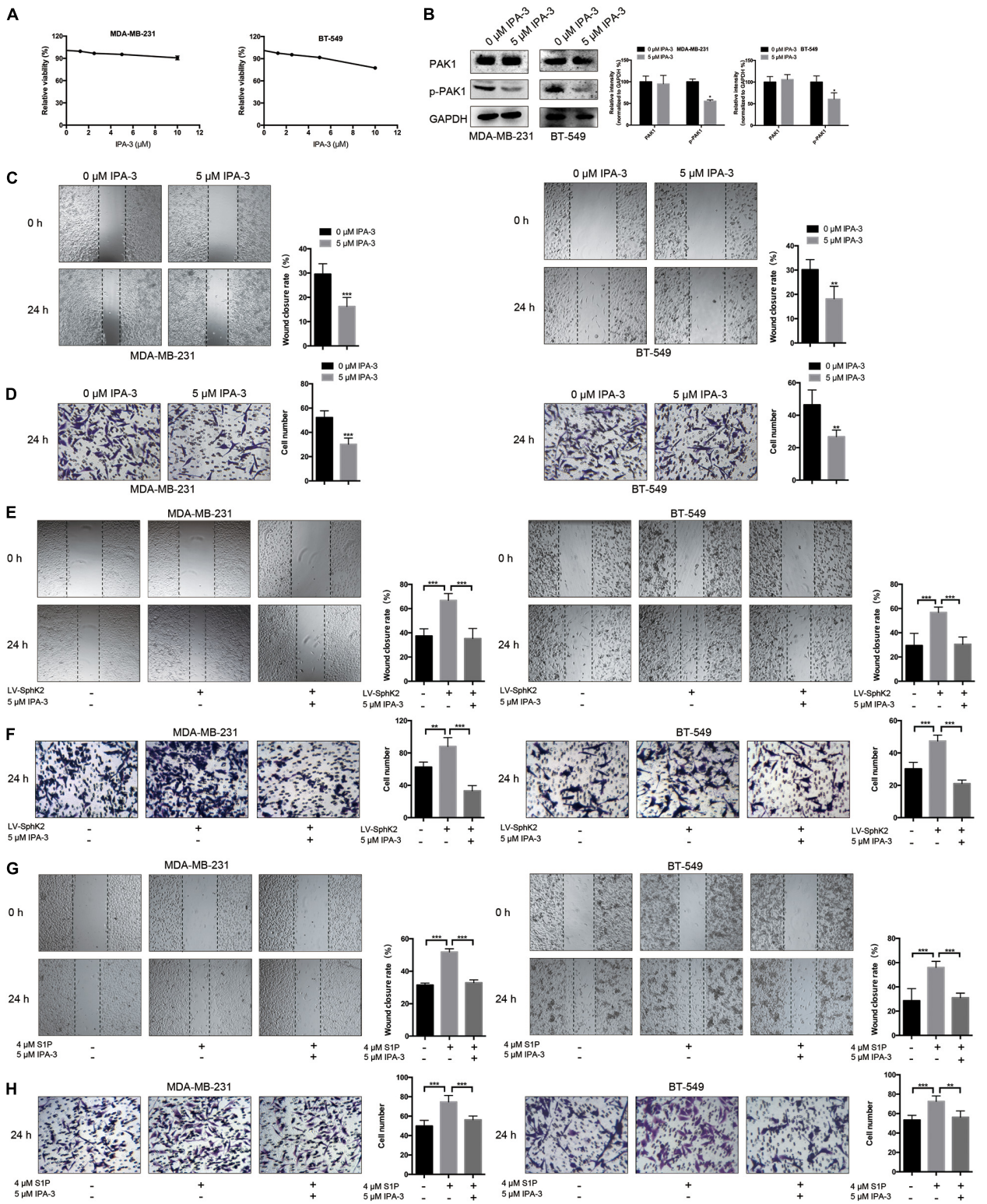

FIGURE 6 | Effects of IPA-3 on TNBC cell migration. **(A)** The influence of IPA-3 on TNBC cell viability was evaluated by a CCK-8 assay. **(B)** The level of phosphorylated PAK1 protein in TNBC cells treated with 5 μM IPA-3 for 24 h was measured by Western blot assay. **(C,D)** TNBC cell migration was examined after treatment with 5 μM IPA-3 by wound-healing and transwell assays. **(E,F)** SphK2-overexpressing TNBC cells were exposed to 5 μM IPA-3, and migration was evaluated. **(G,H)** TNBC cells treated with S1P were exposed to 5 μM IPA-3, and migration was evaluated. The results of each assay are representative of three independent experiments. The bars represent the mean ± SD of three replications of experiments. $^{*}p < 0.05$, $^{**}p < 0.01$, $^{***}p < 0.001$.

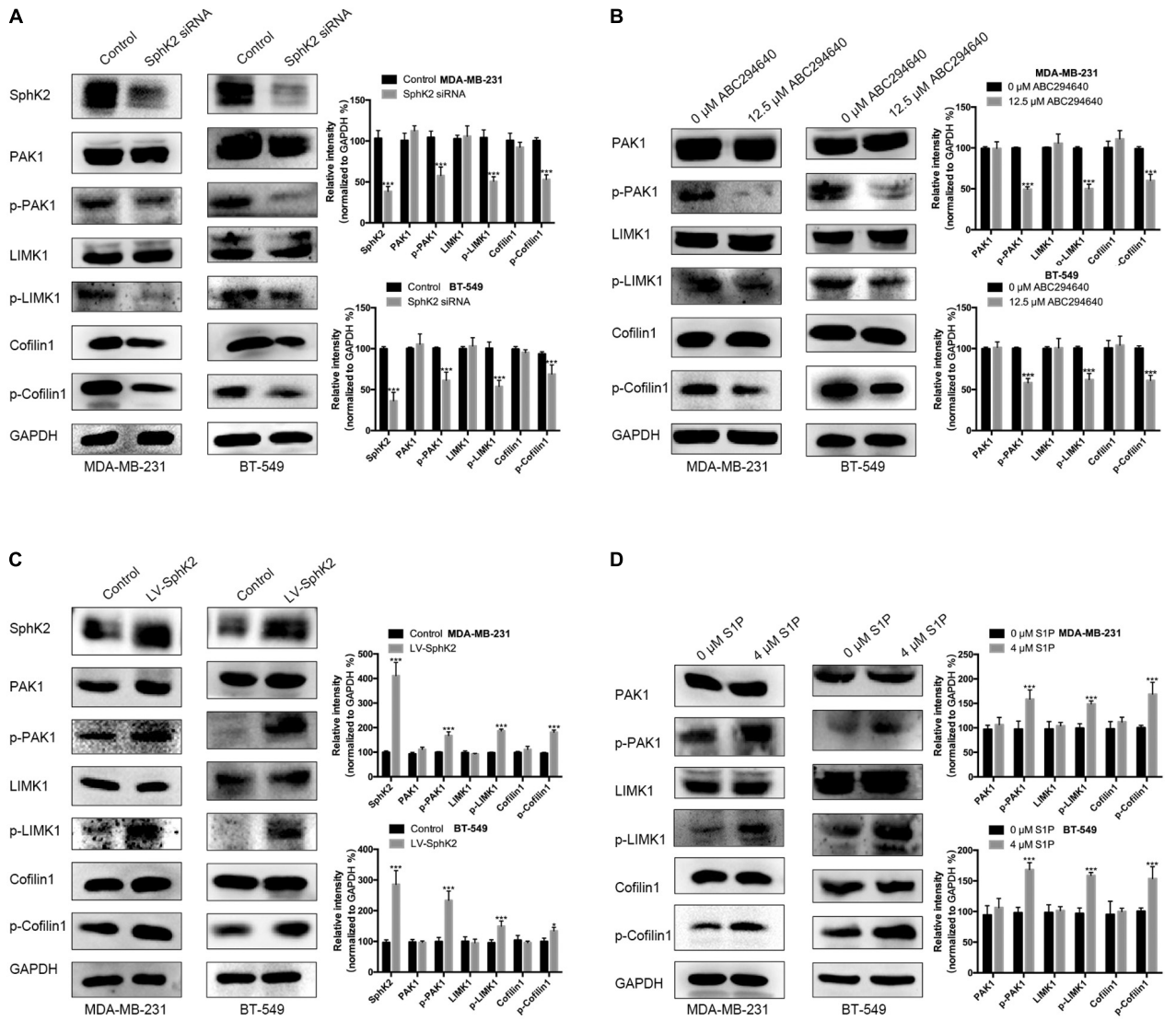

FIGURE 7 | The phosphorylation of PAK1, LIMK1, and Cofilin1 in different cell groups. Western blot assay on **(A)** the phosphorylation of PAK1, LIMK1, and Cofilin1 in TNBC cells transfected with SphK2 siRNA. **(B)** The phosphorylation of PAK1, LIMK1, and Cofilin1 in TNBC cells treated with ABC294640. **(C)** The phosphorylation of PAK1, LIMK1, and Cofilin1 in SphK2-overexpressing TNBC cells. **(D)** The phosphorylation of PAK1, LIMK1, and Cofilin1 in TNBC cells exposed to S1P. The results of each assay are representative of three independent experiments. The bars represent the mean ± SD of three replications of experiments. $^{*}p < 0.05$, $^{***}p < 0.001$.

2006), and stem cells (Ng et al., 2018). Moreover, it has been reported that S1P generated from SphK1 accelerates breast cancer cell migration (Nagahashi et al., 2018). However, whether SphK2/S1P plays the same role in TNBC cell migration is unclear. Here, we reported that SphK2/S1P promotes the migration of TNBC cells. We demonstrated that the inhibition of SphK2 with ABC294640 reduced the S1P level and that the overexpression of SphK2 increased the S1P level in TNBC cells, indicating that the expression of S1P is positively correlated with SphK2. The positive correlation between SphK2 and S1P also existed in murine adenocarcinoma cells (French et al., 2010) and colorectal cancer cells (Xun et al., 2015). However, Gao and Smith (2011) reported contrasting results in which knockdown of SphK2 led to increased S1P production in renal carcinoma cells owing to the elevated expression of SphK1. In the present study, SphK2 knockdown had minimal influence on SphK1 expression. Hait et al. (2005) also showed that SphK2 knockdown did not affect the expression and activity of SphK1 in breast cancer cells. We showed that exogenous S1P stimulation promoted TNBC cell migration and SphK2 knockdown reduced the migratory ability of TNBC cells. Collectively, these results suggest that SphK2 promotes TNBC cell migration through the production of S1P.

Based on the important roles of SphK2/S1P in TNBC cell migration, we further investigated the downstream molecular mechanisms. Our data showed that the PAK1/LIMK1/Cofilin1 cascade, an important regulator of actin cytoskeleton and cell motility (Dummler et al., 2009), was activated by SphK2/S1P in TNBC cells. S1P has been reported to increase PAK1 activity

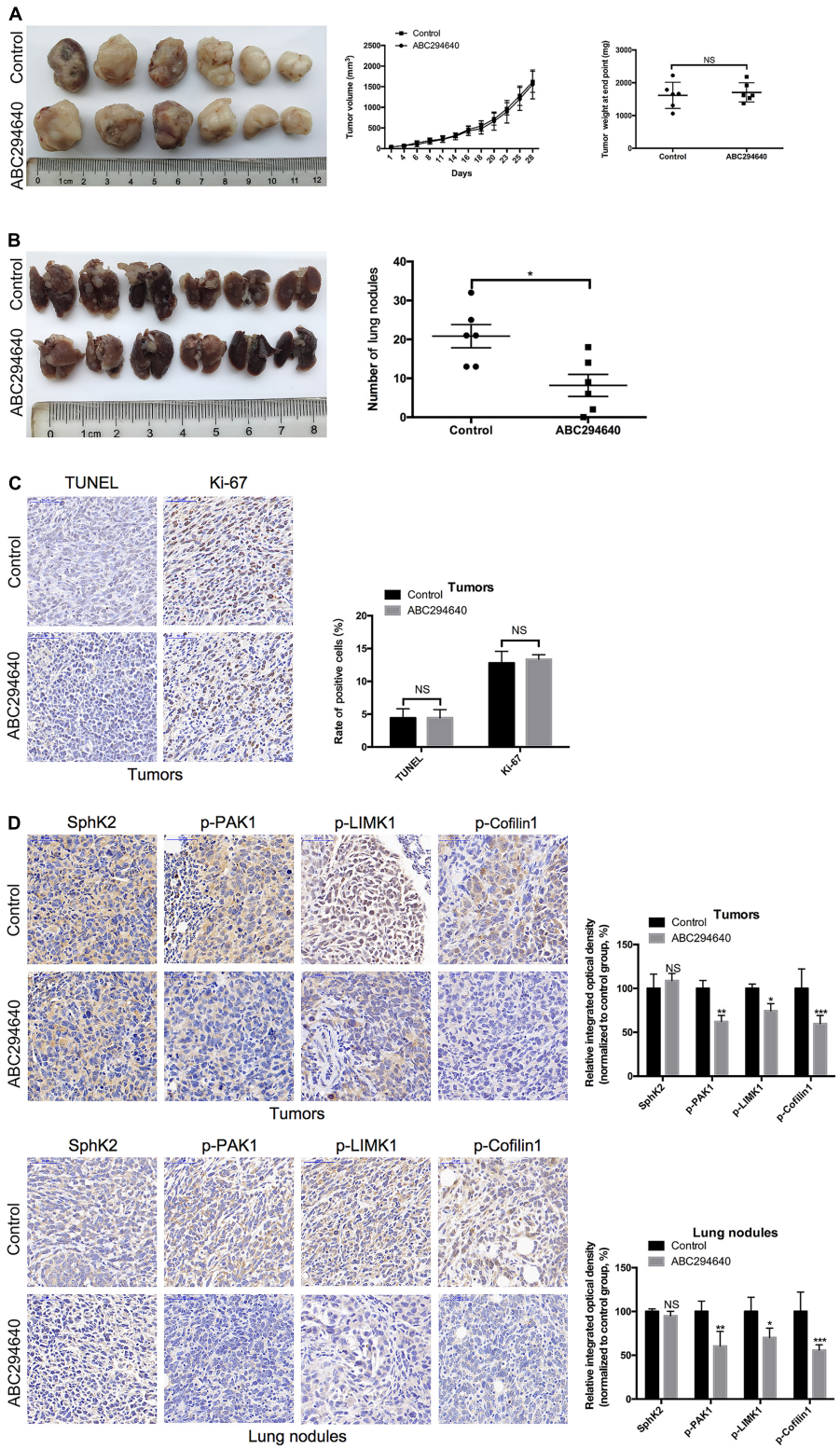

FIGURE 8 | Inhibition of SphK2 activity reduces TNBC metastasis and the phosphorylation of PAK1, LIMK1, and Cofilin1 *in vivo*. **(A)** Representative images of the orthotopic tumors were obtained, and the volumes and weight of tumors were recorded. **(B)** Representative images of the lungs were obtained, and the metastatic nodules were counted. **(C)** Tumor apoptosis and proliferation were evaluated by TUNEL and Ki-67 staining, respectively. **(D)** The levels of SphK2 and phosphorylated PAK1, LIMK1, and Cofilin1 in orthotopic tumors and lung metastatic nodules were measured. The bars represent the mean ± SD of replications of experiments. *$p < 0.05$, **$p < 0.01$, ***$p < 0.001$; NS, not significant.

(Egom et al., 2011) and even directly stimulate PAK1 to induce cell lamellipodia formation and movement (Maceyka et al., 2008). Consistent with these studies, we found that exogenous S1P stimulation increased the phosphorylation of PAK1. In addition, the inhibition of PAK1 by IPA-3 decreased TNBC cell migration and reversed the increased migratory ability of TNBC cells due to SphK2 overexpression or S1P stimulation. These results indicate that PAK1 is the downstream target of SphK2/S1P and contributes to the migration of TNBC cells. Furthermore, the phosphorylation of PAK1, LIMK1, and Cofilin1 was increased in SphK2-overexpressed or S1P-stimulated TNBC cells and decreased in SphK2-inhibited TNBC cells, and was even decreased *in vivo* due to the administration of ABC294640. These results demonstrated that the PAK1/LIMK1/Cofilin1 cascade is the downstream signaling pathway of SphK2/S1P. Generally, we elucidate a novel mechanism linking SphK2/S1P to PAK1/LIMK1/Cofilin1 in TNBC cell migration.

ABC294640, the selective inhibitor of SphK2, was found to have broad antitumor activity. ABC294640 inhibited cell growth both *in vitro* and *in vivo* in various cancers such as colorectal cancer (Xun et al., 2015), non-small cell lung cancer (Dai et al., 2018), and prostate cancer (Schrecengost et al., 2015). ABC294640 also has an effective inhibitory effect on cancer cell migration *in vitro* (French et al., 2010). Remarkably, the present study provided the first evidence that the pharmacological inhibition of SphK2 by ABC294640 at a dose of 40 mg/kg decreased TNBC metastasis in a mouse model, indicating the clinical value of ABC294640 for the treatment of TNBC.

Several limitations of this present study should be noted. Although Antoon et al. (2011) reported that the expression of SphK2 in TNBC cell line MDA-MB-231 was significantly higher than in normal mammary epithelial cell MCF-10A, the evidence of whether SphK2 upregulation present in TNBC tissues is still lacking. Our current study also did not provide expression data of SphK2 in human TNBC tissues, which should be considered as a limitation of the study. Further investigations based on clinical specimens are warranted to provide more evidence supporting SphK2 as a therapeutic target of TNBC. Pharmacokinetics and pharmacodynamics data of ABC294640 in tumor-bearing mice and in patients with advanced solid tumors are available in previously published reports (French et al., 2010; Britten et al., 2017). Interestingly, our results showed that the oral administration of 40 mg/kg ABC294640 three times a week exhibited dramatic activity against TNBC metastasis without inhibiting primary tumor growth. Unfortunately, the plasmatic and intratumoral concentrations of ABC294640 in this metastatic model remain unknown, which is also a limitation of this study. The determination of drug concentrations at which ABC294640 demonstrates metastasis-specific activity will be of great significance in further studies to develop therapeutic strategies against TNBC metastasis.

CONCLUSION

Collectively, we reported that SphK2/S1P promotes TNBC cell migration through the activation of the PAK1/LIMK1/Cofilin1 signaling pathway. Targeting SphK2 with ABC294640 inhibits TNBC xenograft metastasis *in vivo*, and ABC294640 has the potential to be a novel agent for the clinical treatment of TNBC.

MATERIALS AND METHODS

Cell Culture

Human breast carcinoma cell lines MDA-MB-231 and BT-549 and the mouse breast cancer cell line 4T1 were purchased from the Cell Bank of the Chinese Academy of Sciences (Shanghai, China). MDA-MB-231 cells were cultured in Dulbecco's modified Eagle's medium (DMEM) supplemented with 10% (v/v) fetal bovine serum (FBS), 100 U/ml penicillin, and 100 μg/ml streptomycin (all from Wisent, St-Bruno, Canada). BT-549 and 4T1 cells were cultured in Roswell Park Memorial Institute-1640 (RPMI-1640; Wisent, St-Bruno, Canada) medium, and other components of the culture media were the same as for MDA-MB-231 cells. Cells were cultured at 37°C in a humidified 5% CO_2 atmosphere.

Small Interfering RNA Transfection

Sphingosine kinase 2 was downregulated by transfection with sequence-specific siRNA (GenePharma, Shanghai, China). siRNA against human SphK2 (targeted sequence: 5′ GGGUAGUGCCUGAUCAAUGTT 3′) and control siRNA were used. A total of 4 μl of Lipofectamine 2000 (Thermo Fisher Scientific, Waltham, MA, United States) was mixed with 150 μl of Opti-MEM (Wisent, St-Bruno, Canada) and incubated for 5 min at room temperature. siRNA was diluted in 150 μl of Opti-MEM. Following 5 min of incubation, the diluted siRNA was combined with diluted Lipofectamine 2000 (total volume, 300 μl). The solution was mixed gently, incubated for 20 min at room temperature, and then added to a six-well dish containing cells and medium. RT-qPCR and Western blot assays were adopted to assess the knockdown efficiency.

Lentivirus Transfection

Lentivirus transfection was used to obtain TNBC cells with stable ectopic SphK2 expression. Lentivirus expressing SphK2 and corresponding negative control virus were purchased from GeneChem (Shanghai, China). TNBC cells were plated in the six-well plates at a density of 2×10^5 cells per well and were subsequently transfected with lentivirus at a multiplicity of infection (MOI) of 10. Following 48 h of incubation, the antibiotic-resistant transfected cells were selected by applying a culture medium containing puromycin. The SphK2 overexpression efficiency was confirmed by Western blot and RT-qPCR assays.

Cell Counting Kit-8 Assay

For the Cell Counting Kit-8 (CCK-8) assay, the IPA-3 (Selleck, Houston, TX, United States), ABC294640 (Selleck, Houston, TX, United States), and S1P (Avanti Polar Lipids, Alabaster, AL, United States) were dissolved in dimethyl sulfoxide (DMSO) to generate stock solutions at concentrations of 50, 50, and 10 mM, respectively. The final concentration of DMSO in the

treatment medium was below 0.1%. TNBC cells in DMEM containing 10% FBS were seeded into 96-well plates at a concentration of 1×10^4 cells per well and incubated for 24 h. The culture medium was replaced with a fresh medium containing vehicle or testing agents at indicated concentrations. After treating cells with different agents or vehicles for 48 h, CCK-8 solution (10 μl/well) was added to the 96-well plates and incubated for 1 h to detect the viability of TNBC cells. The light absorbance values at 450 nm were measured in a microplate reader (Bio-Rad, Hercules, CA, United States), and cell viability was determined. Relative viability was normalized to the vehicle-treated control cells after background subtraction and was expressed as $OD_{test}/OD_{control}*100\%$. Each treatment was performed in triplicate wells, and three independent experiments were repeated.

Protein Isolation and Western Blot Assays

The cells were lysed with 150 μl of lysis buffer (Beyotime, Shanghai, China) containing 1% protease inhibitors (Thermo Fisher Scientific, Waltham, MA, United States) on ice for 5 min following washing two times with ice-cold phosphate-buffered saline (PBS). The cells were harvested and centrifuged at 12,000 × *g* for 5 min at 4°C. The protein concentrations were determined using a BCA kit (Beyotime, Shanghai, China). Equal amounts of protein (20 μg/lane) dissolved in 20 μl of loading buffer (Beyotime, Shanghai, China) were separated by sodium dodecyl sulfate polyacrylamide gel electrophoresis (SDS-PAGE, Beyotime, Shanghai, China), transferred to polyvinylidene difluoride (PVDF) membranes (Roche Applied Science, Mannheim, Germany), and blocked with 5% non-fat milk for 1 h at room temperature. Immunoblotting was performed by incubation overnight at 4°C with the indicated primary antibodies (Cell Signaling Technology, Beverly, MA, United States except as noted): anti-PAK1, anti-p-PAK1, anti-Cofilin1, anti-p-Cofilin1, anti-LIMK1 (Abcam, Burlingame, CA, United States), anti-p-LIMK1 (Abcam, Burlingame, CA, United States), anti-SphK1 (Proteintech, Wuhan, China), and anti-SphK2 (Proteintech, Wuhan, China). The dilution of primary antibodies against SphK1 and SphK2 was 1:500. Other primary antibodies were diluted at 1:1,000. After the incubation with primary antibodies, the membranes were washed and incubated with horseradish peroxidase (HRP)-linked secondary antibodies (1:5,000 dilution; Proteintech, Wuhan, China) at room temperature for 1 h. The signals were developed with an enhanced chemiluminescence reagent (Biosharp, Beijing, China) under a chemiluminescence camera (Tanon, Beijing, China). The density of each band was measured using ImageJ software (National Institutes of Health, Bethesda, MD, United States) and normalized to internal control [glyceraldehyde 3-phosphate dehydrogenase (GAPDH)] from the same sample. Three independent experiments were repeated.

Real-Time Quantitative PCR

Total RNA was extracted using the TRIzol Reagent (Takara Bio, Otsu, Japan) and reverse transcribed into cDNA using the PrimeScript RT Master Mix (Takara Bio, Otsu, Japan). The relative mRNA expression levels were determined by RT-qPCR with the SYBR Green PCR Master Mix (Takara Bio, Otsu, Japan) on an ABI PRISM 7300 Sequence Detection System (Applied Biosystems, Foster City, CA, United States). The relative mRNA levels were calculated by the $2^{-\Delta\Delta\ Cq}$ method with GAPDH as the internal control. Three independent experiments were repeated.

Wound-Healing Assay

A culture insert (Ibidi, Munich, Germany) was used to generate a wound of 500 μm. The insert was placed on the 24-well plates; then, 2×10^5 cells were seeded in each culture insert and incubated for 24 h. After removing the culture insert, cells were allowed to grow in the media without FBS for 24–48 h. The original area and migration area were measured using ImageJ software, and the wound closure rates are shown according to the ratio of the migration area to the original area. Each treatment was performed in triplicate wells and three independent experiments were repeated.

Transwell Migration Assay

Transwell migration assay was performed using a 6.5-mm transwell insert with 8.0-μm pore polycarbonate membrane (Merck Millipore, Burlington, MA, United States). A total of 300 μl of cell suspension containing 2×10^5 cells without FBS was added to the upper chamber, and 800 μl of medium containing 10% FBS was added to the lower chamber. After incubation for 48 h, cells on the lower chamber were fixed with 4% paraformaldehyde for 20 min and stained with crystal violet for 20 min. Images of each chamber were captured randomly for cell counting. Three independent experiments were repeated.

Quantification of S1P by LC-MS/MS

Cells were washed two times with cold PBS, harvested, and centrifuged at 1,000 rpm for 5 min at 4°C; then, the cells were suspended in 100 μl of distilled water. The cell suspension was mixed with internal standard (1 ng/ml C17-S1P, Avanti Polar Lipids, Alabaster, AL, United States) and 65 μl of methanol and then centrifuged at 1,000 rpm for 5 min. S1P in the supernatant was quantified by LC-MS/MS as described previously at the Virginia Commonwealth University Lipidomics Core (Nagahashi et al., 2013).

Tumor Xenograft Model

Six-week-old female BALB/c mice, weighing approximately 20 g, were purchased from the Model Animal Research Center of Nanjing University (Nanjing, China). The mice were housed in sterile cages in laminar airflow hoods in a specific pathogen-free environment at 22–25°C, 40–60% relative humidity with a 12:12 h day/night light cycle. The mice had free access to autoclaved water and commercial mouse chow (Xietong Biological, Nanjing, China). The study protocol was approved by the Institutional Ethics Committee of the Affiliated Drum Tower Hospital of Nanjing University Medical School. 4T1 cells (2×10^5 cells in 100 μl of PBS) were surgically implanted into the mammary fat pads. When the tumors formed, the

mice were randomly assigned into two groups. Subsequently, ABC294640 at an oral dose of 40 mg/kg body weight or vehicle was administered three times a week. ABC294640 was suspended in an oral vehicle solution containing 2% DMSO + 30% PEG300 (Selleck, Houston, TX, United States) + 5% Tween 80 (Selleck, Houston, TX, United States) + ddH_2O. Tumor volume was measured three times a week using a digital caliper and calculated using the equation (length × width^2)/2. The body weight of mice was also measured three times a week. All mice were sacrificed by cervical dislocation under general anesthesia with isoflurane (RWD Life Science, Shenzhen, China) after 4 weeks of treatment. The tumors and lungs were harvested, and the number of metastatic tumor nodules was recorded.

Hematoxylin & Eosin (H&E), Immunohistochemical, and TUNEL Staining

Tissues fixed with 4% paraformaldehyde were embedded in paraffin and cut into 5-μm thick slices. For H&E staining, the tissue slices were dewaxed in xylene, rehydrated with decreasing concentrations of ethanol, and washed with PBS. The slices were stained with hematoxylin for 30 s with agitation and rinsed with water. Then, the slices were stained with eosin for 10–30 s with agitation and rinsed with water. After staining, the slices were dehydrated, mounted, and covered with coverslips. Immunohistochemical (IHC) staining was performed according to a published protocol (Liu et al., 2017). Samples were incubated with antibodies (Cell Signaling Technology, Beverly, MA, United States, except as noted) against Ki-67, SphK2 (Proteintech, Wuhan, China), p-PAK1, p-LIMK1 (Abcam, Burlingame, CA, United States), and p-Cofilin1. TUNEL staining was performed according to the manufacturer's protocol (Beyotime Biotechnology, Nantong, China). The Ki-67-positive cells, TUNEL-positive cells, and the integrated optical density (IOD) of SphK2, p-PAK1, p-LIMK1, and p-Cofilin1 staining were analyzed using ImageJ software.

Statistical Analysis

Data were analyzed using SPSS 19.0 statistical software (IBM, Chicago, IL, United States) and are expressed as the mean ± SD. Comparisons of different groups were performed using Student's *t*-test or ANOVA analysis. A *p*-value less than 0.05 ($p < 0.05$) was considered to indicate a significant difference.

DATA AVAILABILITY STATEMENT

The raw data supporting the conclusions of this article will be made available by the authors, without undue reservation.

ETHICS STATEMENT

The animal study was reviewed and approved by the Institutional Ethics Committee of the Affiliated Drum Tower Hospital of Nanjing University Medical School.

AUTHOR CONTRIBUTIONS

CJ, JW, ZW, and WS conceived and designed the experiments. WS, DM, YC, LH, SL, DY, SZ, and GZ performed the experiments. WS, DM, YC, LH, and SL analyzed the data. WS and SZ wrote the original manuscript. JW and ZW reviewed and edited the manuscript. CJ, JW, and ZW acquired the funding. All authors contributed to the article and approved the submitted version.

FUNDING

This research was supported by the National Natural Science Foundation of China (81572393, 81602093, and 81972888) and Natural Science Foundation of Jiangsu Province (BK20160118 and BK20141324), and key project was supported by the Medical Science and Technology Development Foundation and Nanjing Municipality Health Bureau (ZKX15020 and ZKX17022).

ACKNOWLEDGMENTS

We thank the Translational Medicine Core facilities of the Medical School of Nanjing University for instrumentation support. This manuscript has been released as a pre-print at ResearchSquare (https://www.researchsquare.com/article/rs-43512/v1) (Shi et al., 2020).

REFERENCES

Antoon, J. W., White, M. D., Meacham, W. D., Slaughter, E. M., Muir, S. E., Elliott, S., et al. (2010). Antiestrogenic effects of the novel sphingosine kinase-2 inhibitor ABC294640. *Endocrinology* 151, 5124–5135. doi: 10.1210/en.2010-0420

Antoon, J. W., White, M. D., Slaughter, E. M., Driver, J. L., Khalili, H. S., Elliott, S., et al. (2011). Targeting NF kappa B mediated breast cancer chemoresistance through selective inhibition of sphingosine kinase-2. *Cancer Biol. Ther.* 11, 678–689. doi: 10.4161/cbt.11.7.14903

Bao, M., Chen, Z., Xu, Y., Zhao, Y., Zha, R., Huang, S., et al. (2012). Sphingosine kinase 1 promotes tumour cell migration and invasion via the S1P/EDG1 axis in hepatocellular carcinoma. *Liver Intern.* 32, 331–338. doi: 10.1111/j.1478-3231.2011.02666.x

Bray, F., Ferlay, J., Soerjomataram, I., Siegel, R. L., Torre, L. A., and Jemal, A. (2018). Global cancer statistics 2018: GLOBOCAN estimates of incidence and mortality worldwide for 36 cancers in 185 countries. *CA Cancer J. Clin.* 68, 394–424. doi: 10.3322/caac.21492

Britten, C. D., Garrett-Mayer, E., Chin, S. H., Shirai, K., Ogretmen, B., Bentz, T. A., et al. (2017). A Phase I study of ABC294640, a first-in-class Sphingosine Kinase-2 inhibitor, in patients with advanced solid tumors. *Clin. Cancer Res.* 23, 4642–4650. doi: 10.1158/1078-0432.CCR-16-2363

Dai, L., Smith, C. D., Foroozesh, M., Miele, L., and Qin, Z. (2018). The sphingosine kinase 2 inhibitor ABC294640 displays anti-non-small cell lung cancer activities in vitro and in vivo. *Int. J. Cancer* 142, 2153–2162. doi: 10.1002/ijc.31234

Datta, A., Loo, S. Y., Huang, B., Wong, L., Tan, S. S. L., Tan, T. Z., et al. (2014). SPHK1 regulates proliferation and survival responses in triple-negative breast cancer. *Oncotarget* 5, 5920–5933. doi: 10.18632/oncotarget.1874

De Laurentiis, M., Cianniello, D., Caputo, R., Stanzione, B., Arpino, G., Cinieri, S., et al. (2010). Treatment of triple negative breast cancer (TNBC): current options and future perspectives. *Cancer Treat. Rev.* 36, S80–S86. doi: 10.1016/s0305-7372(10)70025-6

Dummler, B., Ohshiro, K., Kumar, R., and Field, J. (2009). Pak protein kinases and their role in cancer. *Cancer Metast. Rev.* 28, 51–63. doi: 10.1007/s10555-008-9168-1

Egom, E. E. A., Ke, Y., Solaro, R. J., and Lei, M. (2010). Cardioprotection in ischemia/reperfusion injury: spotlight on sphingosine-1-phosphate and bradykinin signalling. *Prog. Biophys. Mol. Biol.* 103, 142–147. doi: 10.1016/j.pbiomolbio.2010.01.001

Egom, E. E. A., Mohamed, T. M. A., Mamas, M. A., Shi, Y., Liu, W., Chirico, D., et al. (2011). Activation of Pak1/Akt/eNOS signaling following sphingosine-1-phosphate release as part of a mechanism protecting cardiomyocytes against ischemic cell injury. *Am. J. Physiol. Heart Circ. Physiol.* 301, H1487–H1495. doi: 10.1152/ajpheart.01003.2010

Eigenbrod, S., Derwand, R., Jakl, V., Endres, S., and Eigler, A. (2006). Sphingosine kinase and sphingosine-1-phosphate regulate migration, endocytosis and apoptosis of dendritic cells. *Immunol. Invest.* 35, 149–165. doi: 10.1080/08820130600616490

French, K. J., Zhuang, Y., Maines, L. W., Gao, P., Wang, W., Beljanski, V., et al. (2010). Pharmacology and antitumor activity of ABC294640, a selective inhibitor of sphingosine Kinase-2. *J. Pharmacol. Exp. Ther.* 333, 129–139. doi: 10.1124/jpet.109.163444

Gao, P., and Smith, C. D. (2011). Ablation of Sphingosine Kinase-2 inhibits tumor cell proliferation and migration. *Mol. Cancer Res.* 9, 1509–1519. doi: 10.1158/1541-7786.mcr-11-0336

Hait, N. C., Oskeritzian, C. A., Paugh, S. W., Milstien, S., and Spiegel, S. (2006). Sphingosine kinases, sphingosine 1-phosphate, apoptosis and diseases. *Biochim. Biophys. Acta Biomembr.* 1758, 2016–2026. doi: 10.1016/j.bbamem.2006.08.007

Hait, N. C., Sarkar, S., Le Stunff, H., Mikami, A., Maceyka, M., Milstien, S., et al. (2005). Role of sphingosine kinase 2 in cell migration toward epidermal growth factor. *J. Biol. Chem.* 280, 29462–29469. doi: 10.1074/jbc.M502922200

Hla, T., and Brinkmann, V. (2011). Sphingosine 1-phosphate (S1P) physiology and the effects of S1P receptor modulation. *Neurology* 76, S3–S8. doi: 10.1212/WNL.0b013e31820d5ec1

Hwang, S. Y., Park, S., and Kwon, Y. (2019). Recent therapeutic trends and promising targets in triple negative breast cancer. *Pharmacol. Ther.* 199, 30–57. doi: 10.1016/j.pharmthera.2019.02.006

Jang, I., Jeon, B. T., Jeong, E. A., Kim, E.-J., Kang, D., Lee, J. S., et al. (2012). Pak1/LIMK1/cofilin pathway contributes to tumor migration and invasion in human non-small cell lung carcinomas and cell lines. *Korean J. Physiol. Pharmacol.* 16, 159–165. doi: 10.4196/kjpp.2012.16.3.159

Lee, E., Jung, J., Jung, D., Mok, C. S., Jeon, H., Park, C.-S., et al. (2017). Inhibitory effects of novel SphK2 inhibitors on migration of cancer cells. *Anticancer Agents Med. Chem.* 17, 1689–1697. doi: 10.2174/1871520617666170213124856

Li, C., Zheng, S., You, H., Liu, X., Lin, M., Yang, L., et al. (2012). Sphingosine 1-phosphate (S1P)/S1P receptors are involved in human liver fibrosis by action on hepatic myofibroblasts motility. *J. Hepatol.* 56:749. doi: 10.1016/j.jhep.2011.05.006

Li, H., Zhang, B., Liu, Y., and Yin, C. (2014). EBP50 inhibits the migration and invasion of human breast cancer cells via LIMK/cofilin and the PI3K/Akt/mTOR/MMP signaling pathway. *Med. Oncol.* 31:162. doi: 10.1007/s12032-014-0162-x

Liu, H., Toman, R. E., Goparaju, S. K., Maceyka, M., Nava, V. E., Sankala, H., et al. (2003). Sphingosine kinase type 2 is a putative BH3-only protein that induces apoptosis. *J. Biol. Chem.* 278, 40330–40336. doi: 10.1074/jbc.M304455200

Liu, X.-H., Yang, Y.-F., Fang, H.-Y., Wang, X.-H., Zhang, M.-F., and Wu, D.-C. (2017). CEP131 indicates poor prognosis and promotes cell proliferation and migration in hepatocellular carcinoma. *Int. J. Biochem. Cell Biol.* 90, 1–8. doi: 10.1016/j.biocel.2017.07.001

Maceyka, M., Alvarez, S. E., Milstien, S., and Spiegel, S. (2008). Filamin A links sphingosine kinase 1 and sphingosine-1-phosphate receptor 1 at lamellipodia to orchestrate cell migration. *Mol. Cell Biol.* 28, 5687–5697. doi: 10.1128/mcb.00465-08

Nagahashi, M., Kim, E. Y., Yamada, A., Ramachandran, S., Allegood, J. C., Hait, N. C., et al. (2013). Spns2, a transporter of phosphorylated sphingoid bases, regulates their blood and lymph levels, and the lymphatic network. *FASEB J.* 27, 1001–1011. doi: 10.1096/fj.12-219618

Nagahashi, M., Yamada, A., Katsuta, E., Aoyagi, T., Huang, W.-C., Terracina, K. P., et al. (2018). Targeting the SphK1/S1P/S1PR1 axis that links obesity, chronic inflammation, and breast cancer metastasis. *Cancer Res.* 78, 1713–1725. doi: 10.1158/0008-5472.can-17-1423

Ng, M. L., Yarla, N. S., Menschikowski, M., and Sukocheva, O. A. (2018). Regulatory role of sphingosine kinase and sphingosine-1-phosphate receptor signaling in progenitor/stem cells. *World J. Stem Cells* 10, 119–133. doi: 10.4252/wjsc.v10.i9.119

Perou, C. M., Sorlie, T., Eisen, M. B., van de Rijn, M., Jeffrey, S. S., Rees, C. A., et al. (2000). Molecular portraits of human breast tumours. *Nature* 406, 747–752. doi: 10.1038/35021093

Qiu, W., Yang, Z., Fan, Y., and Zheng, Q. (2016). MicroRNA-613 inhibits cell growth, migration and invasion of papillary thyroid carcinoma by regulating SphK2. *Oncotarget* 7, 39907–39915. doi: 10.18632/oncotarget.9530

Schrecengost, R. S., Keller, S. N., Schiewer, M. J., Knudsen, K. E., and Smith, C. D. (2015). Downregulation of critical oncogenes by the selective SK2 inhibitor ABC294640 hinders prostate cancer progression. *Mol. Cancer Res.* 13, 1591–1601. doi: 10.1158/1541-7786.mcr-14-0626

Sekine, Y., Suzuki, K., and Remaley, A. T. (2011). HDL and Sphingosine-1-phosphate activate Stat3 in prostate cancer DU145 cells via ERK1/2 and S1P receptors, and promote cell migration and invasion. *Prostate* 71, 690–699. doi: 10.1002/pros.21285

Shi, W., Ma, D., Cao, Y., Hu, L., Liu, S., and Yan, D. (2020). SphK2/S1P promotes metastasis in triple negative breast cancer through PAK1/LIMK1/Cofilin1 signaling pathway. *ResearchSquare* [Preprint]. Available online at: https://www.researchsquare.com/article/rs-43512/v1 (accessed August 31, 2020).

Shrestha, Y., Schafer, E. J., Boehm, J. S., Thomas, S. R., He, F., Du, J., et al. (2012). PAK1 is a breast cancer oncogene that coordinately activates MAPK and MET signaling. *Oncogene* 31, 3397–3408. doi: 10.1038/onc.2011.515

Wang, S., Liang, Y., Chang, W., Hu, B., and Zhang, Y. (2018). Triple negative breast cancer depends on Sphingosine Kinase 1 (SphK1)/Sphingosine-1-Phosphate (S1P)/Sphingosine 1-Phosphate receptor 3 (S1PR3)/notch signaling for metastasis. *Med. Sci. Monit.* 24, 1912–1923. doi: 10.12659/msm.905833

Xu, D., Zhu, H., Wang, C., Zhao, W., Liu, G., Bao, G., et al. (2017). SphK2 over-expression promotes osteosarcoma cell growth. *Oncotarget* 8, 105525–105535. doi: 10.18632/oncotarget.22314

Xun, C., Chen, M.-B., Qi, L., Zhang, T.-N., Peng, X., Ning, L., et al. (2015). Targeting sphingosine kinase 2 (SphK2) by ABC294640 inhibits colorectal cancer cell growth in vitro and in vivo. *J. Exp. Clin. Cancer Res.* 34:94. doi: 10.1186/s13046-015-0205-y

Conflict of Interest: The authors declare that the research was conducted in the absence of any commercial or financial relationships that could be construed as a potential conflict of interest.

frontiers in Molecular Biosciences

ORIGINAL RESEARCH
published: 13 May 2021
doi: 10.3389/fmolb.2021.674863

CCDC137 Is a Prognostic Biomarker and Correlates With Immunosuppressive Tumor Microenvironment Based on Pan-Cancer Analysis

*Lihao Guo, Boxin Li, Zhaohong Lu, Hairong Liang, Hui Yang, Yuting Chen, Shiheng Zhu, Minjuan Zeng, Yixian Wei, Tonggong Liu, Tikeng Jiang, Mei Xuan and Huanwen Tang**

Dongguan Key Laboratory of Environmental Medicine, Department of Environmental and Occupational Health, School of Public Health, Guangdong Medical University, Dongguan, China

OPEN ACCESS

Edited by:
Haishi Qiao, China Pharmaceutical University, China

Reviewed by:
Dinesh Kumar, Centre of Bio-Medical Research (CBMR), India
Ashok Kumar, All India Institute of Medical Sciences Bhopal, India

***Correspondence:**
Huanwen Tang
thw@gdmu.edu.cn

Specialty section:
This article was submitted to Molecular Diagnostics and Therapeutics, a section of the journal Frontiers in Molecular Biosciences

Received: *02 March 2021*
Accepted: *12 April 2021*
Published: *13 May 2021*

Citation:
Guo L, Li B, Lu Z, Liang H, Yang H, Chen Y, Zhu S, Zeng M, Wei Y, Liu T, Jiang T, Xuan M and Tang H (2021) CCDC137 Is a Prognostic Biomarker and Correlates With Immunosuppressive Tumor Microenvironment Based on Pan-Cancer Analysis. Front. Mol. Biosci. 8:674863. doi: 10.3389/fmolb.2021.674863

Background: The coiled-coil domain containing (CCDC) family proteins have important biological functions in various diseases. However, the coiled-coil domain containing 137 (CCDC137) was rarely studied. We aim to investigate the role of CCDC137 in pan-cancer.

Methods: CCDC137 expression was evaluated in RNA sequence expression profilers of pan-cancer and normal tissues from The Cancer Genome Atlas (TCGA) and Genotype-Tissue Expression (GTEx) database. The influence of CCDC137 on the prognosis of tumor patients was analyzed using clinical survival data from TCGA. Function and pathway enrichment analysis was performed to explore the role of CCDC137 using the R package "clusterProfiler." We further analyzed the correlation of immune cell infiltration score of TCGA samples and CCDC137 expression using TIMER2 online database.

Results: CCDC137 was over-expressed and associated with worse survival status in various tumor types. CCDC137 expression was positively correlated with tumor associated macrophages (TAMs) and cancer associated fibroblasts (CAFs) in Lower Grade Glioma (LGG) and Uveal Melanoma (UVM). In addition, high CCDC137 expression was positively correlated with most immunosuppressive genes, including TGFB1, PD-L1, and IL10RB in LGG and UVM.

Conclusions: Our study identified CCDC137 as an oncogene and predictor of worse survival in most tumor types. High CCDC137 may contribute to elevated infiltration of TAMs and CAFs and be associated with tumor immunosuppressive status.

Keywords: CCDC137, pan-cancer, tumor associated macrophages, immunosuppression status, tumor microenvironment

INTRODUCTION

Tumor microenvironment (TME) has been proved to be composed of complex components, and is crucial for tumor development and prognosis of patients (Cassim and Pouyssegur, 2019). The immune and stromal cells within TME have essential contributions to tumorigenesis and development of tumor (Lei et al., 2020). Tumor associated macrophages (TAMs) could secrete several cytokines and chemokines to alleviate tumor immunity and promote tumor progression. Moreover, the extensive heterogeneity of TAMs enables immune and stromal cells to adapt or alter their phenotypes to conform to the TME, playing an oncogene role in cancer progression and metastasis (Pathria et al., 2019). In addition, cancer associated fibroblasts (CAFs) in TME have abilities to secrete various growth factors, cytokines, and chemokines to promote tumor progression. TGFB1, which was mainly secreted by CAFs and TAMs, was one of the main inducements of tumor immunosuppressive microenvironment (Liao et al., 2019). Therefore, it is urgent to explore the potential molecular mechanism leading to the formation of CAFs and TAMs.

The coiled-coil domain containing (CCDC) family proteins have important biological functions. Many members of CCDC family are involved in the regulation of invasion and metastasis of malignant tumor cells. At present, it has been confirmed that the abnormal expression of CCDC34, CCDC67, and CCDC88A proteins can significantly affect the malignant progress of lung cancer, bladder cancer, thyroid cancer, and pancreatic cancer (Park et al., 2012; Gong et al., 2015; Tanouchi et al., 2016; Geng et al., 2018), which provides a theoretical basis for the application of new medicine in tumor targeted therapy.

CCDC137, a member of CCDC family proteins, was rarely studied in previous researches. In this study, we performed a pan-cancer analysis to explore the role of CCDC137 in tumor progression. In detail, we analyzed the expression level, methylation level, copy-number value, mutation status, and prognostic value of CCDC137 in TCGA pan-cancer. In addition, the associations between CCDC137 and tumor stromal cells, tumor-infiltrating immune cells, and immune related marker genes were investigated. This study revealed the potential role of CCDC137 in TME and its prognostic value in pan-cancer, which may help explore a new drug target.

MATERIALS AND METHODS

Data Collection

The RNA expression profiles and patient survival information of pan-cancer data of TCGA database were downloaded

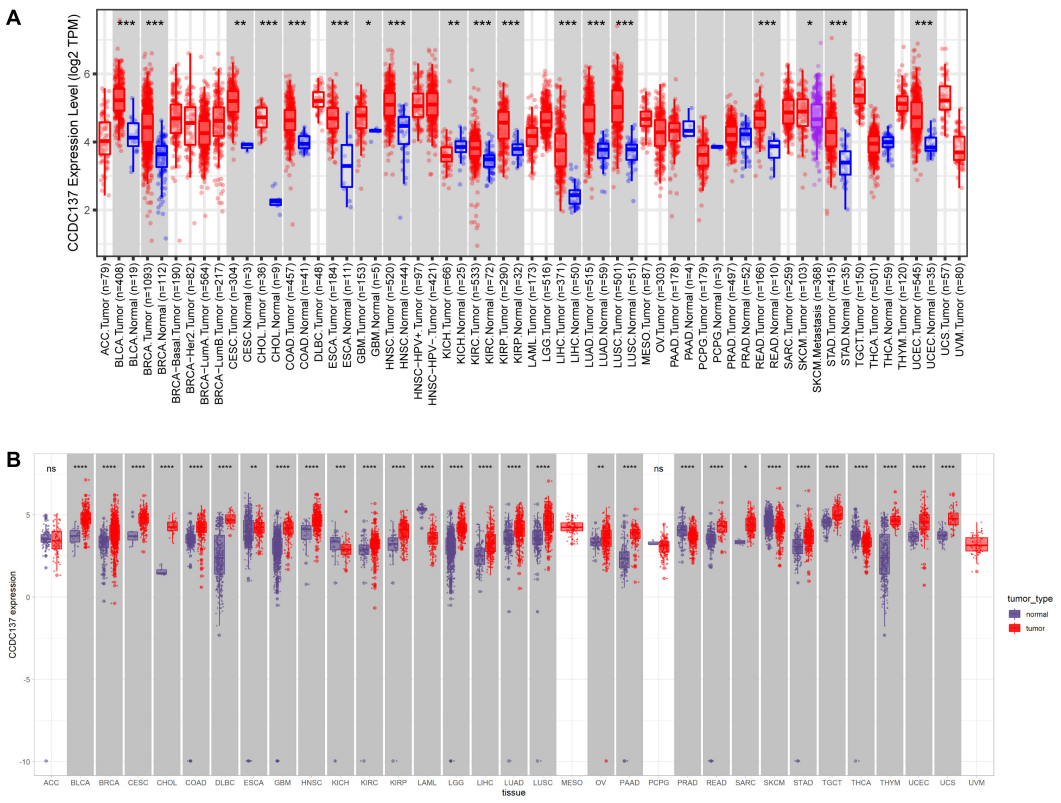

FIGURE 1 | Pan-cancer CCDC137 expression analysis. **(A)** CCDC137 expression in tumor and adjacent normal tissues in pan-cancer data of TCGA cohort. **(B)** CCDC137 expression in tumor tissues from TCGA and normal tissues from TCGA and GTEx cohorts. Data shown as mean ± SD. *$p < 0.05$, **$p < 0.01$, ***$p < 0.001$, and ****$p < 0.0001$.

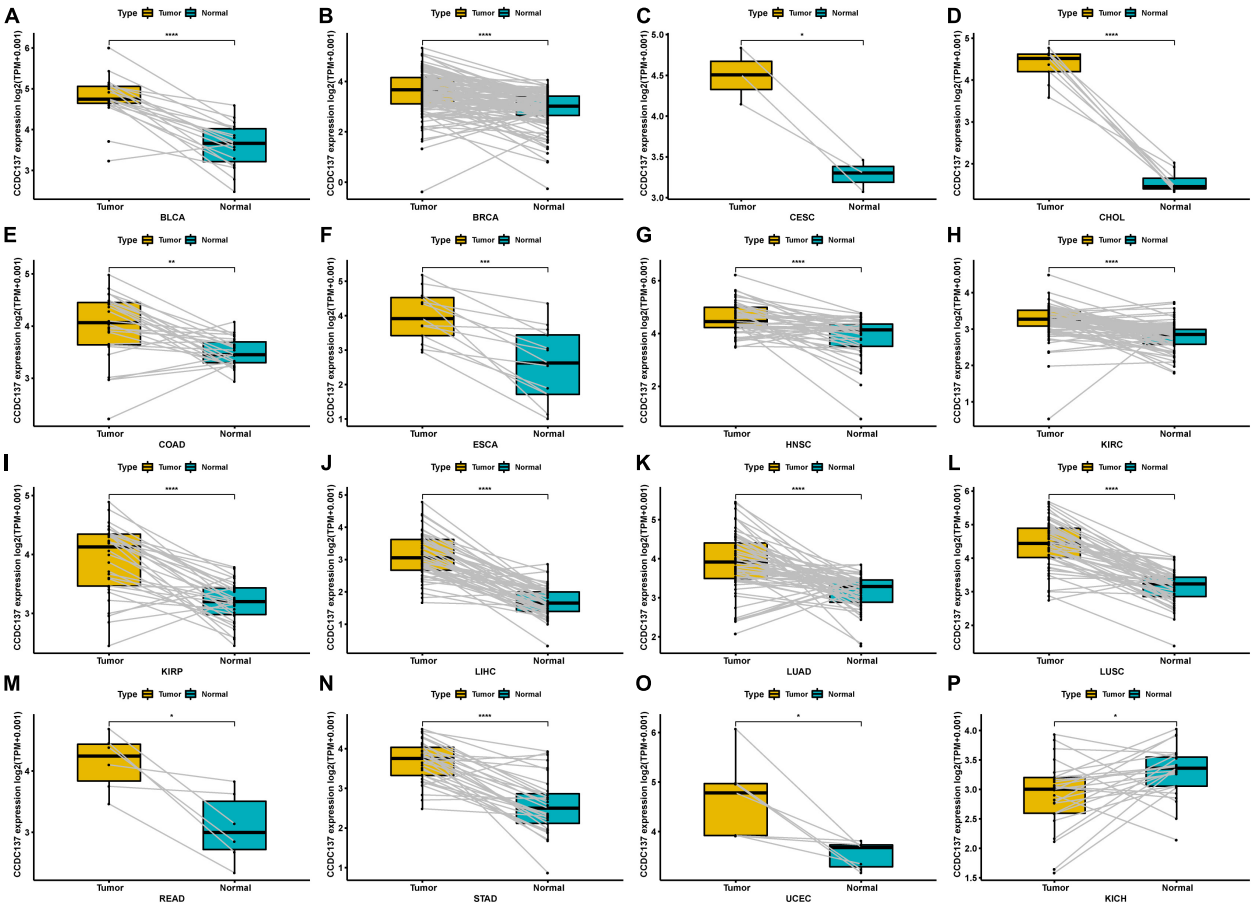

FIGURE 2 | Pan-cancer CCDC137 expression in paired tumor and normal tissues. **(A–P)** CCDC137 expression in paired tumor and adjacent normal tissues in indicated tumor types in TCGA cohort. Data shown as mean ± SD. *$p < 0.05$, **$p < 0.01$, ***$p < 0.001$, and ****$p < 0.0001$.

from UCSC-XENA[1]. The RNA expression profiles of The Genotype-Tissue Expression (GTEx) were downloaded from UCSC-XENA. The methylation level and copy-number value of CCDC137 in TCGA pan-cancer were downloaded from cBioportal[2].

Data Analysis Tools

TIMER2[3] database was used to draw expression difference of CCDC137 using TCGA pan-cancer data. cBioportal database was used to show the alteration frequency of CCDC137 using TCGA data. R packages "survival," and "survminer" were employed to perform Kaplan–Meier survival analysis. For functional enrichment analysis, R package "clusterprofiler" was used to perform Gene Set Enrichment Analysis (GSEA) analysis. Ualcan[4] database was used to evaluate protein and protein phosphorylation level of CCDC137. TISIDB database[5] was used to analysis CCDC137 expression in different molecular subtypes of tumor samples from TCGA.

Immune Cell Infiltration Analysis

TIMER2 database was used to analyze associations between CCDC137 and tumor stromal cells, tumor-infiltrating immune cells. The immunosuppressive gene was obtained from published paper "Pan-cancer Immunogenomic Analyses Reveal Genotype-Immunophenotype Relationships and Predictors of Response to Checkpoint Blockade" (Charoentong et al., 2017).

RESULTS

Pan-Cancer CCDC137 Expression

We first evaluated the mRNA expression of CCDC137 in pan-cancer data of TCGA using TIMER2 database. Results revealed that CCDC137 was highly expressed in 16 tumor types including Bladder Urothelial Carcinoma (BLCA), Breast invasive carcinoma (BRCA), Cervical squamous cell carcinoma and endocervical adenocarcinoma (CESC), Cholangiocarcinoma (CHOL), Colon adenocarcinoma (COAD), Esophageal

[1]https://xenabrowser.net/

[2]https://www.cbioportal.org/

[3]http://timer.cistrome.org/

[4]http://ualcan.path.uab.edu/index.html

[5]http://cis.hku.hk/TISIDB/index.php

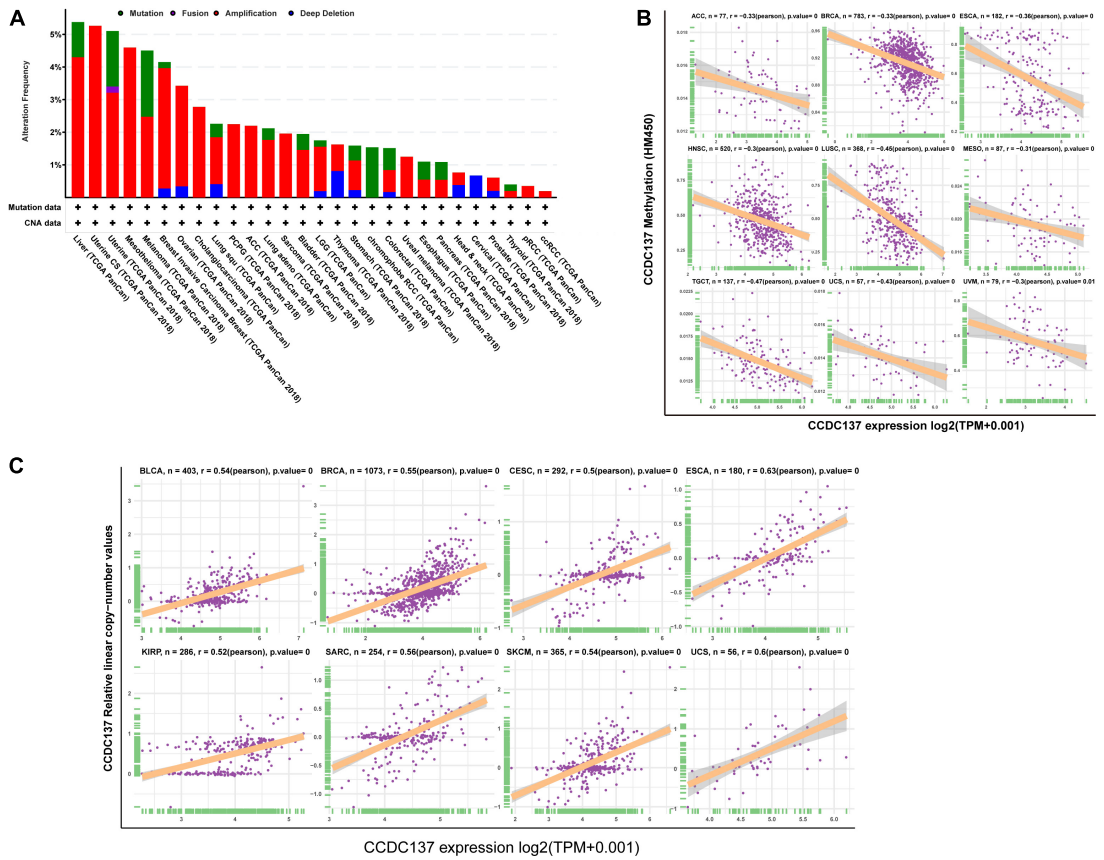

FIGURE 3 | Pan-cancer analysis of CNA and DNA methylation of CCDC137. **(A)** CNA and mutation frequency of CCDC137 in TCGA pan-cancer were accessed using cBioPortal. **(B)** The correlation between DNA methylation and mRNA expression of CCDC137 in TCGA pan-cancer. **(C)** The correlation between CNA and mRNA expression of CCDC137 in TCGA pan-cancer.

carcinoma (ESCA), Glioblastoma multiforme (GBM), Head and Neck squamous cell carcinoma (HNSC), Kidney renal clear cell carcinoma (KIRC), Kidney renal papillary cell carcinoma (KIRP), Liver hepatocellular carcinoma (LIHC), Lung adenocarcinoma (LUAD), Lung squamous cell carcinoma (LUSC), Rectum adenocarcinoma (READ), Stomach adenocarcinoma (STAD), and Uterine Corpus Endometrial Carcinoma (UECE), while only low expressed in Kidney Chromophobe (KICH) (**Figure 1A**). As the number of normal tissues in TCGA is limited, we further analyzed the CCDC137 expression combining normal tissue data of GTEx database with TCGA data. We found that CCDC137 was over-expressed in 24 tumor types. In addition to 16 tumor types mentioned above, there are also Lymphoid Neoplasm Diffuse Large B-cell Lymphoma (DLBC), Brain Lower Grade Glioma (LGG), Ovarian serous cystadenocarcinoma (OV), Pancreatic adenocarcinoma (PAAD), Sarcoma (SARC), Testicular Germ Cell Tumor (TGCT), Thymoma (THYM), and Uterine Carcinosarcoma (UCS). While CCDC137 was low expressed in KICH, Acute Myeloid Leukemia (LAML), Prostate adenocarcinoma (PRAD), Skin Cutaneous Melanoma (SKCM), Thyroid carcinoma (THCA) (**Figure 1B**).

In addition, for paired tumors and adjacent normal tissues in TCGA, CCDC137 was over-expressed in tumor tissues of BLCA, BRCA, CESC, CHOL, COAD, ESCA, HNSC, KIRC, KIRP, LIHC, LUAD, LUSC, READ, STAD, and UCEC (**Figures 2A–O**), while low-expressed in KICH (**Figure 2P**). We then analyzed the CCDC137 expression in different WHO stages and molecular subtypes. We found that CCDC137 expression was higher in relative worse tumor stages in BRCA, LUSC, KIRC, KICH, and HNSC (**Supplementary Figures 1A–E**). We also observed that CCDC137 expression was significantly different in different molecular subtypes of BRCA, HNSC, LGG, LUSC, OV, PCPG, PRAD, STAD, and UCEC (**Supplementary Figures 1A–N**).

DNA Methylation and CNA Alterations of CCDC137 in TCGA Pan-Cancer

To explore the reasons of the high CCDC137 expression in tumor, we evaluated the genetic and epigenetic changes of CCDC137 using TCGA data from cBioPortal. We found that patients with high CCDC137 expression were accompanied by high gene alterations in LIHC, UCEC, BRCA, OV, CHOL, LUSC, and LUAD (**Figure 3A**). For the association between DNA methylation level and mRNA expression of CCDC137, we found that DNA methylation level was significantly negatively

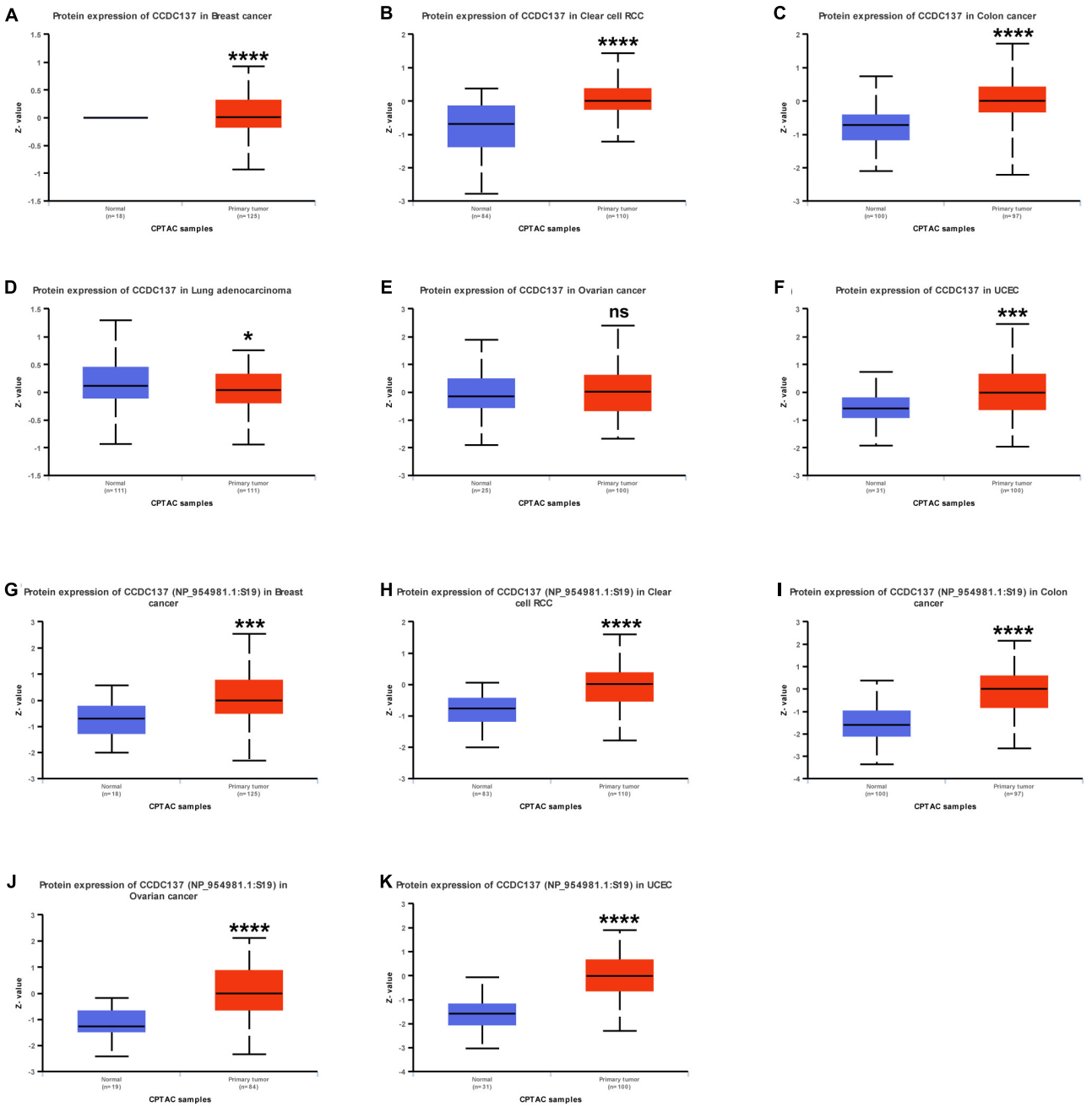

FIGURE 4 | Pan-cancer protein analysis of CCDC137. **(A–F)** CCDC137 protein level in indicated tumor types from TCGA cohort. **(G–K)** CCDC137 protein phosphorylation level in indicated tumor types from TCGA cohort. Data shown as mean ± SD. *$p < 0.05$, **$p < 0.01$, ***$p < 0.001$, and ****$p < 0.0001$.

correlated with CCDC137 expression in nine tumor types, including ACC, BRCA, ESCA, HNSC, LUSC, MESO, TGCT, UCS, and Uveal Melanoma (UVM) (**Figure 3B**). In addition, we further analyzed the association between relative linear copy number values and mRNA expression of CCDC137. The results revealed a significant positive correlation between CCDC137 expression and copy number variation (CNA) in BLCA, BRCA, CESC, ESCA, KIRP, SARC, SKCM, and UCS (**Figure 3C**).

Protein and Protein Phosphorylation Alterations of CCDC137 in TCGA Pan-Cancer

Since protein expression level is the key factor directly affecting molecular function, we further analyzed the protein and protein phosphorylation level of CCDC137 in TCGA pan-cancer using Ualcan database. The results revealed that the protein level of CCDC137 was higher in

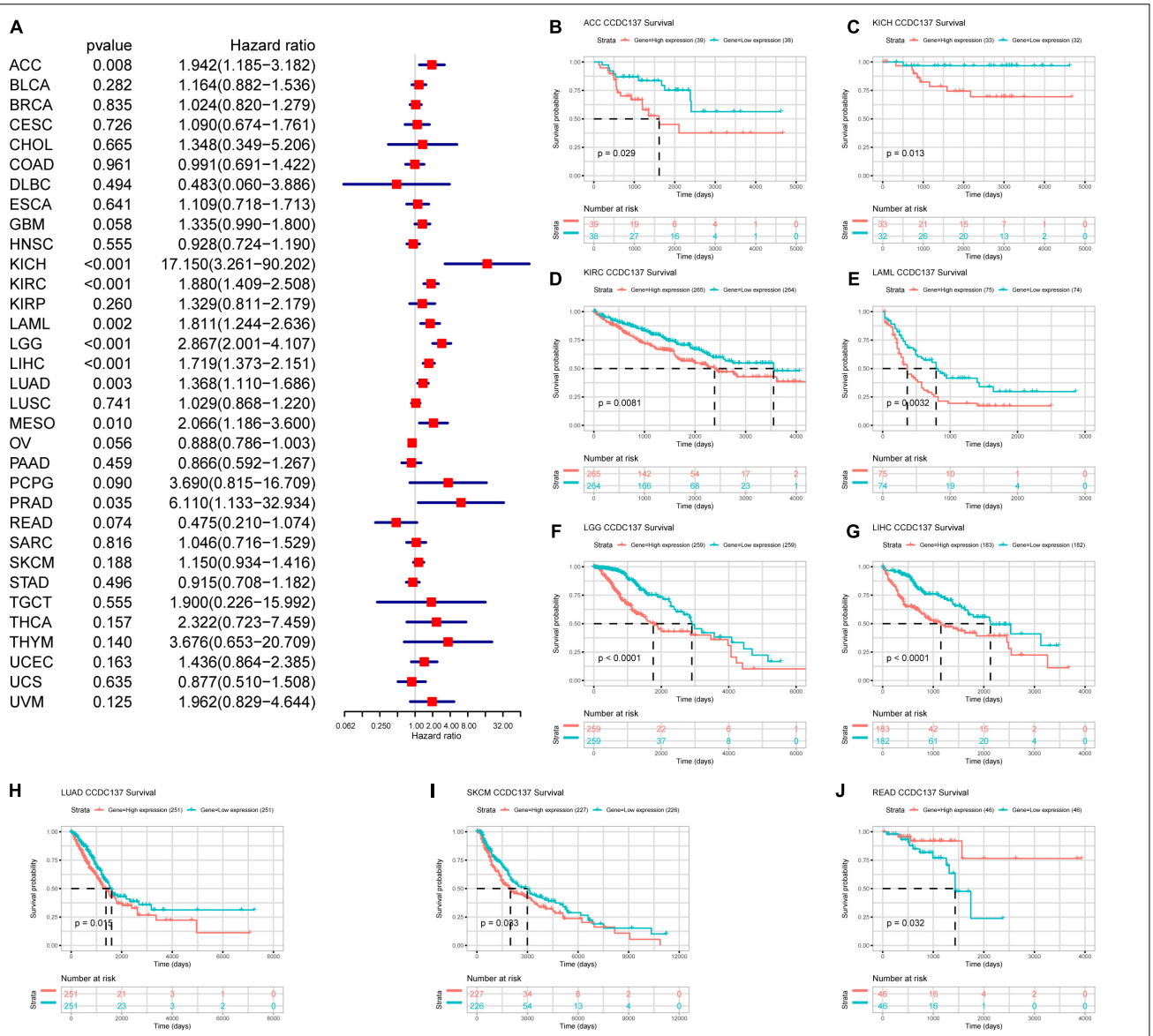

FIGURE 5 | Prognosis value of CCDC137 in TCGA pan-cancer. **(A)** The forest map shows the results of Univariate Cox Regression analysis for OS. **(B–J)** Kaplan–Meier survival analysis of CCDC137 in indicated tumor types. Only tumor types with log rank $p < 0.05$ were displayed.

tumor tissues than that in normal tissues in BRCA, KIRC, COAD, LUAD, and UCEC, while no difference in OV (**Figures 4A–F**). In addition, we found that there was only one phosphorylation site of CCDC137. High phosphorylation level of CCDC137 was observed in BRCA, KIRC, COAD, OV, and UCEC (**Figures 4G–K**).

Prognostic Value of CCDC137 in TCGA Pan-Cancer

Next, we investigated the prognostic value of CCDC137 in TCGA pan-cancer using Univariate Cox Regression analysis and Kaplan–Meier analysis. The Univariate Cox Regression analysis revealed that high expression of CCDC137 was a risk factor of overall survival (OS) in ACC, KICH, KIRC, LAML, LGG, LIHC, LUAD, MESO, and PRAD (**Figure 5A**). For disease free interval (DFI), higher expression of CCDC137 was associated with poorer DFI in ACC, LGG, LIHC, and PRAD (**Supplementary Figure 2A**). For progression free interval (PFI), higher expression of CCDC137 was associated with reduced PFI in ACC, KICH, KIRC, LGG, LIHC, LUSC, MESO, PCPG, PRAD, and UVM, while increased PFI in OV (**Supplementary Figure 2B**). For disease-specific survival (DSS), higher expression of CCDC137 was associated with worse DSS in ACC, KICH, KIRC, LGG, LIHC, LUAD, MESO, PCPG, PRAD, THCA, and THYM, while better DSS in OV (**Supplementary Figure 2C**). The Kaplan–Meier analysis suggested that high CCDC137

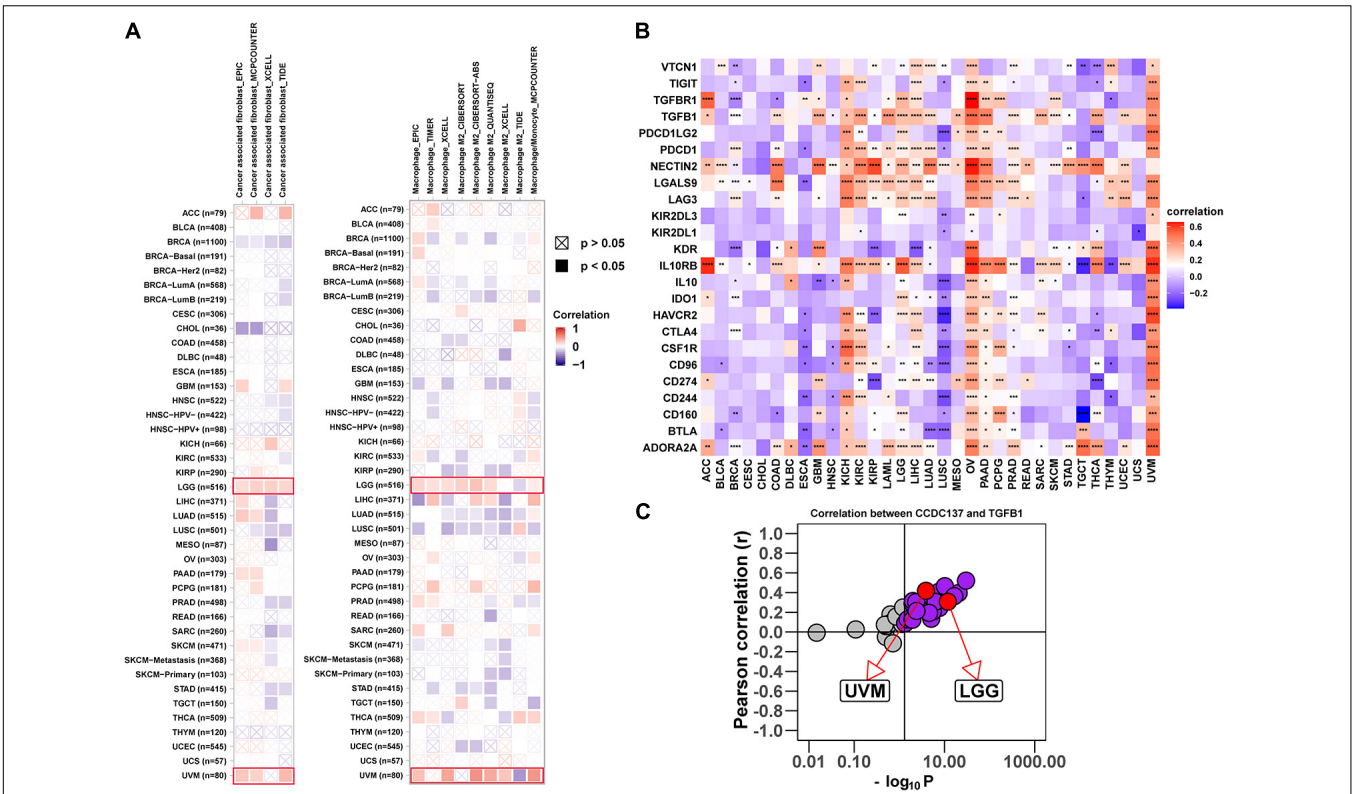

FIGURE 6 | Analysis of the effect of CCDC137 on immune microenvironment. **(A)** The correlation between CCDC137 expression and CAFs (left) or TAMs (right) were shown. Red color represents positive correlation, blue color represents negative correlation, and the deeper the color, the stronger the correlation. **(B)** The heatmap shows the correlation between CCDC137 and immunosuppressive genes in TCGA pan-cancer. **(C)** Correlation coefficient and –log10 (*p* value) of CCDC137 with TGFB1 is shown. Each circle represents a different tumor type from TCGA. Red circles are marked for UVM and LGG. Gray circles mean no correlation.

expression predicted poor OS in ACC, KICH, KIRC, LAML, LGG, LIHC, LUAD, and SKCM, while longer OS time in READ (**Figures 5B–J**).

Immune Cell Infiltration Analysis

Tumor associated macrophages and CAFs, as prominent components of TME, were closely related to the occurrence, development, and metastasis of tumor. Thus, we further investigated the association between CCDC137 expression and infiltration level of TAMs and CAFs using TIMER2 online database. We observed a positive correlation between the infiltration of TAMs/CAFs and CCDC137 expression in the tumors of LGG and UVM based on all or most algorithms (**Figure 6A**). We further selected 24 immunosuppressive marker genes based on published article and performed the correlation analysis with CCDC137 (Charoentong et al., 2017). The results revealed that 17 of 24 immunosuppressive marker genes was positively correlated with CCDC137 expression in LGG and 22 of 24 immunosuppressive marker genes was positively correlated with CCDC137 expression in UVM (**Figure 6B**). In these immunosuppressive marker genes, TGFB1, NECTIN2, LGALS9, LAG3, and IL10RB were significantly correlated with CCDC137 expression in most tumor types. As we have known, there was a significant correlation between TGFB1 expression and TAMs/CAFs. We observed that CCDC137 was significantly correlated with TGFB1 expression in most tumor types including UVM and LGG, which may indicate the potential mechanism of CCDC137 influencing infiltration of TAMs/CAFs (**Figure 6C**).

Gene Set Enrichment Analysis of CCDC137

To better explore the pathways CCDC137 may participate in, we conducted GSEA using R package "clusterprofiler." We observed that CCDC137 was mainly enriched in cell cycle related pathways in most tumor types. For example, CCDC137 was enriched in G1/S Transition in LGG, Cell Cycle, Mitotic in LIHC, Cell Cycle in LUSC, and S Phase in UVM (**Figures 7A–D**). These results indicated that CCDC137 was a major participant in tumor cell cycle process, which provided a potential direction for future research.

DISCUSSION

The CCDC family proteins have important biological functions in various diseases. For example, CCDC43 was proved to accelerate proliferation and metastasis process of gastric cancer (Wang et al., 2020). In addition, CCDC25 was recently observed

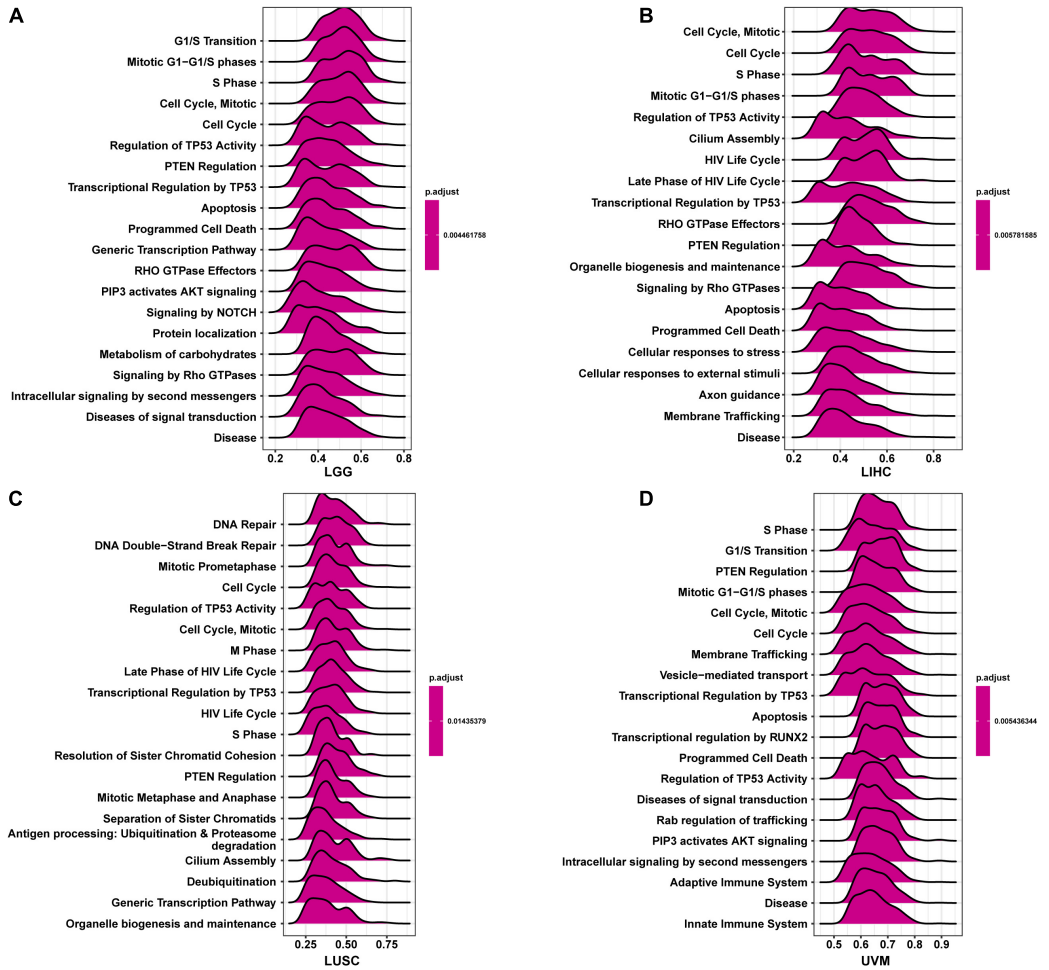

FIGURE 7 | GSEA of CCDC137 in TCGA pan-cancer. **(A–D)** The top 20 GSEA results of CCDC137 in indicated tumor types from TCGA.

to promote cancer metastasis (Yang et al., 2020). However, CCDC137 was rarely studied for now.

In our study, we examined the CCDC137 mRNA and protein expression levels and prognostic value in pan-cancer using TCGA and GTEx data downloaded from UCSC Xena. Based on our results, we found that CCDC137, compared to normal tissues, was over-expressed in 16 tumor types including BLCA, BRCA, CESC, CHOL, COAD, ESCA, GBM, HNSC, KIRC, KIRP, LIHC, LUAD, LUSC, READ, STAD, and UECE. High CCDC137 expression predicts poor OS in ACC, KICH, KIRC, LAML, LGG, LIHC, LUAD, MESO, and PRAD.

Tumor microenvironment, especially tumor immune and stromal microenvironment, constitute a vital element of tumor tissue. Increasing evidence has revealed their clinicopathological significance in predicting outcomes and therapeutic efficacy (Greten and Grivennikov, 2019; Vitale et al., 2019; Suzuki et al., 2021). TAMs and CAFs in TME always accelerate tumor progression (Akins et al., 2020; Liu et al., 2021; Shan et al., 2021). Our results revealed that CCDC137 have close relationships with TAMs and CAFs infiltration in most tumor types. Moreover, the positive correlations between CCDC137 expression and immunosuppressive genes, such as TGFB1, NECTIN2, LGALS9, LAG3, and IL10RB, indicate the key role of CCDC137 in regulating tumor immunology, macrophage polarization, and CAFs formation. TAMs, which are particularly abundant in a tumor mass, contribute much to the immunosuppressive microenvironment (Zeng et al., 2021). TGFB1, mainly secreted by TAMs and CAFs in TME, play an irreplaceable role in inducing immunosuppressive microenvironment. Immunosuppressive genes, such as IL10, IL10RB, LGALS9, and LAG3, were observed to be co-overexpressed with TGFB1 in tumor tissues and predicted poor survival of tumor patients, indicating a potential mechanism by which CCDC137 regulates macrophage polarization, CAFs formation and correlates with several immunosuppressive genes (Kadowaki et al., 2016; Fan et al., 2020; Suzuki et al., 2021; Wang et al., 2021). In addition, the high expression of CCDC137 indicates the immunosuppression status in LGG and UVM, providing a potential drug target for tumor therapy.

In conclusion, CCDC137 may play an important role in macrophage polarization and CAFs formation in TME. Targeting CCDC137 may become a potential treatment for cancer.

DATA AVAILABILITY STATEMENT

The datasets presented in this study can be found in online repositories. The names of the repository/repositories and accession number(s) can be found in the article/ **Supplementary Material**.

AUTHOR CONTRIBUTIONS

LG: conceptualization, methodology, software, formal analysis, writing-original draft, and visualization. BL and ZL: formal analysis, software, visualization, investigation, and validation. HL, HY, and YC: software, validation, and investigation. SZ, MZ, YW, TL, TJ, and MX: investigation and data curation. HT: conceptualization, methodology, writing-review and editing, supervision, and funding acquisition. All authors contributed to the article and approved the submitted version.

FUNDING

This work was supported by the Major Basic Research Project of Guangdong Province (China; No. 2017KZDXM041), Guangdong Provincial University Key Platform Featured Innovation Project (No. 2020KTSCX048), the National Natural Science Foundation of China (No. 82073582), the Provincial Preponderant Key Subjects of Public Health and Preventive Medicine Project (Nos. 4SG20003G and 4SG18004G), and the Public Health and Preventive Medicine Discipline Development Funds of Guangdong Medical University in 2020 (Nos. 4SG20003G and 4SG19013G).

SUPPLEMENTARY MATERIAL

The Supplementary Material for this article can be found online at: https://www.frontiersin.org/articles/10.3389/fmolb.2021.674863/full#supplementary-material

REFERENCES

Akins, E. A., Aghi, M. K., and Kumar, S. (2020). Incorporating tumor-associated macrophages into engineered models of glioma. *iScience* 23:101770. doi: 10.1016/j.isci.2020.101770

Cassim, S., and Pouyssegur, J. (2019). tumor microenvironment: a metabolic player that shapes the immune response. *Int. J. Mol. Sci.* 21:157. doi: 10.3390/ijms21010157

Charoentong, P., Finotello, F., Angelova, M., Mayer, C., Efremova, M., Rieder, D., et al. (2017). Pan-cancer immunogenomic analyses reveal genotype-immunophenotype relationships and predictors of response to checkpoint blockade. *Cell Rep.* 18, 248–262. doi: 10.1016/j.celrep.2016.12.019

Fan, Y., Li, T., Xu, L., and Kuang, T. (2020). Comprehensive analysis of immunoinhibitors identifies LGALS9 and TGFBR1 as potential prognostic biomarkers for pancreatic cancer. *Comput. Math. Methods Med.* 2020:6138039.

Geng, W., Liang, W., Fan, Y., Ye, Z., and Zhang, L. (2018). Overexpression of CCDC34 in colorectal cancer and its involvement in tumor growth, apoptosis and invasion. *Mol Med Rep* 17, 465–473.

Gong, Y., Qiu, W., Ning, X., Yang, X., Liu, L., Wang, Z., et al. (2015). CCDC34 is up-regulated in bladder cancer and regulates bladder cancer cell proliferation, apoptosis and migration. *Oncotarget* 6, 25856–25867. doi: 10.18632/oncotarget.4624

Greten, F. R., and Grivennikov, S. I. (2019). Inflammation and cancer: triggers, mechanisms, and consequences. *Immunity* 51, 27–41. doi: 10.1016/j.immuni.2019.06.025

Kadowaki, A., Miyake, S., Saga, R., Chiba, A., Mochizuki, H., and Yamamura, T. (2016). Gut environment-induced intraepithelial autoreactive CD4(+) T cells suppress central nervous system autoimmunity via LAG-3. *Nat. Commun.* 7:11639.

Lei, X., Lei, Y., Li, J. K., Du, W. X., Li, R. G., Yang, J., et al. (2020). Immune cells within the tumor microenvironment: biological functions and roles in cancer immunotherapy. *Cancer Lett.* 470, 126–133. doi: 10.1016/j.canlet.2019.11.009

Liao, Z., Tan, Z. W., Zhu, P., and Tan, N. S. (2019). Cancer-associated fibroblasts in tumor microenvironment–accomplices in tumor malignancy. *Cell. Immunol.* 343:103729. doi: 10.1016/j.cellimm.2017.12.003

Liu, C., Zhou, X., Long, Q., Zeng, H., Sun, Q., Chen, Y., et al. (2021). Small extracellular vesicles containing miR-30a-3p attenuate the migration and invasion of hepatocellular carcinoma by targeting SNAP23 gene. *Oncogene* 40, 233–245. doi: 10.1038/s41388-020-01521-7

Park, S. J., Jang, H. R., Kim, M., Kim, J. H., Kwon, O. H., Park, J. L., et al. (2012). Epigenetic alteration of CCDC67 and its tumor suppressor function in gastric cancer. *Carcinogenesis* 33, 1494–1501. doi: 10.1093/carcin/bgs178

Pathria, P., Louis, T. L., and Varner, J. A. (2019). Targeting tumor-associated macrophages in cancer. *Trends Immunol.* 40, 310–327.

Shan, G., Zhou, X., Gu, J., Zhou, D., Cheng, W., Wu, H., et al. (2021). Downregulated exosomal microRNA-148b-3p in cancer associated fibroblasts enhance chemosensitivity of bladder cancer cells by downregulating the Wnt/β-catenin pathway and upregulating PTEN. *Cell. Oncol. (Dordr.)* 44, 45–59. doi: 10.1007/s13402-020-00500-0

Suzuki, J., Aokage, K., Neri, S., Sakai, T., Hashimoto, H., Su, Y., et al. (2021). Relationship between podoplanin-expressing cancer-associated fibroblasts and the immune microenvironment of early lung squamous cell carcinoma. *Lung Cancer* 153, 1–10. doi: 10.1016/j.lungcan.2020.12.020

Tanouchi, A., Taniuchi, K., Furihata, M., Naganuma, S., Dabanaka, K., Kimura, M., et al. (2016). CCDC88A, a prognostic factor for human pancreatic cancers, promotes the motility and invasiveness of pancreatic cancer cells. *J. Exp. Clin. Cancer Res.* 35:190.

Vitale, I., Manic, G., Coussens, L. M., Kroemer, G., and Galluzzi, L. (2019). Macrophages and metabolism in the tumor microenvironment. *Cell Metab.* 30, 36–50. doi: 10.1016/j.cmet.2019.06.001

Wang, J., Wu, X., Dai, W., Li, J., Xiang, L., Tang, W., et al. (2020). The CCDC43-ADRM1 axis regulated by YY1, promotes proliferation and metastasis of gastric cancer. *Cancer Lett.* 482, 90–101. doi: 10.1016/j.canlet.2020.03.026

Wang, Z., Chen, S., Wang, G., Li, S., and Qin, X. (2021). CDCA3 is a novel prognostic biomarker associated with immune infiltration in hepatocellular carcinoma. *Biomed. Res. Int.* 2021:6622437.

Yang, L., Liu, Q., Zhang, X., Liu, X., Zhou, B., Chen, J., et al. (2020). DNA of neutrophil extracellular traps promotes cancer metastasis via CCDC25. *Nature* 583, 133–138. doi: 10.1038/s41586-020-2394-6

Zeng, F., Li, G., Liu, X., Zhang, K., Huang, H., Jiang, T., et al. (2021). Plasminogen activator urokinase receptor implies immunosuppressive features and acts as an unfavorable prognostic biomarker in glioma. *Oncologist* 25, 1–10. doi: 10.1002/onco.13750

Conflict of Interest: The authors declare that the research was conducted in the absence of any commercial or financial relationships that could be construed as a potential conflict of interest.

frontiers in Molecular Biosciences

BRIEF RESEARCH REPORT
published: 17 May 2021
doi: 10.3389/fmolb.2021.690665

Association Between Polymorphisms in Gastric Cancer Related Genes and Risk of Gastric Cancer: A Case-Control Study

Yan Pu[1†], Xu Wen[2†], Zhangjun Jia[3†], Yu Xie[4], Changxing Luan[5], Youjia Yu[5], Feng Chen[5], Peng Chen[5], Ding Li[5], Yan Sun[6]*, Jian Zhao[7]* and Haiqin Lv[1]**

[1]School of Medicine, Southeast University, Nanjing, China, [2]Department of General Surgery, Jiangsu Cancer Hospital and Jiangsu Institute of Cancer Research, The Affiliated Cancer Hospital of Nanjing Medical University, Nanjing, China, [3]Department of Clinical Laboratory, Jiangsu Cancer Hospital and Jiangsu Institute of Cancer Research, The Affiliated Cancer Hospital of Nanjing Medical University, Nanjing, China, [4]Department of Geriatrics, Affiliated Nanjing Drum Tower Hospital of Nanjing University Medical School, Nanjing, China, [5]Department of Forensic Medicine, Nanjing Medical University, Nanjing, China, [6]Department of Medical Oncology, Jiangsu Cancer Hospital and Jiangsu Institute of Cancer Research, The Affiliated Cancer Hospital of Nanjing Medical University, Nanjing, China, [7]Department of Radiation Oncology, Jiangsu Cancer Hospital and Jiangsu Institute of Cancer Research, The Affiliated Cancer Hospital of Nanjing Medical University, Nanjing, China*

OPEN ACCESS

Edited by:
Wei Zhao,
City University of Hong Kong, China

Reviewed by:
Zhi-hang Zhou,
Chongqing Medical University, China
Shanzhi Wang,
University of Arkansas at Little Rock, United States

***Correspondence:**
Ding Li
ld@njmu.edu.cn
Yan Sun
sunyan@188.com
Jian Zhao
zhaojiannj@126.com
Haiqin Lv
haiqinlu@seu.edu.cn

[†]These authors have contributed equally to this work

Specialty section:
This article was submitted to Molecular Diagnostics and Therapeutics, a section of the journal Frontiers in Molecular Biosciences

Received: *03 April 2021*
Accepted: *30 April 2021*
Published: *17 May 2021*

Citation:
Pu Y, Wen X, Jia Z, Xie Y, Luan C, Yu Y, Chen F, Chen P, Li D, Sun Y, Zhao J and Lv H (2021) Association Between Polymorphisms in Gastric Cancer Related Genes and Risk of Gastric Cancer: A Case-Control Study. Front. Mol. Biosci. 8:690665. doi: 10.3389/fmolb.2021.690665

Gastric cancer has the second highest incidence among all the malignancies in China, just below lung cancer. Gastric cancer is likewise one of the main sources of cancer related passings. Gastric cancer therefore remains a huge threat to human health. The primary reason is absence of high sensitivity and specificity for early detection while the pathogenesis of GC is stayed muddled. During the last few decades, a lot of GC related genes have been identified. To find candidate GC related variant in these GC related genes, we conducted this case-control study. 29 tagSNPs located in 7 GC related genes were included. 228 gastric cancer patients and 299 healthy controls were enrolled. Significant differences were found between the genotype frequencies of *EFNA1* rs4971066 polymorphism between gastric cancer patients and healthy controls. The result indicated that ephrin-A1 tagSNP rs4971066 GT/TT genotypes was significantly associated with reduced susceptibility of gastric cancer development.

Keywords: EFNA1, gastric cancer, SNP, case-control, biomarker

INTRODUCTION

Gastric cancer (GC) is one of the most well-known reason for cancer-related demise worldwide with the fifth incidence and third mortality (Jiang and Shen, 2019). The five-year survival rate of serious GC patients is still low. GC therefore remains a huge threat to human health. The primary explanation is absence of high sensitivity and specificity for early discovery. Therefore, to identify potential genetic markers such as polymorphisms in GC-related genes, can contribute the potential early diagnosis of GC. During the present study, we have focused on the following GC related genes: Y-box binding protein 1 (YBX1) encodes an exceptionally conserved protein that has wide nucleic acid binding properties. The encoded protein can bind both DNA and RNA then implicating in many cellular processes. Abnormal expression of YBX1 is related with malignant growth multiplication in various tissue including gastric cancer (Fang et al., 2019). ephrin A1 (EFNA1) is a member of the EFN family. For more than 30 years after researchers find this gene, a ton of proof upheld that EFNA1 assumes a basic part in tumor development (eg., Angiogenesis and progression) (Hao and Li, 2020). Gastrokine 2 (GKN2) is a secretory protein, whose expression level decrease in GC.

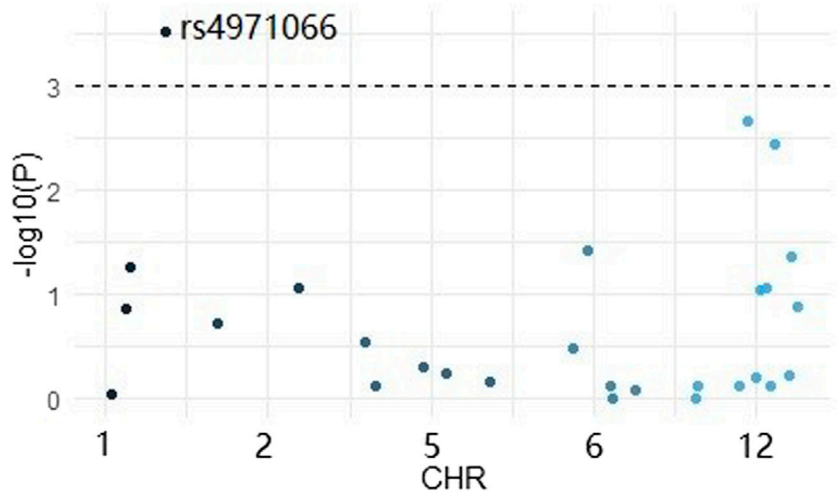

FIGURE 1 | Manhattan plot for the 29 SNPs.

GKN2 can increase sensitivity of GC cells to the drugs which increase ROS levels in tumors (Zhang et al., 2019). MicroRNA 143 (MIR143) has long to be proved to play a tumor suppressive role in gastric cancer. MIR143 is downregulated in GC cell lines. Ectopic expression of MIR143 resulted in inhibition of GC cell proliferation (Wu et al., 2020). Bromodomain containing 2 (BRD2) plays key role in transcription of genes required for cancer. A new report has shown that BRD2 is a direct target of MIR143–3p and increased expression level of BRD2 in gastric tumors was related with shorter survival times for GC patients (Chen et al., 2019). Leucine rich repeat containing G protein-coupled receptor 5 (LGR5) is involved in tissue development and the maintenance of adult stem cells in gastrointestinal tract. LGR5 can regulates gastric adenocarcinoma cell proliferation and invasion via activating Wnt signaling pathway (Wang et al., 2018). HOXC cluster antisense RNA3 (HOXC-AS3) is a long non-coding RNA that essentially increased in gastric cancer tissues and is corresponded with clinical results of gastric cancer (Zhang et al., 2018).

All of these genes have been reported to be associated with the GC development, and we have selected the tagSNPs in these genes and then conducted a case-control study to investigate whether these tagSNPs could contribute to the GC development.

MATERIALS AND METHODS

Subjects

The study population was composed of 228 gastric cancer patients and 299 healthy control individuals. Patients were consecutively recruited from the Jiangsu Cancer Hospital of Nanjing Medical University between Jan 2018 and Sep 2019. The diagnosis of patients was confirmed by histopathological analysis. Clinical information was obtained from hospital records, including gender, age, smoke, drink, differentiation, location, TNM status. Baseline profiles of the study participants have been summarized in **Supplementary Table S1**. The controls were selected from healthy volunteers who visited the Sir Run Hospital of Nanjing Medical University for medical examination. Individuals who had a history of diseases were exclude from the control group.

TagSNP Selection

Population data from 1,000 Genomes phase three were used to screen tagSNPs. A total of 208 individuals from Han Chinese populations were enrolled, including Han Chinese in Beijing, China (CHB) and Southern Han Chinese (CHS). The tagSNP were further screened by using Haploview software. The selected SNPs in the present study were summarized in **Supplementary Table S2**.

Genotyping

Genomic DNA was extracted from 200 μl EDTA-anticoagulated peripheral blood using a commercial extraction kit (Tiangen Biotech Corporation, Beijing, China). We performed polymerase chain reaction–ligase detection reaction (PCR-LDR) assay to detect the genotype of the SNP. The primer used were summarized in **Supplementary Tables S3, S4**. The final production was electrophoresed on ABI3730XL DNA Analyzer (Thermo Fisher Scientific, United States). The SNP was further genotyped by using Genemapper 4.1 (AppliedBiosystems, United States).

Statistical Analysis

All data were analyzed using SPSS 13 (SPSS Inc., Chicago, IL, United States). Genotype frequencies of the SNP were obtained by directed computing. Genotypic association analysis was performed using SNPstats. Odds ratio (OR) and respective 95% confidence intervals were reported to evaluate the effects of any differences between allele and genotype frequencies. Probability of 0.001 (0.05/29) or less was regarded as statistically significant.

RESULTS

Firstly, we conducted a logistic analysis by using plink software and picked out a significant variant *EFNA1* rs4971066 (p value = 0.0003) (**Figure 1**).

TABLE 1 | Association between the rs4971066 and risk of gastric cancer

Genetic model	Genotypes	Patients	Controls	Logistic regression (crude)		Logistic regression (adjusted)[a]	
		n = 228 (%)	*n* = 299 (%)	Or (95% CI)	*p* Value[b]	Or (95%CI)	*p* Value[c]
rs4938723							
Codominant	GG	181 (79.4)	195 (65.2)	1.00		1.00	
	GT	44 (19.3)	90 (30.1)	**0.53 (0.35–0.80)**	**0.002**	**0.36 (0.18–0.72)**	**0.0033**
	TT	3 (1.3)	14 (4.7)	**0.23 (0.07–0.82)**	**0.0099**	0.15 (0.02–1.50)	0.094
Dominant	GG	181 (79.4)	195 (65.2)	1.00	**3e-04**	1.00	
	GT/TT	47 (20.6)	104 (34.8)	**0.49 (0.33–0.73)**		**0.34 (0.17–0.67)**	**0.0013**
Recessive	GG/GT	225 (98.7)	285 (95.3)	1.00	**0.022**	1.00	
	TT	3 (1.3)	14 (4.7)	**0.27 (0.08–0.96)**		0.20 (0.02–1.89)	0.14
Overdominant	GG/TT	184 (80.7)	209 (69.9)	1.00	**0.0044**	1.00	
	GT	44 (19.3)	90 (30.1)	**0.56 (0.37–0.84)**		**0.38 (0.19–0.75)**	**0.0049**

[a]*Adjusted for age and gender using the logistic regression model.*
[b]p *value = 0.0044, multiple testing in a codominant model.*
[c]p *value = 6e-04, multiple testing in a codominant model.*
OR odds ratio; CI confidence interval.
Boldfaced values indicate a significant difference at the 5% level.

Significant difference of *EFNA1* rs4971066 allele frequencies existed between GC patients (G: 0.89 T:0.11) and controls (G: 0.80 T:0.20). Comparing to G allele, T allele carriers have 0.50-fold reduced risk to develop GC ($p = 0.0001$, 95% CI = 0.35–0.71). Then we performed further analysis based on different genetic models. As shown in **Table 1**, significant differences were found between the genotype frequencies of rs4971066 polymorphism between gastric cancer patients and healthy controls. Compared with GG genotype carriers, individuals with GT or TT genotype had 0.53 ($p = 0.002$) or 0.23 ($p = 0.0099$) fold decreased risk to develop gastric cancer in a codominant model, respectively. After adjusted by gender and age, GT genotype carriers still had a 0.36-fold decreased risk to develop gastric cancer ($p = 0.0033$). When compared with GG genotype carriers in a dominant model, GT/TT genotypes carriers had a 0.49- ($P = 3e\text{-}04$) or 0.34- (*adjusted* $p = 0.0013$) fold decreased susceptibility to develop gastric cancer. When compared with GG/TT genotypes carriers, GT genotype carriers had a 0.56- ($p = 0.0044$) or 0.38-fold (*adjusted* $p = 0.0049$) decreased risk to develop gastric cancer in a codominant model.

Furthermore, we divided the patients by their T status, N status, clinical stages, and multifocality. No significant differences were found between patients with different TNM status (**Table 2**).

By enrolling the population data from 1,000 Genome Project, we then compared the frequencies of EFNA1 rs4971066 genotypes in present studied populations and different continental populations. As shown in **Figure 2**, dramatic differences were observed among populations from different continent. The frequency of GC risk rs4971066-GG genotype is highest in EAS population. Consistently, the highest GC incidence was in Asia and the lowest incidence in Africa (Rawla and Barsouk, 2019).

For the single nucleotide polymorphisms in EFNA1, there are couple papers have demonstrated that rs12904 is a gastric cancer related variant (Li et al., 2014; Lee et al., 2015; Zhu et al., 2015). As shown in **Supplementary Figure S1**, strong linkage was found between rs12094 and rs4971066 (D' = 1, r2 = 0.862). This result also indicated that rs4971066 can served as a highly effective genetic marker.

TABLE 2 | Association between the rs4971066 polymorphism and clinical features of GC patients

Clinical features	Genotype frequency		Or (95 CI)	*p*
	N (%)	N (%)		
T Status	T1 and T2	T3 and T4		
GG	78 (83)	95 (80.5)	1.00	
GT	14 (14.9)	22 (18.6)	1.21 (0.57–2.59)	0.496
TT	2 (2.1)	1 (0.8)	0.25 (0.02–3.27)	0.457
G	156 (89.6)	212 (89.8)	1.00	
T	18 (10.3)	24 (10.1)	0.981 (0.515–1.870)	0.954
N status	N0	N1—N3		
GG	83 (83)	69 (78.4)	1.00	
GT	14 (14)	19 (21.6)	1.62 (0.75–3.47)	0.250
TT	3 (3)	0 (0)	0.00 (0.00-NA)	0.254
G	180 (90)	157 (89.2)	1.00	
T	20 (10)	19 (10.7)	1.08 (0.56–2.11)	0.866
Clinical stages	I and II	Ⅲ and IV		
GG	107 (82.3)	66 (80.5)	1.00	
GT	20 (15.4)	16 (19.5)	1.25 (0.60–2.61)	0.574
TT	3 (2.3)	0 (0)	0.00 (0.00-NA)	0.293
G	224 (89.6)	148 (90.2)	1.00	
T	26 (10.4)	16 (9.7)	0.93 (0.48–1.79)	0.86
Multifocality	No	Yes		
GG	167 (81.5)	5 (83.3)	1.00	
GT	35 (17.1)	1 (16.7)	0.97 (0.11–8.64)	0.96
TT	3 (1.5)	0 (0)	0.00 (0.00-NA)	0.76
G	369 (90)	11 (91.6)	1.00	
T	41 (10)	1 (8.3)	0.81 (0.10–6.49)	0.84

DISCUSSION

The Eph family have been associated with controlling cell adhesion, migration and spatial organization of multicellular tissues (Anderton et al., 2021). There are at least 16 receptors and nine ligands recognized in various species belonging to the Eph family, which makes this family the largest family of receptor tyrosine kinases (Brantley-Sieders et al., 2006). These receptors can be partitioned into two classes dependent on homology and binding affinities for two distinct classes of ephrins. EphA-class receptors bind glycosylphosphatidylinositol-anchored ephrin-A ligands, which

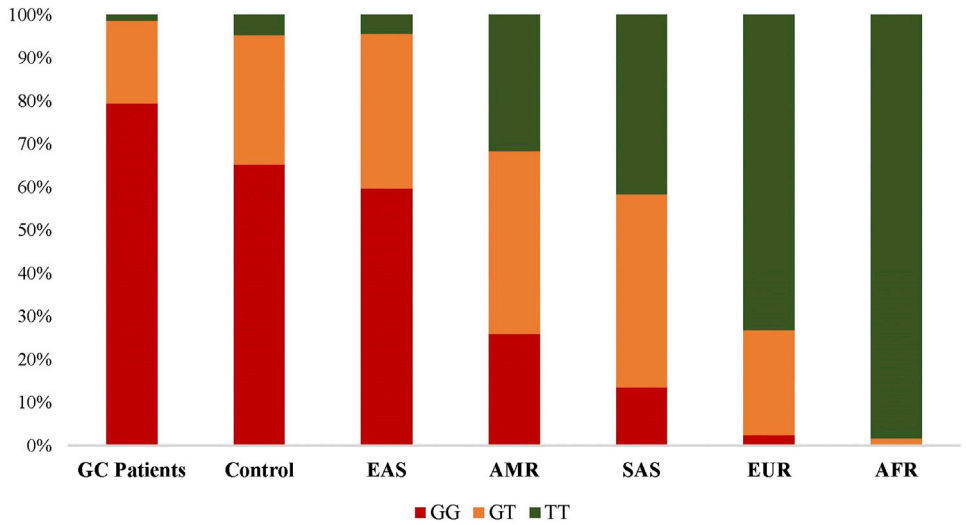

FIGURE 2 | Distributions of *EFNA1* rs4971066 genotypes in studies populations and other ethnic populations.

are bound to the cell membrane. EphB class receptors typically bind to class B ephrins, which are anchored to the cell membrane by a transmembrane spanning domain (Shi et al., 2008). Growing evidences have suggested the roles of A-class receptors and ligands in postnatal angiogenesis regulation, embryonic vascular remodeling and tumor angiogenesis (Pasquale, 2005). Expression analysis of mouse xenograft models and human breast cancer or human Kaposi's sarcoma demonstrated that ephrin-A1 was widely expressed in tumor parenchyma and tumor endothelium (Ogawa et al., 2000). Other studies using inhibitors indicated that A-class receptors are necessary for vascular remodeling in pancreatic islet cell cancer and metastatic mammary adenocancer (Brantley et al., 2002). Scholars found out through a series of experiments in metastatic mammary tumor that membrane-tethered Ephrin-A1 can regulates angiogenic responses from initially distant host endothelium (Brantley-Sieders et al., 2006). The increased expression of ephrin-A1 accelerated the malignant progression of the intestinal adenoma to invasive tumors (Shi et al., 2008). Ephrin-A1 also regulates glutaminolysis through Eph receptor-dependent activation of RhoA GTPases (Youngblood et al., 2016). Ephrin-A1 was recently found it can be targeted by a lncRNA, GMAN, by binding competively to GMAN-AS RNA. Knockdown or knockout of GMAN or EFNA1 in gastric cancer cell lines reduces invasive activity and metastases.

Based on the previous results, it is concluded that the abnormal expression level of ephrin-A1 play a critical role in the tumor occurrence, development and metastasis. As well known, the nucleotide changes in the gene may have additive effect in the function of the specific gene. Not surprisingly, there were several studies have revealed single nucleotide variants in the ephrine-A1 gene that were associated with different diseases. For instances, a SNP rs12904 in the 3′-UTR of ephrin-A1 was found to be associated with gastric cancer susceptibility (Li et al., 2014). A GWAS research of Asian ethnicity has revealed that ephrin-A1 rs4745 and rs12904 were associated with the risk of gastric cancer (Lee et al., 2015). And a SNP rs4745 was found to be significantly associated with type 1 diabetes in a Genome-wide pathway analysis (Lee and Song, 2016). Li et al. identified that rs12904 in ephrin-A1 gene was significantly associated with risk of gastric cancer in a Chinese population. Their data indicated that the OR for carrying AG or GG genotype being 0.65 compared with AA genotype. During the present study, we got a consistent result. Since rs12904 is in strong linkage disequilibrium with rs4971066. The rs12904 AG/GG linked rs4971066 GT/TT genotypes also reduced the risk of gastric cancer. The result of present study demonstrated that rs12904 could be potential genetic marker for predicting the susceptibility of gastric cancer.

The present study has an obvious limitation. As noted in the **Supplementary Table S1** that the ages of patients and controls are significantly different. The controls are younger, and they might develop GC in the future. To further validate the results, healthy independent Han Chinese individuals from 1000 G database were also compared. And the results were consistent.

DATA AVAILABILITY STATEMENT

The original contributions presented in the study are included in the article/**Supplementary Material**, further inquiries can be directed to the corresponding authors.

ETHICS STATEMENT

The studies involving human participants were reviewed and approved by the ethics committee of Nanjing Medical University. The patients/participants provided their written informed consent to participate in this study.

AUTHOR CONTRIBUTIONS

XW, ZJ, YX, CL, JZ, and YS contributed the sample collection and processing. YP, HL, YY, and DL performed the experiments and data analysis. FC and PC contributed to the paper writing.

ACKNOWLEDGMENTS

This work was supported by the National Natural Science Foundation of China (No.81801879, 82002028 and 81922041), the Natural Science Foundation of the Jiangsu Higher Education Institution of China (19KJB340001), the Science and Technology of Jiangsu Province China (BK20170048).

SUPPLEMENTARY MATERIAL

The Supplementary Material for this article can be found online at: https://www.frontiersin.org/articles/10.3389/fmolb.2021.690665/full#supplementary-material

REFERENCES

Anderton, M, Van Der Meulen, E, Blumenthal, MJ, and Schäfer, G (2021). The Role of the Eph Receptor Family in Tumorigenesis. *Cancers* 13 (2). doi:10.3390/cancers13020206

Brantley, D. M., Cheng, N., Thompson, E. J., Lin, Q., Brekken, R. A., Thorpe, P. E., et al. (2002). Soluble Eph A receptors inhibit tumor angiogenesis and progression *in vivo*. *Oncogene* 21 (46), 7011–7026. doi:10.1038/sj.onc.1205679

Brantley-Sieders, D. M., Fang, W. B., Hwang, Y., Hicks, D., and Chen, J. (2006). Ephrin-A1 facilitates mammary tumor metastasis through an angiogenesis-dependent mechanism mediated by EphA receptor and vascular endothelial growth factor in mice. *Cancer Res.* 66 (21), 10315–10324. doi:10.1158/0008-5472.can-06-1560

Chen, Z., Li, Z., Soutto, M., Wang, W., Piazuelo, M. B., Zhu, S., et al. (2019). Integrated Analysis of Mouse and Human Gastric Neoplasms Identifies Conserved microRNA Networks in Gastric Carcinogenesis. *Gastroenterology* 156 (4), 1127–1139.e1128. doi:10.1053/j.gastro.2018.11.052

Fang, J., Hong, H., Xue, X., Zhu, X., Jiang, L., Qin, M., et al. (2019). A novel circular RNA, circFAT1(e2), inhibits gastric cancer progression by targeting miR-548g in the cytoplasm and interacting with YBX1 in the nucleus. *Cancer letters* 442, 222–232. doi:10.1016/j.canlet.2018.10.040

Hao, Y., and Li, G. (2020). Role of EFNA1 in tumorigenesis and prospects for cancer therapy. *Biomedicine & Pharmacotherapy* 130, 110567. doi:10.1016/j.biopha.2020.110567

Jiang, F, and Shen, X (2019). Current prevalence status of gastric cancer and recent studies on the roles of circular RNAs and methods used to investigate circular RNAs. *Cellular & molecular biology letters* 24, 53. doi:10.1186/s11658-019-0178-5

Lee, YH, and Song, GG (2016). Genome-wide pathway analysis for diabetic nephropathy in type 1 diabetes. *Endocr. Res.* 41 (1), 21–7. doi:10.3109/07435800.2015.1044011

Lee, JH, Kim, Y, Choi, JW, and Kim, YS (2015). Genetic variants and risk of gastric cancer: a pathway analysis of a genome-wide association study. *SpringerPlus* 4, 215. doi:10.1186/s40064-015-1005-8

Li, Y., Nie, Y., Cao, J., Tu, S., Lin, Y., Du, Y., et al. (2014). G-A variant in miR-200c binding site ofEFNA1alters susceptibility to gastric cancer. *Mol. Carcinog.* 53 (3), 219–229. doi:10.1002/mc.21966

Ogawa, K., Pasqualini, R., Lindberg, R. A., Kain, R., Freeman, A. L., and Pasquale, E. B. (2000). The ephrin-A1 ligand and its receptor, EphA2, are expressed during tumor neovascularization. *Oncogene* 19 (52), 6043–6052. doi:10.1038/sj.onc.1204004

Pasquale, E. B. (2005). Eph receptor signalling casts a wide net on cell behaviour. *Nat. Rev. Mol. Cell Biol.* 6 (6), 462–475. doi:10.1038/nrm1662

Rawla, P., and Barsouk, A. (2019). Epidemiology of gastric cancer: global trends, risk factors and prevention. *Prz Gastroenterol* 14 (1), 26–38. doi:10.5114/pg.2018.80001

Shi, L., Itoh, F., Itoh, S., Takahashi, S., Yamamoto, M., and Kato, M. (2008). Ephrin-A1 promotes the malignant progression of intestinal tumors in Apcmin/+ mice. *Oncogene* 27 (23), 3265–3273. doi:10.1038/sj.onc.1210992

Wang, X, Wang, X, Liu, Y, et al. (2018). LGR5 regulates gastric adenocarcinoma cell proliferation and invasion via activating Wnt signaling pathway. *Oncogenesis* 7 (8), 57. doi:10.1038/s41389-018-0071-5

Wu, Y, Wan, X, Zhao, X, Song, Z, Xu, Z, Tao, Y, et al. (2020). MicroRNA-143 suppresses the proliferation and metastasis of human gastric cancer cells via modulation of STAT3 expression. *Am. J. Transl. Res.* 12 (3), 867–874.

Youngblood, V. M., Kim, L. C., Edwards, D. N., Hwang, Y., Santapuram, P. R., Stirdivant, S. M., et al. (2016). The Ephrin-A1/EPHA2 Signaling Axis Regulates Glutamine Metabolism in HER2-Positive Breast Cancer. *Cancer Res.* 76 (7), 1825–1836. doi:10.1158/0008-5472.can-15-0847

Zhang, E, He, X, Zhang, C, et al. (2018). A novel long noncoding RNA HOXC-AS3 mediates tumorigenesis of gastric cancer by binding to YBX1. *Genome biology* 19 (1), 154. doi:10.1186/s13059-018-1523-0

Zhang, Z, Xue, H, Dong, Y, et al. (2019). GKN2 promotes oxidative stress-induced gastric cancer cell apoptosis via the Hsc70 pathway. *J. Exp. Clin. Cancer Res.* 38 (1), 338. doi:10.1186/s13046-019-1336-3

Zhu, H., Yang, M., Zhang, H., Chen, X., Yang, X., Zhang, C., et al. (2015). Genome-wide association pathway analysis to identify candidate single nucleotide polymorphisms and molecular pathways for gastric adenocarcinoma. *Tumor Biol.* 36 (7), 5635–5639. doi:10.1007/s13277-015-3236-2

Conflict of Interest: The authors declare that the research was conducted in the absence of any commercial or financial relationships that could be construed as a potential conflict of interest.

frontiers in Molecular Biosciences

ORIGINAL RESEARCH
published: 10 June 2021
doi: 10.3389/fmolb.2021.682594

CORO1C is Associated With Poor Prognosis and Promotes Metastasis Through PI3K/AKT Pathway in Colorectal Cancer

Zongxia Wang[1†], Lizhou Jia[1,2†], Yushu sun[3†], Chunli Li[1], Lingli Zhang[4], Xiangcheng Wang[5,6] and Hao Chen[2,7]**

[1]Cancer Center, Bayannur Hospital, Bayannur, China, [2]Department of Pathology, Wannan Medical College, Wuhu, China, [3]Department of Oncology, Inner Mongolia Autonomous Region Cancer Hospital, Hohhot, China, [4]Department of Ophthalmology, Inner Mongolia Autonomous Region People's Hospital, Hohhot, China, [5]Department of Nuclear Medicine, The Affiliated Hospital of Inner Mongolia Medical University, Hohhot, China, [6]Key Laboratory of Inner Mongolia Autonomous Region Molecular Imaging, Inner Mongolia Medical University, Hohhot, China, [7]Faculty of Medical Science, Jinan University, Guangzhou, China

OPEN ACCESS

Edited by:
Haishi Qiao,
China Pharmaceutical University, China

Reviewed by:
Ren Ke,
Chengdu Medical College, China
Jianfei Huang,
Nantong University, China

***Correspondence:**
Xiangcheng Wang
guyan@nmgfy.com
Hao Chen
ha0chen@wnmc.edu.cn

[†]These authors have contributed equally to this work.

Specialty section:
This article was submitted to Molecular Diagnostics and Therapeutics, a section of the journal Frontiers in Molecular Biosciences

Received: 18 March 2021
Accepted: 28 May 2021
Published: 10 June 2021

Citation:
Wang Z, Jia L, sun Y, Li C, Zhang L, Wang X and Chen H (2021) CORO1C is Associated With Poor Prognosis and Promotes Metastasis Through PI3K/AKT Pathway in Colorectal Cancer. Front. Mol. Biosci. 8:682594. doi: 10.3389/fmolb.2021.682594

Trophoblast cell surface protein 2 (Trop2) is one of the cancer-related proteins that plays a vital role in biological aggressiveness and poor prognosis of colorectal cancer (CRC). The study of the Trop2 related network is helpful for us to understand the mechanism of tumorigenesis. However, the effects of the related proteins interacting with Trop2 in CRC remain unclear. Here, we found that coronin-like actin-binding protein 1C (CORO1C) could interact with Trop2 and the expression of CORO1C in CRC tissues was higher than that in paracarcinoma tissues. The expression of CORO1C was associated with histological type, lymph node metastasis, distant metastasis, AJCC stage, venous invasion, and perineural invasion. The correlation between CORO1C expression and clinical characteristics was analyzed demonstrating that high CORO1C expression in CRC patients were associated with poor prognosis. Furthermore, CORO1C knockdown could decrease the cell proliferation, colony formation, migration and invasion *in vitro* and tumor growth *in vivo*. The underlying mechanisms were predicted by bioinformatics analysis and verified by Western blotting. We found that PI3K/AKT signaling pathway was significantly inhibited by CORO1C knockdown and the tuomr-promoting role of CORO1C was leastwise partly mediated by PI3K/AKT signaling pathway. Thus, CORO1C may be a valuable prognostic biomarker and drug target in CRC patients.

Keywords: CORO1C, colorectal cancer, prognosis, metastasis, AKT

INTRODUCTION

Colorectal cancer (CRC) is the third most common cancer worldwide, and the incidence rate and mortality of CRC are increasing year by year (Siegel et al., 2020). Metastasis continues to be the leading cause of significant clinical problems and more than 90% cancer-related mortalities (Guan, 2015). Liver is the most common site of distant relapse in CRC patients, followed by lung, hilar/perihepatic lymph nodes, and peritoneum (Jiang et al., 2021). Approximately 25% of CRC patients present distant metastasis at initial diagnosis, and 50% of them develop metastatic disease within 3 years (Vatandoust et al., 2015). Cell migration underlies malignant tumor invasion and metastasis.

Human trophoblast cell surface protein 2 (Trop2) is a cell-surface glycoprotein highly expressed in a variety of tumors, and the high expression of Trop2 protein is associated with poor survival prognosis of cancer patients (Zhao et al., 2017; Zimmers et al., 2018; Sun et al., 2020). Trop2 plays a key role in inducing epithelial-mesenchymal transition (EMT) and regulating cell migration (Li et al., 2017; Wu et al., 2017; Gu et al., 2018). Trop2 physically interacts with β-catenin which is a vital molecule of EMT, and Trop2-induced β-catenin accumulation in the nucleus accelerates gastric tumor metastasis (Zhao et al., 2019). Due to the complicated mechanisms of Trop2, it remains necessary to investigate the interacting proteins of Trop2 in the process of exploring tumorigenesis.

When it comes to the potential function of Trop2, we found that coronin-like actin-binding protein 1C (CORO1C) has interacted with it. CORO1C belongs to the highly conserved coronin family that affects the actin cytoskeleton (Liu et al., 2016). It is enriched at the leading edge of lamellipodia, as well as folds of the invasive cell membrane (Brayford et al., 2016). CORO1C regulates F-actin, Arp2/3 complex, and ADF/cofilin proteins, inhibiting actin dynamics (Chan et al., 2011). It also selectively interferes with Rac1, which is a nexus in membrane protrusion and migration regulation (Williamson et al., 2015). Furthermore, CORO1C is differentially expressed in various solid tumors, such as glioblastoma cancer (Thal et al., 2008), hepatocellular cancer (Wu et al., 2010b), breast cancer (Wang et al., 2014) and lung cancer (Mataki et al., 2015). CORO1C has been confirmed to promote cellular proliferation and metastasis through regulating cyclin D1 and vimentin in gastric cancer (Cheng et al., 2019), but little is known about the role of CORO1C in CRC.

In this study, we investigated the proteins conjugated with Trop2 and speculated that CORO1C plays a vital role in CRC metastasis. The expression of CORO1C in CRC was detected, and the associations between CORO1C and clinicopathological features of CRC patients were investigated Also, the effects of CORO1C on CRC cells and the underlying mechanisms were explored *in vitro* and *in vivo*. Our research confirmed the biological function of CORO1C in CRC cells and provided a novel insight to CRC development and progression.

MATERIALS AND METHODS

Cell Line and Cell Culture

293T cell line and colorectal cancer cell lines SW480, SW620, COCA2, LOVO, HCT116,HT-29, and the normal colorectal epithelial cell line (NCM460) were purchased from Keygen Biotech Co., Ltd. and maintained in DMEM medium (Gibco, United States) with 10% fetal bovine serum (Gibco, United States), 50 units/ml penicillin (Gibco, United States) and 50 μg/ml streptomycin (Gibco, United States). The cell line was incubated in a moist environment with 5% CO_2 at 37°C. AKT inhibitor (Miltefosine) was perchased (Selleck Chemicals LLC,S3056) and the used concentration was 50 μM.

Lentivirus-Mediated Transfection for Trop2 and CORO1C Over-Expression

The lentivirus-mediated Trop2-cDNA, CORO1C-cDNA (GeneCopoeia, Guangzhou, China) inserted in the pcDNA3.1 were used to overexpress Trop2 in 293T cells. Lipofectamine 2000 Transfection Reagent (Invitrogen, United States) was utilized to perform the transfections according to the instruction.

shRNA for CORO1C Down-Expression

The shRNA of CORO1C was designed according to the sequence of CORO1C gene (sense sequence: GGTAGTCAGCTGGGAAAG TCT), and BLAST test showed no homology with the coding sequence of other genes. CORO1C knockdown plasmids were synthesized by GeneCopoeia Co., Ltd. (Top strand: 5′-CACCGG TAGTCAGCTGGGAAAGTCTCGAAAGACTTTCCCAGCTGA CTACC-3'. Bottom strand: 5′- AAAAGGTAGTCAGCTGGGAAA GTCTTTCGAGACTTTCCCAGCTGACTACC -3′). The plasmid was transformed into *Escherichia coli* DH5α for amplification, and then extracted by EndoFree Maxi Plasmid Kit (TianGen, Beijing, China) according the instructions. Lipofectamine 2000 Transfection Reagent (Invitrogen, United States) was utilized to perform the transfections according to the instructions.

Quantitative Polymerase Chain Reaction (qPCR) Array

Total RNA was extracted from 293T cells using Trizol reagent (#12096028, Invitrogen, United States) and reverse transcribed into cDNA using High Capacity cDNA Reverse Transcription Kits (#4374966, Applied Biosystems, United States) according to the instruction. Quantitative real-time PCR was performed using SYBR Advantage qPCR Premix (#638321, Takara, Japan) on an ABI StepOnePlus Real-Time PCR System following the steps below: 95°C for 20 s; 40 cycles of amplification at 95°C for 15 s and 56°C for 1 min; 95°C for 15 s, 60°C for 1 min, 95°C for 15 s. Following primers were used for the reaction: human Trop2 forward, 5′-ACAACGATGGCCTCTACGAC-3′, and reverse, 5′-GTCCAGGTCTGAGTGGTTGAA-3′, and GAPDH forward, 5′-GGAGCGAGATCCCTCCAAAAT-3′, and reverse, 5′-GGCTGT TGTCATACTTCTCATGG-3′. Results were normalized to GAPDH and all experiments were repeated in triplicate.

Protein Extraction and Western Blotting

293T cells were dissolved by RIPA Lysis Buffer (#89901, Thermo, United States) in accordance with the protocol. The lysate was kept on ice for 5 min and then centrifuged at 12,000 g for 20 min. Protein samples were mixed with SDS-PAGE sample loading buffer (#P0015, Beyotime, China) and then heated to 95°C for 10 min. The protein sample was loaded onto an polyacrylamide gel for electrophoresis and then transferred to a PVDF membrane. The blots were blocked at room temperature for 2 h and then incubated with appropriate primary antibodies overnight at 4°C. After washing three times with PBST, the membrane was incubated with corresponding secondary antibodies at room temperature for

1 h. Proteins were visualized by chemiluminescent substrate (#34580, Thermo, United States) and ChemiDoc XRS + system (Bio-Rad, United States). Primary antibodies was used to detect Trop2 (1:1,000, #90540, CST, United States), CORO1C (1:500, #14749-1-AP, Proteintech, United States) and GAPDH (1:1,000, #97166, CST, United States).

Immunoprecipitation and Mass Spectrometry

10 μg anti-Trop2 IgG (#90540, CST, United States) was incubated with 50 μL dynabeads (#20423, Thermo, United States) for 10 min with rotation at room temperature. The protein sample was incubated with dynabead-IgG complex for 10 min at room temperature with rotation. The complex was washed with PBST three times and then resuspended by glycine (50 nM, pH2.8) for 2 min with rotation. The eluate obtained from the IP experiment was incubated with 1 mmol DTT and 200 μL UA buffer (8 MUrea, 150 mM TrisHCl,pH8.0) at room temperature for 1 h. The mixture was transferred into 10 kDa ultrafiltration centrifuge tube, centrifuged for 15 min (14,000 g). The tube was added with 14,000 μL IAA (50 mM), shocked for 1 min, incubated in room temperature for 30 min, and centrifugated at 14,000 g for 10 min. Ammonium bicarbonate (300 μL, 100 mmol) was added to the tube, and the tube was centrifuged in 14, 000 g for 20 min. The tube was added with 8 μL Trypsin buffer (4 μg Trypsin) and incubated in 37°C for 16 h. The filtrate was collected by centrifugation at 14, 000 g for 10 min and detected by TripleTOF 5,600 + mass spectrometer (AB SCIEX, United States). The data was analyzed by MaxQuant 1.5.2.8 software, and then the peptides and proteins were identified by Maxquant algorithm. The filtration parameters were set as: peptide FDR ≤0.01 and protein FDR ≤0.01.

Patients and Tissue Specimens

In this study, 581 patients with CRC diagnosed in the Affiliated Hospital of Nantong University during 2014–2018 were recruited. A total of 734 formalin-fixed, paraffin-embedded (FFPE) CC tissue samples were investigated, including CRC tissues (n = 581), matched paracarcinoma tissues (n = 117), and colonitis tissues (n = 36). None of the patients had been treated with radiotherapy, chemotherapy, or immunotherapy. The clinical information, including age, gender, location, histologic type, differentiation, depth of invasion, lymph node metastasis, distant metastasis, AJCC stage, venous invasion, perineural invasion, preoperative CEA, preoperative CA199, and Ki67 about the patients enrolled in this study were recorded.

Tissue Microarrays and Immunohistochemistry

The TMAs were constructed in the Department of Pathology, Affiliated Hospital of Nantong University, Nantong, Jiangsu, China, using the Quick-Ray tissue system (UNITMA, Korea). Graded alcohol was used for deparaffinage and rehydration. 3% H_2O_2 was utilized to block endogenous peroxidase. Antigens were retrieved by heating in 0.01 M citrate buffer (pH 6.0). CORO1C was detected by a anti-human CORO1C rabbit polyclonal antibody (dilution 1:200) (#14749-1-AP, Proteintech, United States). Hematoxylin was used for counterstain. Staining was scored independently by two pathologists unaware of clinical characteristics. CORO1C expression was quantified according to the semi-quantitative H-score method, using staining intensity scores as follow: 0 indicated negative expression; 1 indicated weakly positive staining; 2 indicated moderately positive staining; and 3 indicated strongly positive staining. Single staining intensity score = score × the percentage of cells in the corresponding intensity × 100. Final staining scores were the sum of four staining intensity scores. The minimum possible final staining score was 0 (no staining) and maximum possible score was 300 (100% of cells with 3 staining intensity) (Zhao et al., 2016).

CCK-8 Proliferation Assay

The cells in each group were seeded into 96-well plates with 5 × 10^3 cell/well, and cell proliferation was detected using CCK-8 kit according to the instruction. Diluted CCK-8 reagents were added into each well at 24, 48, 72 and 96 h respectively. After incubation in 37°C for 2 h, the absorbance of cells in each group at 450 nm was detected by a microplate reader.

Clone Formation Assay

The cells in each group were seeded into 6-well plates with 1 × 10^3 cell/well. After incubation for 2 weeks, cells were fixed with formaldehyde for 30 min, and then stained with 0.01% crystal violet for 30 min. Cell clones were counted and photographed.

Transwell Migration/Invasion Assay

Medium containing 10% serum was added in the lower chamber, cell suspension without serum was added in the upper chamber (containing matrigel glue for invasion assay). After incubation for 48 h, the membrane of the upper chamber was sucked and then fixed with formaldehyde for 30 min. Cells on the membrane were stained with 0.01% crystal violet for 30 min. Average values of 5 visual fields were randomly selected for statistical analysis.

Nude Mouse Tumorigenicity Assay

HCT116-shControl and HCT116-shCORO1C were collected in the logarithmic growth phase, respectively, and 100 μL cell suspension with a density of 1 × 10^8/ ml was prepared with RPMI 1640 medium and injected into the oxter of nude mice. The tumor size was measured with Vernier calipers every 3 days. Tumor volume = longest diameter × shortest diameter^2/2. The protocols of animal study were approved by the laboratory animal center of Inner Mongolia Medical University.

Gene Ontology Analysis and Gene Set Enrichment Analysis

Ualcan database (http://ualcan.path.uab.edu/) was searched, and 395 genes were identified to be closely associated with CORO1C

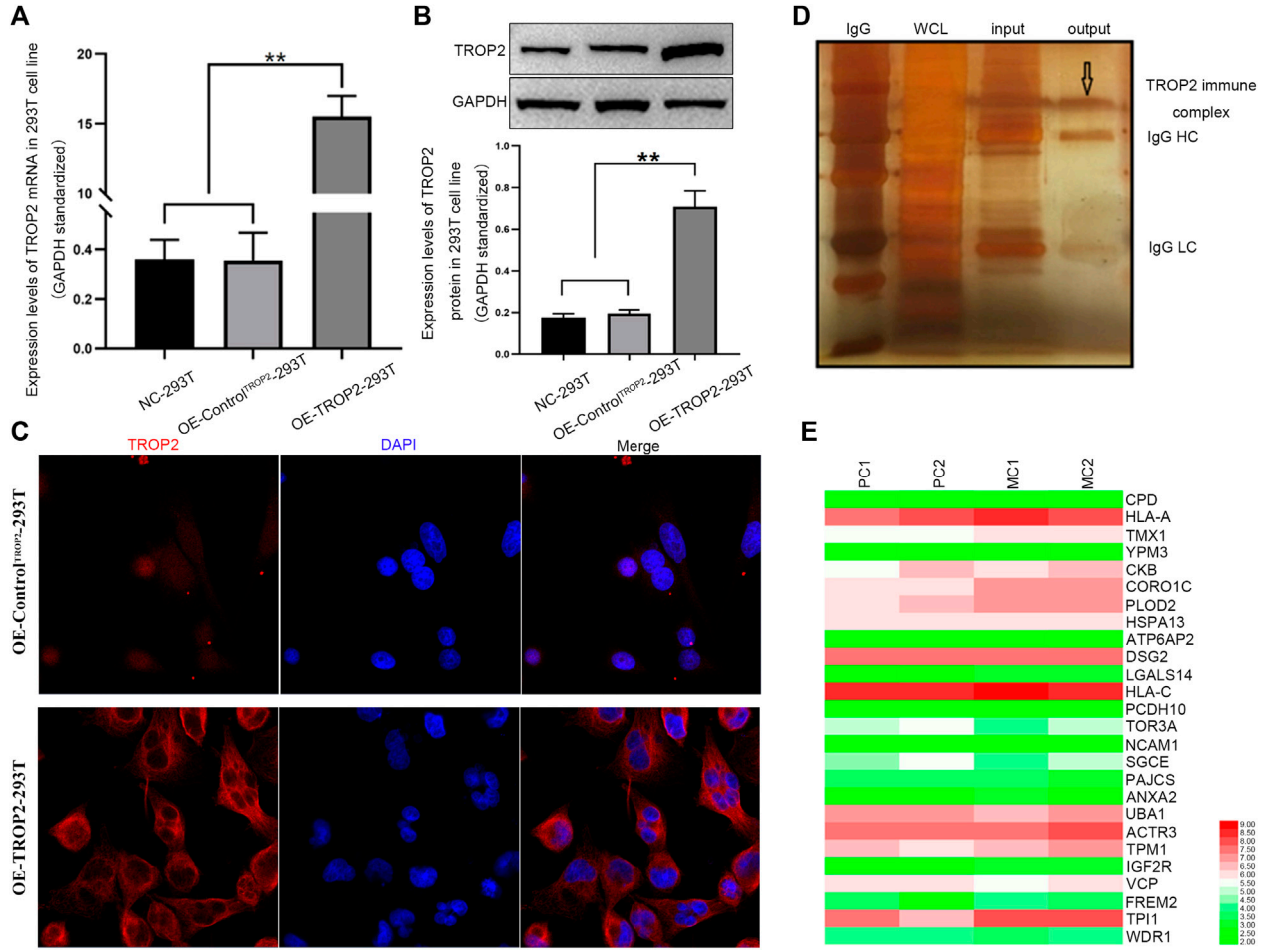

FIGURE 1 | Associations between CORO1C, TROP2, and CRC metastasis. Overexpression of Trop2 in 293T cells was confirmed by **(A)** qRT-PCR, **(B)** Western blotting, and **(C)** Immunofluorescence. **(D)** Trop2 immunocomplex by Co-IP; **(E)** Heatmap of proteins interacting with Trop2 in PC and MC. The RNA-seq data were obtained from GSE28702. Red and green colors represent high and low gene expression, respectively. PC: primary CRC; MC: metastatic CRC, $^{**}p < 0.01$.

(pearson correlation coefficient ≥0.5, data not shown). Next, we performed GO analysis and GSEA of these CORO1C-related genes by DAVID database (https://david.ncifcrf.gov/). These genes were classified into three functional groups: molecular function group, biological process group, and cellular component group. Terms in each group and signaling pathways in KEGG were selected if $p < 0.001$ and false discovery rate <0.1. Data were visualized using Sangerbox online tool (http://sangerbox.com/).

Statistical Analysis

All statistics were analyzed by SPSS 19.0 statistical software (SPSS Inc., Chicago, IL). All the experiments were repeated three times with similar results. The correlation between CORO1C expression and clinical features was analyzed by Pearson's χ^2 test. The differences between the two groups were analyzed using an unpaired Student's *t*-test. Three or more groups were compared using one-way analysis of variance (ANOVA), followed by Tukey's multiple comparison test. Cumulative patient survival was estimated by Kaplan-Meier analysis. The survival curves were compared by log-rank test. $p < 0.05$ indicated statistical significance.

RESULTS

CORO1C is Related to Colorectal Cancer Cell Migration and Invasion

To identify the proteins interacting with Trop2, we first overexpressed Trop2 in 293T cells using the lentivirus-mediated Trop2-cDNA. qPCR, Western blotting, and immunofluorescence were performed to confirm Trop2 overexpression (**Figures 1A–C**). Coimmunoprecipitation (Co-IP) and mass spectrometry were used to define the proteins (CPD, HLA-A, PLOD2, and CORO1C) interacting with Trop2 (**Figure 1D**, **Supplementary Table S1**). Bioinformatics analysis confirmed that CORO1C is strongly associated with invasion and metastasis (**Figure 1E**, **Supplementary Table S2**).

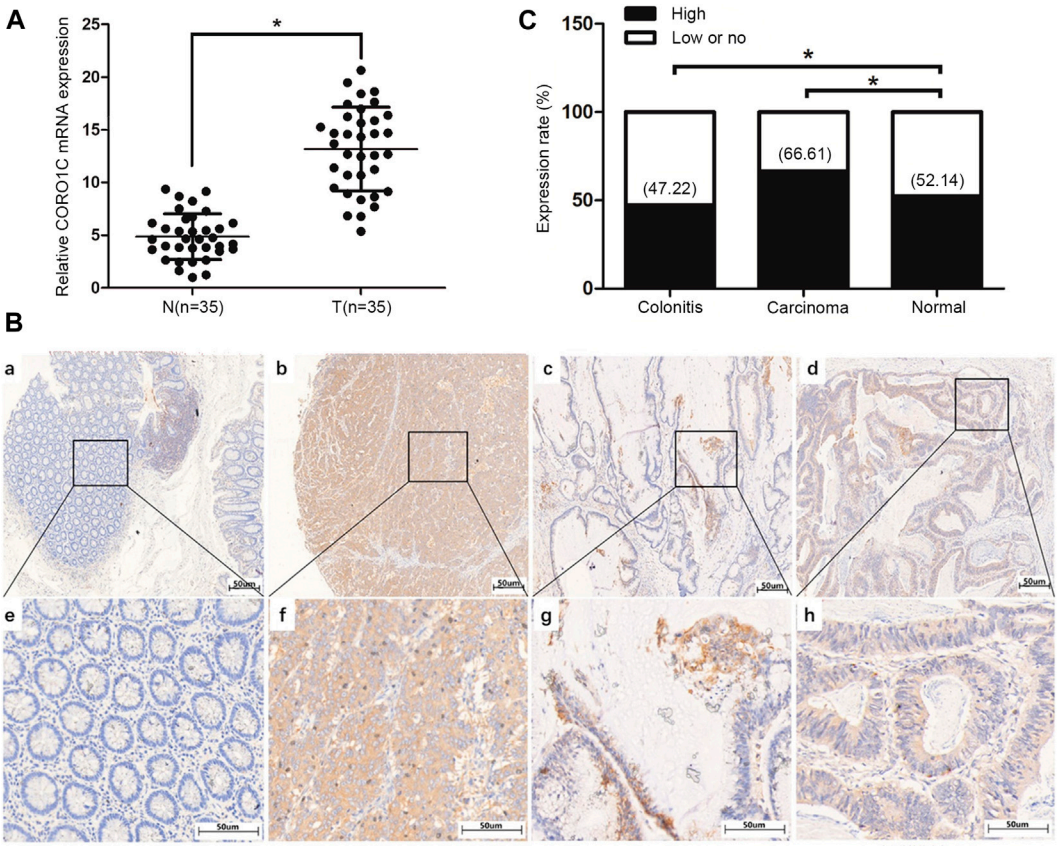

FIGURE 2 | Expression of CORO1C in CRC patients. **(A)** CORO1C mRNA levels in the 35 CRC tissues. **(B)** Representative images of CORO1C protein expression in colorectal tissues: a. Negative expression of CORO1C in normal colorectal tissues; b. Positive expression of CORO1C in moderately differentiated tubular adenocarcinoma tissues; c. Positive expression of CORO1C in mucinous adenocarcinoma tissues; d. Positive expression of CORO1C in highly differentiated tubular adenocarcinoma tissues. **(C)** Positive rate of high CORO1C in CRC tissues was higher than in normal tissues, $^*p < 0.05$.

CORO1C Protein was Overexpressed in Colorectal Cancer Tissues Compared to Adjacent Tissues

The mRNA level of *COR O 1C* in CRC tissues was confirmed to be higher than that in normal tissues (**Figure 2A**). The protein subcellular localization of CORO1C, detected by IHC assay was in the cytoplasm in CRC tissues (**Figure 2B**). The χ-tile software program for TMA data analysis was utilized to estimate the level of CORO1C protein in CRC patients. The score between 0 and 130 was considered low or no expression, while the counts >130 were considered high expression. The CORO1C expression was classified as high or low or no. The frequency of high CORO1C expression in CRC tissues (66.61%, 387/581) was higher than that in pericarcinomatous tissue (52.14%, 61/117) (**Figure 2C**).

CORO1C Overexpression was Associated With Increased Invasiveness and Metastasis in Colorectal Cancer Patients

We investigated the relationship between CORO1C expression and pathological parameters in CRC patients. The results showed that the expression of CORO1C was significantly related to the histological type ($\chi^2 = 7.6419$, $p = 0.006$), lymph node metastases ($\chi^2 = 19.1615$, $p < 0.001$), distant metastases ($\chi^2 = 9.5623$, $p = 0.002$), AJCC stage ($\chi^2 = 17.7192$, $p = 0.001$), venous invasion ($\chi^2 = 22.1337$, $p < 0.001$), and perineural invasion ($\chi^2 = 21.1141$, $p < 0.001$). However, no significant difference was detected between CORO1C expression and gender, age, location, differentiation, tumor size, preoperative CEA, preoperative CA199, and Ki67 (**Table 1**).

High CORO1C Expression was Associated With Poor Prognosis in Colorectal Cancer

Univariate analysis showed that the overall survival (OS) was significantly associated with CORO1C expression, differentiation, lymph node status, distant metastasis, TNM stage, venous invasion, perineural invasion, and preoperative CEA. Multivariate analysis indicated that only CORO1C expression, distant metastases, TNM stage, and venous invasion were independent prognostic factors for OS (**Table 2**). Moreover, Kaplan–Meier survival curves displayed that high CORO1C expression and increased distant metastasis exerted a negative effect on OS (**Figure 3**).

TABLE 1 | Association between CORO1C expression and clinicopathological characteristics in CRC patients.

Characteristic	*n*	CORO1C(%)		Pearsonχ2	*P*
		High	Low or no		
Total	581	465 (63.35)	269 (36.65)		
Gender				1.0839	0.298
Male	348	226 (64.94)	122 (35.56)		
Female	233	161 (69.10)	72 (30.90)		
Age				0.5923	0.442
< 60	212	137 (64.62)	75 (35.38)		
≥60	369	250 (67.75)	119 (32.25)		
Location				2.1214	0.548
Right	186	119 (63.98)	67 (36.02)		
Transverse	76	49 (64.47)	27 (35.53)		
Left	113	74 (65.49)	39 (34.51)		
Sigmoid	206	145 (70.39)	61 (29.61)		
Histological type				7.6419	0.006*
Adenocarcinoma	519	336 (64.74)	183 (35.26)		
Mucinous/SRCC	62	51 (82.26)	11 (17.74)		
Differentiation				1.6203	0.655
Well	154	98 (63.64)	56 (36.36)		
Moderate	312	215 (68.91)	97 (31.09)		
Poor	98	63 (64.29)	35 (35.71)		
Others	17	11 (64.71)	68 (35.29)		
T stage				1.2279	0.746
T1	41	27 (65.85)	14 (34.15)		
T2	60	39 (65.00)	21 (35.00)		
T3	198	127 (64.14)	71 (35.86)		
T4	282	194 (68.79)	88 (31.21)		
N stage				19.1615	<0.001*
N0	326	193 (59.20)	133 (40.80)		
N1	166	123 (74.10)	43 (25.90)		
N2	89	71 (79.78)	18 (25.90)		
M stage				9.5623	0.002*
M0	485	310 (63.92)	175 (36.08)		
M1	96	77 (80.21)	19 (19.79)		
AJCC stage				17.7192	0.001*
I	62	35 (56.45)	27 (43.55)		
II	197	114 (57.87)	83 (42.13)		
III	231	173 (74.89)	58 (25.11)		
IV	91	65 (71.43)	26 (28.57)		
Venous invasion				22.1337	<0.001*
Negative	498	313 (62.85)	185 (37.15)		
Positive	83	74 (89.16)	9 (10.84)		
Perineural invasion				21.1141	<0.001*
Negative	504	318 (63.10)	186 (36.90)		
Positive	77	69 (89.61)	8 (10.39)		
Preoperative CEA, ng/ml				1.9482	0.378
≤5	257	166 (64.59)	91 (35.41)		
> 5	283	196 (69.26)	87 (30.74)		
Unknown	41	25 (60.98)	16 (39.02)		
Preoperative CA199,ng/ml				2.6548	<0.265
≤37	259	164 (63.32)	95 (36.68)		
> 37	279	195 (69.89)	84 (30.11)		
Unknown	43	28 (65.12)	15 (34.88)		
Ki67				0.4627	0.496
Negative	178	115 (64.61)	63 (35.39)		
Positive	403	272 (67.49)	131 (32.51)		

Downregulation of CORO1C Inhibited Proliferation, Migration, and Invasion of CRC Cells *in Vitro* and *in Vivo*

We measured the levels of CORO1C expression in six CRC cell lines, namely SW480, SW620, COCA2, LOVO, HCT116, HT-29, and the normal colorectal epithelial cell line (NCM460) by western blotting. We found that CORO1C was highly expressed in COCA2 and HCT116 cells, and weakly expressed in SW620 and LOVO cells (**Figure 4A**). In the follow-up experiments, COCA2 and HCT116 cells were used to down-express CORO1C. SW620 and LOVO cells were used to over-express CORO1C.

TABLE 2 | Univariate and multivariate analysis of prognostic factors for overall survival in CRC.

	Univariate analysis			Multivariate analysis		
	HR	***p*-value**	**95%CI**	**HR**	***p*-value**	**95%CI**
CORO1C						
High vs. low or No	0.981	<0.001*	0.978–0.984	2.113	<0.001*	1.642–2.721
Age						
< 60 vs. ≥60	1.151	0.338	0.864–1.533	—	—	—
Gender						
Male vs. female	1.150	0.350	0.858–1.540	—	—	—
Location						
Right vs. transverse vs. left vs. sigmoid	1.001	0.982	0.919–1.091	—	—	—
Histological type						
Adenocarcinoma vs. Mutinous/SRCC	0.981	0.892	0.744–1.294	—	—	—
Differentiation						
Well vs. moderate vs. poor vs. others	1.208	0.008*	1.051–1.389	—	—	—
TNM						
0 vs.Ⅰvs.Ⅱvs.Ⅲvs.Ⅳ	1.249	0.007*	1.063–1.467	1.178	0.007*	1.045–1.327
T stage						
T1 vs. T2 vs. T3 vs. T4	1.089	0.281	0.932–1.273	—	—	—
N stage						
N0 vs. N1 vs. N2 vs. N3	0.711	0.001*	0.582–0.870	—	—	—
M stage						
M0 vs. M1	2.243	<0.001*	1.502–3.350	3.305	<0.001*	2.529–4.320
Venous invasion						
Negative vs. positive	2.720	<0.001*	2.127–3.478	3.326	<0.001*	2.511–4.170
Perineural invasion						
Negative vs. positive	2.523	<0.001*	1.678–3.794	—	—	—
Preoperative CEA, ng/ml						
≤5 vs. > 5 vs. unknown	1.025	0.824	0.827–1.270	—	—	—
Preoperative CA199,ng/ml						
≤37 vs. > 37vs. unknown	0.955	0.674	0.771–1.184	—	—	—
Ki67						
Negative vs. positive	0.990	0.930	0.800–1.227	—	—	—

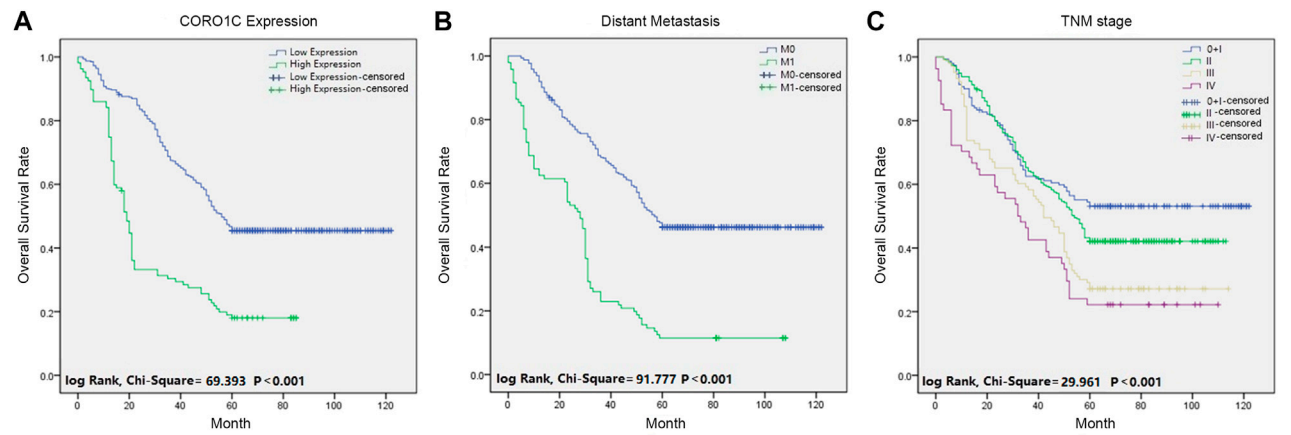

FIGURE 3 | Survival curves of CRC patients using the Kaplan-Meier method and the log-rank test. **(A)** OS curves for patients with low CORO1C expression (blue line) and patients with high CORO1C expression (green line). **(B)** OS curves for distant metastases, M0 (blue line), and M1 (green line). **(C)** OS curves by TNM stage, TNM 0 and I (blue line), TNM II (green line), TNM III (gray line), and TNM IV (purple line).

To confirm the effects of CORO1C on CRC cells behaviors, shRNA against CORO1C was constructed and transfected into COCA2 and HCT116 cell lines. The significant downregulation of CORO1C after transfection was confirmed by Western blotting (**Figure 4B**). The knockdown of CORO1C in both cells suppressed cell proliferation (**Figure 4C**), clone formation

(**Figure 4D**), migration (**Figure 4E**), and invasion (**Figure 4F**). A nude mouse xenograft model was constructed by HCT116 cells transfected with shRNA-CORO1C to confirm the role of CORO1C in CRC proliferation. The results showed that volumes (785.221 ± 134.681 mm^3) and weights (0.442 ± 0.093 g) of tumors from the shCORO1C group (275.171 ± 98.854 mm^3, 0.146 ± 0.057 g) were decreased than those from the control group, and CORO1C knockdown reduced the growth rate of CRC *in vivo* (**Figure 4G**).

AKT Inhibition Reversed the Effects of CORO1C on Migration and Invasion in CRC Cells

As shown in **Figure 5A**, in the biological process, CROR1C-related genes were mainly enriched in leukocyte migration, movement of a cell or subcellular component, and cell adhesion. In the cellular component group, CROR1C-related genes were mainly enriched in focal adhesion, cadherin binding, and cell-cell junction. Regarding the molecular function, CROR1C-related genes were enriched in protein binding, cadherin binding, and GTP binding. The findings of GSEA confirmed that CORO1C was related to focal adhesion, regulation of actin cytoskeleton, gap junction, and PI3K/AKT signaling pathway (**Figure 5B**). In COCA2 and HCT116 cell lines transfected with shRNA-CORO1C, the expression of fibronectin and vimentin protein was decreased, and E-cadherin expression showed an opposite trend. In addition, CORO1C knockdown inhibited the phosphorylation of the PI3K/AKT signaling pathway (**Figure 5C**).

To further explore whether CORO1C1 facilitates migration and invasion of CRC cells via PI3K/AKT signaling pathway. CORO1C1 was overexpressed in SW620 and LOVO cell lines. We found that the effects of CORO1C1 were reversed by inhibition of AKT (**Figure 5D–E**). Taken together, the effects of CORO1C on migration and invasion might be mediated leastwise by PI3K/AKT signaling pathway in CRC cells.

DISCUSSION

In this study, we showed that a large number of proteins were connected with Trop2. The expression of these proteins was compared between primary CRC and secondary CRC, and CORO1C was markedly up-regulated in secondary CRC. Reportedly, CORO1C overexpression is related to poor prognosis in hepatocellular carcinoma, primary effusion lymphoma, and gastric cancer (Wu et al., 2010a; Luan et al., 2010; Cheng et al., 2019). To determine the role of CORO1C in CRC, we examined TMAs that included 734 samples of colorectal tissues and the relevant clinical data. With respect to Trop2 expression in colorectal tissues (Ohmachi et al., 2006), high CORO1C expression was detected more often in CRC tissues (66.61%) than in paracancerous tissues (52.14%). The CORO1C expression was associated with histological type, lymph node metastases, distant metastases, AJCC stage, venous invasion, and perineural invasion, indicating the aggressive characteristic of the cancer type. Furthermore, CRC patients with high CORO1C expression had a poor prognosis. Our findings suggested that CORO1C promotes CRC invasiveness and metastasis, i.e., poor disease-free survival and OS rates in patients.

In order to verify the influence of CORO1C on CRC, its expression was downregulated in COCA2 and HCT116 cells, which was inhibited clone formation, cell proliferation, migration, and invasion *in vitro*. The silencing also suppressed the tumor growth *in vivo*. As a target of several microRNAs, CORO1C promotes cell proliferation, invasion, and migration in non-small lung cancer, hepatocellular carcinoma, and triple-negative breast cancer (Wang et al., 2014; Han et al., 2020; Liao and Peng, 2020). It was demonstrated that knockdown of CORO1C dramatically suppressed cell viability, colony formation, mitosis, and metastasis and promotes apoptosis of gastric cancer cells (Cheng et al., 2019). These studies supported our findings that CORO1C plays a tumor-promoting role in CRC.

In order to elucidate the possible mechanisms, GO analysis and GSEA of CORO1C in CRC were performed. The CORO1C-related genes were classified into the biological process group, cellular component group, and molecular function group, indicating that CORO1C is associated with cell adhesion and migration. Cell invasion and metastasis require the involvement of the actin cytoskeleton, which is composed of filamentous actin (F-actin) (Jung et al., 2016). CORO1C is an actin-binding protein with three binding sites, directly regulating the activity of F-actin (Mikati et al., 2015). Several studies suggested a critical role of CORO1C in tumor metastasis. For example, it promotes gastric cancer metastasis via interaction with Arp2, MMP-9, and cathepsin K (Ren et al., 2012; Sun et al., 2014), increases matrix degradation and invasion and decreases adhesion and formation of invadopodia-like extensions in glioblastoma cells (Ziemann et al., 2013). The knockdown of CORO1C impairs cell polarity and cytoskeleton in hepatocellular carcinoma cells (Wang et al., 2013). GSEA demonstrated that CORO1C-related genes are enriched in PI3/AKT signaling pathway. Trop2 increases IGF-1R signaling-mediated AKT/β-catenin/Slug expression essential for cell survival and EMT (Shvartsur and Bonavida, 2015). As a binding protein of Trop2, CORO1C induces EMT through PI3/AKT pathway, which was confirmed by subsequent experiments. With CORO1C knockdown, the expression of EMT biomarkers such as fibronectin and vimentin was decreased, and that of E-cadherin was increased, suggesting that shCORO1C inhibits EMT in CRC cells. The downregulation of CORO1C also reduced the phosphorylation levels of the PI3K/AKT signaling pathway.

Our study nevertheless has some limitations. The other proteins besides CORO1C interacting with Trop2 on CRC were not explored. It's necessary if we want to fully understand the function of Trop2. In addition, the results will be more valuable if the detailed network around CORO1C and the downstream signaling pathways are investigated. These questions need to be researched in the future.

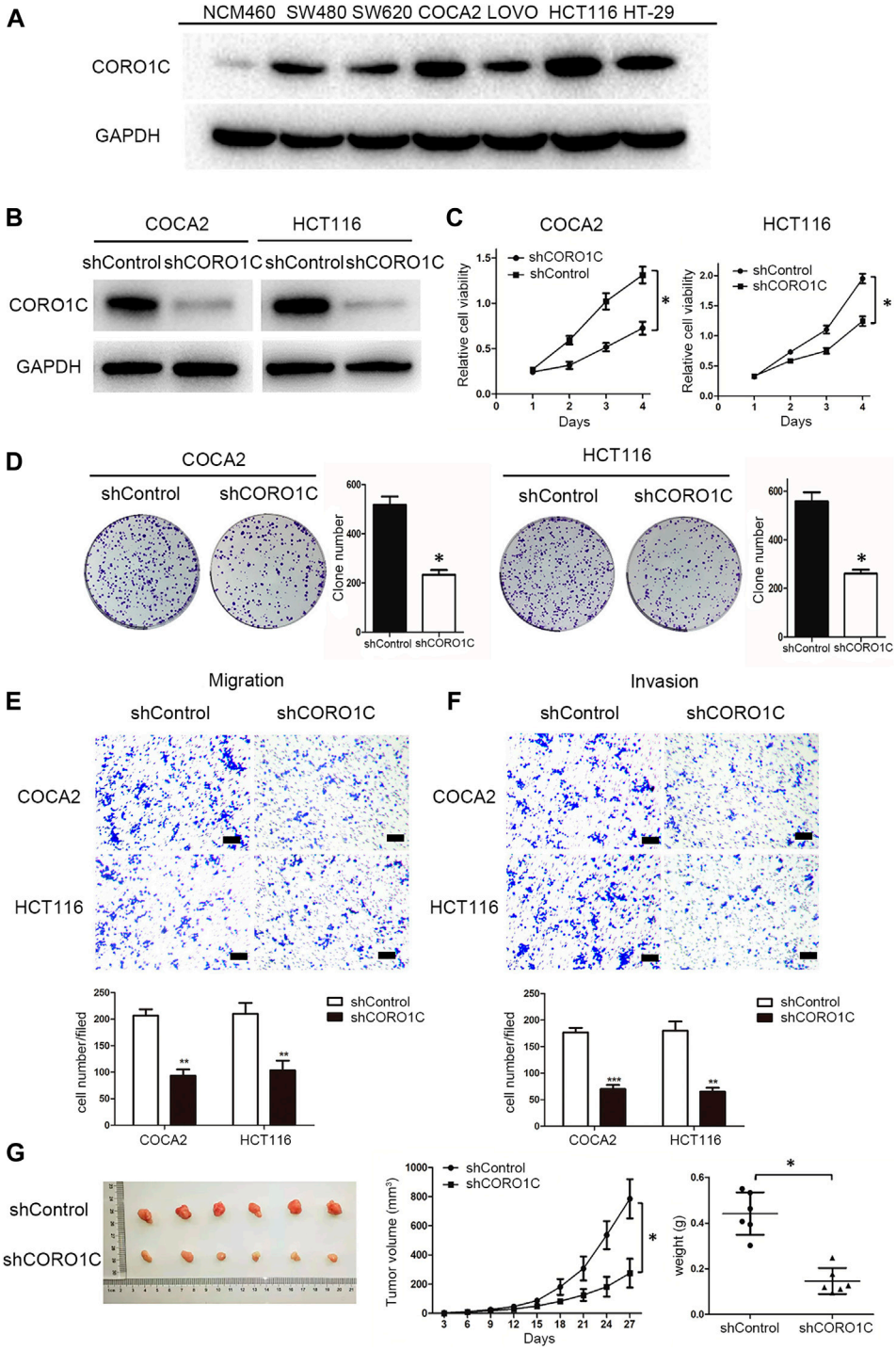

FIGURE 4 | The effects of CORO1C knockdown on CRC growth and metastasis *in vitro* and *in vivo*. **(A)** Levels of CORO1C1 protein expression in CRC cell lines and normal colorectal epithelial cells (NCM460) determined by western blotting. **(B)** COCA2 and HCT116 cells showed a significant decrease in protein level after shCORO1C transfection. **(C)** CORO1C downregulation significantly inhibited the proliferation of both cell lines. **(D)** A significant decrease in cell anchorage-dependent growth was detected after CORO1C knockdown. **(E, F)** Decreased CORO1C expression impaired abilities of migration **(E)** and invasion **(F)** of CRC cells (scale bar, 150 μm). All quantitative data of *in vitro* assays were generated from three replicates **(G)**. The effects of CORO1C downregulation on the tumor growth in the xenograft mouse model (n = 6 mice/per group). $^{*}p < 0.05$, $^{**}p < 0.01$, $^{***}p < 0.001$.

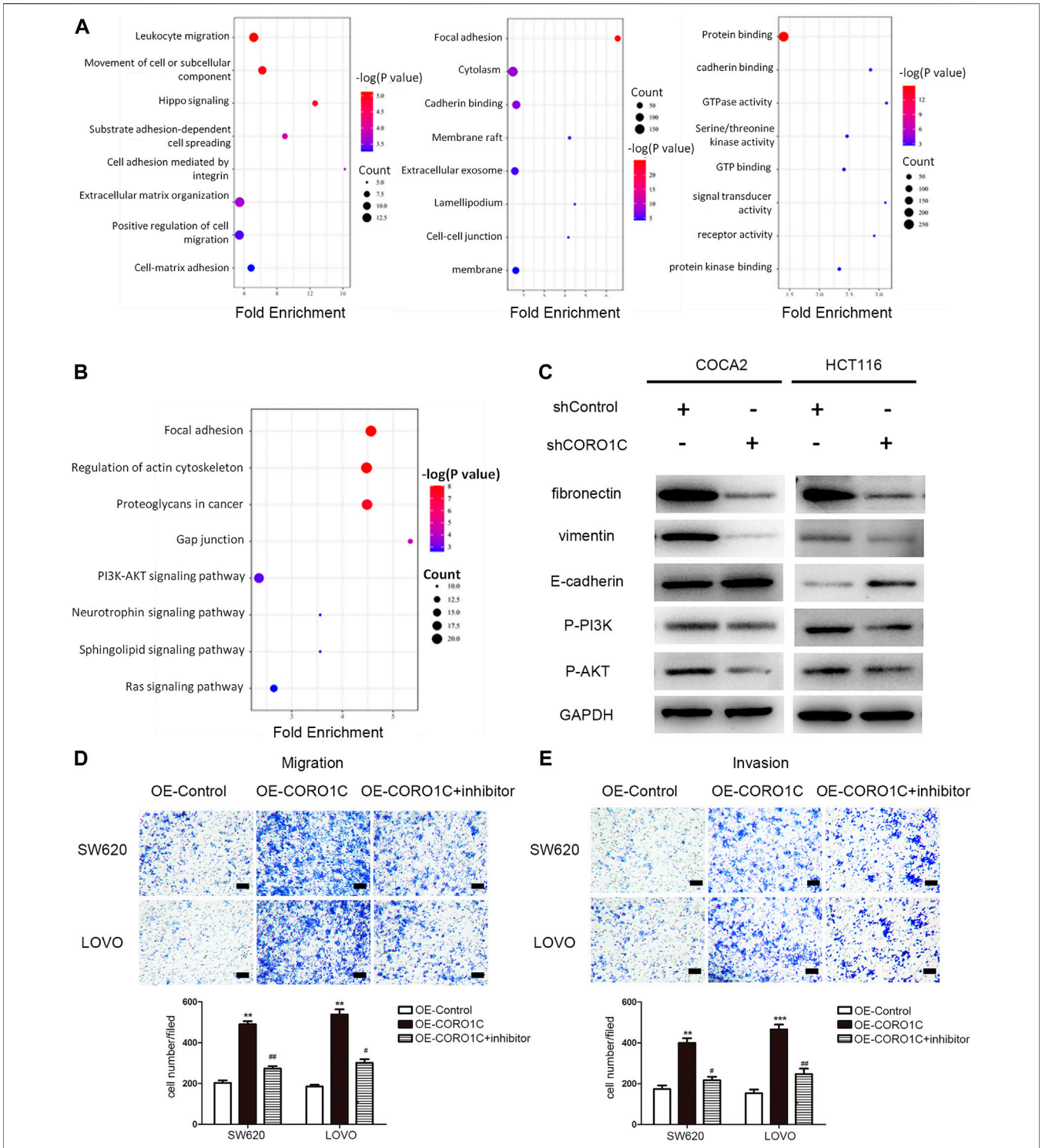

FIGURE 5 | Underlying mechanism of CORO1C in CRC. **(A)** GO analysis of CORO1C-related genes in CRC. **(B)** GSEA of CORO1C-related genes in CRC. **(C)** Expression changes of EMT-related proteins and PI3K/AKT signaling pathway after CORO1C knockdown. **(D, E)** The effects of AKT inhibitor (Miltefosine) on the abilities of migration **(D)** and invasion **(E)** of CRC cells (scale bar, 150 μm). All quantitative data were generated from three replicates. *$p < 0.05$, **$p < 0.01$, ***$p < 0.001$ vs. OE-Control group, #$p < 0.05$, ##$p < 0.01$ vs. OE-CORO1C group.

CONCLUSION

In summary, we demonstrated that high CORO1C expression was associated with increased metastasis and poor prognosis. CORO1C induced EMT of CRC cells via PI3K/AKT signaling pathway and then promoted CRC invasion and metastasis. Therefore, CORO1C may be a potential prognostic biomarker and a therapeutic target for CRC patients.

DATA AVAILABILITY STATEMENT

The original contributions presented in the study are included in the article/**Supplementary Material**, further inquiries can be directed to the corresponding authors.

ETHICS STATEMENT

All animals were maintained according to the guidelines of the laboratory animal center of Inner Mongolia Medical University. The studies involving human participants were reviewed and approved by the Human Research Ethics Committees of the Affiliated Hospital of Nantong University. The participants provided written informed consent to participate in this study.

AUTHOR CONTRIBUTIONS

ZW, LJ, and YS conducted all experiments and prepared the figures and the manuscript. CL and LZ assisted in the study design and critically revised the raw manuscript. XW and HC designed the study, supervised the project and edited the manuscript. All the authors were involved in writing the manuscript, read and approved the final manuscript.

FUNDING

This work was supported by grants from National Natural Science Foundation of China (81960318, 81860534 and 82060438), Natural Science Foundation of Inner Mongolia Autonomous Region (2017MS0837, 2017MS08104 and 2020MS08002), Inner Mongolia Autonomous Region Science and Technology Plan Project (2020GG0273), Inner Mongolia medical university talent team project (NYTD-2017016), Inner Mongolian Science and Technology Innovation Project (201702113), the Natural Science Foundation of the Anhui Higher Education Institutions of China (KJ2020A0611), the Scientific Research Foundation for PhD of Wannan Medical College (WYRCQD2019010), the Scientific Research Project at School-level of Wannan Medical College (WK2020S04, WK202019 and WK2020F09), and the College Student Innovation Training Program of Anhui (S202010368100).

SUPPLEMENTARY MATERIAL

The Supplementary Material for this article can be found online at: https://www.frontiersin.org/articles/10.3389/fmolb.2021.682594/full#supplementary-material

REFERENCES

Brayford, S., Bryce, N. S., Schevzov, G., Haynes, E. M., Bear, J. E., Hardeman, E. C., et al. (2016). Tropomyosin Promotes Lamellipodial Persistence by Collaborating with Arp2/3 at the Leading Edge. *Curr. Biol.* 26, 1312–1318. doi:10.1016/j.cub.2016.03.028

Chan, K. T., Creed, S. J., and Bear, J. E. (2011). Unraveling the enigma: Progress towards Understanding the Coronin Family of Actin Regulators. *Trends Cel Biol.* 21, 481–488. doi:10.1016/j.tcb.2011.04.004

Cheng, X., Wang, X., Wu, Z., Tan, S., Zhu, T., and Ding, K. (2019). CORO1C Expression Is Associated with Poor Survival Rates in Gastric Cancer and Promotes Metastasis *In Vitro*. *FEBS Open Bio*. 9, 1097–1108. doi:10.1002/2211-5463.12639

Gu, Q. Z., Nijiati, A., Gao, X., Tao, K. L., Li, C. D., Fan, X. P., et al. (2018). TROP2 Promotes Cell Proliferation and Migration in Osteosarcoma through PI3K/AKT Signaling. *Mol. Med. Rep.* 18, 1782–1788. doi:10.3892/mmr.2018.9083

Guan, X. (2015). Cancer Metastases: Challenges and Opportunities. *Acta Pharmaceutica Sinica B* 5, 402–418. doi:10.1016/j.apsb.2015.07.005

Han, S., Ding, X., Wang, S., Xu, L., Li, W., and Sun, W. (2020). Mir-133a-3p Regulates Hepatocellular Carcinoma Progression through Targeting Coro1c. *Cmar* 12, 8685–8693. doi:10.2147/CMAR.S254617

Jiang, K., Chen, H., Fang, Y., Chen, L., Zhong, C., Bu, T., et al. (2021). Exosomal ANGPTL1 Attenuates Colorectal Cancer Liver Metastasis by Regulating Kupffer Cell Secretion Pattern and Impeding MMP9 Induced Vascular Leakiness. *J. Exp. Clin. Cancer Res.* 40, 21. doi:10.1186/s13046-020-01816-3

Jung, W., Murrell, M. P., and Kim, T. (2016). F-actin Fragmentation Induces Distinct Mechanisms of Stress Relaxation in the Actin Cytoskeleton. *ACS Macro Lett.* 5, 641–645. doi:10.1021/acsmacrolett.6b00232

Li, X., Teng, S., Zhang, Y., Zhang, W., Zhang, X., Xu, K., et al. (2017). TROP2 Promotes Proliferation, Migration and Metastasis of Gallbladder Cancer Cells by Regulating PI3K/AKT Pathway and Inducing EMT. *Oncotarget* 8, 47052–47063. doi:10.18632/oncotarget.16789

Liao, M., and Peng, L. (2020). MiR-206 May Suppress Non-small Lung Cancer Metastasis by Targeting CORO1C. *Cell. Mol. Biol. Lett.* 25, 22. doi:10.1186/s11658-020-00216-x

Liu, X., Gao, Y., Lin, X., Li, L., Han, X., and Liu, J. (2016). The Coronin Family and Human Disease. *Cpps* 17, 603–611. doi:10.2174/1389203717666151201192011

Luan, S.-L., Boulanger, E., Ye, H., Chanudet, E., Johnson, N., Hamoudi, R. A., et al. (2010). Primary Effusion Lymphoma: Genomic Profiling Revealed Amplification of SELPLG and CORO1C Encoding for Proteins Important for Cell Migration. *J. Pathol.* 222, 166–179. doi:10.1002/path.2752

Mataki, H., Enokida, H., Chiyomaru, T., Mizuno, K., Matsushita, R., Goto, Y., et al. (2015). Downregulation of the microRNA-1/133a Cluster Enhances Cancer Cell Migration and Invasion in Lung-Squamous Cell Carcinoma via Regulation of Coronin1C. *J. Hum. Genet.* 60, 53–61. doi:10.1038/jhg.2014.111

Mikati, M. A., Breitsprecher, D., Jansen, S., Reisler, E., and Goode, B. L. (2015). Coronin Enhances Actin Filament Severing by Recruiting Cofilin to Filament Sides and Altering F-Actin Conformation. *J. Mol. Biol.* 427, 3137–3147. doi:10.1016/j.jmb.2015.08.011

Ohmachi, T., Tanaka, F., Mimori, K., Inoue, H., Yanaga, K., and Mori, M. (2006). Clinical Significance of TROP2 Expression in Colorectal Cancer. *Clin. Cancer Res.* 12, 3057–3063. doi:10.1158/1078-0432.CCR-05-1961

Ren, G., Tian, Q., An, Y., Feng, B., Lu, Y., Liang, J., et al. (2012). Coronin 3 Promotes Gastric Cancer Metastasis via the Up-Regulation of MMP-9 and Cathepsin K. *Mol. Cancer* 11, 67. doi:10.1186/1476-4598-11-67

Shvartsur, A., and Bonavida, B. (2014). Trop2 and its Overexpression in Cancers: Regulation and Clinical/Therapeutic Implications. *Genes Cancer* 6, 84–105. doi:10.18632/genesandcancer.40

Siegel, R. L., Miller, K. D., and Jemal, A. (2020). Cancer Statistics, 2020. *CA A. Cancer J. Clin.* 70, 7–30. doi:10.3322/caac.21590

Sun, Y., Shang, Y., Ren, G., Zhou, L., Feng, B., Li, K., et al. (2014). Coronin3 Regulates Gastric Cancer Invasion and Metastasis by Interacting with Arp2. *Cancer Biol. Ther.* 15, 1163–1173. doi:10.4161/cbt.29501

Sun, X., Xing, G., Zhang, C., Lu, K., Wang, Y., and He, X. (2020). Knockdown of Trop2 Inhibits Proliferation and Migration and Induces Apoptosis of Endometrial Cancer Cells via AKT/β-catenin Pathway. *Cell Biochem. Funct.* 38, 141–148. doi:10.1002/cbf.3450

Thal, D., Xavier, C.-P., Rosentreter, A., Linder, S., Friedrichs, B., Waha, A., et al. (2008). Expression of Coronin-3 (coronin-1C) in Diffuse Gliomas Is Related to Malignancy. *J. Pathol.* 214, 415–424. doi:10.1002/path.2308

Vatandoust, S., Price, T. J., and Karapetis, C. S. (2015). Colorectal Cancer: Metastases to a Single Organ. *Wjg* 21, 11767. doi:10.3748/wjg.v21.i41.11767

Wang, Z.-G., Jia, M.-K., Cao, H., Bian, P., and Fang, X.-D. (2013). Knockdown of Coronin-1C Disrupts Rac1 Activation and Impairs Tumorigenic Potential in Hepatocellular Carcinoma Cells. *Oncol. Rep.* 29, 1066–1072. doi:10.3892/or.2012.2216

Wang, J., Tsouko, E., Jonsson, P., Bergh, J., Hartman, J., Aydogdu, E., et al. (2014). miR-206 Inhibits Cell Migration through Direct Targeting of the Actin-Binding Protein Coronin 1C in Triple-Negative Breast Cancer. *Mol. Oncol.* 8, 1690–1702. doi:10.1016/j.molonc.2014.07.006

Williamson, R. C., Cowell, C. A. M., Reville, T., Roper, J. A., Rendall, T. C. S., and Bass, M. D. (2015). Coronin-1C Protein and Caveolin Protein Provide Constitutive and Inducible Mechanisms of Rac1 Protein Trafficking. *J. Biol. Chem.* 290, 15437–15449. doi:10.1074/jbc.M115.640367

Wu, L., Hou, J. X., Peng, C. W., Zhang, Y. H., Chen, C., Chen, L. D., et al. (2010a). Increased coronin-1C Expression Is Related to Hepatocellular Carcinoma Invasion and Metastasis. *Zhonghua Gan Zang Bing Za Zhi* 18, 516–519. doi:10.3760/CMA.J.ISSN.1007-3418.2010.07.011

Wu, L., Peng, C.-W., Hou, J.-X., Zhang, Y.-H., Chen, C., Chen, L.-D., et al. (2010b). Coronin-1C Is a Novel Biomarker for Hepatocellular Carcinoma Invasive Progression Identified by Proteomics Analysis and Clinical Validation. *J. Exp. Clin. Cancer Res.* 29, 17. doi:10.1186/1756-9966-29-17

Wu, B., Yu, C., Zhou, B., Huang, T., Gao, L., Liu, T., et al. (2017). Overexpression of TROP2 Promotes Proliferation and Invasion of Ovarian Cancer Cells. *Exp. Ther. Med.* 14, 1947–1952. doi:10.3892/etm.2017.4788

Zhao, W., Zhu, H., Zhang, S., Yong, H., Wang, W., Zhou, Y., et al. (2016). Trop2 Is Overexpressed in Gastric Cancer and Predicts Poor Prognosis. *Oncotarget* 7, 6136–6145. doi:10.18632/oncotarget.6733

Zhao, W., Ding, G., Wen, J., Tang, Q., Yong, H., Zhu, H., et al. (2017). Correlation between Trop2 and Amphiregulin Coexpression and Overall Survival in Gastric Cancer. *Cancer Med.* 6, 994–1001. doi:10.1002/cam4.1018

Zhao, W., Jia, L., kuai, X., Tang, Q., Huang, X., Yang, T., et al. (2019). The Role and Molecular Mechanism of Trop2 Induced Epithelial-Mesenchymal Transition through Mediated β-catenin in Gastric Cancer. *Cancer Med.* 8, 1135–1147. doi:10.1002/cam4.1934

Ziemann, A., Hess, S., Bhuwania, R., Linder, S., Kloppenburg, P., Noegel, A. A., et al. (2013). CRN2 Enhances the Invasiveness of Glioblastoma Cells. *Neuro. Oncol.* 15, 548–561. doi:10.1093/neuonc/nos388

Zimmers, S. M., Browne, E. P., Williams, K. E., Jawale, R. M., Otis, C. N., Schneider, S. S., et al. (2018). TROP2 Methylation and Expression in Tamoxifen-Resistant Breast Cancer. *Cancer Cel Int.* 18, 94. doi:10.1186/s12935-018-0589-9

Conflict of Interest: The authors declare that the research was conducted in the absence of any commercial or financial relationships that could be construed as a potential conflict of interest.

frontiers in Molecular Biosciences

ORIGINAL RESEARCH
published: 28 June 2021
doi: 10.3389/fmolb.2021.690500

TRPV4 is a Prognostic Biomarker that Correlates with the Immunosuppressive Microenvironment and Chemoresistance of Anti-Cancer Drugs

*Kai Wang[1,2], Xingjun Feng[2], Lingzhi Zheng[2], Zeying Chai[2], Junhui Yu[2], Xinxin You[2], Xiaodan Li[2] and Xiaodong Cheng[1]**

[1]Department of Gynecologic Oncology, Women's Hospital, School of Medicine, Zhejiang University, Hangzhou, China, [2]Department of Obstetrics and Gynecology, Taizhou Hospital of Zhejiang Province Affiliated to Wenzhou Medical University, Linhai, China

OPEN ACCESS

Edited by:
Wei Zhao,
City University of Hong Kong, Hong Kong

Reviewed by:
Alfredo Ferro,
University of Catania, Italy
Jacopo Junio Valerio Branca,
University of Florence, Italy
Cj Chang,
Hangzhou Normal University, China

***Correspondence:**
Xiaodong Cheng
chengxd@zj.edu.cn

Specialty section:
This article was submitted to Molecular Diagnostics and Therapeutics, a section of the journal Frontiers in Molecular Biosciences

Received: *03 April 2021*
Accepted: *03 June 2021*
Published: *28 June 2021*

Citation:
Wang K, Feng X, Zheng L, Chai Z, Yu J, You X, Li X and Cheng X (2021) TRPV4 is a Prognostic Biomarker that Correlates with the Immunosuppressive Microenvironment and Chemoresistance of Anti-Cancer Drugs. Front. Mol. Biosci. 8:690500. doi: 10.3389/fmolb.2021.690500

Background: Transient receptor potential cation channel subfamily V member 4 (TRPV4) has been reported to regulate tumor progression in many tumor types. However, its association with the tumor immune microenvironment remains unclear.

Methods: TRPV4 expression was assessed using data from The Cancer Genome Atlas (TCGA) and the Genotype-Tissue Expression (GTEx) database. The clinical features and prognostic roles of TRPV4 were assessed using TCGA cohort. Gene set enrichment analysis (GSEA) of TRPV4 was conducted using the R package clusterProfiler. We analyzed the association between TRPV4 and immune cell infiltration scores of TCGA samples downloaded from published articles and the TIMER2 database. The IC50 values of 192 anti-cancer drugs were downloaded from the Genomics of Drug Sensitivity in Cancer (GDSC) database and the correlation analysis was performed.

Results: TRPV4 was highly expressed and associated with worse overall survival (OS), disease-specific survival (DSS), disease-free interval (DFI), and progression-free interval (PFI) in colon adenocarcinoma (COAD) and ovarian cancer. Furthermore, TRPV4 expression was closely associated with immune regulation-related pathways. Moreover, tumor-associated macrophage (TAM) infiltration levels were positively correlated with TRPV4 expression in TCGA pan-cancer samples. Immunosuppressive genes such as PD-L1, PD-1, CTLA4, LAG3, TIGIT, TGFB1, and TGFBR1 were positively

Abbreviations: BLCA, bladder urothelial carcinoma; BRCA, breast invasive carcinoma; CNA, copy number alteration; COAD, colon adenocarcinoma; DFI, disease-free interval; DLBCL, diffuse large B-cell lymphoma; DSS, disease-specific survival; ESCA, esophageal carcinoma; GDSC, genomics of drug sensitivity in cancer; KICH, kidney chromophobe; KIRC, kidney renal clear cell carcinoma; LGG, low-grade glioma; LIHC, liver hepatocellular carcinoma; LUAD, lung adenocarcinoma; LUSC, lung squamous cell carcinoma; OS, overall survival; PFI, progression-free interval; PRAD, prostate adenocarcinoma; READ, rectum adenocarcinoma; SKCM, skin cutaneous melanoma; STAD, stomach adenocarcinoma; TAM, tumor-associated macrophage; TCGA, the Cancer genome atlas; TGCT, testicular germ cell tumors; THCA, thyroid carcinoma; UCEC, uterine corpus endometrial carcinoma; UCS, uterine carcinosarcoma.

correlated with TRPV4 expression in most tumors. In addition, patients with high expression of TRPV4 might be resistant to the treatment of Cisplatin and Oxaliplatin.

Conclusion: Our results suggest that TRPV4 is an oncogene and a prognostic marker in COAD and ovarian cancer. High TRPV4 expression is associated with tumor immunosuppressive status and may contribute to TAM infiltration based on TCGA data from pan-cancer samples. Patients with high expression of TRPV4 might be resistant to the treatment of Cisplatin and Oxaliplatin.

Keywords: TRPV4, tumor immune microenvironment, pan-cancer, tumor immunosuppressive status, tumor-associated macrophage

BACKGROUND

TRPV4 is a broadly expressed polymodally activated ion channel. It is reported to be involved in tumor progression in several tumor types, playing different or even opposite roles therein. For example, overexpression of TRPV4 promotes epithelial to mesenchymal transition in breast cancer cells (Huang et al., 2021). TRPV4 also promotes metastasis of endometrial cancer cells by regulating the RhoA/ROCK1 pathway (Li et al., 2020). In contrast, TRPV4 activation inhibits glioma progression (Huang et al., 2021). Despite these reports, the role of TRPV4 in most tumor types remains unclear.

A number of studies indicate that the tumor immune microenvironment (TIME) has clinicopathological significance

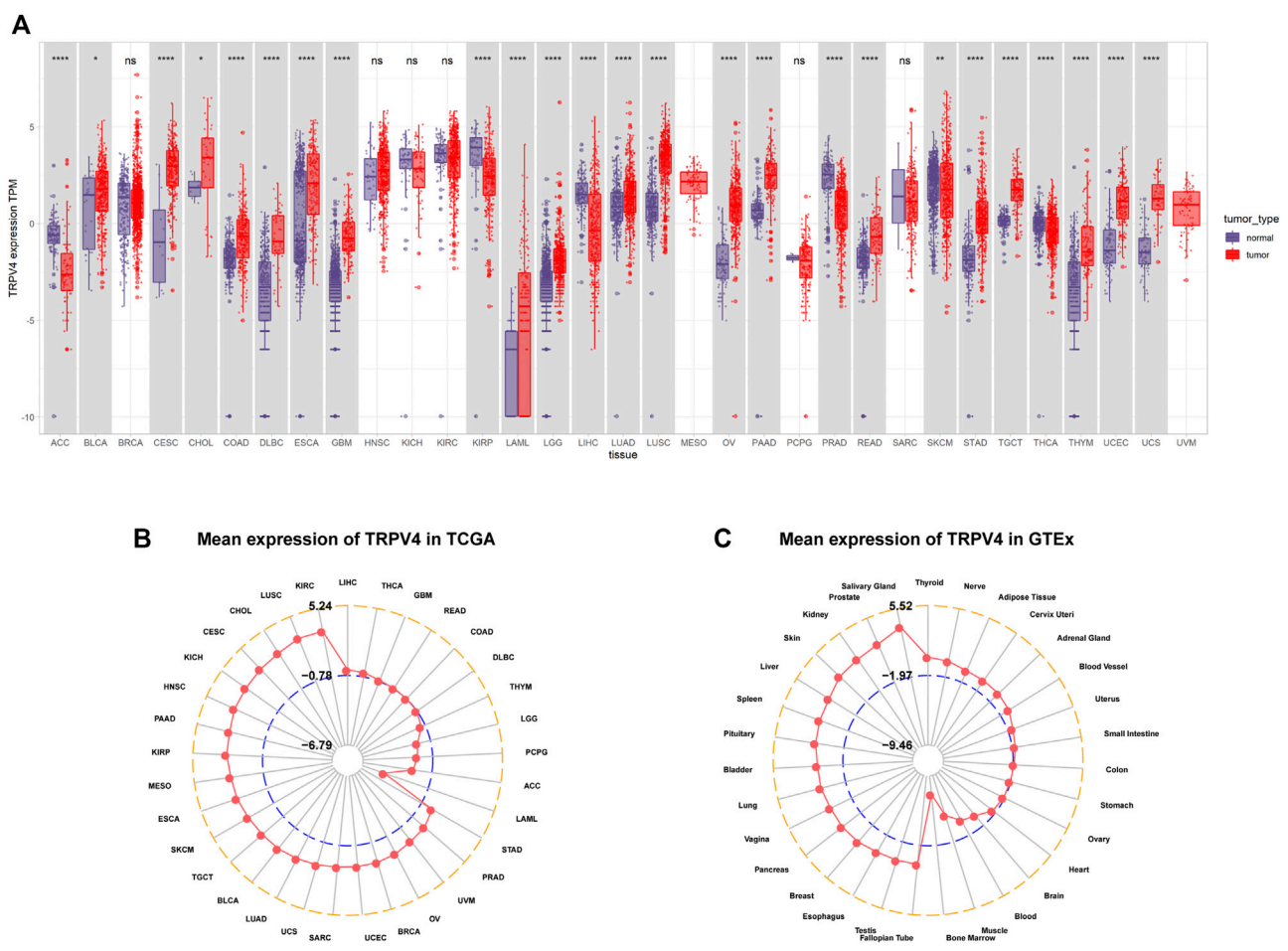

FIGURE 1 | Pan-cancer TRPV4 expression analysis. **(A)** Pan-cancer TRPV4 expression between tumor tissues from TCGA and normal tissues from TCGA and the GTEx database. **(B)** Radar plot shows TRPV4 expression levels in tumor tissues from TCGA. **(C)** Radar plot shows TRPV4 expression levels in normal tissues from the GTEx database.

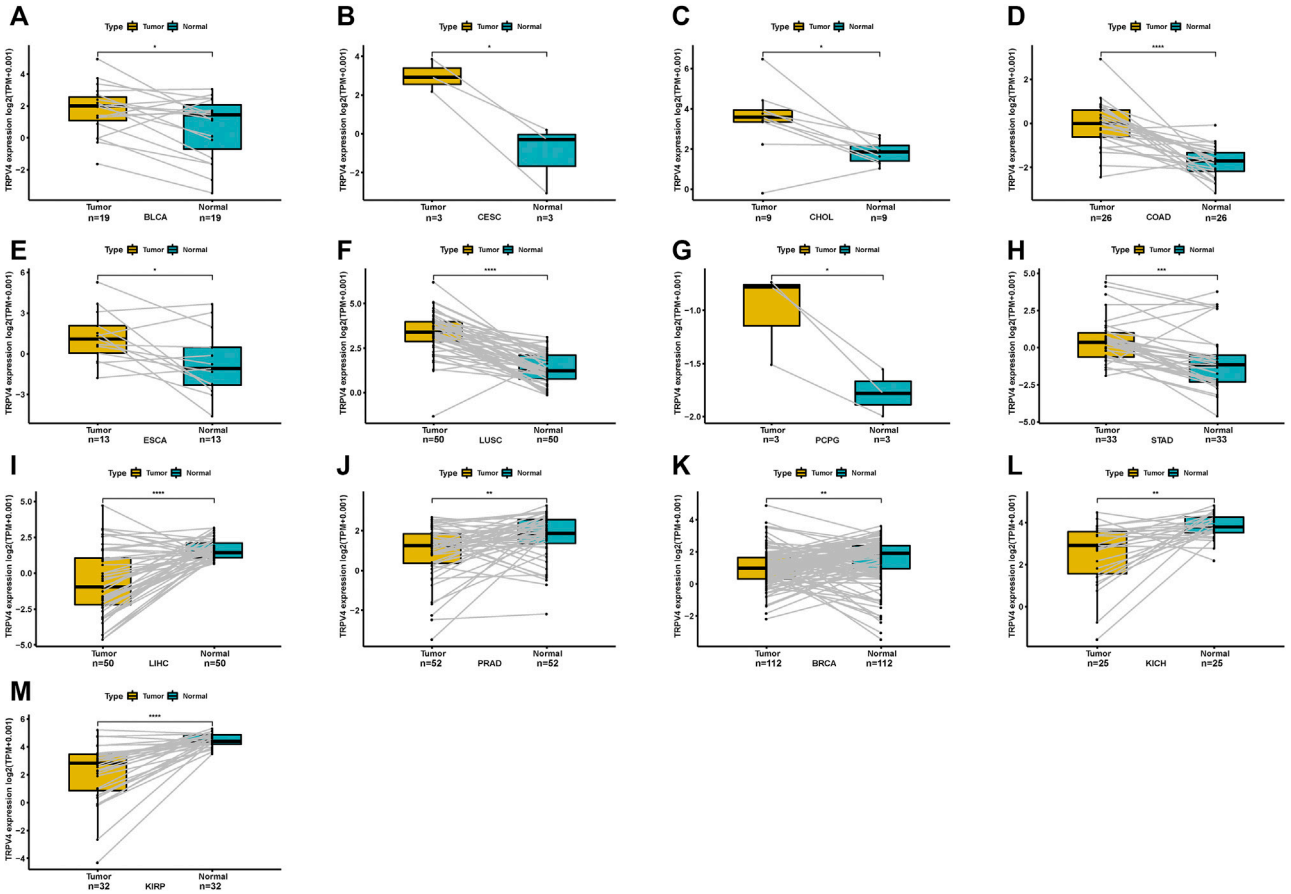

FIGURE 2 | Pan-cancer TRPV4 expression in paired tumor and adjacent normal tissues. **(A–M)** Pan-cancer TRPV4 expression in paired tumor and adjacent normal tissues in indicated tumor types from TCGA.

in predicting therapeutic effect and prognosis in tumor patients (Hubert et al., 2021; Li et al., 2021; Liu et al., 2021). It has been confirmed that solid tumors are composed of malignant, non-malignant, hematopoietic, and mesenchymal cells. Among the non-malignant cells, tumor-associated macrophages (TAMs) play an essential role in promoting tumor progression (Deng et al., 2021; Gill et al., 2021). High TAM levels in tumor tissues influence the immune escape status of tumors, rendering immunotherapy ineffective (Bi et al., 2021). Thus, exploring the relationship between TRPV4 and TAM is helpful to understand the role of TRPV4 in tumor progression.

In our study, we assessed TRPV4 expression using data from The Cancer Genome Atlas (TCGA) and the Genotype-Tissue Expression (GTEx) database and found that TRPV4 was differentially expressed in 25 tumor types. Furthermore, in patients with colon adenocarcinoma (COAD) or ovarian cancer, high TRPV4 expression was associated with worse overall survival (OS), disease-specific survival (DSS), disease-free interval (DFI), and progression-free interval (PFI). TRPV4 is predicted to influence immune regulation-related pathways. We further assessed the association between TRPV4 expression and immune cell infiltration scores and immunosuppressive genes in TCGA pan-cancer samples and found that TRPV4 expression was positively correlated with TAM infiltration and immunosuppressive genes such as PD-L1, PD-1, CTLA4, LAG3, TIGIT, TGFB1, and TGFBR1 in pan-cancer samples. In addition, we further assessed the influence of TRPV4 on resistance of patients to anti-cancer drugs.

Our study explored the role of TRPV4 in TCGA pan-cancer and further highlight a potential function whereby TRPV4 may regulate TAM infiltration and tumor immunosuppressive microenvironment.

METHODS

Data Sources

TCGA and GTEx expression and clinical data were obtained from the UCSC Xena database (https://xenabrowser.net/datapages/). DNA copy number and methylation data were downloaded from the cBioPortal database (https://www.cbioportal.org/). The IC_{50} values of drugs and gene expression profiles in the relative cell lines were downloaded from the Genomics of Drug Sensitivity in

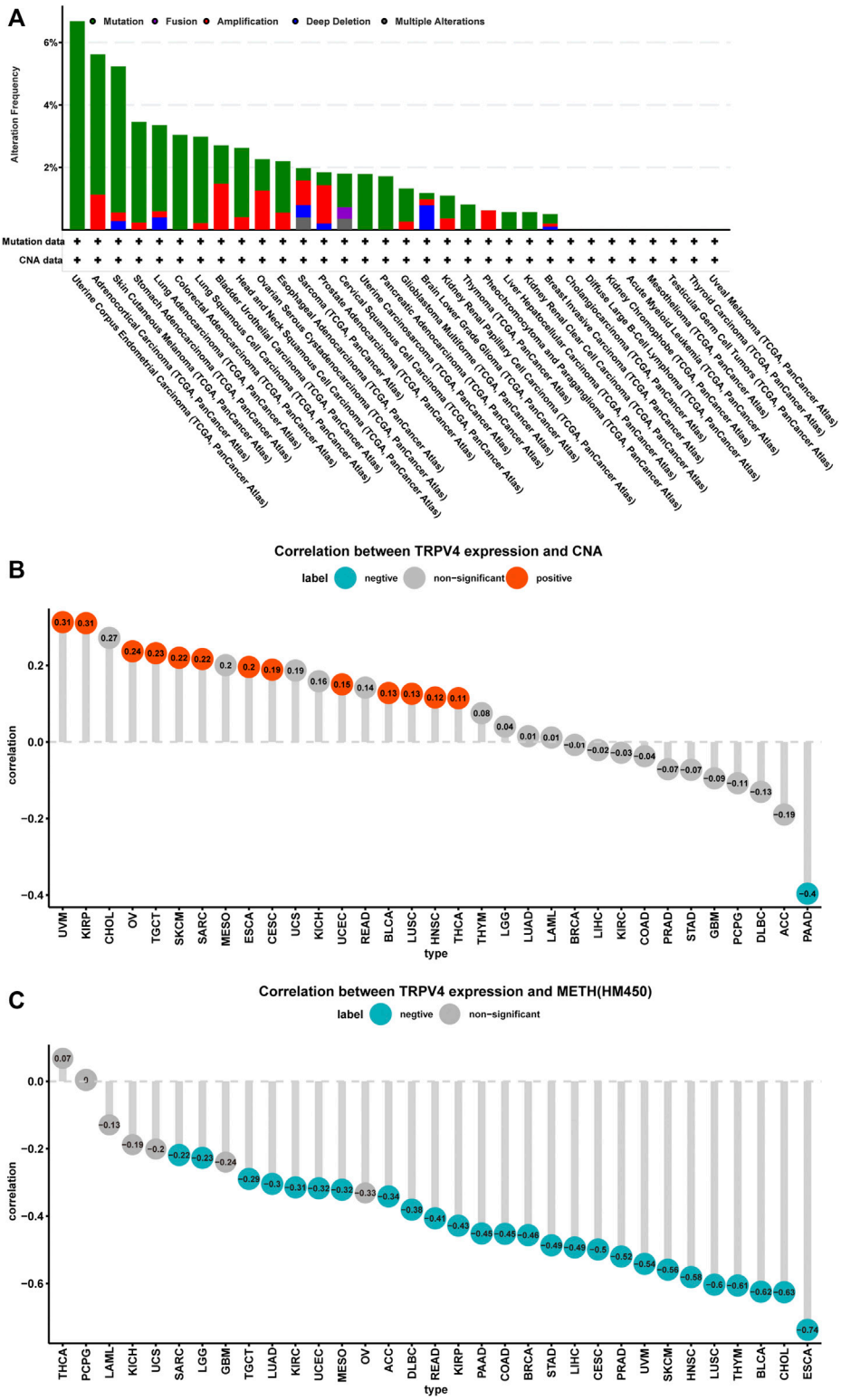

FIGURE 3 | TRPV4 gene alterations in pan-cancer. **(A)** CNA and mutation status of TRPV4 in TCGA pan-cancer samples. **(B)** The correlation between TRPV4 expression and linear copy-number value in TCGA pan-cancer samples. **(C)** The correlation between TRPV4 expression and methylation levels of TRPV4 as a promoter in TCGA pan-cancer samples. The pearson's correlation coefficient was calculated using R software.

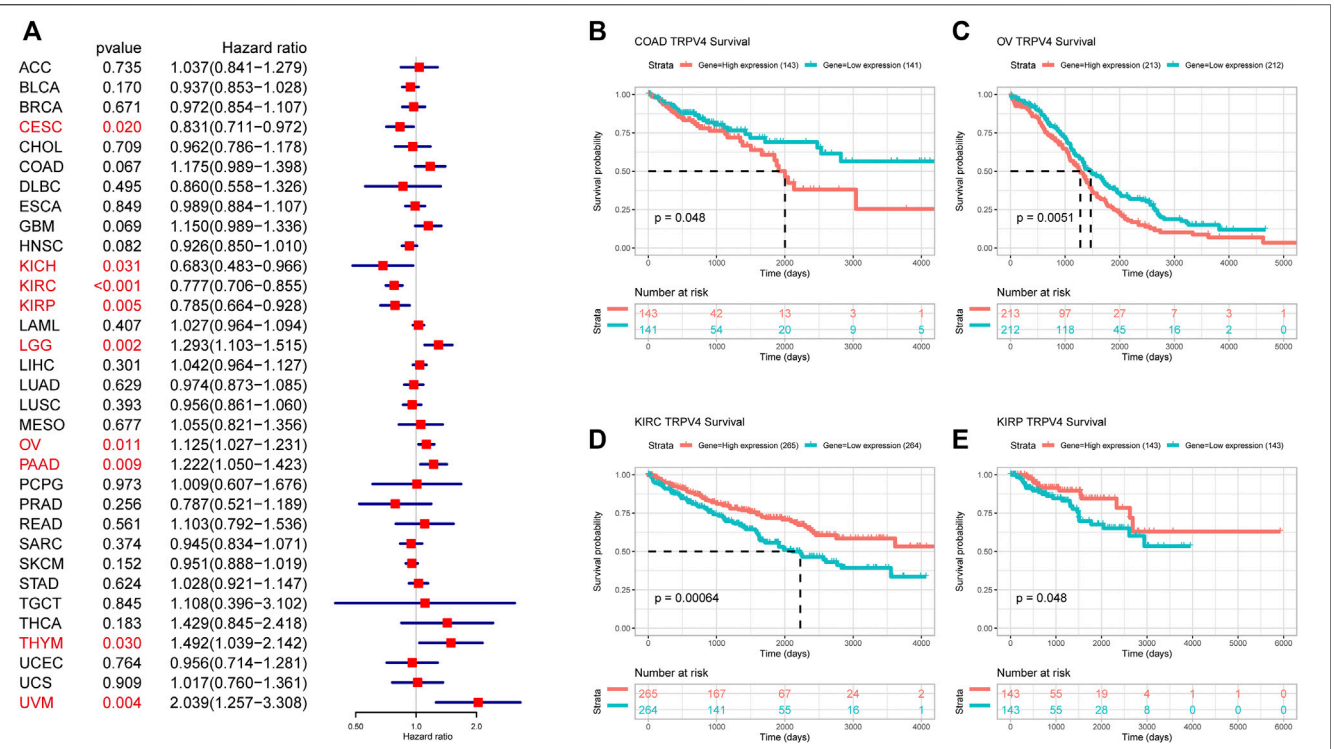

FIGURE 4 | OS analysis of TRPV4 in pan-cancer. **(A)** Forest map shows the univariate Cox regression analysis results for TRPV4 in TCGA pan-cancer samples. Red indicates significant results. **(B)** Kaplan-Meier survival analysis results for TRPV4 in indicated tumor types. The median values of TRPV4 in COAD, OV, KIRC, and KIRP were respectively -0.6416, 0.9493, 3.4129, and 2.4479.

Cancer (GDSC) database (https://www.cancerrxgene.org/). The number of samples used in this study as follows:

1. TCGA tumor samples: ACC-77; BLCA-407; BRCA-1098; CESC-306; CHOL-36; COAD-288; DLBC-47; ESCA-182; GBM-163; HNSC-520; KICH-66; KIRC-531; KIRP-289; LAML-173; LGG-522; LIHC-371; LUAD-515; LUSC-498; MESO-87; OV-427; PAAD-179; PCPG-182; PRAD-496; READ-92; SARC-262; SKCM-469; STAD-414; TGCT-137; THCA-512; UCEC-181; THYM-119; UCS-57; UVM-79.
2. TCGA normal samples: ACC-0; BLCA-19; BRCA-113; CESC-3; CHOL-9; COAD-41; DLBC-0; ESCA-13; GBM-0; HNSC-44; KICH-25; KIRC-72; KIRP-32; LAML-0; LGG-0; LIHC-50; LUAD-59; LUSC-50; MESO-0; OV-0; PAAD-4; PCPG-3; PRAD-52; READ-10; SARC-2; SKCM-1; STAD-36; TGCT-0; THCA-59; UCEC-13; THYM-0; UCS-0; UVM-0.
3. GTEx normal samples: ACC-128; BLCA-9; BRCA-179; CESC-10; CHOL-0; COAD-308; DLBC-444; ESCA-653; GBM-1152; HNSC-0; KICH-28; KIRC-28; KIRP-28; LAML-70; LGG-1152; LIHC-110; LUAD-288; LUSC-288; MESO-0; OV-88; PAAD-167; PCPG-0; PRAD-167; READ-308; SARC-0; SKCM-812; STAD-174; TGCT-165; THCA-279; UCEC-78; THYM-444; UCS-78; UVM-0.

Data Analysis Tools

Copy number alteration (CNA) and mutation status of TRPV4 in TCGA pan-cancer samples were analyzed using the cBioPortal database. The TIMER2 (http://timer.cistrome.org/) database was used to analyze the correlation between immune cell infiltration and TRPV4. R packages ggplot2, ggpubr, and gridExtra were used to draw TRPV4 expression patterns in the R software (3.6.2). R packages survival and survminer were used to perform Kaplan-Meier survival analysis and univariate Cox regression analysis, respectively. Gene set enrichment analysis (GSEA) was performed using the R package clusterProfiler.

TIME Analysis

Immune cell infiltration correlation analysis was performed using two methods: 1) the TIMER2 database was used to analyze the correlation between immune cell infiltration and TRPV4; and 2) the immune cell infiltration scores of TCGA pan-cancer samples were downloaded from the ImmuCellAI database (http://bioinfo.life.hust.edu.cn/web/ImmuCellAI/) to perform the correlation analysis. To compare levels of immune cell infiltration, tumor samples from each tumor type were divided into two groups (high-TRPV4 and low-TRPV4 groups) according to the median expression of TRPV4 in each tumor types.

Statistical Analysis

Data are presented as the mean ± SD. Differences between the groups were analyzed using Student's t-test. Statistical analysis was performed using R 3.6.2. $p < 0.05$ (two-tailed) was considered statistically significant: $^{*}p < 0.05$, $^{**}p < 0.01$, $^{***}p < 0.001$, and $^{****}p < 0.0001$.

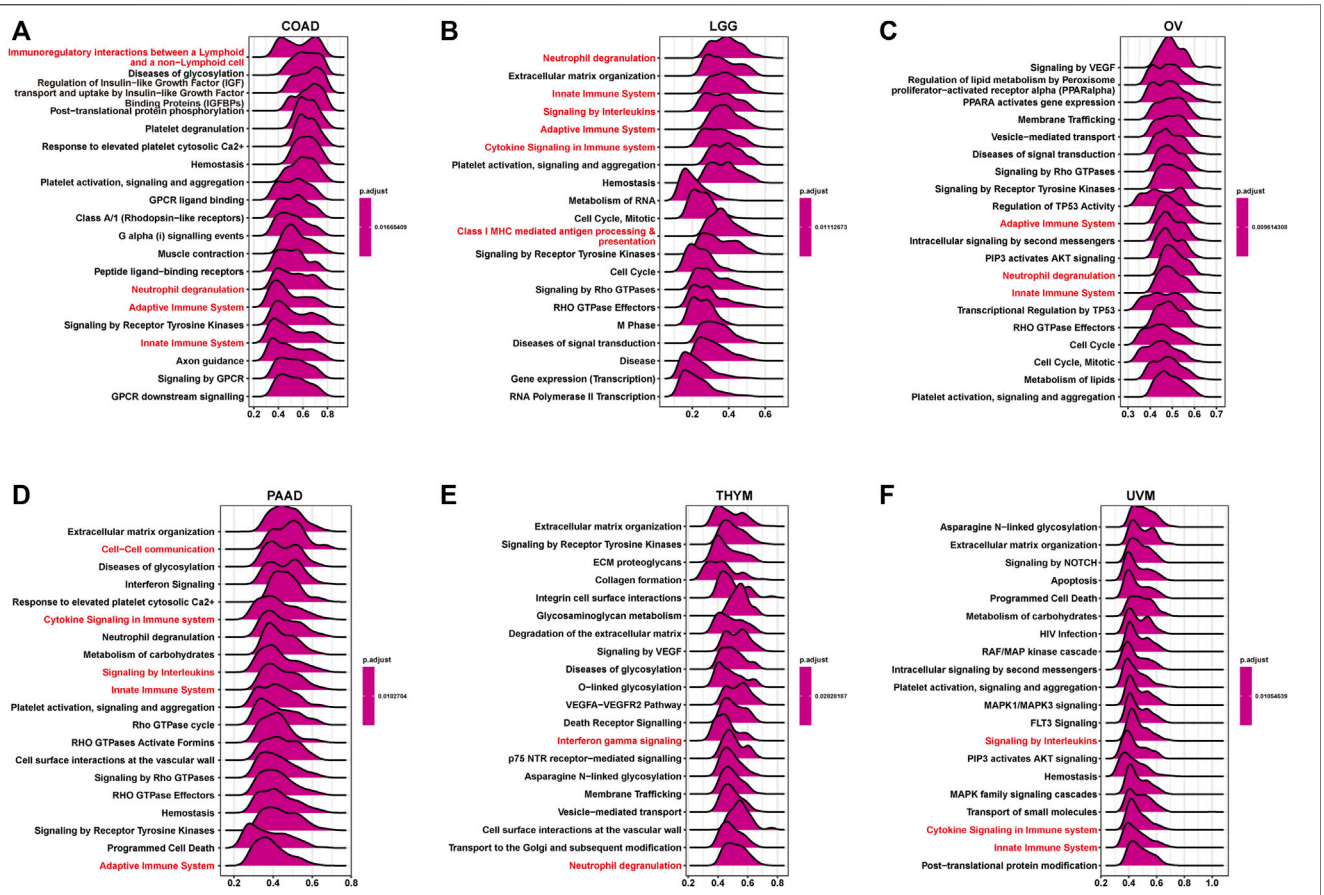

FIGURE 5 | GSEA of TRPV4 in pan-cancer. **(A–F)** The top 20 GSEA results in indicated tumor types (NES ≥ 1.5, adjusted *p*-value < 0.05). Red indicates cell cycle-related or immune regulation-related terms.

RESULTS

TRPV4 Expression in Pan-Cancer

We first assessed TRPV4 expression in tumor tissue samples from TCGA and normal tissue samples from TCGA and the GTEx database. We found that TRPV4 was overexpressed in 19 cancer types, namely, bladder urothelial carcinoma (BLCA), cervical squamous cell carcinoma and endocervical adenocarcinoma (CESC), cholangiocarcinoma (CHOL), colon adenocarcinoma (COAD), lymphoid neoplasm diffuse large B-cell lymphoma (DLBCL), esophageal carcinoma (ESCA), glioblastoma multiforme (GBM), acute myeloid leukemia (LAML), brain low-grade glioma (LGG), lung adenocarcinoma (LUAD), lung squamous cell carcinoma (LUSC), ovarian serous cystadenocarcinoma, pancreatic adenocarcinoma (PAAD), rectum adenocarcinoma (READ), stomach adenocarcinoma (STAD), testicular germ cell tumors (TGCTs), thymoma (THYM), uterine corpus endometrial carcinoma (UCEC), and uterine carcinosarcoma (UCS). In contrast, low TRPV4 expression was observed in only six cancer types, namely, adrenocortical carcinoma (ACC), kidney renal papillary cell carcinoma (KIRP), liver hepatocellular carcinoma (LIHC), prostate adenocarcinoma (PRAD), skin cutaneous melanoma (SKCM), and thyroid carcinoma (THCA) (**Figure 1A**). For tumor tissue data mined from TCGA, TRPV4 expression was highest in kidney renal clear cell carcinoma (KIRC) and lowest in LAML (**Figure 1B**). For normal tissue data from the GTEx database, the highest TRPV4 expression was observed in the salivary gland and prostate, while the lowest expression was detected in bone marrow (**Figure 1C**).

For paired tumors and normal tissues in TCGA, TRPV4 was overexpressed in BLCA, CESC, CHOL, COAD, ESCA, LUSC, pheochromocytoma/paraganglioma (PCPG), and STAD (**Figures 2A–H**), while low TRPV4 expression was observed in LIHC, PRAD, breast invasive carcinoma (BRCA), kidney chromophobe (KICH), and KIRP (**Figures 2I–M**).

TRPV4 Alteration Analysis

We further explored TRPV4 gene alterations in TCGA pan-cancer samples using cBioPortal and observed that patients with UCEC and ACC presented high gene alteration frequencies, including mutations and amplifications (**Figure 3A**). In addition, we downloaded copy number and methylation data

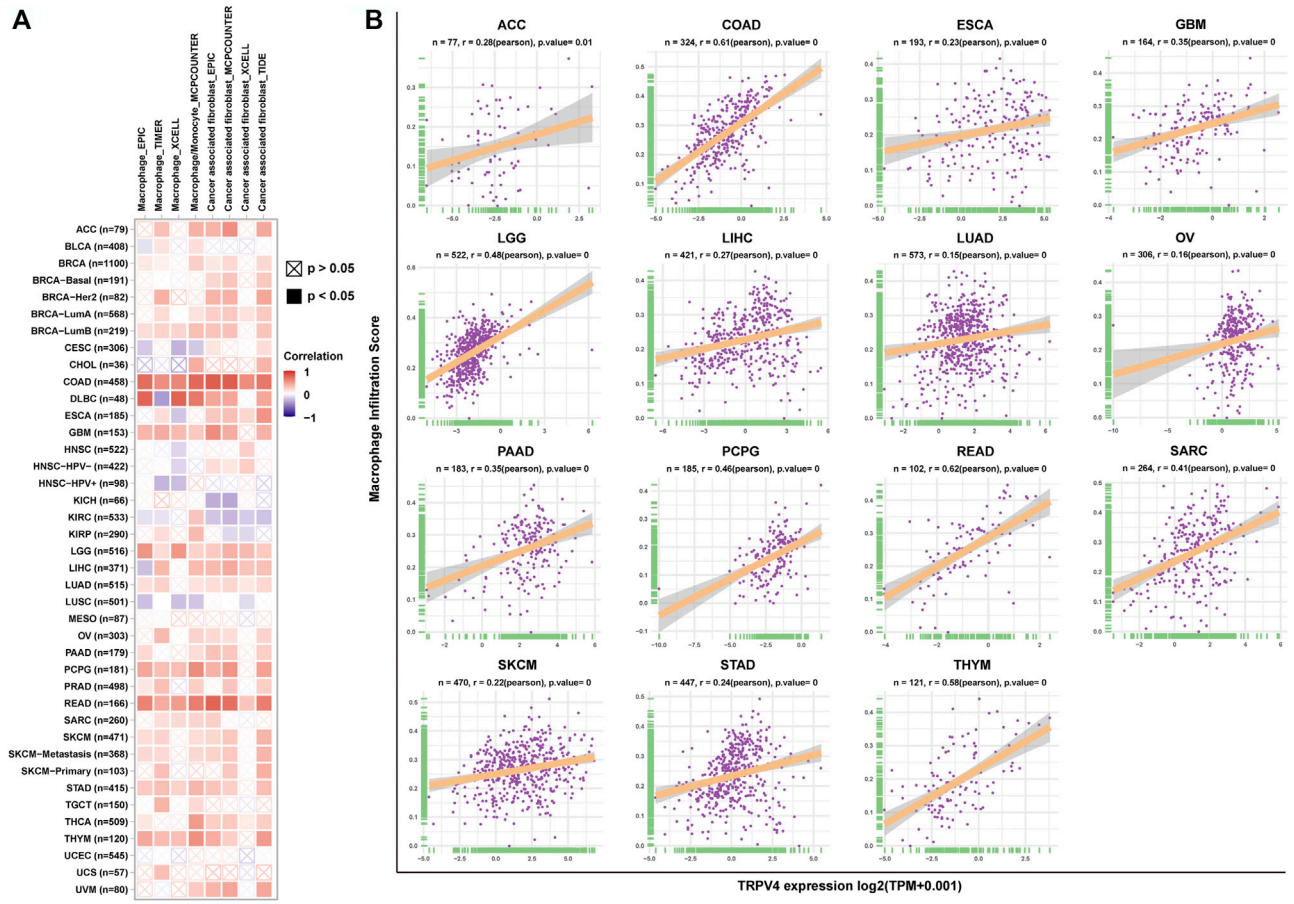

FIGURE 6 | Immune cell infiltration analysis. **(A)** The correlation between TRPV4 expression and TAM and CAF infiltration levels in TCGA pan-cancer samples using the TIMER2 database. **(B)** The correlation between TRPV4 expression and TAM infiltration levels in TCGA pan-cancer samples using data from the ImmuCellAI database. The pearson's correlation coefficient was calculated using R software.

for TRPV4 and performed a correlation analysis. The results revealed that copy number values were positively correlated with TRPV4 expression (**Figure 3B**), while methylation levels were negatively correlated with TRPV4 expression in most tumor types from TCGA (**Figure 3C**). These results indicate that high copy number values and low methylation levels contribute to high TRPV4 expression in pan-cancer.

Prognostic Role of TRPV4

To further evaluate the significance of TRPV4 as a prognostic marker in tumor patients, we performed univariate Cox regression analysis and Kaplan-Meier survival analysis using TCGA pan-cancer data. Results from the univariate Cox regression analysis suggested that TRPV4 was a risk factor for OS in LGG, ovarian cancer, PAAD, THYM, and UVM patients, while it was a protective factor in CESC, KICH, KIRC, and KIRP (**Figure 4A**). Kaplan-Meier survival analysis revealed that high TRPV4 expression predicted poorer OS in patients with ACC, HNSC, KIRP, LIHC, LUAD, and UVM and better OS in patients with KIRC and KIRP (**Figure 4B**). We further conducted DFI, PFI, and DSS assessments using univariate Cox regression analysis. For DFI, TRPV4 was a risk factor in PAAD and a protective factor in UCEC and UCS (**Supplementary Figure S1A**). For PFI, TRPV4 was a risk factor in COAD, LGG, PAAD, and UVM and a protective factor in KICH, KIRC, KIRP, and UCEC (**Supplementary Figure S1B**). For DSS, TRPV4 was a risk factor in COAD, GBM, LGG, LUSC, ovarian cancer, PAAD, THYM, and UVM and a protective factor in CESC, KICH, KIRC, KIRP, and LUSC (**Supplementary Figure S1C**).

GSEA of TRPV4

GSEA based on the Reactome pathway database was used to predict pathways in which TRPV4 may be involved in pan-cancer. The GSEA results revealed that TRPV4 participates in immune regulation-related pathways in pan-cancer such as immunoregulatory interactions between lymphoid and non-lymphoid cells, the adaptive immune system, and the innate immune system (**Figures 5A–F**).

TIME Analysis

Having predicted that TRPV4 is closely related to immune regulation pathways through GSEA analysis, we focused on

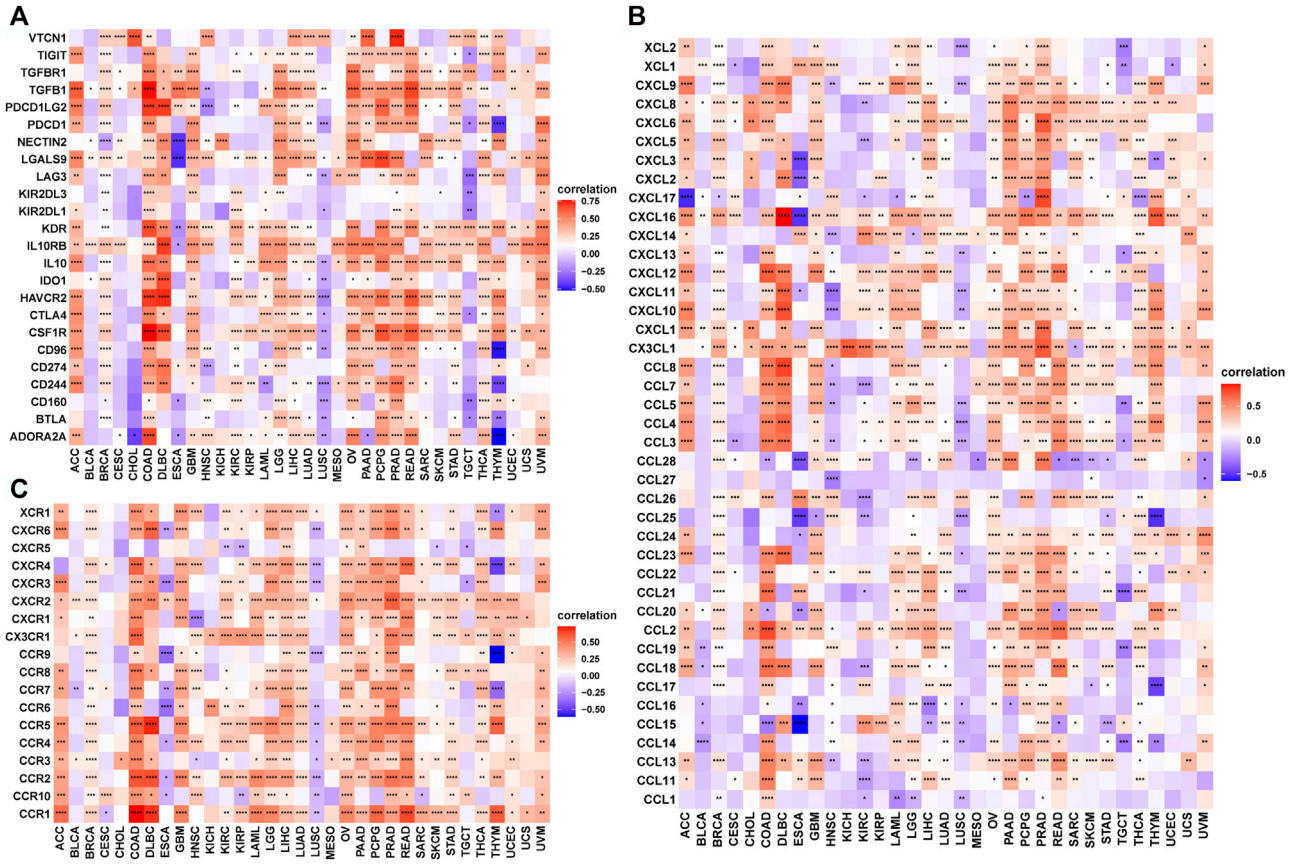

FIGURE 7 | The correlation between TRPV4 and immunosuppressive genes. **(A)** Heatmap representing the correlation between TRPV4 expression and immunosuppressive status-related genes. **(B)** Heatmap representing the correlation between TRPV4 expression and chemokine genes. **(C)** Heatmap representing the correlation between TRPV4 expression and chemokine receptor genes. The pearson's correlation coefficient was calculated using R software.

the infiltration of immune cells in the tumor microenvironment. We found that TRPV4 expression was positively correlated with the infiltration level of TAMs and tumor associated fibroblasts (CAFs) in pan-cancer using the TIMER2 database (**Figure 6A**). To validate this result, we downloaded immune cell infiltration data from the ImmuCellAI database and performed a correlation analysis, obtaining the same result that TRPV4 expression was positively correlated with the level of TAMs in pan-cancer (**Figure 6B**).

Next, we explored the correlation between TRPV4 with immune checkpoints, immunosuppressive genes, chemokines, and chemokine receptors. Immune checkpoint and immunosuppressive genes such as PD-L1, PD-1, CTLA4, LAG3, TIGIT, TGFB1, and TGFBR1 were positively correlated with TRPV4 in most tumors (**Figure 7A**). Chemokines and chemokine receptors such as CCL5, CCL5, CCR4, and CCR5 were also positively correlated with TRPV4 expression in most tumors (**Figures 7B,C**).

Drug Resistance Analysis

We downloaded the IC_{50} values of anti-cancer drugs and gene expression profiles in the relative cell lines from the GDSC database. To explore the influence of TRPV4 expression on the sensitivity of anti-cancer drugs, we divided the tumor cells into high- and low-TRPV4 groups and compared their IC_{50} values. We found that the IC_{50} values of several anti-cancer drugs decreased in the high-TRPV4 group, including sapitinib (an EGFR inhibitor) and selumetinib (a MEK1/2 inhibitor) (**Figure 8A**), indicating that patients exhibiting high TRPV4 expression levels are relatively sensitive to these anti-cancer drugs. In comparison, the IC_{50} values of platinum drugs such as cisplatin and oxaliplatin increased in the high-TRPV4 group (**Figures 8A–C**). Moreover, the IC_{50} values of cisplatin and oxaliplatin were positively correlated with TRPV4 expression (**Figures 8D,E**). These results indicate that patients exhibiting high TRPV4 expression levels may be resistant to cisplatin and oxaliplatin treatment.

DISCUSSION

TRPV4 is an omnipresent polymodally activated ion channel. Recent studies have shown that TRPV4 plays a role in a number of different functions in the body, including cancer. Moreover, the functions of TRPV4 are different or even opposite in different tumors. TRPV4 plays an oncogenic role in breast cancer,

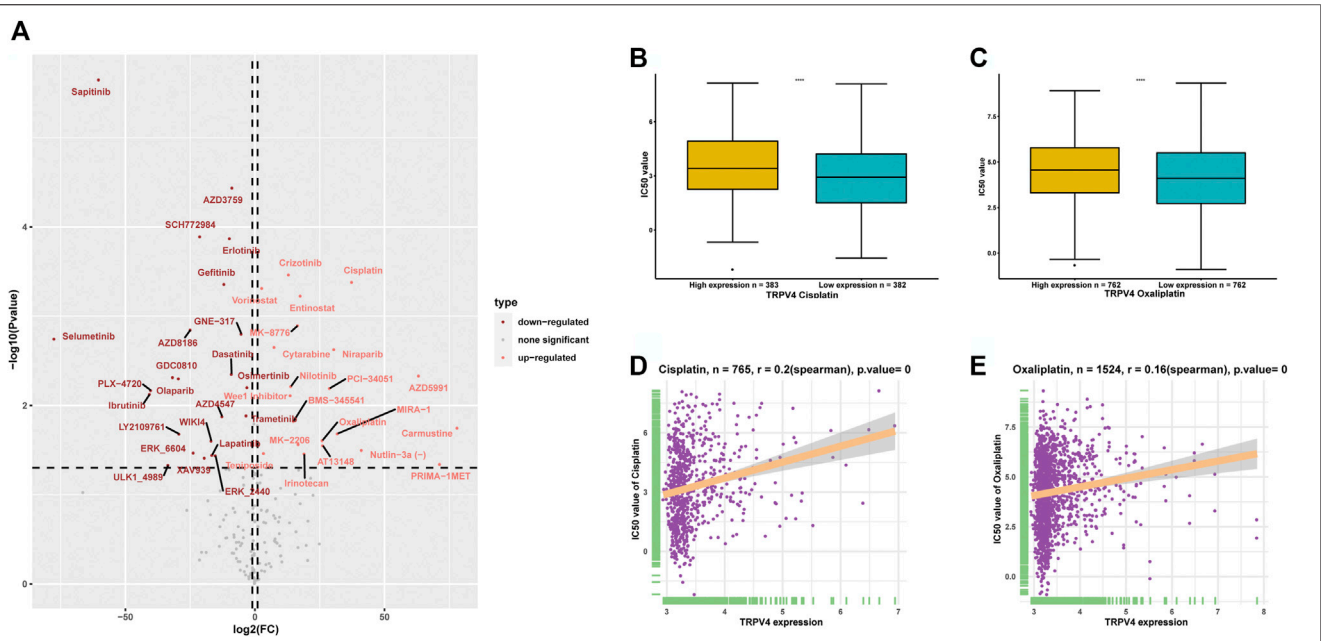

FIGURE 8 | Anti-cancer drug sensitivity analysis. **(A)** Volcano map representing the differences in IC_{50} values of anti-cancer drugs between high- and low-TRPV4 groups. **(B)** IC_{50} values of cisplatin in high- and low-TRPV4 groups. **(C)** IC_{50} values of oxaliplatin in high- and low-TRPV4 groups. **(D)** The correlation between TRPV4 expression and IC_{50} values of cisplatin. **(E)** The correlation between TRPV4 expression and IC_{50} values of oxaliplatin. The spearman's correlation coefficient was calculated using R software.

endometrial cancer, gastric cancer, oral squamous cell carcinoma, and COAD (Arbabian et al., 2020; Azimi et al., 2020; Fujii et al., 2020; Li et al., 2020; Wang et al., 2020) and a suppressor gene role in glioma (Huang et al., 2021). However—in many other tumor types—the function of TRPV4 remains unclear.

We first assessed TRPV4 expression using tumor tissue data from TCGA and normal tissue data from TCGA and the GTEx database. We found that TRPV4 was overexpressed in 19 cancer types, namely, BLCA, CESC, CHOL, COAD, DLBCL, ESCA, GBM, LAML, LGG, LUAD, LUSC, ovarian cancer, PAAD, READ, STAD, TGCT, THYM, UCEC, and UCS. In contrast, low TRPV4 expression was observed in only six cancer types, namely, ACC, KIRP, LIHC, PRAD, SKCM, and THCA. In COAD and ovarian cancer, TRPV4 was over-expressed; moreover, high expression levels of TRPV4 predicted worse OS in tumor patients. It has been reported that TRPV4 promotes the progression of COAD (Arbabian et al., 2020), while no reports on TRPV4 in ovarian cancer are available.

Tumor-acclimatized immune and stromal cells in the tumor microenvironment such as TAMs and CAFs play a vital role in accelerating tumor progression. The remodeling of immune cells by tumor cells can lead to immune escape (Komohara and Takeya, 2017). In our study, we predicted that TRPV4 is involved in immune regulation-related pathways using GSEA. Moreover, we proved that TRPV4 expression was positively correlated with TAMs and CAFs using two different methods: the TIMER2 and ImmuCellAI databases. Our results revealed that TRPV4 regulates the infiltration levels of TAMs and CAFs either directly or indirectly. Based on these results, we further explored the correlation between TRPV4 and immune checkpoints, immunosuppressive genes, chemokines, and chemokine receptors. Immune checkpoint and immunosuppressive genes such as PD-L1, PD-1, CTLA4, LAG3, TIGIT, TGFB1, and TGFBR1 were positively correlated with TRPV4 in most tumors. Chemokines and chemokine receptors such as CCL5, CCL5, CCR4, and CCR5 were also positively correlated with TRPV4 expression in most tumors. These results indicate that TRPV4 is closely associated with immune regulation. Patients with tumors exhibiting high TRPV4 expression levels may manifest an immunosuppressive status.

To explore the indicator function of TRPV4 in anti-cancer drug selection, we analyzed the association between TRPV4 expression and IC_{50} values of anti-cancer drugs using data from the GDSC database. We found that the IC_{50} values of several anti-cancer drugs, including sapitinib (an EGFR inhibitor) and selumetinib (a MEK1/2 inhibitor), decreased in the high-TRPV4 group, indicating that patients exhibiting high TRPV4 expression levels may be relatively sensitive to these anti-cancer drugs. In comparison, the IC_{50} values of platinum drugs—such as cisplatin and oxaliplatin—increased in the high-TRPV4 group. Moreover, the IC_{50} values of cisplatin and oxaliplatin were positively correlated with TRPV4 expression. These results indicate that patients exhibiting high TRPV4 expression levels may be resistant to cisplatin and oxaliplatin treatment.

CONCLUSION

We conducted a comprehensive assessment of TRPV4, revealing its potential cancer-promoting effect as well as its role as an indicator of patient prognosis. Importantly, high TRPV4 expression often indicates tumor immunosuppression, which may render immune checkpoint inhibitors unsuitable for treatment. Finally, we found that patients exhibiting high TRPV4 expression levels may be resistant to cisplatin and oxaliplatin treatment and sensitive to sapitinib (an EGFR inhibitor) and selumetinib (a MEK1/2 inhibitor) treatment. The impact of TRPV4 on the progression of numerous cancers requires a comprehensive understanding of its role as a biomarker for patient prognosis based on its broad influence on anti-cancer drug efficacy.

DATA AVAILABILITY STATEMENT

The datasets presented in this study can be found in online repositories. The names of the repository/repositories and accession number(s) can be found in the article/ **Supplementary Material**.

ETHICS STATEMENT

The studies involving human participants were reviewed and approved by Ethical Committee of taizhou Hospital of Zhejiang Province. The patients/participants provided their written informed consent to participate in this study. Written informed consent was obtained from the individual(s) for the publication of any potentially identifiable images or data included in this article.

AUTHOR CONTRIBUTIONS

XC, XF and KW conceived the project and participated in the study design and interpretation of the results. KW wrote the manuscript. XC, LZ and JY participated in the study design and helped draft the manuscript. ZC, XY and LX participated in data interpretation and provided a critical review of the manuscript. All authors have read and approved the final manuscript.

FUNDING

This study was supported by the Science and Technology Bureau of Zhejiang Province (Grant No. LGF19H160019), Taizhou Science and Technology Project, Zhejiang Province (1802KY10, 1902ky29), and the Scientific Innovation Foundation of Taizhou Hospital of Zhejiang Province (18EZZDC7, 15EZD15).

ACKNOWLEDGMENTS

We thank the public database TCGA, GTEx, Reactome, ImmuCellAI, GDSC, and cBioportal for providing data for our research.

SUPPLEMENTARY MATERIAL

The Supplementary Material for this article can be found online at: https://www.frontiersin.org/articles/10.3389/fmolb.2021.690500/full#supplementary-material

REFERENCES

Arbabian, A., Iftinca, M., Altier, C., Singh, P. P., Isambert, H., and Coscoy, S. (2020). Mutations in Calmodulin-Binding Domains of TRPV4/6 Channels Confer Invasive Properties to colon Adenocarcinoma Cells. *Channels*. 14 (1), 101–109. doi:10.1080/19336950.2020.1740506

Azimi, I., Robitaille, M., Armitage, K., So, C. L., Milevskiy, M. J. G., Northwood, K., et al. (2020). Activation of the Ion Channel TRPV4 Induces Epithelial to Mesenchymal Transition in Breast Cancer Cells. *Int J Mol Sci*. 21 (24), 9417. doi:10.3390/ijms21249417

Bi, K., He, M. X., Bakouny, Z., Kanodia, A., Napolitano, S., Wu, J., et al. (2021). Tumor and Immune Reprogramming during Immunotherapy in Advanced Renal Cell Carcinoma. *Cancer Cell*. 39, 649–661. doi:10.1016/j.ccell.2021.02.015

Deng, X.-X., Jiao, Y.-N., Hao, H.-F., Xue, D., Bai, C.-C., and Han, S.-Y. (2021). Taraxacum Mongolicum Extract Inhibited Malignant Phenotype of Triple-Negative Breast Cancer Cells in Tumor-Associated Macrophages Microenvironment through Suppressing IL-10/STAT3/PD-L1 Signaling Pathways. *J. Ethnopharmacology*. 274, 113978. doi:10.1016/j.jep.2021.113978

Fujii, S., Tajiri, Y., Hasegawa, K., Matsumoto, S., Yoshimoto, R. U., Wada, H., et al. (2020). The TRPV4-AKT axis Promotes Oral Squamous Cell Carcinoma Cell Proliferation via CaMKII Activation. *Lab. Invest.* 100 (2), 311–323. doi:10.1038/s41374-019-0357-z

Gill, C. M., D'Andrea, M. R., Tomita, S., Suhner, J., Umphlett, M., Zakashansky, K., et al. (2021). Tumor Immune Microenvironment in Brain Metastases from Gynecologic Malignancies. *Cancer Immunol. Immunother.* [Epub ahead of print]. doi:10.1007/s00262-021-02909-4

Huang, T., Xu, T., Wang, Y., Zhou, Y., Yu, D., Wang, Z., et al. (2021). Cannabidiol Inhibits Human Glioma by Induction of Lethal Mitophagy through Activating TRPV4. *Autophagy*, 1–15. doi:10.1080/15548627.2021.1885203

Hubert, P., Roncarati, P., Demoulin, S., Pilard, C., Ancion, M., Reynders, C., et al. (2021). Extracellular HMGB1 Blockade Inhibits Tumor Growth through Profoundly Remodeling Immune Microenvironment and Enhances Checkpoint Inhibitor-Based Immunotherapy. *J. Immunother. Cancer*. 9 (3), e001966. doi:10.1136/jitc-2020-001966

Komohara, Y., and Takeya, M. (2017). CAFs and TAMs: Maestros of the Tumour Microenvironment. *J. Pathol.* 241 (3), 313–315. doi:10.1002/path.4824

Li, R., Liu, Y., Yin, R., Yin, L., Li, K., Sun, C., et al. (2021). The Dynamic Alternation of Local and Systemic Tumor Immune Microenvironment during Concurrent Chemoradiotherapy of Cervical Cancer: A Prospective Clinical Trial. *Int. J. Radiat. Oncology Biology Physics.*, S0360–S3016(21)00243-251. doi:10.1016/j.ijrobp.2021.03.003

Li, X., Cheng, Y., Wang, Z., Zhou, J., Jia, Y., He, X., et al. (2020). Calcium and TRPV4 Promote Metastasis by Regulating Cytoskeleton through the RhoA/ROCK1 Pathway in Endometrial Cancer. *Cell Death Dis.* 11 (11), 1009. doi:10.1038/s41419-020-03181-7

Liu, C., Zhou, X., Long, Q., Zeng, H., Sun, Q., Chen, Y., et al. (2021). Small Extracellular Vesicles Containing miR-30a-3p Attenuate the Migration and Invasion of Hepatocellular Carcinoma by Targeting SNAP23 Gene. *Oncogene*. 40 (2), 233–245. doi:10.1038/s41388-020-01521-7

Wang, H., Zhang, B., Wang, X., Mao, J., Li, W., Sun, Y., et al. (2020). TRPV4 Overexpression Promotes Metastasis through Epithelial-Mesenchymal Transition in Gastric Cancer and Correlates with Poor Prognosis. *Onco Targets Ther*. 13, 8383–8394. doi:10.2147/OTT.S256918

Conflict of Interest: The authors declare that the research was conducted in the absence of any commercial or financial relationships that could be construed as a potential conflict of interest.

frontiers in Molecular Biosciences

ORIGINAL RESEARCH
published: 30 June 2021
doi: 10.3389/fmolb.2021.691143

Development and Validation of a Prognostic Classifier Based on Lipid Metabolism–Related Genes in Gastric Cancer

Xiao-Li Wei[1†], Tian-Qi Luo[2†], Jia-Ning Li[3†], Zhi-Cheng Xue[2], Yun Wang[4], You Zhang[5], Ying-Bo Chen[2] and Chuan Peng[6*]*

[1]Department of Medical Oncology, Sun Yat-sen University Cancer Center, State Key Laboratory of Oncology in South China, Collaborative Innovation Center for Cancer Medicine, Guangzhou, China, [2]Department of Gastric Surgery, Sun Yat-sen University Cancer Center, State Key Laboratory of Oncology in South China, Collaborative Innovation Center for Cancer Medicine, Guangzhou, China, [3]Department of Clinical Research, Sun Yat-sen University Cancer Center, State Key Laboratory of Oncology in South China, Collaborative Innovation Center for Cancer Medicine, Guangzhou, China, [4]Department of Hematologic Oncology, Sun Yat-sen University Cancer Center, State Key Laboratory of Oncology in South China, Collaborative Innovation Center for Cancer Medicine, Guangzhou, China, [5]Zhongshan School of Medicine, Sun Yat-sen University Cancer Center, Guangzhou, China, [6]Department of Ultrasound, Sun Yat-sen University Cancer Center, State Key Laboratory of Oncology in South China, Collaborative Innovation Center for Cancer Medicine, Guangzhou, China

Background: Dysregulation of lipid metabolism plays important roles in the tumorigenesis and progression of gastric cancer (GC). The present study aimed to establish a prognostic model based on the lipid metabolism–related genes in GC patients.

Materials and Methods: Two GC datasets from the Gene Expression Atlas, GSE62254 (n = 300) and GSE26942 (n = 217), were used as training and validation cohorts to establish a risk predictive scoring model. The efficacy of this model was assessed by ROC analysis. The association of the risk predictive scores with patient characteristics and immune cell subtypes was evaluated. A nomogram was constructed based on the risk predictive score model and other prognostic factors.

Results: A risk predictive score model was established based on the expression of 19 lipid metabolism–related genes (LPL, IPMK, PLCB3, CDIPT, PIK3CA, DPM2, PIGZ, GPD2, GPX3, LTC4S, CYP1A2, GALC, SGMS1, SMPD2, SMPD3, FUT6, ST3GAL1, B4GALNT1, and ACADS). The time-dependent ROC analysis revealed that the risk predictive score model was stable and robust. Patients with high risk scores had significantly unfavorable overall survival compared with those with low risk scores in both the training and validation cohorts. A higher risk score was associated with more aggressive features, including a higher tumor grade, a more advanced TNM stage, and diffuse type of Lauren classification of GC. Moreover, distinct immune cell subtypes and signaling pathways were found between the high–risk and low–risk score groups. A nomogram containing patients' age, tumor stage, adjuvant chemotherapy, and the risk predictive score could accurately predict the survival probability of patients at 1, 3, and 5 years.

OPEN ACCESS

Edited by:
Zhe-Sheng Chen,
St. John's University, United States

Reviewed by:
Yingyan Yu,
Shanghai Jiao Tong University, China
Lei Shi,
Georgia State University, United States
Mingyue Li,
University of Pennsylvania, United States

***Correspondence:**
Ying-Bo Chen
chenyb@sysucc.org.cn
Chuan Peng
pengchuan@sysucc.org.cn

[†]These authors have contributed equally to this work

Specialty section:
This article was submitted to Molecular Diagnostics and Therapeutics, a section of the journal Frontiers in Molecular Biosciences

Received: *05 April 2021*
Accepted: *07 June 2021*
Published: *30 June 2021*

Citation:
Wei X-L, Luo T-Q, Li J-N, Xue Z-C, Wang Y, Zhang Y, Chen Y-B and Peng C (2021) Development and Validation of a Prognostic Classifier Based on Lipid Metabolism–Related Genes in Gastric Cancer. Front. Mol. Biosci. 8:691143. doi: 10.3389/fmolb.2021.691143

Conclusion: A novel 19-gene risk predictive score model was developed based on the lipid metabolism–related genes, which could be a potential prognostic indicator and therapeutic target of GC.

Keywords: gastric cancer, prognostic model, lipid metabolism, nomogram, gene expression omnibus dataset, gene panel

INTRODUCTION

Gastric cancer (GC) is one of the leading causes of cancer-related death worldwide, ranking the third in males and the fifth in females (Bray et al., 2018). Current treatments of GC, including surgery, chemotherapy, and targeted regimens, improve the survival of patients to some extent (Johnston and Beckman, 2019). New prognostic biomarkers remain needed to lower risk, stratify patients, and guide future research for potential new therapeutic targets.

Deregulation of lipid metabolism has a critical role in the promotion of tumorigenesis and tumor progression (Röhrig and Schulze, 2016; Yu et al., 2018; Yang et al., 2020; Esposito et al., 2019). It also participates in the regulation of T cell function, including T cell proliferation and differentiation (Lochner et al., 2015; Raud et al., 2018). Dysregulation of lipid metabolism contributes to various aspects of tumor growth (Lochner et al., 2015; Raud et al., 2018). Lipoproteins, high lipid droplets, and excessive cholesteryl ester storage are hallmarks of aggressiveness of cancers (Yue et al., 2014; Liu et al., 2017). Therefore, targeting deregulated lipid metabolism is a promising strategy for cancer treatment (Liu et al., 2017; Iannelli et al., 2018).

GC progression is closely associated with alterations of lipid metabolism. A low level of serum high-density lipoprotein predicted a high risk of GC development, a high rate of lymphatic and vascular invasion, an advanced nodal metastasis, and a poor prognosis in patients with GC (Guo et al., 2007; Tamura et al., 2012; Nam et al., 2019). Adipocytes and fatty acids fueled metastasis and conferred a poor prognosis of GC (Duan et al., 2016; Tan et al., 2018; Jiang et al., 2019). Various lipid metabolites and genes involved in lipid metabolism also shared some roles in GC tumorigenesis or progression (Abbassi-Ghadi et al., 2013; Tao et al., 2019; Huang et al., 2020; Zhang et al., 2020). For example, adipocytes promoted peritoneal metastasis of GC through reprogramming of fatty acid metabolism mediated by phosphatidylinositol transfer protein, cytoplasmic 1 (PITPNC1) (Tan et al., 2018). Enhanced fatty acid carnitinylation and oxidation mediated by carnitine palmitoyltransferase 1C (CPT1C) promoted proliferative ability of GC (Chen et al., 2020).

The mechanisms of deregulation of lipid metabolism in cancers are complicated, including alteration in pathways involved in *de novo* lipogenesis, lipid uptake, lipid storage, and lipolysis and generating enhanced synthesis, uptake, consumption, and storage of fatty acids (Liu et al., 2017). However, an overall view of the prognostic value of lipid metabolism–related genes in GC remained to be explored (Liu et al., 2017). Identification of genes associated with clinical outcomes is important for further research in this area. In the current study, lipid metabolism–related gene sets were extracted and analyzed for their prognostic value in patients with GC. A novel lipid metabolism–related gene panel was developed and validated for its capability of predicting patient outcomes.

MATERIALS AND METHODS

Study Subjects

Two GEO (Gene Expression Omnibus, https://www.ncbi.nlm.nih.gov/geo/) datasets, GSE62254 and GSE26942, were used for analyses. Patients eligible for analyses were as follows: 1) histologically diagnosed with gastric adenocarcinoma, 2) having available mRNA expression data, and having 3) available complete clinical and survival information. There were 300 and 217 patients in the GSE62254 and GSE26942 datasets, respectively. 17 patients were excluded from the GSE26942 dataset due to not meeting the inclusion criteria, including 12 cases of normal tissue, 3 cases of gastric stromal tumor, and 2 cases without available survival information. Finally, the 300-patient cohort from the GSE62254 dataset was used as the training cohort for our risk predictive score model development, and the 200-patient cohort from the GSE26942 dataset was used as the validation cohort. The risk predictive score was also validated in another two public GC datasets, including the TCGA dataset (n = 350) and GSE84437 dataset (n = 432).

Risk Predictive Model Development in the Training Cohort

The normalized gene expression data of the GSE62254 dataset were downloaded from GEO. Prognosis relevant genes from lipid metabolism–related gene sets were identified using the "survival" package. All the lipid metabolism–related genes were subjected to the univariate Cox regression model, and 63 genes were identified to be associated with overall survival (OS). The 63 genes were further subjected to the LASSO Cox regression model analysis using the glmnet package, and then 19 genes were selected for construction of the risk prognostic scoring system. Calculation of risk scores was performed using the generated coefficients and corresponding expression. According to the risk scores, patients were classified into low-risk and high-risk groups with a cut-off value (risk score = −3.793587), which best stratified patients with different OS.

Risk Predictive Model Validation in the Validation Cohort

The same model and coefficients in the training cohort were applied in the validation cohort (GSE26942 dataset). The

normalized gene expression data of GSE26942 were downloaded. The efficacy of risk score prognostic classification was evaluated by ROC analysis with the timeROC package. The survival analysis was conducted as mentioned above and was also validated with another two gene sets (TCGA GC and GSE84437).

Risk Predictive Model Assessment

The timeROC package of R software was applied to perform the time-dependent receiver-operating characteristic curve (ROC) analysis. Survival analysis with Kaplan–Meier plots and the log-rank test, and the univariate and multivariate Cox hazard model were performed. GO and KEGG functional enrichment analyses were conducted through the R package clusterProfiler.

Evaluating the Relevance of the Risk Predictive Model With Immune Cells

The expression matrices of GSE62254 and GSE26942 datasets were uploaded to CIBERSORT to determine the tumor-infiltrating immune cell fractions, which were calculated according to the LM22 signature with 1,000 permutations, as described previously (Newman et al., 2015). The genes and the immune cell markers are listed in **Supplementary File 1**. The immune cell subtype fractions were compared between the low–risk and high–risk score groups.

Construction of a Nomogram

Independent prognostic factors were identified through univariate and multivariate Cox regression analysis. The independent prognostic factors were used to construct the prognostic nomogram, which assessed the OS probability at 1, 3, and 5 years with the "rms" package in R software.

Statistical Analysis

Student's *t*-test, the chi-squared test, and the Mann–Whitney U test were used to examine the differences between groups. Spearman analysis was adopted to assess the correlation between gene expression levels. All calculations were performed with R 3.5.3 software (http://www.R-project.org). A two-tailed p value < 0.05 was considered statistically significant.

RESULTS

Construction of a Risk Prognostic Model Based on Lipid Metabolism–Related Genes

Human lipid metabolism–related pathways were downloaded from the KEGG (https://www.kegg.jp/) database. 13 lipid metabolism–related pathways were included for analysis (**Supplementary Table S1**). The characteristics of patients in the GSE62254 and GSE26942 datasets are listed in **Supplementary Table S2**. The study procedures are shown in **Supplementary Figure S1**.

The risk prognostic model was developed using the training dataset (GSE62254). The univariate Cox regression model was used to identify genes with prognostic relevance for overall survival (OS). As a result, 63 genes were found to have statistically significant relevance with OS, and their correlations with each other were validated (**Supplementary Figure S2A**). The LASSO algorithm was used to reduce overfitting and construct the model. The LASSO algorithm is known to have the following features: it is simple and visible, can reduce variance through reduction of coefficients, and can increase interpretability and decrease overfitting through eliminating irrelevant variables. The risk score was built using the LASSO Cox regression model (**Supplementary Figures S2B,S2C**). 19 genes were selected for the construction of the risk prognostic scoring system (**Supplementary Table S3**). The correlations between these genes are shown in Supplementary Figure 2D. The risk score was calculated as follows based on the 19 genes:

Risk score = (0.100 * LPL) + (−0.374 * IPMK) + (−0.122 * PLCB3) + (0.311 * CDIPT) + (0.146 * PIK3CA) + (−0.263 * DPM2) + (0.310 * PIGZ) + (−0.594 * GPD2) + (0.043 * GPX3) + (0.077 * LTC4S) + (−0.782 * CYP1A2) + (−0.102 * GALC) + (−0.189 * SGMS1) + (−0.061 * SMPD2) + (−0.184 * SMPD3) + (−0.081 * FUT6) + (0.130 * ST3GAL1) + (0.549 * B4GALNT1) + (−0.040 * ACADS).

Validation of the Risk Prognostic Model and Its Efficiency

The GSE26942 dataset was adopted as the validation dataset. With a cut-off value of −3.793587, which stratified patients into two groups with the largest OS difference, patients were classified into low-risk and high-risk groups. The difference between the low-risk and high-risk groups in OS was statistically significant in the training dataset, the validation dataset, and both datasets combined. Kaplan–Meier curves are displayed in **Figures 1A–C**. Our constructed risk score also had significant prognostic relevance when validated with another two gene sets, TCGA GC and GSE84437 (**Supplementary Figure S3**). Subgroup analyses of Kaplan–Meier curves stratified by adjuvant chemotherapy (no/yes) and TNM stage (I + II/III + IV) in the combined dataset are displayed in **Supplementary Figure S4**. Time-dependent ROC analysis for the risk prognostic model at 1, 3, and 5 years is shown in **Figures 1D–F**. The area under the curve (AUC) was, respectively, 0.74 (95% CI: 0.67–0.82), 0.78 (95% CI: 0.73–0.83), and 0.78 (95% CI: 0.73–0.83) at 1, 3, and 5 years in the training dataset. The AUC was, respectively, 0.61 (95% CI: 0.50–0.72), 0.60 (95% CI: 0.51–0.68), and 0.63 (95% CI: 0.53–0.73) at 1, 3, and 5 years in the validation dataset and 0.69 (95% CI: 0.63–0.75), 0.71 (95% CI: 0.67–0.76), and 0.73 (95% CI: 0.68–0.77) at 1, 3, and 5 years in the combined dataset.

Univariate and multivariate Cox regression analysis in the combined dataset showed that the risk prognostic score model was an independent and significant prognostic factor for OS (**Figures 1G,H**). Patients with a high risk score had significantly worse OS (HR and 95% CI: 2.51 [1.93–3.28]) after being adjusted by other independent prognostic factors. The continuous patient risk score, survival state, and expression of the 19 genes of both datasets are shown in **Supplementary Figure S5**.

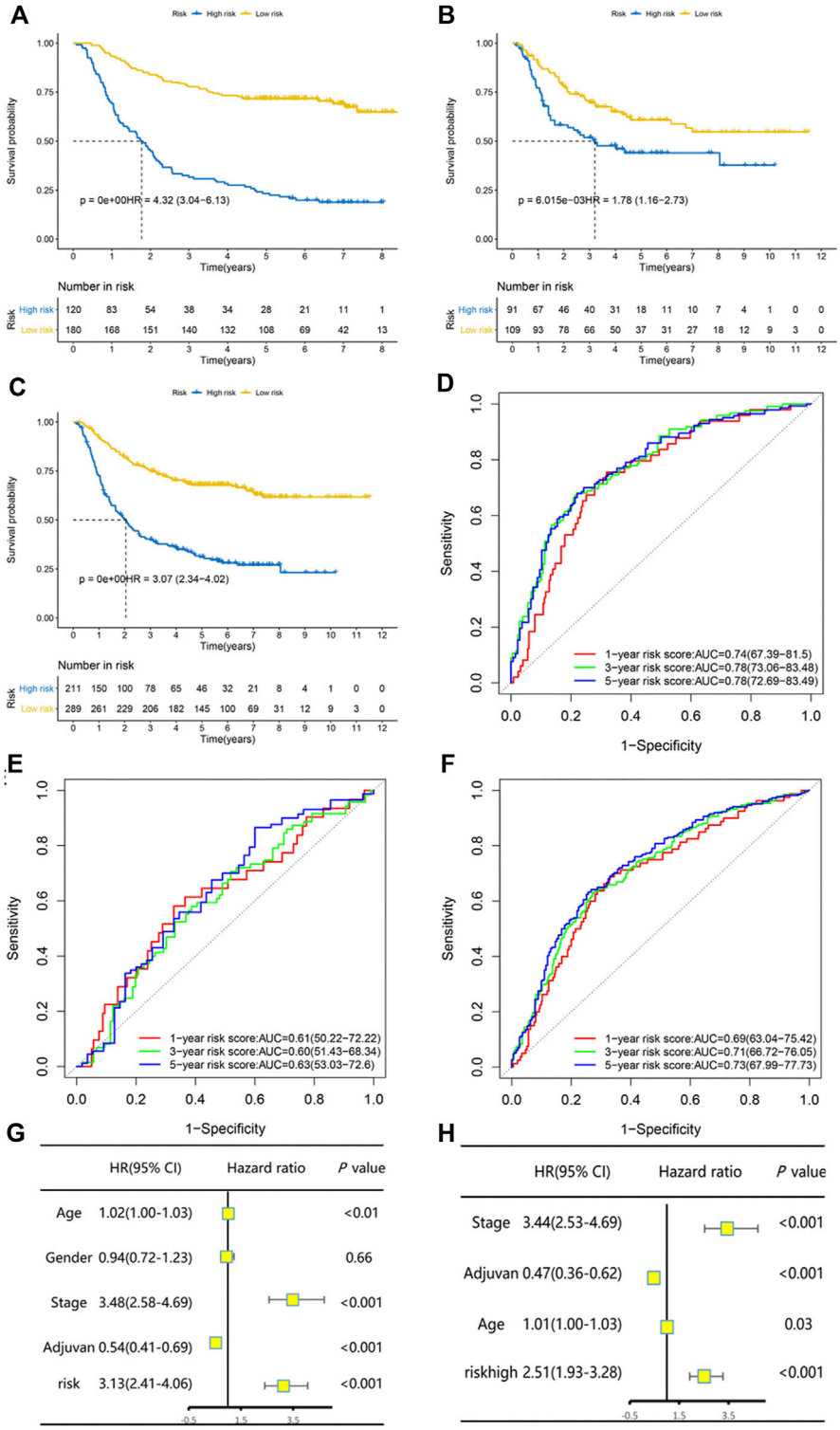

FIGURE 1 | The risk predictive score model had high efficacy of prediction in the training set, the validation set, and the combination of both datasets. Kaplan–Meier curves of overall survival stratified by risk score (low/high) in the training set **(A)**, validation set **(B)**, and both datasets **(C)**. Time-dependent ROC analysis for the risk predictive model at 1, 3, and 5 years in the training set **(D)**, validation set **(E)**, and both datasets **(F)**. Univariate and multivariate Cox regression analysis for overall survival in both datasets **(G–H)**.

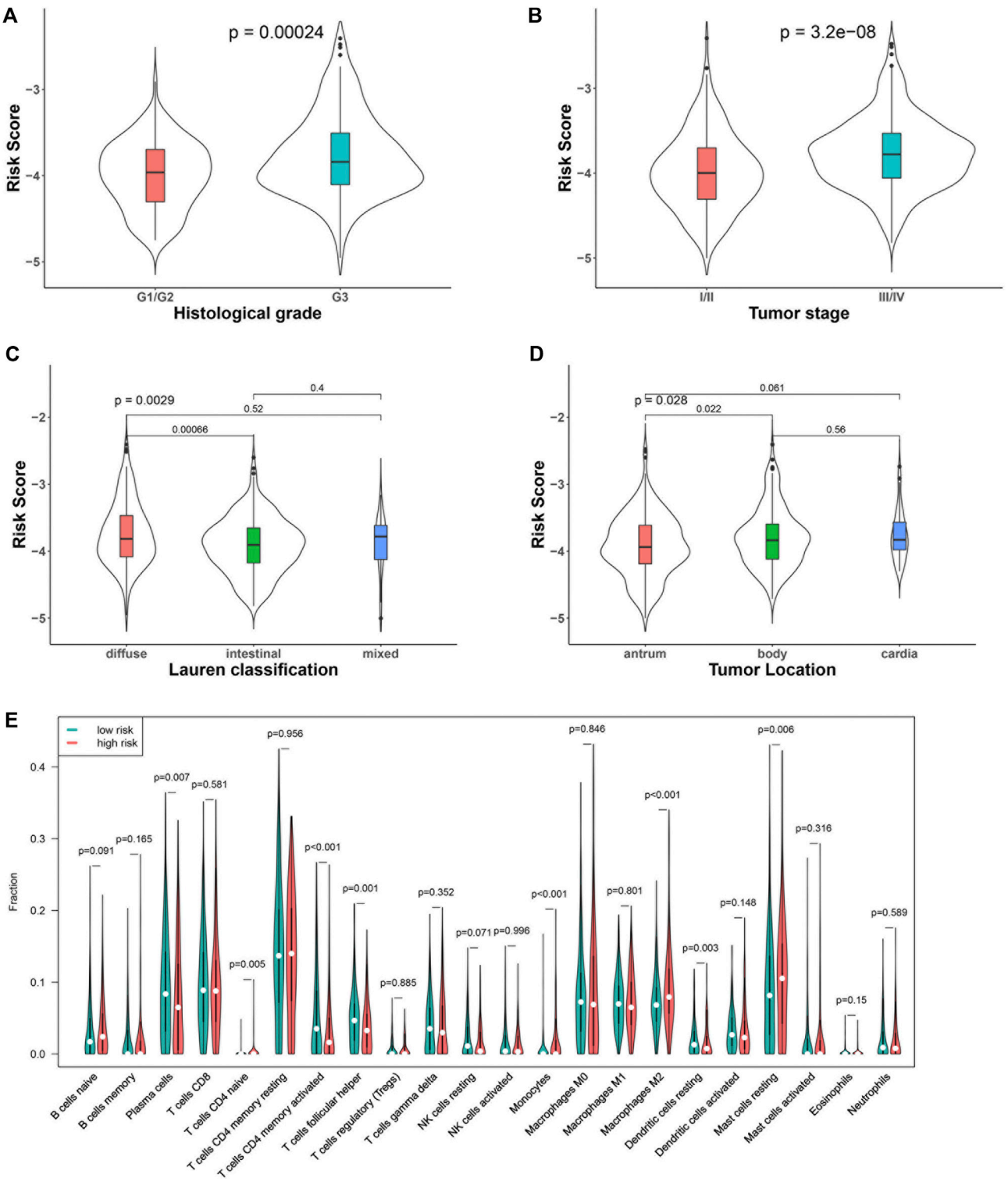

FIGURE 2 | Association of the risk score with clinical characteristics and immune cells: tumor grade **(A)**, stage **(B)**, Lauren classification **(C)**, tumor location **(D)**, and immune cell subtypes **(E)**.

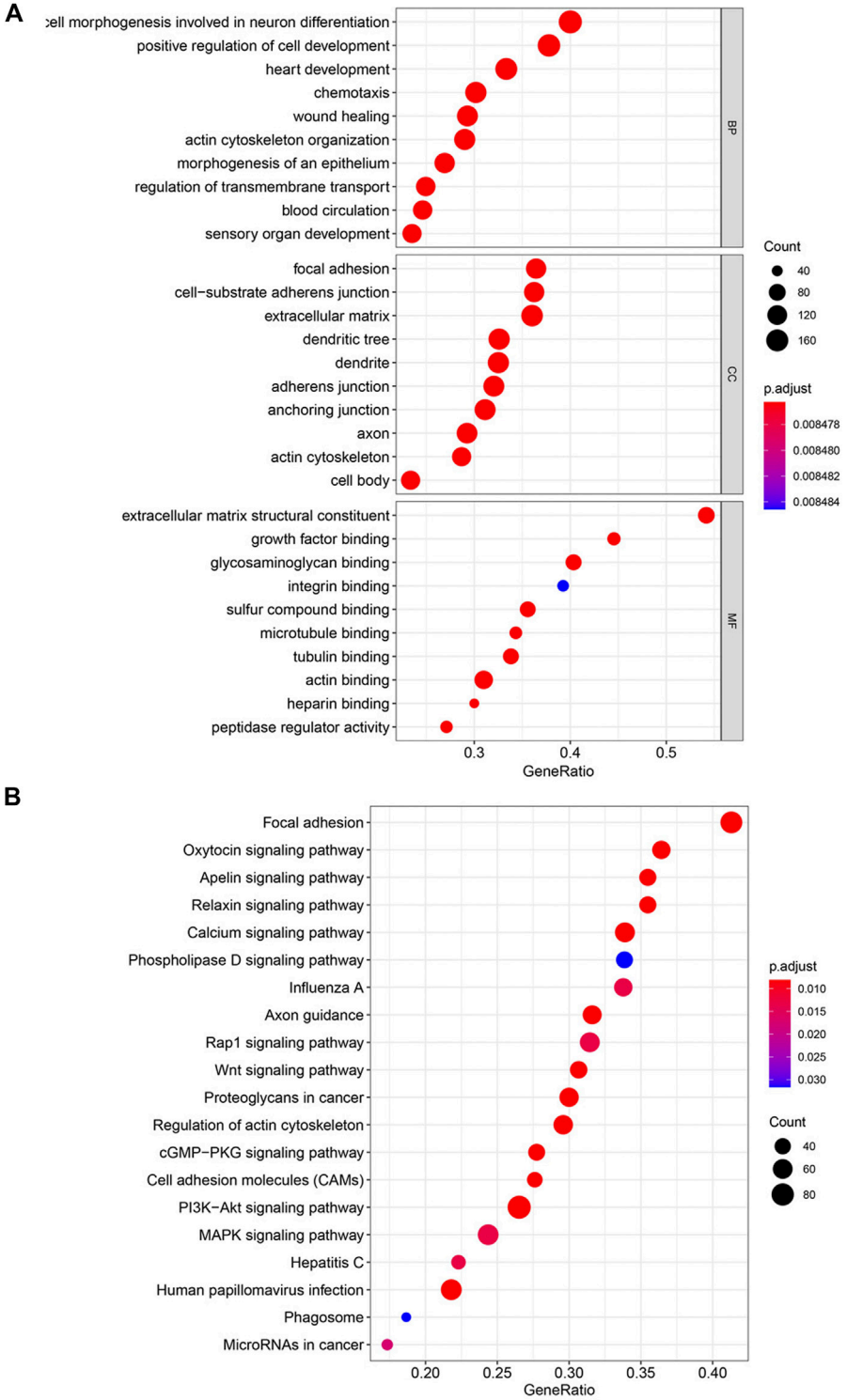

FIGURE 3 | Enriched pathways by risk score with KEGG and GO functional enrichment analyses. **(A)** Top 10 GO terms in the biological process (BP), cellular component (CC), and molecular function (MF). **(B)** Top 20 enriched pathways in KEGG.

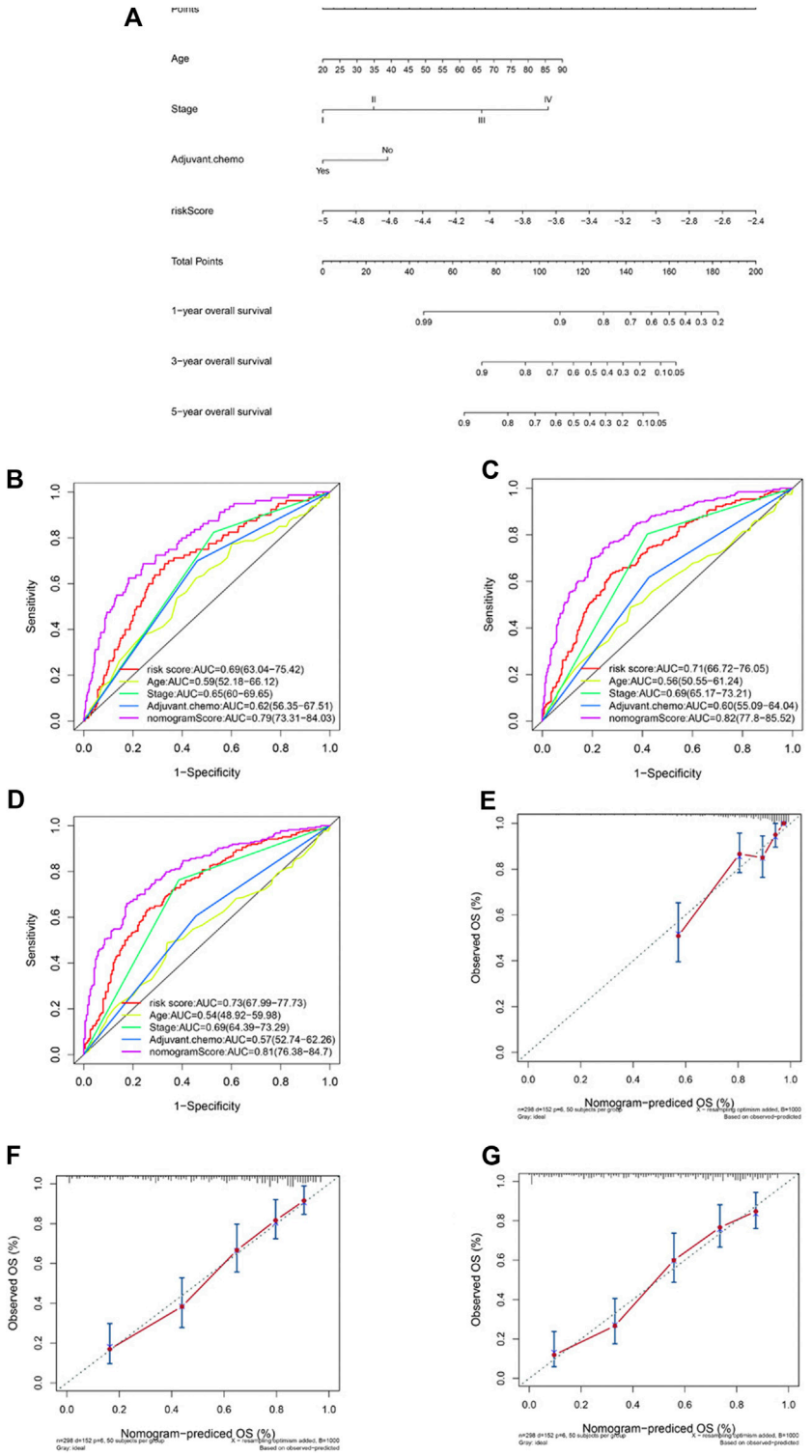

FIGURE 4 | Construction of a nomogram based on the risk predictive score and other prognostic factors. Nomogram constructed based on the risk score and three other factors **(A)**. ROC analysis comparing the AUCs at survival of 1 year **(B)**, 3 years **(C),** and 5 years **(D)** among the nomogram, risk score model, age, stage, and adjuvant chemotherapy. Comparisons between the predicted overall survival of 1-year **(E)**, 3-year **(F)**, and 5-year **(G)** nomogram models and the ideal model.

Association of Risk Score With Clinical Characteristics and Immune Cells

We compared the risk score between patients with different clinical characteristics. The results showed that the risk score between patients with different age (<60 or ≥60 years) was comparative (p = 0.11), so it was between males and females (p = 0.84). Tumors with more aggressive features generally had a higher risk score than those with less aggressive features. In particular, patients with a higher grade (G3) tumor had a higher risk score than those with a lower grade (G1/G2) tumor (p < 0.001, **Figure 2A**). Patients in stage III/IV had a higher risk score than those in stage I/II (p < 0.001, **Figure 2B**). In terms of Lauren classification, diffused tumors had a higher risk score compared with the intestinal tumors (p < 0.001, **Figure 2C**). In addition, tumors located in the gastric body had a higher risk score than those located in the gastric antrum (p = 0.02, **Figure 2D**).

We analyzed the percentage of 22 immune cell subtypes in the tumors of both datasets and compared their level between patients with low and high risk scores (**Figure 2E**). The levels of some immune cells, including plasma cells (p = 0.007), activated CD4 memory cells (p < 0.001), follicular helper T cells (p = 0.001), and resting dendritic cells, were significantly lower in the high–risk score group (p = 0.003), while some immune cells, including naïve CD4 T cells (p = 0.005), monocytes (p < 0.001), M2 macrophages (p < 0.001), and resting mast cells, were higher in the high–risk score group (p = 0.006).

Differentially Expressed Genes and Pathways Based on the Risk Prognostic Score

Functional analysis of differentially expressed genes was performed with KEGG and GO functional enrichment analyses. The top 10 GO genes were found to be associated with the biological process (BP), cellular component (CC), and molecular function (MF) (**Figure 3A**). These genes are associated with positive regulation of cell development, focal adhesion, cell-substrate adherens junction, extracellular matrix structural constituent, growth factor binding, etc. The top 20 enriched pathways are shown in **Figure 3B**, with the focal adhesion signaling pathway as the most significantly differently expressed pathway. Some other cancer-related pathways, including the Wnt signaling pathway, PI3K–Akt signaling pathway, and MAPK signaling pathway, were also significantly enriched in the high–risk score group.

Construction of a Nomogram Model

Factors identified by univariate and multivariate Cox regression analysis as independent and significant prognostic factors were applied in the construction of a nomogram model (**Figure 4A**). As shown in **Figures 1G,H**, those factors included patients' age, tumor stage, adjuvant chemotherapy, and the risk prognostic score. The predictive accuracy of the nomogram at 1 year (AUC = 0.79, **Figure 4B**), 3 years (AUC = 0.82, **Figure 4C**), and 5 years (AUC = 0.81, **Figure 4D**) was calculated and assessed by ROC analysis. The comparisons between the 1-, 3-, and 5-year nomogram models and the ideal model are shown in **Figures 4E–G** that displayed consistent indices and indicated relatively high accuracy of the nomogram models. The decision curve analysis (DCA) showed high predicting efficiency of the nomogram for the 3- and 5-year overall survival in the training dataset, the validation dataset, and the combination of both datasets (**Supplementary Figures S6A–S6F**).

DISCUSSION

GC has long been recognized as a recalcitrant cancer for its high incidence, high mortality, aggressive behavior, refractory traits, and poor prognosis (Van Cutsem et al., 2016). Identification of genetic factors that drive tumor progression and contribute to unfavorable outcomes is of key importance, for both improving patient care and developing potential therapeutics. As one of the most important basic metabolites, lipid has been demonstrated to be involved in the development and progression of malignancies in recent years, including GC (Huang et al., 2020). Although some studies have suggested important roles of lipid metabolites and lipid metabolism–related genes in GC (Huang et al., 2020), no reports have given an overall view of the prognostic value of lipid metabolism–related genes in GC.

In this study, we develop a novel prognostic scoring model based on the expression of lipid metabolism–related genes in gastric cancer. We used independent datasets from GEO to construct and validate the risk predictive scoring system containing 19 lipid metabolism–related genes. This scoring system was demonstrated to be efficient in predicting patient survival by ROC analysis. Patients had a significant and remarkable difference of OS between the high–risk and low–risk score groups. We further generated a nomogram integrating the risk predictive scoring system and three other prognostic factors (patients' age, TNM stage, and adjuvant chemotherapy) that improved the efficiency of prognostic value of the nomogram and accurately predicted the 1-, 3-, and 5-year OS of GC patients in the GEO datasets.

The risk predictive score calculated with our scoring system was significantly associated with the aggressiveness of GC. Patients with a higher grade tumor and in an advanced stage were shown to have a higher risk score, suggesting that dysregulation of lipid metabolism not just was associated with cancer progression in GC but also served as a driving factor for the aggressiveness of GC. Some of the genes included in our risk scoring system had been found to be involved in cancers, such as lipoprotein lipase (LPL) (Zaidi et al., 2013), phosphate 3-kinase catalytic subunit alpha (PIK3CA) (Arafeh and Samuels, 2019), mitochondrial glycerol-3-phosphate dehydrogenase (GPD2) (Singh, 2014), leukotriene C4 synthase (LTC4S) (Halvorsen et al., 2014), galactosylceramidase (GALC) (Halvorsen et al., 2014), sphingomyelin phosphodiesterase 3 (SMPD3) (Singh et al., 2014), fucosyltransferase 6 (FUT6) (Singh et al., 2014), and β-galactoside α-2,3-sialyltransferase-1 (ST3Gal1) (Wu et al., 2018). Except for PIK3CA, which was found to be frequently

altered in GC and was associated with unfavorable prognosis (Cancer Genome Atlas Research Network, 2014; Kim et al., 2017), although most of these genes were less studied, studies have suggested some roles of them in GC. LPL, which encodes lipoprotein lipase, a key enzyme in triglyceride metabolism, was reported to promote the progression of GC (Chang et al., 2017). Phospholipase C beta 3 (PLCB3), which encodes a member of the phosphoinositide phospholipase C beta enzyme family, was found to be one of the critical altered genes involved in aristolochic acid–induced gastric benign or malignant tumors (Wang et al., 2020). The polymorphism of cytochrome P450 family 1 subfamily A member 2 (CYP1A2) was repeatedly found to be associated with GC risk (Xue et al., 2014) and could modulate susceptibility to GC in patients with *Helicobacter pylori* infection (Ghoshal et al., 2014). Our study presented evidence for the prognostic value of these genes in GC, demonstrating their potential to be targets for anti-GC therapeutic research and development in the future.

Interestingly, the present study also revealed that patients with high and low risk scores had distinct features in tumor-infiltrating immune cells. Patients with high risk scores had significantly reduced number of plasma cells, activated CD4 memory cells, follicular helper T cells, and resting dendritic cells and increased number of naïve CD4 T cells, monocytes, M2 macrophages, and resting mast cells. Activated CD4 memory cells were associated with favorable outcomes in patients with cervical cancer (Ju et al., 2020) and favorable outcomes after radiotherapy in patients with multiple cancers (Ju et al., 2020; Wen et al., 2020). In gastric cancer, patients with low risk scores had increased number of activated CD4 memory cells and had superior prognosis (Zhao et al., 2020). Dendritic cells are specialized antigen-presenting cells which are key to the initiation of immune responses, including anti-tumor immune responses (Wculek et al., 2020). The increased number of dendritic cells induced by neoadjuvant chemotherapy was reported to be related to improved survival in GC (Hu et al., 2014). Naïve CD4 T cells were developed to form Treg cells in the tumor microenvironment and predicted poor prognosis in breast cancer (Su et al., 2017). M2 macrophages are a well-known tumor-promoting immunosuppressive cell type, and they have been proposed as a therapeutic target in GC (Gambardella et al., 2020). Immunotherapy has been established as a novel treatment in GC, but as monotherapy, PD-1 antibodies have limited benefit because the majority of patients do not respond (Xie et al., 2021). Novel combination options with immunotherapy are in great need in GC. Lipid metabolism not only impacts the proliferation and migration of tumor cells but also shapes the immuno-microenvironment by affecting the recruitment and function of tumor-infiltrating immune cells (He et al., 2021). In our study, patients with high risk scores had an immunosuppressive tumor microenvironment, indicating a possible role of treatments targeting lipid metabolism–related genes with immunotherapy in GC.

The major limitation of the present study was the lack of validation in larger patient cohorts from multicenter real-world clinical practice. Thus, the risk predictive score was still far from being able to be used in clinical practice. Another important limitation was that most of the genes used to construct this risk predictive score model were scarcely investigated in cancers. In addition, we did not perform the basic experiment to validate their roles and related mechanisms in GC cells. The biological mechanism was unclear and needed further experimental validation. However, as a prognostic risk score, our model was repeatedly validated and achieved consensus results, so the conclusions of our study are still convincing despite the lack of experimental validation of each gene's role in GC.

CONCLUSION

In the present study, a novel lipid metabolism–related gene-based risk predictive score model was constructed and validated in datasets of patients with GC. This risk predictive scoring system could efficiently predict patient outcomes and had significant correlation with immune cell subtypes. A nomogram containing the risk score was generated, and it improved the prognostic predictive value of the current TNM staging system. This study will be helpful in biomarker and therapeutics development for GC patients.

DATA AVAILABILITY STATEMENT

The datasets presented in this study can be found in online repositories. The names of the repository/repositories and accession number(s) can be found in the article/ **Supplementary Material**.

ETHICS STATEMENT

The study followed the Declaration of Helsinki and was approved by the Clinical Research Ethics Committee of Sun Yat-sen University Cancer Center. Because of the retrospective nature of the study, patient consent for inclusion was waived.

AUTHOR CONTRIBUTIONS

CP, Y-BC, and X-LW designed the study. T-QL, J-NL, and Z-CX retrieved the data and conducted analysis. T-QL, YW, and YZ drew the tables and figures. X-LW, T-QL, and J-NL wrote the manuscript. All authors read and approved the manuscript.

FUNDING

This study was supported by the Guangdong Basic and Applied Basic Research Foundation (2019A1515110171).

ACKNOWLEDGMENTS

The authors would like to thank the authors who submitted the related data on the GEO website.

SUPPLEMENTARY MATERIAL

The Supplementary Material for this article can be found online at: https://www.frontiersin.org/articles/10.3389/fmolb.2021.691143/full#supplementary-material

Supplementary Figure 1 | Flowchart of the study. Two GEO datasets, GSE62254 and GSE26942, were used as the training and validation datasets for the risk predictive score model construction. Further comparisons and establishment of a nomogram based on the risk scores were conducted.

Supplementary Figure 2 | Construction of a risk predictive score model based on lipid metabolism–related genes. 63 prognostic relevant genes in lipid metabolism–related pathways were screened **(A)**. The risk predictive score system was constructed using the LASSO Cox regression model **(B,C)**. Correlation between the 19 selected genes **(D)**.

Supplementary Figure 3 | Kaplan–Meier curves of overall survival stratified by risk score (low/high) in another two datasets: TCGA GC dataset **(A)** and GSE84437 dataset **(B)**.

Supplementary Figure 4 | Subgroup analyses of Kaplan–Meier curves for overall survival stratified by adjuvant chemotherapy (no/yes) and TNM stage (I + II/III + IV) in the combined dataset. Adjuvant chemotherapy—no **(A)**, adjuvant chemotherapy—yes **(B)**, TNM stage—I + II **(C)**, and TNM stage—III + IV **(D)**.

Supplementary Figure 5 | Expression of 19 genes **(A)**, continuous patient risk score **(B)**, and survival state **(C)** in both datasets.

Supplementary Figure 6 | Decision curve analysis (DCA) for 3-year OS and 5-year OS. DCA for 3-year OS in the training dataset **(A)**, validation dataset **(B),** and both datasets **(C)**; DCA for 5-year OS in the training dataset **(D)**, validation dataset **(E),** and both datasets **(F)**.

REFERENCES

Abbassi-Ghadi, N., Kumar, S., Huang, J., Goldin, R., Takats, Z., and Hanna, G. B. (2013). Metabolomic Profiling of Oesophago-Gastric Cancer: a Systematic Review. *Eur. J. Cancer* 49, 3625–3637. doi:10.1016/j.ejca.2013.07.004

Arafeh, R., and Samuels, Y. (2019). PIK3CA in Cancer: The Past 30 Years. *Semin. Cancer Biol.* 59, 36–49. doi:10.1016/j.semcancer.2019.02.002

Bray, F., Ferlay, J., Soerjomataram, I., Siegel, R. L., Torre, L. A., and Jemal, A. (2018). Global Cancer Statistics 2018: GLOBOCAN Estimates of Incidence and Mortality Worldwide for 36 Cancers in 185 Countries. *CA: A Cancer J. Clinicians* 68, 394–424. doi:10.3322/caac.21492

Chang, W.-C., Huang, S.-F., Lee, Y.-M., Lai, H.-C., Cheng, B.-H., Cheng, W.-C., et al. (2017). Cholesterol Import and Steroidogenesis Are Biosignatures for Gastric Cancer Patient Survival. *Oncotarget* 8, 692–704. doi:10.18632/oncotarget.13524

Chen, T., Wu, G., Hu, H., and Wu, C. (2020). Enhanced Fatty Acid Oxidation Mediated by CPT1C Promotes Gastric Cancer Progression. *J. Gastrointest. Oncol.* 11, 695–707. doi:10.21037/jgo-20-157

Cancer Genome Atlas Research Network 2014). Comprehensive Molecular Characterization of Gastric Adenocarcinoma. *Nature.* 513, 202–209.doi:10.1038/nature13480

Duan, J., Sun, L., Huang, H., Wu, Z., Wang, L., and Liao, W. (2016). Overexpression of Fatty Acid Synthase Predicts a Poor Prognosis for Human Gastric Cancer. *Mol. Med. Rep.* 13, 3027–3035. doi:10.3892/mmr.2016.4902

Esposito, M., Mondal, N., Greco, T. M., Wei, Y., Spadazzi, C., Lin, S.-C., et al. (2019). Bone Vascular Niche E-Selectin Induces Mesenchymal-Epithelial Transition and Wnt Activation in Cancer Cells to Promote Bone Metastasis. *Nat. Cel Biol* 21, 627–639. doi:10.1038/s41556-019-0309-2

Gambardella, V., Castillo, J., Tarazona, N., Gimeno-Valiente, F., Martínez-Ciarpaglini, C., Cabeza-Segura, M., et al. (2020). The Role of Tumor-Associated Macrophages in Gastric Cancer Development and Their Potential as a Therapeutic Target. *Cancer Treat. Rev.* 86, 102015. doi:10.1016/j.ctrv.2020.102015

Ghoshal, U., Tripathi, S., Kumar, S., Mittal, B., Chourasia, D., Kumari, N., et al. (2014). Genetic Polymorphism of Cytochrome P450 (CYP) 1A1, CYP1A2, and CYP2E1 Genes Modulate Susceptibility to Gastric Cancer in Patients with *Helicobacter pylori* Infection. *Gastric Cancer* 17, 226–234. doi:10.1007/s10120-013-0269-3

Guo, E., Chen, L., Xie, Q., Chen, J., Tang, Z., and Wu, Y. (2007). Serum HDL-C as a Potential Biomarker for Nodal Stages in Gastric Cancer. *Ann. Surg. Oncol.* 14, 2528–2534. doi:10.1245/s10434-007-9401-0

Halvorsen, A. R., Helland, A., Fleischer, T., Haug, K. M., Grenaker Alnæs, G. I., Nebdal, D., et al. (2014). Differential DNA Methylation Analysis of Breast Cancer Reveals the Impact of Immune Signaling in Radiation Therapy. *Int. J. Cancer* 135, 2085–2095. doi:10.1002/ijc.28862

He, S., Cai, T., Yuan, J., Zheng, X., and Yang, W. (2021). Lipid Metabolism in Tumor-Infiltrating T Cells. *Adv. Exp. Med. Biol.* 1316, 149–167. doi:10.1007/978-981-33-6785-2_10

Hu, M., Li, K., Maskey, N., Xu, Z., Peng, C., Wang, B., et al. (2014). Decreased Intratumoral Foxp3 Tregs and Increased Dendritic Cell Density by Neoadjuvant Chemotherapy Associated with Favorable Prognosis in Advanced Gastric Cancer. *Int. J. Clin. Exp. Pathol.* 7, 4685–4694.

Huang, S., Guo, Y., Li, Z., Zhang, Y., Zhou, T., You, W., et al. (2020). A Systematic Review of Metabolomic Profiling of Gastric Cancer and Esophageal Cancer. *Cancer Biol. Med.* 17, 181–198. doi:10.20892/j.issn.2095-3941.2019.0348

Iannelli, F., Lombardi, R., Milone, M. R., Pucci, B., De Rienzo, S., Budillon, A., et al. (2018). Targeting Mevalonate Pathway in Cancer Treatment: Repurposing of Statins. *Pra* 13, 184–200. doi:10.2174/1574892812666171129141211

Jiang, M., Wu, N., Xu, B., Chu, Y., Li, X., Su, S., et al. (2019). Fatty Acid-Induced CD36 Expression via O-GlcNAcylation Drives Gastric Cancer Metastasis. *Theranostics* 9, 5359–5373. doi:10.7150/thno.34024

Johnston, F. M., and Beckman, M. (2019). Updates on Management of Gastric Cancer. *Curr. Oncol. Rep.* 21, 67. doi:10.1007/s11912-019-0820-4

Ju, M., Qi, A., Bi, J., Zhao, L., Jiang, L., Zhang, Q., et al. (2020). A Five-mRNA Signature Associated with post-translational Modifications Can Better Predict Recurrence and Survival in Cervical Cancer. *J. Cel Mol Med* 24, 6283–6297. doi:10.1111/jcmm.15270

Kim, J.-W., Lee, H. S., Nam, K. H., Ahn, S., Kim, J. W., Ahn, S.-H., et al. (2017). PIK3CA Mutations Are Associated with Increased Tumor Aggressiveness and Akt Activation in Gastric Cancer. *Oncotarget* 8, 90948–90958. doi:10.18632/oncotarget.18770

Liu, Q., Luo, Q., Halim, A., and Song, G. (2017). Targeting Lipid Metabolism of Cancer Cells: A Promising Therapeutic Strategy for Cancer. *Cancer Lett.* 401, 39–45. doi:10.1016/j.canlet.2017.05.002

Lochner, M., Berod, L., and Sparwasser, T. (2015). Fatty Acid Metabolism in the Regulation of T Cell Function. *Trends Immunol.* 36, 81–91. doi:10.1016/j.it.2014.12.005

Nam, S. Y., Park, B. J., Nam, J. H., and Kook, M.-C. (2019). Effect of *Helicobacter pylori* Eradication and High-Density Lipoprotein on the Risk of De Novo Gastric Cancer Development. *Gastrointest. Endosc.* 90, 448–456. doi:10.1016/j.gie.2019.04.232

Newman, A. M., Liu, C. L., Green, M. R., Gentles, A. J., Feng, W., Xu, Y., et al. (2015). Robust Enumeration of Cell Subsets from Tissue Expression Profiles. *Nat. Methods* 12, 453–457. doi:10.1038/nmeth.3337

Raud, B., McGuire, P. J., Jones, R. G., Sparwasser, T., and Berod, L. (2018). Fatty Acid Metabolism in CD8+T Cell Memory: Challenging Current Concepts. *Immunol. Rev.* 283, 213–231. doi:10.1111/imr.12655

Röhrig, F., and Schulze, A. (2016). The Multifaceted Roles of Fatty Acid Synthesis in Cancer. *Nat. Rev. Cancer* 16, 732–749. doi:10.1038/nrc.2016.89

Singh, G. (2014). Mitochondrial FAD-Linked Glycerol-3-Phosphate Dehydrogenase: A Target for Cancer Therapeutics. *Pharmaceuticals* 7, 192–206. doi:10.3390/ph7020192

Singh, R., Pochampally, R., Watabe, K., Lu, Z., and Mo, Y.-Y. (2014). Exosome-mediated Transfer of miR-10b Promotes Cell Invasion in Breast Cancer. *Mol. Cancer* 13, 256. doi:10.1186/1476-4598-13-256

Su, S., Liao, J., Liu, J., Huang, D., He, C., Chen, F., et al. (2017). Blocking the Recruitment of Naive CD4+ T Cells Reverses Immunosuppression in Breast Cancer. *Cell Res* 27, 461–482. doi:10.1038/cr.2017.34

Tamura, T., Inagawa, S., Hisakura, K., Enomoto, T., and Ohkohchi, N. (2012). Evaluation of Serum High-Density Lipoprotein Cholesterol Levels as a Prognostic Factor in Gastric Cancer Patients. *J. Gastroenterol. Hepatol.* 27, 1635–1640. doi:10.1111/j.1440-1746.2012.07189.x

Tan, Y., Lin, K., Zhao, Y., Wu, Q., Chen, D., Wang, J., et al. (2018). Adipocytes Fuel Gastric Cancer Omental Metastasis via PITPNC1-Mediated Fatty Acid Metabolic Reprogramming. *Theranostics* 8, 5452–5468. doi:10.7150/thno.28219

Tao, L., Yu, H., Liang, R., Jia, R., Wang, J., Jiang, K., et al. (2019). Rev-erbα Inhibits Proliferation by Reducing Glycolytic Flux and Pentose Phosphate Pathway in Human Gastric Cancer Cells. *Oncogenesis* 8, 57. doi:10.1038/s41389-019-0168-5

Van Cutsem, E., Sagaert, X., Topal, B., Haustermans, K., and Prenen, H. (2016). Gastric Cancer. *The Lancet* 388, 2654–2664. doi:10.1016/s0140-6736(16)30354-3

Wang, L., Li, C., Tian, J., Liu, J., Zhao, Y., Yi, Y., et al. (2020). Genome-wide Transcriptional Analysis of Aristolochia Manshuriensis Induced Gastric Carcinoma. *Pharm. Biol.* 58, 98–106. doi:10.1080/13880209.2019.1710219

Wculek, S. K., Cueto, F. J., Mujal, A. M., Melero, I., Krummel, M. F., and Sancho, D. (2020). Dendritic Cells in Cancer Immunology and Immunotherapy. *Nat. Rev. Immunol.* 20, 7–24. doi:10.1038/s41577-019-0210-z

Wen, P., Gao, Y., Chen, B., Qi, X., Hu, G., Xu, A., et al. (2020). Pan-Cancer Analysis of Radiotherapy Benefits and Immune Infiltration in Multiple Human Cancers. *Cancers (Basel)* 12. doi:10.3390/cancers12040957

Wu, X., Zhao, J., Ruan, Y., Sun, L., Xu, C., and Jiang, H. (2018). Sialyltransferase ST3GAL1 Promotes Cell Migration, Invasion, and TGF-B1-Induced EMT and Confers Paclitaxel Resistance in Ovarian Cancer. *Cell Death Dis* 9, 1102. doi:10.1038/s41419-018-1101-0

Xie, J., Fu, L., and Jin, L. (2021). Immunotherapy of Gastric Cancer: Past, Future Perspective and Challenges. *Pathol. - Res. Pract.* 218, 153322. doi:10.1016/j.prp.2020.153322

Xue, H., Lu, Y., Xue, Z., Lin, B., Chen, J., Tang, F., et al. (2014). The Effect of CYP1A1 and CYP1A2 Polymorphisms on Gastric Cancer Risk Among Different Ethnicities: a Systematic Review and Meta-Analysis. *Tumor Biol.* 35, 4741–4756. doi:10.1007/s13277-014-1620-y

Yang, M., Jiang, Z., Yao, G., Wang, Z., Sun, J., Qin, H., et al. (2020). GALC Triggers Tumorigenicity of Colorectal Cancer via Senescent Fibroblasts. *Front. Oncol.* 10, 380. doi:10.3389/fonc.2020.00380

Yu, X. H., Ren, X. H., Liang, X. H., and Tang, Y. L. (2018). Roles of Fatty Acid Metabolism in Tumourigenesis: Beyond Providing Nutrition (Review). *Mol. Med. Rep.* 18, 5307–5316. doi:10.3892/mmr.2018.9577

Yue, S., Li, J., Lee, S.-Y., Lee, H. J., Shao, T., Song, B., et al. (2014). Cholesteryl Ester Accumulation Induced by PTEN Loss and PI3K/AKT Activation Underlies Human Prostate Cancer Aggressiveness. *Cel Metab.* 19, 393–406. doi:10.1016/j.cmet.2014.01.019

Zaidi, N., Lupien, L., Kuemmerle, N. B., Kinlaw, W. B., Swinnen, J. V., and Smans, K. (2013). Lipogenesis and Lipolysis: the Pathways Exploited by the Cancer Cells to Acquire Fatty Acids. *Prog. Lipid Res.* 52, 585–589. doi:10.1016/j.plipres.2013.08.005

Zhang, H., Deng, T., Liu, R., Ning, T., Yang, H., Liu, D., et al. (2020). CAF Secreted miR-522 Suppresses Ferroptosis and Promotes Acquired Chemo-Resistance in Gastric Cancer. *Mol. Cancer* 19, 43. doi:10.1186/s12943-020-01168-8

Zhao, E., Zhou, C., and Chen, S. (2020). A Signature of 14 Immune-Related Gene Pairs Predicts Overall Survival in Gastric Cancer. *Clin. Transl Oncol.* 23, 265–274. doi:10.1007/s12094-020-02414-7

Conflict of Interest: The authors declare that the research was conducted in the absence of any commercial or financial relationships that could be construed as a potential conflict of interest.

frontiers in Molecular Biosciences

REVIEW
published: 26 July 2021
doi: 10.3389/fmolb.2021.707461

MicroRNAs in Transforming Growth Factor-Beta Signaling Pathway Associated With Fibrosis Involving Different Systems of the Human Body

Xiaoyang Xu, Pengyu Hong, Zhefu Wang, Zhangui Tang and Kun Li**

Department of Oral and Maxillofacial Surgery, Xiangya Stomatological Hospital and School of Stomatology, Central South University, Changsha, China

Fibrosis, a major cause of morbidity and mortality, is a histopathological manifestation of many chronic inflammatory diseases affecting different systems of the human body. Two types of transforming growth factor beta (TGF-β) signaling pathways regulate fibrosis: the canonical TGF-β signaling pathway, represented by SMAD-2 and SMAD-3, and the noncanonical pathway, which functions without SMAD-2/3 participation and currently includes TGF-β/mitogen-activated protein kinases, TGF-β/SMAD-1/5, TGF-β/phosphatidylinositol-3-kinase/Akt, TGF-β/Janus kinase/signal transducer and activator of transcription protein-3, and TGF-β/rho-associated coiled-coil containing kinase signaling pathways. MicroRNA (miRNA), a type of non-coding single-stranded small RNA, comprises approximately 22 nucleotides encoded by endogenous genes, which can regulate physiological and pathological processes in fibrotic diseases, particularly affecting organs such as the liver, the kidney, the lungs, and the heart. The aim of this review is to introduce the characteristics of the canonical and non-canonical TGF-β signaling pathways and to classify miRNAs with regulatory effects on these two pathways based on the influenced organ. Further, we aim to summarize the limitations of the current research of the mechanisms of fibrosis, provide insights into possible future research directions, and propose therapeutic options for fibrosis.

Keywords: TGF-β, signaling pathway, miRNA, mechanism, fibrosis

OPEN ACCESS

Edited by:
Wei Zhao,
City University of Hong Kong, China

Reviewed by:
Ye Ding,
Georgia State University, United States
Ravindra K. Sharma,
University of Florida, United States

****Correspondence:***
Zhangui Tang
tangzhangui@aliyun.com
Kun Li
406889138@qq.com

Specialty section:
This article was submitted to Molecular Diagnostics and Therapeutics, a section of the journal Frontiers in Molecular Biosciences

Received: *10 May 2021*
Accepted: *08 July 2021*
Published: *26 July 2021*

Citation:
Xu X, Hong P, Wang Z, Tang Z and Li K (2021) MicroRNAs in Transforming Growth Factor-Beta Signaling Pathway Associated With Fibrosis Involving Different Systems of the Human Body. Front. Mol. Biosci. 8:707461. doi: 10.3389/fmolb.2021.707461

INTRODUCTION

Fibrosis is a histopathological manifestation of many chronic inflammatory diseases (Wynn, 2007). Some fibroproliferative diseases, such as progressive kidney disease, hepatitis, pulmonary fibrosis, cardiovascular disease, scleroderma, and systemic sclerosis, eventually cause high morbidity and mortality by influencing diverse systems of the human body (Wynn, 2007). Fibrosis is characterized by the undue aggregation of extracellular interstitial constituents in and around injured or inflamed tissues, such as collagen and fibronectin (Wynn, 2008). If the causative disease continues to progress, fibrosis leads to collapse of tissue structure, loss of organ function, and finally death. Factors causing fibrotic diseases are genetic, inflammatory, environmental, etc. (Wynn, 2008) Research is underway for the molecular mechanism of fibrotic diseases and valid treatments to prevent or reverse the progression of these diseases (Wynn, 2008; Meng et al., 2016).

Transforming growth factor beta (TGF-β), a key molecule in the development of fibrosis, can regulate a series of biological processes, including the cell growth cycle, cell differentiation, immune regulation, and extracellular matrix (ECM) deposition (Ikushima and Miyazono, 2012; Meng et al., 2016). Two types of TGF-β signaling pathways regulate fibrosis: the canonical signaling pathway, represented by SMAD-2/3, and the noncanonical pathway, which does not involve SMAD-2/3 participation (Meng et al., 2016; Finnson et al., 2020). Increasing evidence confirms that the pathogenesis of fibrosis includes the canonical TGF-β signaling pathway and abnormal activation of the noncanonical TGF-β pathway (Finnson et al., 2020). Therefore, further research of the molecular mechanism of these signaling pathways regulating fibrotic diseases and potential molecular targets for treatments is warranted in the future.

MicroRNA (miRNA), a type of non-coding single-stranded small RNA, comprises approximately 22 nucleotides encoded by endogenous genes, which can regulate physiological and pathological processes in fibrotic diseases (Liu et al., 2018). Its central role in the research of fibrotic disease treatment and pathogenesis has garnered widespread attention in recent years (Banerjee et al., 2011; Liu et al., 2018; Li et al., 2019). Accumulating evidence confirms that miRNAs, such as miR-125a-5p, miR-29a-3p, miR-181a-5p, and miR-216a, can positively and negatively regulate the canonical TGF-β/SMAD pathway to affect myofibroblast transformation, collagen synthesis, and ECM deposition in fibrotic diseases (Yang et al., 2016; Henry et al., 2019; Srivastava et al., 2019). Several studies support the regulatory mechanism of miRNAs in noncanonical TGF-β signaling pathway-mediated fibrotic diseases (Yang et al., 2016). Since miRNAs are commonly involved in regulating the canonical and noncanonical TGF-β signaling pathways, they have diagnostic and therapeutic potentials in many fibroproliferative diseases (Yang et al., 2016). The aim of this review is to comprehensively generalize the regulatory role of miRNAs in canonical and noncanonical TGF-β pathway-intervened fibrosis and identify their characteristics in different organs, with focus on the most recent literature to provide the current valuable knowledge in this area.

CANONICAL TGF-β SIGNALING PATHWAY

In the canonical TGF-β signaling pathway, active TGF-β is first isolated from the latent TGF-β complex in the extracellular space, which maintains TGF-β in the inactive form (Meng et al., 2016). The inactive molecule then binds to the TGF-β type II receptor (TGF-βRII), which in turn binds and phosphorylates the TGF-β type I receptor ALK5, leading to its activation. Subsequently, Smad2 and Smad3 proteins are continuously phosphorylated by ALK5 in the cytoplasm and then form a complex with Smad4, which finally assembles in the nucleus to further regulate fibrosis-related transcription (Hill, 2009; Wrighton et al., 2009; Thatcher, 2010). In addition, the inhibitory function of SMAD-7 competes with SMAD-2/3 to bind with phosphorylated ALK5 (Yan et al., 2009; Hu et al., 2018).

NONCANONICAL TGF-β SIGNALING PATHWAY

During fibrotic progression, complex regulatory networks composed of multiple TGF-β-related signaling pathways work together (Yang et al., 2016; Finnson et al., 2020). Therefore, in addition to canonical pathways, we should pay attention to noncanonical TGF-β signaling pathways, including ALK1/Smad1/5, Janus kinases (JAKs)/signal transducer and activator of transcription protein-3 (STAT3), phosphatidylinositol-3-kinase (PI3K), mitogen-activated protein (MAP) kinases (ERK, p38, and JNK), and rho-like GTPases in different cell types (Finnson et al., 2020).

Unlike the canonical ALK5-SMAD-2/3 pathway, the TGF-β type I receptor ALK1 forms a complex with ALK5 under stimulation by TGF-β, leading to activation of SMAD-1/5 and suppression of ALK5-SMAD-2/3 signaling (Goumans et al., 2003; Finnson et al., 2008). Moreover, the activation of SMAD-1 and SMAD-5 are both inhibited by SMAD-6 and SMAD-7, which respond to TGF-β-related bone morphogenetic proteins (Katsuno et al., 2018). Pannu et al. showed that in systemic sclerosis, the up-regulation of extracellular interstitial components, which depend on ALK5, is not associated with SMAD-2/3 activation but reconciled by ALK1/SMAD-1 and ERK-1/2 signalings (Pannu et al., 2007).

MAPK, which includes three major classical types, i.e., ERK, JNK, and p38 MAPK, is commonly involved in the up-regulation of key molecules that sustain cell proliferation, growth, differentiation, and survival processes (Braicu et al., 2019). After TGF-β-induced phosphorylation, TβRII and ALK5 can sequentially activate Ras, Raf, and MEK-1/2 to activate ERK-1/2 by recruiting adaptor protein growth factor receptor-bound protein 2/Son of Sevenless. Fibrosis-related genes, without or in collaboration with activated SMAD complexes, are controlled by some transcription factors, which are phosphorylated by activated ERK, such as jun and fos (Zhang, 2017). Moreover, ERKs can negatively regulate SMAD protein activity by directly phosphorylating the linker region of SMAD proteins (Kretzschmar et al., 1997; Kretzschmar et al., 1999). In fibrotic processes, intramolecular polyubiquitination of TNF receptor-associated factor 6 (TRAF-6) at Lys63 is conducted by the interplay between activated TGF-β receptors and TRAF-6 (Yamashita et al., 2008). Subsequently, TAK1 is recruited by polyubiquitinated TRAF-6 to activate JNK and p38 *via* activations of MKK4 and MKK3/6, respectively. Finally, the activated JNK and p38 continuously activate the downstream transcription factors c-jun and ATF-2, which then regulate SMAD activity through phosphorylation (Zhang, 2009; Zhang, 2017).

The PI3K/AKT/mammalian target of rapamycin (mTOR) signaling cascade, which comprises the core units of phosphatidylinositide 3-kinases and their downstream mediators AKT and mTOR, mediate cell proliferation, survival, and metabolism and control cellular differentiation (Yu and Cui, 2016; Marquard and Jücker, 2020). TGF-β regulates PI3K/AKT signaling through two mechanisms: SMAD-dependent and SMAD-independent (Zhang, 2017). In

the SMAD-dependent pathway, TGF-β-driven SMAD signaling induces the lipid phosphatase SH2-containing inositol 5′-phosphatase, which can then inhibit PI3K/AKT signaling (Valderrama-Carvajal et al., 2002). Similar to TGF-β-induced JNK/p38 activation, in the SMAD-independent mechanism, ubiquitinated TRAF6 stimulates PI3K/AKT signaling and induces ubiquitination and activation of AKT (Yang et al., 2009). Although its specific function in fibrotic diseases is unclear, increasing evidence suggests that PI3K/AKT signaling plays a critical role in profibrotic processes in organs such as the liver, the heart, the kidney, the lungs, skin, and even oral mucosa (Dai et al., 2015; Li et al., 2017; Chaigne et al., 2019; Mi et al., 2019; Wang et al., 2019a; Zhou et al., 2019; Yin et al., 2020).

ROCK is the eventful cellular regulator of rho GTPases that organizes the actin cytoskeleton and facilitates myofibroblast differentiation and ECM production in fibroblasts of diverse tissues (Akhmetshina et al., 2008; Ji et al., 2014; Manickam et al., 2014; Lai et al., 2019). RhoA (a GTPase) and ROCK can be activated by TGF-β to induce actin polymerization through SMAD-dependent or SMAD-independent mechanisms(Zhang, 2017). The rho-like GTPases Cdc42 and Rac can also be recruited by TGF-β to combinate with the TGF-β receptor complex, which is involved in cell-to-cell connection dissociation and cell migration during epithelial to mesenchymal transition (EMT) (Zhang, 2017).

JAK, which is a receptor-associated tyrosine kinase, acts as regulators of cytokine and growth factor signaling. JAK2 is a regulator of the profibrotic results of TGF-β in many fibrotic diseases (O'Shea et al., 2015; Cao et al., 2019; Zhao et al., 2019; Qin et al., 2020). STAT3, a STAT protein and a downstream regulator of JAK2 signaling, is crucial to many fibrotic diseases in a TGF-β-dependent manner (O'Shea et al., 2015; Chakraborty et al., 2017; Oh et al., 2018). In this signaling, first, JAK2 is phosphorylated when cytokines bind to cell receptors. Subsequently, the phosphorylates downstream STAT3, which participates in various biological processes, such as cell proliferation, differentiation, and apoptosis (O'Shea et al., 2015).

ROLE OF miRNAs IN THE CANONICAL AND NONCANONICAL TGF-β SIGNALING PATHWAYS IN FIBROTIC DISEASES AFFECTING DIFFERENT ORGANS

Kidney

In recent years, the vital role of miRNAs in renal pathophysiology has been evidenced by clinical and experimental models (Van der Hauwaert et al., 2019). During the progression of renal fibrosis mediated by SMAD-3, miR-29 and miR-200 are downregulated, and miR-21 and miR-192 are upregulated (Meng et al., 2015). The miR-29 family, including miR-29a, miR-29b, and miR-29c, acts as a negative modulator of some fibrotic diseases through canonical TGF-β-SMAD-2/3 signaling, thereby playing a protective role in the fibrotic process (He et al., 2013). Expression of disintegrin metalloproteases Adams, mainly Adam10, Adam12, Adam17, and Adam19, is significantly upregulated *in vivo* and *in vitro* through the regulation of the TGF-β-SMAD-2/3 pathway. Overexpression of miR-29 can downregulate Adam12 and Adam19 expressions, partially mitigating fibrosis (Ramdas et al., 2013). Although the function of Adam in fibrosis and its specific mechanism in the fibrotic process are clear, accumulating evidence indicates that they significantly correlate with the development of fibrosis and that multiple miR-29 binding sites are present in the 3′-UTR region of the mRNA of Adams (Ramdas et al., 2013). In addition, Sole et al. showed that patients with lupus nephritis accompanied by high renal chronicity indexes have significantly reduced miR-29c levels in urinary exosomes, suggesting the early diagnostic value of miR-29c in renal fibrosis (Solé et al., 2015). Although significant downregulation of miR-200b occurs in renal fibrosis related to TGF-β signaling (Meng et al., 2015). Tang et al. postulated that miR-200b represses TGF-β1-induced EMT by inhibiting ZEB1 and ZEB2 and ECM protein fibronectin by directly targeting the 3′UTR region of the mRNA, which is not directly associated with the TGF-β signaling pathway (Tang et al., 2013). A study showed that in paclitaxel-treated renal fibrosis animal models, inhibition of TGF-β/SMAD-2/3 signaling and mitigation of renal fibrosis, which were accompanied by downregulation of miR-192, probably implied the regulatory relationship between miR-192 and the canonical TGF-β signaling pathway (Sun et al., 2011). Diabetic nephropathy (DN) is characterized by basement membrane thickening, glomerular hypertrophy, and ECM deposition, eventually leading to renal interstitial fibrosis. Ma et al. showed that miR-130b is related to fibrosis in DN, and its overexpression can not only promote the mRNA and protein expressions of collagen types I and IV and fibronectin but also increase its downstream signal TGF-β1, t-Smad2/3, P-SMAD-2/3, and SMAD-4 expressions, thus implying a profibrotic role of miR-130b in DN and its strong correlation with the canonical TGF-β/SMAD-2/3 signaling pathway (Ma et al., 2019). Another study verified the negative regulatory role of miR-101a in chronic kidney disease (Ding et al., 2020). KDM3A, a histone demethylase, which is a key regulator of histone modification, accelerates chronic renal fibrosis by directly regulating the YAP-TGF-β-SMAD signaling pathway or indirectly mediating TGF-β-SMAD signaling by suppressing the expression of TGIF1 (Ding et al., 2020). However, overexpressed miR-101a can alleviate chronic renal fibrosis by downregulating the protein and mRNA expressions of KDM3A. The inhibitory effect of miR-101a on this disease can also be partially reversed by overexpression of YAP/TGF-β2 or inhibition of TGIF (Ding et al., 2020). Taken together, the aforementioned miRNAs mainly affect the progression of renal fibrosis through the canonical TGF-β signaling pathway.

Several studies indicated that miR-21 is strongly associated with renal fibrosis and plays a key role in the profibrotic process (Zarjou et al., 2011; Ben-Dov et al., 2012; Glowacki et al., 2013; Chen et al., 2015; Luo et al., 2019). For example, in an *in vivo* study, the kidneys with unilateral ureteral obstruction presented with elevated levels of miR-21 compared to those without the obstruction in mouse models, (Glowacki et al., 2013) and blockade of miR-21 in this model alleviated fibrosis (Zarjou

et al., 2011). In humans, the enhanced expression of miR-21 can be tested in renal allografts with severe interstitial fibrosis compared to those without fibrosis (Ben-Dov et al., 2012; Glowacki et al., 2013). A study by Chen et al. showed that elevated levels of miR-21 led to the upregulation of phosphorylated AKT and downregulation of PTEN, which sped up the fibrotic process during long-term nephrotoxicity induced by calcineurin inhibitors (Chen et al., 2015). In addition, Luo et al. indicated that Smilax glabra Roxb (PTFS), a traditional Chinese herb, showed powerful anti-EMT and anti-fibrosis effects both *in vitro* and *in vivo*, and the mechanism underlying them may be associated with the miR-21/PTEN/PI3K/Akt signaling pathway and their complicated upstream molecular regulatory network involving TGF-β signaling (Luo et al., 2019).

In early years, miR-132 was demonstrated to affect cell proliferation during wound healing by regulating the STAT3 and ERK pathways (Li et al., 2015a). Subsequently, Bijkerk et al. suggested that miR-132 may coordinately mediate genes involved in TGF-β signaling, STAT3/ERK pathways, and cell proliferation (Foxo3/p300) related to promoting trans-differentiation and proliferation of myofibroblasts during the formation of renal fibrosis (Bijkerk et al., 2016). A study by Wang et al. supported that p53 could physically interplay with the promoter region of miR-199a-3p by using chromatin immunoprecipitation assays (Wang et al., 2012a). Yang et al. reported a novel modulatory mechanism of promoting renal fibrosis in which miR-199a-3p suppresses the suppressors of cytokine signaling-7 (SOCS7), a SOCS family, to upregulate STAT3 activation, which is directly induced by TGF-β-driven p53 upregulation. *In vitro* and *in vivo* experiments also confirmed that the TGF-β/p53/miR-199a-3p/SOCS7/STAT3 axis may play a critical role in human renal fibrosis (Yang et al., 2017a). In addition to miR-199a-3p, miR-206 is associated with the JAK/STAT3 pathway, according to a study by Zhao et al. (2019). In that study, miR-206 attenuated EMT in chronic kidney disease by suppressing JAK/STAT signaling by directly targeting Annexin A1. Wu et al. reported that overexpression of miR-455-3p attenuates renal fibrosis by directly targeting the 3′-UTR region of ROCK2 in the DN model, providing a testimony for the protective effect of miR-455-3p in DN (Wu et al., 2018). Thus, these miRNAs affect renal fibrosis by regulating the non-canonical TGF-β signaling pathway.

Liver

In studies related to liver fibrosis, miR-193a/b, miR-942, miR-96, and miR-21 play central roles in the canonical TGF-β signaling pathway (Roderburg et al., 2013; Luo et al., 2018; Tao et al., 2018; Ju et al., 2019). In concanavalin A-induced hepatic fibrosis mice models, miR-193a/b-3p played a protective role by alleviating concanavalin A-induced hepatic fibrosis through apoptosis and cell cycle arrest of hepatic stellate cells (HSCs) and inhibition of HSCs activation (Ju et al., 2019). During this process, the expression of TGF-β1 and phosphorylation of SMAD-2/3 are restrained, and CAPRIN1, a cell cycle-related protein, is confirmed to be the target gene of miR-193a/b-3p by the dual luciferase reporter system (Ju et al., 2019). Another study showed the prominent role of miR-942 in the progression of liver fibrosis infected by the hepatitis B virus (Tao et al., 2018). The miR-942 in activated HSCs was upregulated in cell models and liver specimens of patients with hepatitis B virus-related liver fibrosis and correlated inversely with bone morphogenic proteins and activin membrane-bound inhibitor (BAMBI), which interfered with TGF-β1 signaling by capturing TGF-β receptor I (TβRI/ALK-5) (Tao et al., 2018). Thus, with the degradation of BAMBI, the activity of the TGF-β/SMAD-2/3 signaling pathway is enhanced, which promotes the process of fibrosis (Tao et al., 2018). Schistosomiasis, a severe subtropical parasitic disease, induces liver fibrosis and results in portal hypertension, which are the main causes of host mortality. Luo et al. (2018) indicated that schistosomiasis-infected mice showed significant hepatic fibrosis, accompanied by high expressions of miR-96, TGF-β, and Smad2/3 and suppression of Smad7 (Luo et al., 2018). Subsequently, transfection of the miR-96 inhibitor through recombinant adeno-associated virus 8 could significantly alleviate liver fibrosis, and the dual luciferase reporter assay proved that Smad7 is its target gene (Luo et al., 2018). A study indicated unchanged levels of overall miR-133a in whole RNA extracted from the fibrotic murine and human livers but specifically downregulated in HSC during fibrogenesis (Roderburg et al., 2013). The addition of TGF-β in HSC downregulated the expression of miR-133 more sharply, which aggravated the rate of hepatofibrogenesis, but overexpression of miR-133 could partly reverse this (Roderburg et al., 2013). Thus, miR-133 may be a diagnostic biomarker and a target for therapeutic strategies in hepatic fibrosis (Roderburg et al., 2013).

The role of miR-21 in liver fibrosis is supported by the literature (Yang et al., 2017b; Wang et al., 2017; Huang et al., 2019). In recent years, some studies have found that some drugs used for hepatic fibrosis exert anti-fibrosis effects by acting on miR-21-related signal axes (Yang et al., 2017b; Wang et al., 2017; Huang et al., 2019). The most reported drugs are chlorogenic acid (CGA) and methyl helicterate (Yang et al., 2017b; Wang et al., 2017; Huang et al., 2019). CGA, a phenolic acid abundantly found in nature, has various pharmacological effects, including anti-inflammatory, anti-hypertensive, and anti-oxidant capacities (Yang et al., 2017b). miR-21 can enhance the activity of the TGF-β/SMAD-2/3 signaling pathway by inhibiting the expression of Smad7, which promotes the fibrotic process in the liver, which is reversible by CGA *in vitro* and *in vivo* (Yang et al., 2017b). The therapeutic mechanism of CGA in liver fibrosis caused by schistosomiasis is also consistent with the aforementioned result, whereby significant downregulation of miR-21 expression is accompanied by upregulation of Smad7, reductions of p-Smad2 and p-Smad3, and conspicuous alleviation of fibrosis (Wang et al., 2017). Methyl helicterate is the main ingredient of *Helicteres angustifolia*, which has been utilized as a traditional Chinese medicine to treat immune disorders and liver diseases (Huang et al., 2019). Activation of the ERK1 pathway can promote the deposition of collagen and the expression of α-SMA to accelerate the process of fibrosis, while SPRY2 can inhibit this pathway, but miR-21 can bind to the 3′UTR region of SPRY2 to reverse its effect (Huang et al., 2019). A study showed that methyl helicterate could mitigate liver fibrosis by inhibiting miR-21-mediated ERK and TGFβ/SMAD 2/3 pathways and, therefore,

has potential as a therapeutic drug for liver fibrosis (Huang et al., 2019).

Compared to normal liver tissue, miR-101 is significantly downregulated in hepatitis B virus-related cirrhosis, hepatic fibrosis, and hepatocellular carcinoma (Lei et al., 2019). A study showed that the expression of miR-101 in CCL_4-induced fibrotic liver tissue in mice was significantly reduced, contrary to the high expressions of TGF-β, p-PI3K, p-Akt, p-mTOR, and fibrosis-related proteins (Lei et al., 2019). However, overexpression of miR-101 completely reversed this, so downregulating the PI3K/Akt/mTOR signaling pathway may be feasible against hepatic fibrosis (Lei et al., 2019). Similar to miR-101, miR-29b could also downregulate the PI3K/Akt signal axis to inhibit the fibrotic process in the liver (Wang et al., 2015). In addition, it could cause cell cycle arrest in the G1 phase of cells by downregulating cyclinD1 and p21, thereby suppressing hepatocyte viability and colony formation (Wang et al., 2015). In contrast, miR-33a plays a reverse role in promoting hepatic fibrosis by regulating the PI3K/Akt signaling pathway (Li et al., 2014). The activity of the JAK2/STAT3 signal axis in hepatic fibrosis also cannot be underestimated. Yang et al. reported that the low expression of miR-375-3p in the mouse liver can induce the JAK2/STAT3 pathway to activate the TGF-β1/SMAD signal and promote EMT, whereas the addition of miR-375-3p mimic has an antifibrotic effect (Yang et al., 2019). Taken together, these findings indicate the active regulatory functions of miRNAs in liver fibrosis affected by the non-canonical TGF-β signaling pathway.

Lung

TGF-β receptors are important elements in the canonical TGF-β/SMAD 2/3 signaling pathway (Wrighton et al., 2009). Some studies reported that miRNAs, including miR-18a-5p, miR-153, and miR-1344, play anti-pulmonary fibrosis effects for targeting TGF-β receptors to inhibit downstream SMAD-2/3 expression (Liang et al., 2015; Stolzenburg et al., 2016; Zhang et al., 2017). Among them, miR-18a-5p and miR-153 directly target TGF-βRII, whereas miR-1344 can not only target TGF-βRII but also TGF-βRI (ALK5), which showed anti-fibrotic effects in lung fibrosis models (Liang et al., 2015; Stolzenburg et al., 2016; Zhang et al., 2017). miR-101 influences the proliferation and activation of lung fibroblasts in pulmonary fibrosis through two signaling pathways (Huang et al., 2017). Regarding the proliferation of pulmonary fibroblasts, miR-101 reverses this process by targeting frizzled receptor 4/6 (FZD4/6) to inhibit WNT5a-FZD4/6-NFATc2 signaling, which is a form of the Wnt signaling pathway (Huang et al., 2017). To activate lung fibroblasts, miR-101 reduces the degree of fibroblast activation by directly targeting TGF-βRI (ALK5) to further inhibit the phosphorylation of SMAD-2/3 (Huang et al., 2017). The expression of miR-411-3p in silicosis rats and lung fibroblasts induced by TGF-β was significantly reduced, and the overexpression of miR-411-3p reversed the phenomenon and relieved the development of pulmonary fibrosis (Gao et al., 2020). The underlying mechanism is that miR-411-3p has an inhibitory effect on the expression of SMAD ubiquitination regulator 2 (Smurf2) and reduces the ubiquitination degradation of Smad7 under control of Smurf2, which results in blocking TGF-β/Smads signaling (Gao et al., 2020). In contrast, miR-21 promotes the transduction of the TGF-β/SMAD-2/3 signaling pathway by directly targeting Smad7 to accelerate the process of pulmonary fibrosis (Wang et al., 2018). In addition, miR-21 can also sharply reduce the phosphorylation levels of ERK, p38, and JNK, which were induced by resveratrol, thereby promoting the process of fibrosis by affecting the non-canonical TGF-β/MAPK signaling pathway (Wang et al., 2018). The miR-200 family is useful in pulmonary fibrosis (Cao et al., 2018). An article reported that miR-200b/c exerts a protective effect by targeting ZEB1/2, which may be related to the inhibition of p38 MAPK and TGF-β/SMAD-3 signaling pathway (Cao et al., 2018). Autophagy, a method of fibrotic regulation, is significantly reduced during fibrosis, and a study showed that miR-449a activates autophagy by targeting Bcl2 induced by the TGF-β1/ERK/MAPK pathway, thereby alleviating the development of lung fibrosis (Han et al., 2016). In addition, miR-344a-5p plays a vital role in anti-pulmonary fibrosis through MAPK signaling pathways, including map3k11 (Liu et al., 2017). As for the mechanism, miR-344a-5p inhibits the proliferation of myofibroblasts by targeting the mRNA of map3k11 to alleviate pulmonary fibrosis (Liu et al., 2017). lncRNA PCF is upregulated, which is affected by the activation of TGF-β1, to act as the ceRNA of miR-344a-5p and reverse its effect (Liu et al., 2017).

In pulmonary fibrosis induced by the non-canonical TGF-β/PI3K-Akt signaling pathway, miR-193a, miR-542-5p, miR-31/184, and miR-301a are crucial (Yuan et al., 2018; Liu et al., 2019; Wang et al., 2020a). The upregulation of miR-193a in paraquat-induced pulmonary fibrosis leads to the downregulation of the PI3K/AKT/mTOR axis and the upregulation of its downstream autophagy-related LC3-II/LC3-I and Beclin1, which induced the autophagy of lung fibroblasts and then reduced the expression of pulmonary fibrosis marker protein α-SMA and collagen deposition (Liu et al., 2019). The decrease of miR-542-5p in silica-induced mouse pulmonary fibrosis was shown by the miRNAs microarray analysis in a study by Yuan et al. (2018) In that study, miR-542-5p was confirmed to reverse TGF-β1 or silica-induced mouse lung fibrosis by directly targeting integrin α6, which inhibited fibroblast activation and reduced the phosphorylation levels of FAK/PI3K/AKT *in vitro* (Yuan et al., 2018). MiR-31 and miR-184 play contradictory roles in pulmonary fibrosis, which was verified by Wang et al. (2020a). In that study, miR-31 was enhanced, and miR-184 was suppressed *in vitro*, accompanied by the upregulation of TGF-β-SMAD-2 and TGF-β-PI3K-AKT signaling pathways and increase of some profibrotic factors, matrix metallopeptidase 7 (MMP7) and Runt-related protein 2 (RUNX2) (Wang et al., 2020a). As for the mechanism, the 3′UTR region of SMAD 6 was confirmed to be the binding site of miR-31, which promoted SMAD 2 phosphorylation to further enhance the SMAD 2/SMAD-4 dimer formation and translocation (Wang et al., 2020a). Thus, downregulating miR-31 and upregulating miR-184 may effectively ameliorate pulmonary fibrosis (Wang et al., 2020a). In the noncanonical TGF-β/JAK2/STAT3 pathway in lung fibrosis, miR-125a-3p plays a pivotal role. In a study by Xu et al., miR-125a-3p directly targetted 3′UTR of Fyn and then lead

to the inactivation of the Fyn downstream effector STAT3, which inhibited the progression of silica-induced murine pulmonary fibrosis and TGF-β1-treated fibroblast lines (Xu et al., 2019).

Heart

In cardiac fibrosis, miRNAs related to the regulation of the canonical TGF-β/Smad2/3 signaling pathway should first be miR-150-5p (Che et al., 2019). In a study by Che et al., miR-150-5p inhibited the binding of Smad7 to ALK5 by directly targeting smad7, which promoted the increase of the binding of Smad2/3 to ALK5, thereby promoting the high expression of TGF-β/Smad2/3 signal, accelerating extracellular collagen deposition, and exacerbating the process of myocardial fibrosis (Che et al., 2019). miR-328 has the same effect as miR-150-5p in cardiac fibrosis, and its inhibition can also significantly reduce the expression level of the TGF-β/Smad2/3 signaling pathway, but its specific target molecule is unclear (Du et al., 2016). The canonical effectors of the TGF-β signaling pathway, p-SMAD2 and p-SMAD3, can also control the nuclear steps of miRNA biogenesis, which promotes transcriptional activation of pri-miRNAs and regulates the subsequent post-transcriptional conversion of pri-miRNAs into pre-miRNAs by DROSHA (Siomi and Siomi, 2010). This mechanism is well reflected in the regulation of the conversion of pri-miR-21 into pre-miR-21 (Davis-Dusenbery and Hata, 2011). Moreover, p-SMAD2/3 can interact with the DICER enzyme in the cytoplasm to enhance the cleavage efficiency of DICER for pre-miR-21 in the form of a complex of p-SMAD2/3/DICER, which promotes pre-miR-21 to mature miR-21 transformation (García et al., 2015). In addition, the direct target effect of miR-21 on the 3′UTR region of SMAD7 in cardiac fibrosis was demonstrated in that article, which further clarified the pro-fibrotic mechanism of miR-21 (García et al., 2015). Unlike the aforementioned miRNAs, miR-24 has the contradictory effect of inhibiting cardiac fibrosis (Wang et al., 2012b). The overexpressed miR-24 downregulates the expression of the TGF-β/SMAD2/3 signaling pathway to slow down the fibrosis process by directly targeting furin, which is a protease that controls latent TGF-β activation processing (Wang et al., 2012b).

In the non-canonical TGF-β/MAPKs signaling pathway, a study on miR-433 characterized its crucial role in regulating cardiac fibrosis (Tao et al., 2016). In that study, miR-433 was highly expressed in fibroblasts of cardiac fibrosis tissue, and its knockdown could significantly inhibit the transdifferentiation of cardiac fibroblasts into myofibroblasts (Tao et al., 2016). As for the mechanism, miR-433 directly targets JNK1, which leads to the activation of ERK and p38 kinase, and subsequent SMADs activity, particularly SMAD3 activity (Tao et al., 2016). miR-7a/b has a contradictory effect compared to miR-433 in the progression of cardiac fibrosis (Li et al., 2015b). Although the potential target of miR-7a/b is unclear, it similarly affects TGF-β/MAPKs signaling in the dynamic of the regulation of cardiac fibrosis (Li et al., 2015b).

Other Organs

Hypertrophic scar (HS) is a pathological scar resulting from abnormal wound healing (Shen et al., 2020). A study by Shen et al. reported that miR-145-5p could remarkably ameliorate HS by directly targeting the canonical TGF-β effectors SMAD-2/3 (Shen et al., 2020). Thus, it may be an available therapeutic drug for treating HS (Shen et al., 2020). The same effect could be found in the regulated function of miR-29b in HS, but its specific target in the canonical TGF-β signaling pathway requires further research (Guo et al., 2017).

Bladder outlet obstruction (BOO) is commonly encountered in the field of urology, often accompanying fibrosis of the bladder structure (Fusco et al., 2018). Wang et al. showed that miR-101b has protective function in hypoxia-induced fibrosis coursed by BOO, which is mainly associated with the canonical TGF-β/SMAD-2/3 signaling pathway (Wang et al., 2019b). As for the mechanism, the TGF-β type 1 receptor was inhibited by direct targeting of miR-101b, subsequently affecting the phosphorylation of its downstream molecule SMAD2/3, which ultimately caused the downregulation of the canonical TGF-β/SMAD2/3 signaling pathway (Wang et al., 2019b).

Oral submucous fibrosis (OSMF) is a chronic, progressive, pre-malignant condition mainly related to the consumption of betel nuts (Singh et al., 2018). In recent years, many studies have investigated miRNAs related to OSMF, including miR-21, miR-10b, and miR-942-5p (Singh et al., 2018; Fang et al., 2020; Wang et al., 2020b). Among them, the most in-depth research is of miR-942-5p, reported by Wang et al. (2020b) In that study, miR-942-5p showed significantly low expression in oral squamous carcinoma in the background of OSMF and could directly target latent transforming growth factor beta binding protein 2 (LTBP2), which further blocked the PI3K/Akt/mTOR signaling pathway (Wang et al., 2020b). The regulatory mechanisms of miRNAs in the canonical and non-canonical TGF-β signaling pathway are summarized as shown in **Figure 1**. In addition, the miRNAs in canonical and non-canonical TGF-β signaling in fibrotic diseases of different organs are also listed in the **Table 1**.

DISCUSSION

Previous studies have suggested that the TGF-β signaling pathway, which plays a major regulatory role in fibrotic diseases, is widely regulated by miRNAs. Some of these miRNAs can affect various fibrotic diseases *via* canonical or non-canonical TGF-β signaling, including miR-21, miR-101, miR-29, miR-200, miR-942, and miR-193. Among them, miR-21 has been widely confirmed to promote the occurrence and development of fibrosis of organs, such as the kidney (Zarjou et al., 2011; Ben-Dov et al., 2012; Glowacki et al., 2013; Chen et al., 2015; Luo et al., 2019), liver (Yang et al., 2017b; Wang et al., 2017; Huang et al., 2019), lung (Wang et al., 2018) and heart (Davis-Dusenbery and Hata, 2011; García et al., 2015), by targeting the canonical TGF-β/SMAD2/3 signaling pathway and the non-canonical TGF-β/PI3K/AKT signaling pathway. miR-101 plays an active role in inhibiting fibrotic diseases, such as renal (Ding et al., 2020), hepatic (Lei et al., 2019), or pulmonary fibrosis (Huang et al., 2017) and bladder outlet obstruction (Wang et al., 2019b), by directly targeting ALK5 in

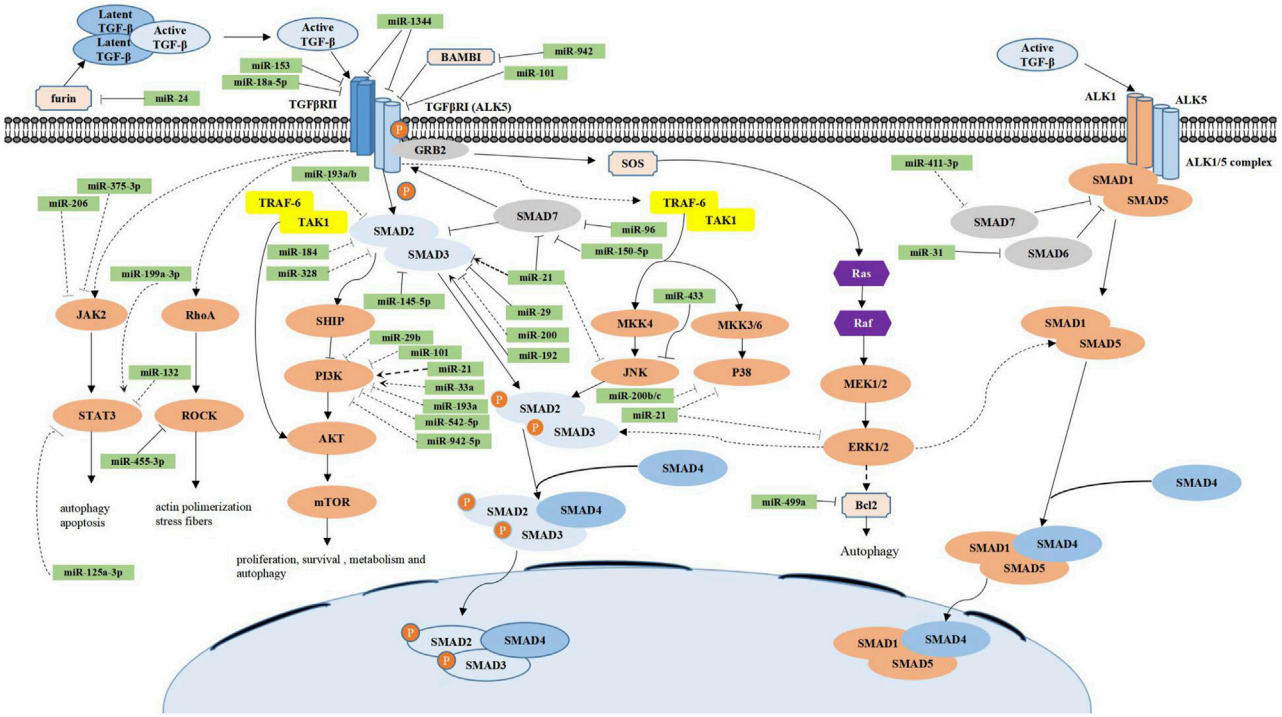

FIGURE 1 | Regulatory mechanisms of miRNAs in the canonical and noncanonical TGF-β signaling pathways. In the canonical TGF-β signaling pathway (blue), active TGF-β is first isolated from the latent TGF-β complex in the extracellular space and then binds to the TGF-β type II receptor (TGF-βRII), which in turn binds and phosphorylates TGF-β type I receptor (ALK5), causing its activation. ALK5 continues to phosphorylate intracellular SMAD-2 and SMAD-3 proteins, which constitute a complex with SMAD-4 and finally accumulate in the nucleus and further regulate fibrosis-related gene expression. In addition, the inhibitory function of SMAD-7 competes with SMAD 2/3 to bind with phosphorylated ALK5, thereby inhibiting the TGF-β signaling pathway. The noncanonical TGF-β signaling pathway (orange) most commonly includes the TGF-β/Smad1/5, TGF-β/PI3K/AKT/mTOR, TGF-β/MAPK (ERKs, JNKs, and p38), TGF-β/JAK2/STAT3, and TGF-β/RhoA/ROCK signaling pathways. Their functions are also listed in the figure. Numerous miRs have been implicated in the regulation of the canonical and noncanonical TGF-β signaling pathways. miRs are grouped to have the direct (solid line) or indirect (dotted line) effect as well as the promotion (arrowhead) or inhibition (flathead) effect.

the canonical TGF-β signaling pathway. miR-29 can ameliorate renal fibrosis (Ramdas et al., 2013; Solé et al., 2015) and HS (Guo et al., 2017) by targeting the canonical TGF-β signaling-related disintegrin metalloprotease Adams but inhibit liver fibrosis (Wang et al., 2015) by regulating the non-canonical TGF-β/PI3K/AKT signaling pathway. miR-200 exerts anti-fibrosis effects on the kidney (Tang et al., 2013) and lung (Cao et al., 2018) by directly targeting ZEB1/2. miR-942 can promote liver fibrosis (Tao et al., 2018) but plays a contrary regulatory role in oral submucous fibrosis (Wang et al., 2020b). In addition, miR-193 plays a protective role in pulmonary (Liu et al., 2019) and hepatic fibrosis (Ju et al., 2019) by regulating canonical TGF-β/SMAD2/3 and non-canonical TGF-β/PI3K/AKT/mTOR signaling pathways, respectively. Thus, the aforementioned miRNAs can become therapeutic targets or molecular drugs for fibrotic diseases owing to their regulatory effects in various fibrotic diseases.

Fibrosis offers the advantage of promoting tissue repair and healing. However, excessive fibrosis can cause tissue and organ dysfunctions (Diegelmann and Evans, 2004). During tissue repair, temporary ECM deposition occurs first, followed by the recruited inflammatory cells, the proliferated fibroblasts, and angiogenesis replacing the temporary ECM deposition and, finally, capillaries and fibroblasts degenerating with epithelial regeneration (Diegelmann and Evans, 2004). In contrast, fibrosis represents a disorder of the tissue repair process, during which excessive deposition of ECM rich in fibrous collagen, induction and proliferation of myofibroblasts, and repeated inflammatory responses lead to the replacement of normal parenchymal tissues and formation of non-functioning scar tissue (Diegelmann and Evans, 2004). Canonical and non-canonical TGF-β signaling pathways are the main signal axis regulating the fibrosis process (Meng et al., 2016; Finnson et al., 2020). miRNAs can promote or inhibit the progression of fibrotic diseases by targeting the upstream or downstream signal molecules of the TGF-β signaling network (Banerjee et al., 2011; Liu et al., 2018; Li et al., 2019). Therefore, miRNAs can be used as molecular drugs or targets to diagnose and treat fibrotic diseases. The intervention of miRNAs in the early manifestations of fibrosis related to the TGF-β signaling pathway may induce tissue healing and prevent the occurrence of fibrosis.

TABLE 1 | MiRNAs in canonical and noncanonical TGF-β signaling in fibrotic diseases of different organs. HS, hypertrophic scar; BOO, bladder outlet obstruction; OSF, oral submucous fibrosis; TGF-β, transforming growth factor-β; Smad2/3, *drosophila* mothers against decapentaplegic protein 2/3; PI3K, phosphatidylinositol 3-kinase; Akt, protein kinase B; MAPK, mitogen-activated protein kinase; JAK2, Janus kinase 2; STAT3, signal transducer and activator of transcription 3; ROCK, rho-associated coiled-coil containing kinase.

Location	Source	Disease	Mechanism	microRNAs	References
Kidney	Human	Renal fibrosis	TGF-β/Smad2/3 signaling pathway	miR-29	He et al. (2013), Ramdas et al. (2013), Solé et al. (2015)
			TGF-β/Smad2/3 signaling pathway	miR-21	Glowacki et al. (2013), Zarjou et al. (2011), Ben-Dov et al. (2012)
			TGF-β/Smad2/3 signaling pathway	miR-192	Sun et al. (2011)
			TGF-β/Smad2/3 signaling pathway	miR-101a	Ding et al. (2020)
			TGF-β/PI3K/Akt signaling pathway	miR-21	Chen et al. (2015), Luo et al. (2019)
			TGF-β/JAK2/STAT3 signaling pathway	miR-132	Li et al. (2015a), Bijkerk et al. (2016)
			TGF-β/JAK2/STAT3 signaling pathway	miR-199a-3p	Wang et al. (2012a), Yang et al. (2017a)
			TGF-β/JAK2/STAT3 signaling pathway	miR-206	Zhao et al. (2019)
			TGF-β/ROCK signaling pathway	miR-455-3p	Wu et al. (2018)
Liver	Human	Hepatic fibrosis	TGF-β/Smad2/3 signaling pathway	miR-193a/b	Ju et al. (2019)
			TGF-β/Smad2/3 signaling pathway	miR-942	Tao et al. (2018)
			TGF-β/Smad2/3 signaling pathway	miR-96	Luo et al. (2018)
			TGF-β/Smad2/3 signaling pathway	miR-133	Roderburg et al. (2013)
			TGF-β/Smad2/3 signaling pathway	miR-21	Yang et al. (2017b), Wang et al. (2017), Huang et al. (2019)
			TGF-β/PI3K/Akt signaling pathway	miR-101	Lei et al. (2019)
			TGF-β/PI3K/Akt signaling pathway	miR-29b	Wang et al. (2015)
			TGF-β/PI3K/Akt signaling pathway	miR-33a	Li et al. (2014)
			TGF-β/JAK2/STAT3 signaling pathway	miR-375-3p	Yang et al. (2019)
			TGF-β/MAPK signaling pathway	miR-21	Huang et al. (2019)
Lung	Human	Pulmonary fibrosis	TGF-β/Smad2/3 signaling pathway	miR-18a-5p	Zhang et al. (2017)
			TGF-β/Smad2/3 signaling pathway	miR-153	Liang et al. (2015)
			TGF-β/Smad2/3 signaling pathway	miR-1344	Stolzenburg et al. (2016)
			TGF-β/Smad2/3 signaling pathway	miR-411-3p	Gao et al. (2020)
			TGF-β/Smad2/3 signaling pathway	miR-21	Wang et al. (2018)
			TGF-β/Smad2/3 signaling pathway	miR-200b/c	Cao et al. (2018)
			TGF-β/MAPK signaling pathway	miR-21	Wang et al. (2018)
			TGF-β/MAPK signaling pathway	miR-344a-5p	Liu et al. (2017)
			TGF-β/MAPK signaling pathway	miR-200b/c	Cao et al. (2018)
			TGF-β/PI3K/Akt signaling pathway	miR-193a	Liu et al. (2019)
			TGF-β/PI3K/Akt signaling pathway	miR-542-5p	Yuan et al. (2018)
			TGF-β/PI3K/Akt signaling pathway	miR-31/184	Wang et al. (2020a)
			TGF-β/JAK2/STAT3 signaling pathway	miR-125a-3p	Xu et al. (2019)
Heart	Human	Cardiac fibrosis	TGF-β/Smad2/3 signaling pathway	miR-150-5p	Che et al. (2019)
			TGF-β/Smad2/3 signaling pathway	miR-328	Du et al. (2016)
			TGF-β/Smad2/3 signaling pathway	miR-21	Davis-Dusenbery and Hata (2011), García et al. (2015)
			TGF-β/Smad2/3 signaling pathway	miR-24	Wang et al. (2012b)
			TGF-β/MAPK signaling pathway	miR-433	Tao et al. (2016)
Other organs	Human	HS	TGF-β/Smad2/3 signaling pathway	miR-145-5p	Shen et al. (2020)
			TGF-β/Smad2/3 signaling pathway	miR-29b	Guo et al. (2017)
		BOO	TGF-β/Smad2/3 signaling pathway	miR-101b	Fusco et al. (2018)
		OSF	TGF-β/PI3K/Akt signaling pathway	miR-942-5p	Wang et al. (2020b)
			TGF-β/PI3K/Akt signaling pathway	miR-21	Singh et al. (2018)

CONCLUSION AND PROSPECTS

Fibrosis is often the final histopathological change in the development of chronic inflammatory diseases and can occur in almost all tissues and organs throughout the body. According to the current research results of fibrotic diseases of various organs, the developmental mechanisms of tissue and organ fibrosis mainly involve the canonical TGF-β/SMAD2/3 signaling pathway and the non-canonical TGF-β pathway, including the TGF-β/ALK1/Smad1/5 pathway, the TGF-β/MAPK pathway, the TGF-β/PI3K-Akt pathway, the TGF-β/JAK2/STAT3 pathway, and the TGF-β/ROCK pathway. MiRNA, which is involved in various physiological and pathological processes, with important roles in the canonical or noncanonical TGF-β signaling pathways, has received widespread attention in recent years. The regulating function of miRNAs in fibrosis is mainly to promote or ameliorate fibrosis by inhibiting the expression of effect molecules in the fibrosis signal pathway at the mRNA level. However, current research on the regulation of miRNA in fibrotic diseases mainly focuses on fibrosis of organs such as the liver, the kidneys, the lungs,

and the heart, whereas the fibrosis-related research of other tissues and organs is limited and not in-depth. In addition, for the current mechanism research, the specific targets of many miRNAs and the upstream and downstream regulatory relationships are not comprehensive or sufficiently thorough.

In the future, many questions concerning the mechanisms of the pathogenesis of fibrotic diseases should be solved. For example, in addition to the few aforementioned organs, fibrosis of other tissues and organs has unique features and developmental progression, carrying research value. Therefore, more in-depth research should be performed. There may be more than five non-canonical TGF-β signaling pathways that affect the development of fibrosis. The related miRNAs are not limited to pathways, and long-term continuous exploration is required. The pathogenesis of fibrotic diseases is complex. Therefore, a single target therapy cannot have a complete effect, and combination treatment with multiple targets and signaling pathway may be more reasonable. Hence, the next step should be to explore the mechanisms of fibrotic diseases from different tissue and organs, investigating more signaling pathways related to fibrosis and more functional miRNAs in these diseases and trying combination therapeutic methods with multiple targets and multiple pathways.

AUTHOR CONTRIBUTIONS

XX, PH, ZW, KL, and ZT designed the concept. XX searched the literature, wrote the manuscript and made the figure and table. XX, PH, ZW, KL, and ZT revised the manuscript. All authors read and approved the final manuscript.

FUNDING

This work has been supported by the National Natural Science Foundation of China (81800952), National Natural Science Foundation of China (81671003), and the Natural Science Foundation of Hunan Province, China (2018JJ3712).

REFERENCES

Akhmetshina, A., Dees, C., Pileckyte, M., Szucs, G., Spriewald, B. M., Zwerina, J., et al. (2008). Rho-associated Kinases Are Crucial for Myofibroblast Differentiation and Production of Extracellular Matrix in Scleroderma Fibroblasts. *Arthritis Rheum.* 58, 2553–2564. doi:10.1002/art.23677

Banerjee, J., Chan, Y. C., and Sen, C. K. (2011). MicroRNAs in Skin and Wound Healing. *Physiol. Genomics* 43, 543–556. doi:10.1152/physiolgenomics.00157.2010

Ben-Dov, I. Z., Muthukumar, T., Morozov, P., Mueller, F. B., Tuschl, T., and Suthanthiran, M. (2012). MicroRNA Sequence Profiles of Human Kidney Allografts with or without Tubulointerstitial Fibrosis. *Transplantation* 94, 1086–1094. doi:10.1097/TP.0b013e3182751efd

Bijkerk, R., de Bruin, R. G., van Solingen, C., van Gils, J. M., Duijs, J. M. G. J., van der Veer, E. P., et al. (2016). Silencing of microRNA-132 Reduces Renal Fibrosis by Selectively Inhibiting Myofibroblast Proliferation. *Kidney Int.* 89, 1268–1280. doi:10.1016/j.kint.2016.01.029

Braicu, C., Buse, M., Busuioc, C., Drula, R., Gulei, D., Raduly, L., et al. (2019). A Comprehensive Review on MAPK: A Promising Therapeutic Target in Cancer. *Cancers* 11, 1618. doi:10.3390/cancers11101618

Cao, G., Zhu, R., Jiang, T., Tang, D., Kwan, H. Y., and Su, T. (2019). Danshensu, a Novel Indoleamine 2,3-dioxygenase1 Inhibitor, Exerts Anti-hepatic Fibrosis Effects via Inhibition of JAK2-STAT3 Signaling. *Phytomedicine* 63, 153055. doi:10.1016/j.phymed.2019.153055

Cao, Y., Liu, Y., Ping, F., Yi, L., Zeng, Z., and Li, Y. (2018). miR-200b/c Attenuates Lipopolysaccharide-Induced Early Pulmonary Fibrosis by Targeting ZEB1/2 via P38 MAPK and TGF-β/smad3 Signaling Pathways. *Lab. Invest.* 98, 339–359. doi:10.1038/labinvest.2017.123

Chaigne, B., Clary, G., Le Gall, M., Dumoitier, N., Fernandez, C., Lofek, S., et al. (2019). Proteomic Analysis of Human Scleroderma Fibroblasts Response to Transforming Growth Factor-ß. *Prot. Clin. Appl.* 13, 1800069. doi:10.1002/prca.201800069

Chakraborty, D., Šumová, B., Mallano, T., Chen, C.-W., Distler, A., Bergmann, C., et al. (2017). Activation of STAT3 Integrates Common Profibrotic Pathways to Promote Fibroblast Activation and Tissue Fibrosis. *Nat. Commun.* 8, 1130. doi:10.1038/s41467-017-01236-6

Che, H., Wang, Y., Li, Y., Lv, J., Li, H., Liu, Y., et al. (2019). Inhibition of microRNA-150-5p Alleviates Cardiac Inflammation and Fibrosis via Targeting Smad7 in High Glucose-treated Cardiac Fibroblasts. *J. Cel Physiol* 235, 7769–7779. doi:10.1002/jcp.29386

Chen, J., Zmijewska, A., Zhi, D., and Mannon, R. B. (2015). Cyclosporine-mediated Allograft Fibrosis Is Associated with Micro-RNA-21 through AKT Signaling. *Transpl. Int.* 28, 232–245. doi:10.1111/tri.12471

Dai, J.-P., Zhu, D.-X., Sheng, J.-T., Chen, X.-X., Li, W.-Z., Wang, G.-F., et al. (2015). Inhibition of Tanshinone IIA, Salvianolic Acid A and Salvianolic Acid B on Areca Nut Extract-Induced Oral Submucous Fibrosis *In Vitro*. *Molecules* 20, 6794–6807. doi:10.3390/molecules20046794

Davis-Dusenbery, B. N., and Hata, A. (2011). Smad-mediated miRNA Processing. *RNA Biol.* 8, 71–76. doi:10.4161/rna.8.1.14299

Diegelmann, R. F., and Evans, M. C. (2004). Wound Healing: An Overview of Acute, Fibrotic and Delayed Healing. *Front. Biosci.* 9, 283–289. doi:10.2741/1184

Ding, H., Xu, Y., and Jiang, N. (2020). Upregulation of miR-101a Suppresses Chronic Renal Fibrosis by Regulating KDM3A via Blockade of the YAP-TGF-β-Smad Signaling Pathway. *Mol. Ther. - Nucleic Acids* 19, 1276–1289. doi:10.1016/j.omtn.2020.01.002

Du, W., Liang, H., Gao, X., Li, X., Zhang, Y., Pan, Z., et al. (2016). MicroRNA-328, a Potential Anti-fibrotic Target in Cardiac Interstitial Fibrosis. *Cell Physiol Biochem* 39, 827–836. doi:10.1159/000447793

Fang, C.-Y., Yu, C.-C., Liao, Y.-W., Hsieh, P.-L., Ohiro, Y., Chu, P.-M., et al. (2020). miR-10b Regulated by Twist Maintains Myofibroblasts Activities in Oral Submucous Fibrosis. *J. Formos. Med. Assoc.* 119, 1167–1173. doi:10.1016/j.jfma.2020.03.005

Finnson, K. W., Almadani, Y., and Philip, A. (2020). Non-canonical (Non-smad2/3) TGF-β Signaling in Fibrosis: Mechanisms and Targets. *Semin. Cel Develop. Biol.* 101, 115–122. doi:10.1016/j.semcdb.2019.11.013

Finnson, K. W., Parker, W. L., ten Dijke, P., Thorikay, M., and Philip, A. (2008). ALK1 Opposes ALK5/Smad3 Signaling and Expression of Extracellular Matrix Components in Human Chondrocytes. *J. Bone Miner Res.* 23, 896–906. doi:10.1359/jbmr.080209

Fusco, F., Creta, M., De Nunzio, C., Iacovelli, V., Mangiapia, F., Li Marzi, V., et al. (2018). Progressive Bladder Remodeling Due to Bladder Outlet Obstruction: a Systematic Review of Morphological and Molecular Evidences in Humans. *Bmc Urol.* 18, 15. doi:10.1186/s12894-018-0329-4

Gao, X., Xu, H., Xu, D., Li, S., Wei, Z., Li, S., et al. (2020). MiR-411-3p Alleviates Silica-Induced Pulmonary Fibrosis by Regulating Smurf2/TGF-β Signaling. *Exp. Cel Res.* 388, 111878. doi:10.1016/j.yexcr.2020.111878

García, R., Nistal, J. F., Merino, D., Price, N. L., Fernández-Hernando, C., Beaumont, J., et al. (2015). p-SMAD2/3 and DICER Promote Pre-miR-21 Processing during Pressure Overload-Associated Myocardial Remodeling. *Biochim. Biophys. Acta (Bba) - Mol. Basis Dis.* 1852, 1520–1530. doi:10.1016/j.bbadis.2015.04.006

Glowacki, F., Savary, G., Gnemmi, V., Buob, D., Van der Hauwaert, C., Lo-Guidice, J.-M., et al. (2013). Increased Circulating miR-21 Levels Are Associated with Kidney Fibrosis. *PLoS One* 8, e58014. doi:10.1371/journal.pone.0058014

Goumans, M.-J., Valdimarsdottir, G., Itoh, S., Lebrin, F., Larsson, J., Mummery, C., et al. (2003). Activin Receptor-like Kinase (ALK)1 Is an Antagonistic Mediator of Lateral TGFβ/ALK5 Signaling. *Mol. Cel* 12, 817–828. doi:10.1016/s1097-2765(03)00386-1

Guo, J., Lin, Q., Shao, Y., Rong, L., and Zhang, D. (2017). miR-29b Promotes Skin Wound Healing and Reduces Excessive Scar Formation by Inhibition of the TGF-β1/Smad/CTGF Signaling Pathway. *Can. J. Physiol. Pharmacol.* 95, 437–442. doi:10.1139/cjpp-2016-0248

Han, R., Ji, X., Rong, R., Li, Y., Yao, W., Yuan, J., et al. (2016). MiR-449a Regulates Autophagy to Inhibit Silica-Induced Pulmonary Fibrosis through Targeting Bcl2. *J. Mol. Med.* 94, 1267–1279. doi:10.1007/s00109-016-1441-0

He, Y., Huang, C., Lin, X., and Li, J. (2013). MicroRNA-29 Family, a Crucial Therapeutic Target for Fibrosis Diseases. *Biochimie* 95, 1355–1359. doi:10.1016/j.biochi.2013.03.010

Henry, T. W., Mendoza, F. A., and Jimenez, S. A. (2019). Role of microRNA in the Pathogenesis of Systemic Sclerosis Tissue Fibrosis and Vasculopathy. *Autoimmun. Rev.* 18, 102396. doi:10.1016/j.autrev.2019.102396

Hill, C. S. (2009). Nucleocytoplasmic Shuttling of Smad Proteins. *Cell Res* 19, 36–46. doi:10.1038/cr.2008.325

Hu, H.-H., Chen, D.-Q., Wang, Y.-N., Feng, Y.-L., Cao, G., Vaziri, N. D., et al. (2018). New Insights into TGF-β/Smad Signaling in Tissue Fibrosis. *Chemico-Biological Interactions* 292, 76–83. doi:10.1016/j.cbi.2018.07.008

Huang, C., Xiao, X., Yang, Y., Mishra, A., Liang, Y., Zeng, X., et al. (2017). MicroRNA-101 Attenuates Pulmonary Fibrosis by Inhibiting Fibroblast Proliferation and Activation. *J. Biol. Chem.* 292, 16420–16439. doi:10.1074/jbc.M117.805747

Huang, Q., Zhang, X., Bai, F., Nie, J., Wen, S., Wei, Y., et al. (2019). Methyl Helicterte Ameliorates Liver Fibrosis by Regulating miR-21-Mediated ERK and TGF-β1/Smads Pathways. *Int. Immunopharmacology* 66, 41–51. doi:10.1016/j.intimp.2018.11.006

Ikushima, H., and Miyazono, K. (2012). TGF-β Signal Transduction Spreading to a Wider Field: a Broad Variety of Mechanisms for Context-dependent Effects of TGF-β. *Cell Tissue Res* 347, 37–49. doi:10.1007/s00441-011-1179-5

Ji, H., Tang, H., Lin, H., Mao, J., Gao, L., Liu, J., et al. (2014). Rho/Rock Cross-Talks with Transforming Growth Factor-β/Smad Pathway Participates in Lung Fibroblast-Myofibroblast Differentiation. *Biomed. Rep.* 2, 787–792. doi:10.3892/br.2014.323

Ju, B., Nie, Y., Yang, X., Wang, X., Li, F., Wang, M., et al. (2019). miR-193a/b-3p Relieves Hepatic Fibrosis and Restrains Proliferation and Activation of Hepatic Stellate Cells. *J. Cel Mol Med* 23, 3824–3832. doi:10.1111/jcmm.14210

Katsuno, Y., Qin, J., Oses-Prieto, J., Wang, H., Jackson-Weaver, O., Zhang, T., et al. (2018). Arginine Methylation of SMAD7 by PRMT1 in TGF-β-Induced Epithelial-Mesenchymal Transition and Epithelial Stem-Cell Generation. *J. Biol. Chem.* 293, 13059–13072. doi:10.1074/jbc.RA118.002027

Kretzschmar, M., Doody, J., and Massagu, J. (1997). Opposing BMP and EGF Signalling Pathways Converge on the TGF-β Family Mediator Smad1. *Nature* 389, 618–622. doi:10.1038/39348

Kretzschmar, M., Doody, J., Timokhina, I., and Massague, J. (1999). A Mechanism of Repression of TGFbeta/Smad Signaling by Oncogenic Ras. *Genes Develop.* 13, 804–816. doi:10.1101/gad.13.7.804

Lai, S. S., Fu, X., Cheng, Q., Yu, Z. H., Jiang, E. Z., Zhao, D. D., et al. (2019). HSC-specific Knockdown of GGPPS Alleviated CCl4-Induced Chronic Liver Fibrosis through Mediating RhoA/Rock Pathway. *Am. J. Transl Res.* 11, 2382–2392.

Lei, Y., Wang, Q.-I., Shen, L., Tao, Y.-Y., and Liu, C.-H. (2019). MicroRNA-101 Suppresses Liver Fibrosis by Downregulating PI3K/Akt/mTOR Signaling Pathway. *Clin. Res. Hepatol. Gastroenterol.* 43, 575–584. doi:10.1016/j.clinre.2019.02.003

Li, D., Wang, A., Liu, X., Meisgen, F., Grünler, J., Botusan, I. R., et al. (2015a). MicroRNA-132 Enhances Transition from Inflammation to Proliferation during Wound Healing. *J. Clin. Invest.* 125, 3008–3026. doi:10.1172/jci79052

Li, K., Wu, Y., Yang, H., Hong, P., Fang, X., and Hu, Y. (2019). H19/miR-30a/C8orf4 axis Modulates the Adipogenic Differentiation Process in Human Adipose Tissue-derived Mesenchymal Stem Cells. *J. Cel Physiol* 234, 20925–20934. doi:10.1002/jcp.28697

Li, R., Xiao, J., Qing, X., Xing, J., Xia, Y., Qi, J., et al. (2015b). Sp1 Mediates a Therapeutic Role of MiR-7a/b in Angiotensin II-Induced Cardiac Fibrosis via Mechanism Involving the TGF-β and MAPKs Pathways in Cardiac Fibroblasts. *Plos One* 10, e0125513. doi:10.1371/journal.pone.0125513

Li, X., Zhang, Z.-L., and Wang, H.-F. (2017). Fusaric Acid (FA) Protects Heart Failure Induced by Isoproterenol (ISP) in Mice through Fibrosis Prevention via TGF-β1/SMADs and PI3K/AKT Signaling Pathways. *Biomed. Pharmacother.* 93, 130–145. doi:10.1016/j.biopha.2017.06.002

Li, Z.-J., Ou-Yang, P.-H., and Han, X.-P. (2014). Profibrotic Effect of miR-33a with Akt Activation in Hepatic Stellate Cells. *Cell Signal.* 26, 141–148. doi:10.1016/j.cellsig.2013.09.018

Liang, C., Li, X., Zhang, L., Cui, D., Quan, X., and Yang, W. (2015). The Anti-fibrotic Effects of microRNA-153 by Targeting TGFBR-2 in Pulmonary Fibrosis. *Exp. Mol. Pathol.* 99, 279–285. doi:10.1016/j.yexmp.2015.07.011

Liu, H., Lei, C., He, Q., Pan, Z., Xiao, D., and Tao, Y. (2018). Nuclear Functions of Mammalian MicroRNAs in Gene Regulation, Immunity and Cancer. *Mol. Cancer* 17, 64. doi:10.1186/s12943-018-0765-5

Liu, H., Wang, B., Zhang, J., Zhang, S., Wang, Y., Zhang, J., et al. (2017). A Novel Lnc-PCF Promotes the Proliferation of TGF-β1-Activated Epithelial Cells by Targeting miR-344a-5p to Regulate Map3k11 in Pulmonary Fibrosis. *Cell Death Dis* 8, e3137. doi:10.1038/cddis.2017.500

Liu, M.-W., Su, M.-X., Tang, D.-Y., Hao, L., Xun, X.-H., and Huang, Y.-Q. (2019). Ligustrazin Increases Lung Cell Autophagy and Ameliorates Paraquat-Induced Pulmonary Fibrosis by Inhibiting PI3K/Akt/mTOR and Hedgehog Signalling via Increasing miR-193a Expression. *Bmc Pulm. Med.* 19, 35. doi:10.1186/s12890-019-0799-5

Luo, Q., Cai, Z., Tu, J., Ling, Y., Wang, D., and Cai, Y. (2019). Total Flavonoids from Smilax Glabra Roxb Blocks Epithelial-mesenchymal Transition and Inhibits Renal Interstitial Fibrosis by Targeting miR-21/PTEN Signaling. *J. Cel Biochem* 120, 3861–3873. doi:10.1002/jcb.27668

Luo, X., Zhang, D., Xie, J., Su, Q., He, X., Bai, R., et al. (2018). MicroRNA-96 Promotes Schistosomiasis Hepatic Fibrosis in Mice by Suppressing Smad7. *Mol. Ther. - Methods Clin. Develop.* 11, 73–82. doi:10.1016/j.omtm.2018.10.002

Ma, Y., Shi, J., Wang, F., Li, S., Wang, J., Zhu, C., et al. (2019). MiR-130b Increases Fibrosis of HMC Cells by Regulating the TGF-β1 Pathway in Diabetic Nephropathy. *J. Cel Biochem* 120, 4044–4056. doi:10.1002/jcb.27688

Manickam, N., Patel, M., Griendling, K. K., Gorin, Y., and Barnes, J. L. (2014). RhoA/Rho Kinase Mediates TGF-β1-Induced Kidney Myofibroblast Activation through Poldip2/Nox4-Derived Reactive Oxygen Species. *Am. J. Physiology-Renal Physiol.* 307, F159–F171. doi:10.1152/ajprenal.00546.2013

Marquard, F. E., and Jücker, M. (2020). PI3K/AKT/mTOR Signaling as a Molecular Target in Head and Neck Cancer. *Biochem. Pharmacol.* 172, 113729. doi:10.1016/j.bcp.2019.113729

Meng, X.-M., Nikolic-Paterson, D. J., and Lan, H. Y. (2016). TGF-β: the Master Regulator of Fibrosis. *Nat. Rev. Nephrol.* 12, 325–338. doi:10.1038/nrneph.2016.48

Meng, X.-M., Tang, P. M.-K., Li, J., and Lan, H. Y. (2015). TGF-Î²/Smad Signaling in Renal Fibrosis. *Front. Physiol.* 6, 82. doi:10.3389/fphys.2015.00082

Mi, X.-J., Hou, J.-G., Jiang, S., Liu, Z., Tang, S., Liu, X.-X., et al. (2019). Maltol Mitigates Thioacetamide-Induced Liver Fibrosis through TGF-β1-Mediated Activation of PI3K/Akt Signaling Pathway. *J. Agric. Food Chem.* 67, 1392–1401. doi:10.1021/acs.jafc.8b05943

O'Shea, J. J., Schwartz, D. M., Villarino, A. V., Gadina, M., McInnes, I. B., and Laurence, A. (2015). The JAK-STAT Pathway: Impact on Human Disease and Therapeutic Intervention. *Annu. Rev. Med.* 66, 311–328. doi:10.1146/annurev-med-051113-024537

Oh, R. S., Haak, A. J., Smith, K. M. J., Ligresti, G., Choi, K. M., Xie, T., et al. (2018). RNAi Screening Identifies a Mechanosensitive ROCK-JAK2-STAT3 Network central to Myofibroblast Activation. *J. Cel Sci* 131. doi:10.1242/jcs.209932

Pannu, J., Nakerakanti, S., Smith, E., Dijke, P. T., and Trojanowska, M. (2007). Transforming Growth Factor-β Receptor Type I-dependent Fibrogenic Gene Program Is Mediated via Activation of Smad1 and ERK1/2 Pathways. *J. Biol. Chem.* 282, 10405–10413. doi:10.1074/jbc.M611742200

Qin, Y., Zhao, P., Chen, Y., Liu, X., Dong, H., Zheng, W., et al. (2020). Lipopolysaccharide Induces Epithelial-Mesenchymal Transition of Alveolar Epithelial Cells Cocultured with Macrophages Possibly via the JAK2/STAT3 Signaling Pathway. *Hum. Exp. Toxicol.* 39, 224–234. doi:10.1177/0960327119881678

Ramdas, V., McBride, M., Denby, L., and Baker, A. H. (2013). Canonical Transforming Growth Factor-β Signaling Regulates Disintegrin Metalloprotease Expression in Experimental Renal Fibrosis via miR-29. *Am. J. Pathol.* 183, 1885–1896. doi:10.1016/j.ajpath.2013.08.027

Roderburg, C., Luedde, M., Vargas Cardenas, D., Vucur, M., Mollnow, T., Zimmermann, H. W., et al. (2013). miR-133a Mediates TGF-β-dependent Derepression of Collagen Synthesis in Hepatic Stellate Cells during Liver Fibrosis. *J. Hepatol.* 58, 736–742. doi:10.1016/j.jhep.2012.11.022

Shen, W., Wang, Y., Wang, D., Zhou, H., Zhang, H., and Li, L. (2020). miR-145-5p Attenuates Hypertrophic Scar via Reducing Smad2/Smad3 Expression. *Biochem. Biophysical Res. Commun.* 521, 1042–1048. doi:10.1016/j.bbrc.2019.11.040

Singh, P., Srivastava, A. N., Sharma, R., Mateen, S., Shukla, B., Singh, A., et al. (2018). Circulating MicroRNA-21 Expression as a Novel Serum Biomarker for Oral Sub-mucous Fibrosis and Oral Squamous Cell Carcinoma. *Asian Pac. J. Cancer Prev.* 19, 1053–1057. doi:10.22034/APJCP.2018.19.4.1053

Siomi, H., and Siomi, M. C. (2010). Posttranscriptional Regulation of microRNA Biogenesis in Animals. *Mol. Cel* 38, 323–332. doi:10.1016/j.molcel.2010.03.013

Solé, C., Cortés-Hernández, J., Felip, M. L., Vidal, M., and Ordi-Ros, J. (2015). miR-29c in Urinary Exosomes as Predictor of Early Renal Fibrosis in Lupus Nephritis. *Nephrol. Dial. Transpl.* 30, 1488–1496. doi:10.1093/ndt/gfv128

Srivastava, S. P., Hedayat, A. F., Kanasaki, K., and Goodwin, J. E. (2019). microRNA Crosstalk Influences Epithelial-To-Mesenchymal, Endothelial-To-Mesenchymal, and Macrophage-To-Mesenchymal Transitions in the Kidney. *Front. Pharmacol.* 10, 904. doi:10.3389/fphar.2019.00904

Stolzenburg, L. R., Wachtel, S., Dang, H., and Harris, A. (2016). miR-1343 Attenuates Pathways of Fibrosis by Targeting the TGF-β Receptors. *Biochem. J.* 473, 245–256. doi:10.1042/Bj20150821

Sun, L., Zhang, D., Liu, F., Xiang, X., Ling, G., Xiao, L., et al. (2011). Low-dose Paclitaxel Ameliorates Fibrosis in the Remnant Kidney Model by Down-regulating miR-192. *J. Pathol.* 225, 364–377. doi:10.1002/path.2961

Tang, O., Chen, X.-M., Shen, S., Hahn, M., and Pollock, C. A. (2013). MiRNA-200b Represses Transforming Growth Factor-β1-Induced EMT and Fibronectin Expression in Kidney Proximal Tubular Cells. *Am. J. Physiology-Renal Physiol.* 304, F1266–F1273. doi:10.1152/ajprenal.00302.2012

Tao, L., Bei, Y., Chen, P., Lei, Z., Fu, S., Zhang, H., et al. (2016). Crucial Role of miR-433 in Regulating Cardiac Fibrosis. *Theranostics* 6, 2068–2083. doi:10.7150/thno.15007

Tao, L., Xue, D., Shen, D., Ma, W., Zhang, J., Wang, X., et al. (2018). MicroRNA-942 Mediates Hepatic Stellate Cell Activation by Regulating BAMBI Expression in Human Liver Fibrosis. *Arch. Toxicol.* 92, 2935–2946. doi:10.1007/s00204-018-2278-9

Thatcher, J. D. (2010). The TGF- Signal Transduction Pathway. *Sci. Signaling* 3, tr4. doi:10.1126/scisignal.3119tr4

Valderrama-Carvajal, H., Cocolakis, E., Lacerte, A., Lee, E.-H., Krystal, G., Ali, S., et al. (2002). Activin/TGF-β Induce Apoptosis through Smad-dependent Expression of the Lipid Phosphatase SHIP. *Nat. Cel Biol* 4, 963–969. doi:10.1038/ncb885

Van der Hauwaert, C., Glowacki, F., Pottier, N., and Cauffiez, C. (2019). Non-Coding RNAs as New Therapeutic Targets in the Context of Renal Fibrosis. *Int. J. Mol. Sci.* 20, 1977. doi:10.3390/ijms20081977

Wang, C.-J., Li, B.-B., Tan, Y.-J., Zhang, G.-M., Cheng, G.-L., and Ren, Y.-S. (2020a). MicroRNA-31/184 Is Involved in Transforming Growth Factor-β-Induced Apoptosis in A549 Human Alveolar Adenocarcinoma Cells. *Life Sci.* 242, 117205. doi:10.1016/j.lfs.2019.117205

Wang, J., Chu, E. S. H., Chen, H.-Y., Man, K., Go, M. Y. Y., Huang, X. R., et al. (2015). microRNA-29b Prevents Liver Fibrosis by Attenuating Hepatic Stellate Cell Activation and Inducing Apoptosis through Targeting PI3K/AKT Pathway. *Oncotarget* 6, 7325–7338. doi:10.18632/oncotarget.2621

Wang, J., He, F., Chen, L., Li, Q., Jin, S., Zheng, H., et al. (2018). Resveratrol Inhibits Pulmonary Fibrosis by Regulating miR-21 through MAPK/AP-1 Pathways. *Biomed. Pharmacother.* 105, 37–44. doi:10.1016/j.biopha.2018.05.104

Wang, J., He, Q., Han, C., Gu, H., Jin, L., Li, Q., et al. (2012a). p53-facilitated miR-199a-3p Regulates Somatic Cell Reprogramming. *Stem Cells* 30, 1405–1413. doi:10.1002/stem.1121

Wang, J., Huang, W., Xu, R., Nie, Y., Cao, X., Meng, J., et al. (2012b). MicroRNA-24 Regulates Cardiac Fibrosis after Myocardial Infarction. *J. Cel. Mol. Med.* 16, 2150–2160. doi:10.1111/j.1582-4934.2012.01523.x

Wang, J., Jiang, C., Li, N., Wang, F., Xu, Y., Shen, Z., et al. (2020b). The circEPSTI1/mir-942-5p/LTBP2 axis Regulates the Progression of OSCC in the Background of OSF via EMT and the PI3K/Akt/mTOR Pathway. *Cel Death Dis* 11, 682. doi:10.1038/s41419-020-02851-w

Wang, J., Zhu, H., Huang, L., Zhu, X., Sha, J., Li, G., et al. (2019a). Nrf2 Signaling Attenuates Epithelial-To-Mesenchymal Transition and Renal Interstitial Fibrosis via PI3K/Akt Signaling Pathways. *Exp. Mol. Pathol.* 111, 104296. doi:10.1016/j.yexmp.2019.104296

Wang, N., Duan, L., Ding, J., Cao, Q., Qian, S., Shen, H., et al. (2019b). MicroRNA-101 Protects Bladder of BOO from Hypoxia-Induced Fibrosis by Attenuating TGF-β-Smad2/3 Signaling. *Iubmb Life* 71, 235–243. doi:10.1002/iub.1968

Wang, Y., Yang, F., Xue, J., Zhou, X., Luo, L., Ma, Q., et al. (2017). Antischistosomiasis Liver Fibrosis Effects of Chlorogenic Acid through IL-13/miR-21/Smad7 Signaling Interactions *In Vivo* and *In Vitro*. *Antimicrob. Agents Chemother.* 61, e01347–16. doi:10.1128/AAC.01347-16

Wrighton, K. H., Lin, X., and Feng, X.-H. (2009). Phospho-control of TGF-β Superfamily Signaling. *Cel Res* 19, 8–20. doi:10.1038/cr.2008.327

Wu, J., Liu, J., Ding, Y., Zhu, M., Lu, K., Zhou, J., et al. (2018). MiR-455-3p Suppresses Renal Fibrosis through Repression of ROCK2 Expression in Diabetic Nephropathy. *Biochem. Biophysical Res. Commun.* 503, 977–983. doi:10.1016/j.bbrc.2018.06.105

Wynn, T. A. (2007). Common and Unique Mechanisms Regulate Fibrosis in Various Fibroproliferative Diseases. *J. Clin. Invest.* 117, 524–529. doi:10.1172/jci31487

Wynn, T. (2008). Cellular and Molecular Mechanisms of Fibrosis. *J. Pathol.* 214, 199–210. doi:10.1002/path.2277

Xu, Q., Liu, Y., Pan, H., Xu, T., Li, Y., Yuan, J., et al. (2019). Aberrant Expression of miR-125a-3p Promotes Fibroblast Activation via Fyn/STAT3 Pathway during Silica-Induced Pulmonary Fibrosis. *Toxicology* 414, 57–67. doi:10.1016/j.tox.2019.01.007

Yamashita, M., Fatyol, K., Jin, C., Wang, X., Liu, Z., and Zhang, Y. E. (2008). TRAF6 Mediates Smad-Independent Activation of JNK and P38 by TGF-β. *Mol. Cel* 31, 918–924. doi:10.1016/j.molcel.2008.09.002

Yan, X., Liu, Z., and Chen, Y. (2009). Regulation of TGF- Signaling by Smad7. *Acta Biochim. Biophys. Sinica* 41, 263–272. doi:10.1093/abbs/gmp018

Yang, C., Zheng, S.-D., Wu, H.-J., and Chen, S.-J. (2016). Regulatory Mechanisms of the Molecular Pathways in Fibrosis Induced by MicroRNAs. *Chin. Med. J. (Engl)* 129, 2365–2372. doi:10.4103/0366-6999.190677

Yang, F., Luo, L., Zhu, Z.-D., Zhou, X., Wang, Y., Xue, J., et al. (2017b). Chlorogenic Acid Inhibits Liver Fibrosis by Blocking the miR-21-Regulated TGF-β1/Smad7 Signaling Pathway *In Vitro* and *In Vivo*. *Front. Pharmacol.* 8, 929. doi:10.3389/fphar.2017.00929

Yang, R., Xu, X., Li, H., Chen, J., Xiang, X., Dong, Z., et al. (2017a). p53 Induces miR199a-3p to Suppress SOCS7 for STAT3 Activation and Renal Fibrosis in UUO. *Sci. Rep.* 7, 43409. doi:10.1038/srep43409

Yang, W.-L., Wang, J., Chan, C.-H., Lee, S.-W., Campos, A. D., Lamothe, B., et al. (2009). The E3 Ligase TRAF6 Regulates Akt Ubiquitination and Activation. *Science* 325, 1134–1138. doi:10.1126/science.1175065

Yang, Y.-Z., Zhao, X.-J., Xu, H.-J., Wang, S.-C., Pan, Y., Wang, S.-J., et al. (2019). Magnesium Isoglycyrrhizinate Ameliorates High Fructose-Induced Liver Fibrosis in Rat by Increasing miR-375-3p to Suppress JAK2/STAT3 Pathway and TGF-β1/Smad Signaling. *Acta Pharmacol. Sin* 40, 879–894. doi:10.1038/s41401-018-0194-4

Yin, Z.-F., Wei, Y.-I., Wang, X., Wang, L.-N., and Li, X. (2020). Buyang Huanwu Tang Inhibits Cellular Epithelial-To-Mesenchymal Transition by Inhibiting TGF-β1 Activation of PI3K/Akt Signaling Pathway in Pulmonary Fibrosis Model *In Vitro*. *BMC Complement. Med. Ther.* 20, 13. doi:10.1186/s12906-019-2807-y

Yu, J. S. L., and Cui, W. (2016). Proliferation, Survival and Metabolism: the Role of PI3K/AKT/mTOR Signalling in Pluripotency and Cell Fate Determination. *Development* 143, 3050–3060. doi:10.1242/dev.137075

Yuan, J., Li, P., Pan, H., Li, Y., Xu, Q., Xu, T., et al. (2018). miR-542-5p Attenuates Fibroblast Activation by Targeting Integrin α6 in Silica-Induced Pulmonary Fibrosis. *Int. J. Mol. Sci.* 19, 3717. doi:10.3390/ijms19123717

Zarjou, A., Yang, S., Abraham, E., Agarwal, A., and Liu, G. (2011). Identification of a microRNA Signature in Renal Fibrosis: Role of miR-21. *Am. J. Physiology-Renal Physiol.* 301, F793–F801. doi:10.1152/ajprenal.00273.2011

Zhang, Q., Ye, H., Xiang, F., Song, L.-J., Zhou, L.-L., Cai, P.-C., et al. (2017). miR-18a-5p Inhibits Sub-pleural Pulmonary Fibrosis by Targeting TGF-β Receptor II. *Mol. Ther.* 25, 728–738. doi:10.1016/j.ymthe.2016.12.017

Zhang, Y. E. (2009). Non-Smad Pathways in TGF-β Signaling. *Cel Res* 19, 128–139. doi:10.1038/cr.2008.328

Zhang, Y. E. (2017). Non-Smad Signaling Pathways of the TGF-β Family. *Cold Spring Harb Perspect. Biol.* 9, a022129. doi:10.1101/cshperspect.a022129

Zhao, S. Q., Shen, Z. C., Gao, B. F., and Han, P. (2019). microRNA-206 Overexpression Inhibits Epithelial-mesenchymal Transition and Glomerulosclerosis in Rats with Chronic Kidney Disease by Inhibiting JAK/STAT Signaling Pathway. *J. Cel Biochem* 120, 14604–14617. doi:10.1002/jcb.28722

Zhou, C., Zeldin, Y., Baratz, M. E., Kathju, S., and Satish, L. (2019). Investigating the Effects of Pirfenidone on TGF-β1 Stimulated Non-SMAD Signaling Pathways in Dupuytren's Disease -derived Fibroblasts. *BMC Musculoskelet. Disord.* 20, 135. doi:10.1186/s12891-019-2486-3

Conflict of Interest: The authors declare that the research was conducted in the absence of any commercial or financial relationships that could be construed as a potential conflict of interest.

Publisher's Note: All claims expressed in this article are solely those of the authors and do not necessarily represent those of their affiliated organizations, or those of the publisher, the editors and the reviewers. Any product that may be evaluated in this article, or claim that may be made by its manufacturer, is not guaranteed or endorsed by the publisher.

frontiers in Molecular Biosciences

ORIGINAL RESEARCH
published: 29 September 2021
doi: 10.3389/fmolb.2021.753218

LncRNA-MCM3AP-AS1 Promotes the Progression of Infantile Hemangiomas by Increasing miR-138-5p/HIF-1α Axis-Regulated Glycolysis

*Haijun Mei, Hua Xian and Jing Ke**

Department of General Surgery, Affiliated Hospital of Nantong University, Nantong, China

Infantile hemangioma (IH) is a common benign tumor of endothelial cells in infants. Most hemangiomas are self-limited, but a few may develop and lead to serious complications that affect the normal life of children. Therefore, finding an effective treatment strategy for IH is a pressing need. Recent studies have demonstrated that non-coding RNAs affect the progression of multiple tumors. This study aims to investigate the mechanism by which LncRNA-MCM3AP-AS1 promotes glycolysis in the pathogenesis of IH. We first documented that the expression of LncRNA MCM3AP-AS1 was significantly upregulated in IH. Furthermore, we demonstrated that MCM3AP-AS1 bound to miR-106b-3p which promotes glycolysis in IH. In addition, we found that inhibition of HIF-1α contributed to the transformation of glycolysis to normal aerobic oxidation, partially reversed the promoting effect on glycolysis by the up-regulation of LncRNA MCM3AP-AS1 in IH disease. More importantly, we demonstrated this phenomenon existed in IH patients. Taken together, we demonstrate that LncRNA-MCM3AP-AS1 promotes the progression of infantile hemangiomas by increasing the glycolysis via regulating miR-138-5p/HIF-1α axis.

Keywords: LncRNA-MCM3AP-AS1, miR-138-5p, HIF-1α, infantile hemangiomas, glycolysis

OPEN ACCESS

Edited by:
Wei Zhao,
City University of Hong Kong, Hong Kong, SAR China

Reviewed by:
Hongbao Yang,
China Pharmaceutical University, China
Yi Si,
Fudan University, China

****Correspondence:***
Jing Ke
kjljy@163.com

Specialty section:
This article was submitted to Molecular Diagnostics and Therapeutics, a section of the journal Frontiers in Molecular Biosciences

Received: *04 August 2021*
Accepted: *13 September 2021*
Published: *29 September 2021*

Citation:
Mei H, Xian H and Ke J (2021) LncRNA-MCM3AP-AS1 Promotes the Progression of Infantile Hemangiomas by Increasing miR-138-5p/HIF-1α Axis-Regulated Glycolysis. Front. Mol. Biosci. 8:753218. doi: 10.3389/fmolb.2021.753218

INTRODUCTION

Infantile hemangiomas (IH) is a common benign skin tumor in children with vascular endothelial cell proliferation as the main pathological characteristic (Chamli et al., 2021). The incidence of IH is about 10% in Caucasians under 1 year old, and it is most common in females, with a male to female ratio of 1:3–4 (Chang et al., 2008). Potential complications of IH include permanent disfigurement, ulcers, scarring, bleeding, visual impairment, airway obstruction, congestive heart failure and death (Baselga et al., 2016). Compared with localized IH lesions, deep lesions are at greater risk of ulceration and dysfunction, and therefore require early and aggressive clinical intervention and treatment (Cheng and Friedlander, 2016). According to the course of disease, IH can be divided into proliferating phase stage, involuting stage and involuted stage (Yoon et al., 2021). Hemangiomas can recede spontaneously, but 90% of IH patients need 9–10 years or more to recede completely (Darrow et al., 2015). Most of the subsided tumors will leave scar or fibrous fat deposition, therefore early active intervention and treatment would be preferred. The tendency of spontaneous regression is an important feature of the course of IH, and its pathological basis is the disappearance of juvenile capillary degeneration, replaced by deposition of fiber and adipose tissues (Caussé et al., 2013). Promoting the transition from early stage to regression stage is the main goal of current treatment.

However, due to the unknown mechanism of progression of infantile hemangioma, especially the mechanism of spontaneous regression, no effective treatment is available.

Long non-coding RNAs (lncRNAs) are a group of RNAs over 200 bp in length that do not have complete protein coding function and lack a specific open reading frame (Ørom and Shiekhattar, 2011). Previous studies have shown that lncRNAs affect the progression of multiple tumors (Ørom and Shiekhattar, 2011). LncRNA antisense 1 to micro-chromosome maintenance protein 3-associated protein (MCM3AP-AS1) gene was located on chromosome 21. In recent years, it has been reported that MCM3AP-AS1 plays an important role in the progression of glioblastoma and liver cancer (Yang et al., 2017; Wang et al., 2019a). Reports have shown that LncRNA MCM3AP-AS1 is up-regulated in glioma endothelial cells and hepatocellular carcinoma. Interference or silencing of its expression inhibits the proliferation and invasion of glioma cells. In papillary thyroid carcinoma, MCM3AP-AS1 expression is upregulated and promotes proliferation, migration, and invasion of cancer cells. However, the role of lncRNA MCM3AP-AS1 in hemangioma remains unknown.

MicroRNAs (miRNAs) are non-coding RNA molecules with highly conserved sequences (Dong et al., 2013). MiRNAs are involved in the regulation of a series of physiological processes, including cell proliferation, differentiation, apoptosis, signal transduction and organ development (Sarkar and Kumar, 2021). In prostate cancer, miRNA-34c down-regulates Bcl-2 protein expression, thereby inhibiting cell proliferation and promoting cell apoptosis (Hagman et al., 2010). In glioblastoma, miRNA-153 promotes apoptosis by down-regulating Bcl-2 protein expression (Xu et al., 2011). However, it is not clear whether miR-138-5p plays a role in hemangioma.

Due to the infinite proliferation of malignant tumor cells, their demand for energy and biomacromolecules increases dramatically (Zhang et al., 2017). The Warburg effect is known as the preferential conversion of glucose to lactic acid (aerobic glycolysis) for energy in cancer cells, even when oxygen is available (Wan et al., 2017). Interestingly, the vascular endothelial cells produce most of their ATP through aerobic glycolysis, despite that hemangioma contains abundant oxygen (Wang et al., 2019b). A variety of genes are often altered by changing their metabolic patterns during the process of tumor cells adapting to hypoxia. Among them, the most important gene is hypoxia-inducible factor 1a (HIF-1α) (Nyga et al., 2019). Under hypoxic conditions, HIF-1α promotes the occurrence of glycolysis in tumor cells by activating the expression of key protein involved in extracellular glucose input such as glucose transporter 1 (GLUT1) and intracellular glycolytic enzymes such as phosphofructokinase 1 (PFK1) (Quiroga et al., 2021; Zhang et al., 2021). Therefore, the therapeutic value of the glycolysis pathway in the pathogenesis of IH should be investigated.

In this study, we used bioinformatics method, combined with qPCR, WB, flow cytometry and other research methods to study the regulation of LncRNA MCM3AP-AS1 and miRNA/HIF-1α signaling pathway in the occurrence and development of hemangioma to explore the molecular mechanism of hemangioma.

RESULTS

LncRNA MCM3AP-AS1 Expression was Up-Regulated in IH Clinical Samples and HemECs, and Affected the Prognosis of IH

The qPCR was used to detect the expression of common lncRNAs to investigate their differential expression in IH and normal tissues. The results showed that among a variety of lncRNAs, only LncRNA MCM3AP-AS1 was up-regulated in IH compared to normal tissue (**Figure 1A**). We then compared the expression of these lncRNAs in hemangioma cell lines and normal cell lines, and our experimental results demonstrated that the expression of LncRNA MCM3AP-AS1 was significantly up-regulated in HemECs compared to the HUVECs that was taken as controls (**Figure 1B**). Since LncRNA MCM3AP-AS1 was up-regulated in both IH tissues and HemECs, the data from the SEER database were used to analyze whether LncRNA MCM3AP-AS1 affects the prognosis of hemangioma patients. The result indicated that patients with low expression of LncRNA MCM3AP-AS1 had significantly better overall survival (**Figure 1C**). These results suggest that the overexpression of lncRNA MCM3AP-AS1 aggravates the progression of IH.

Knockdown of LncRNA MCM3AP-AS1 Inhibited the Proliferation of Hemangioma Cells

Previous research has reported the tumor-promoting effect of LncRNAs on several tumors. We explored whether LncRNA MCM3AP-AS1 has the similar effect on IH cells. CCK-8 analysis demonstrated that the cell viability of HemECs was significantly reduced by knock-down of LncRNA MCM3AP-AS1 (**Figure 2A**). We further analyzed whether LncRNA MCM3AP-AS1 induces apoptosis in HemECs. FACS analysis was employed to estimate the effect of silence of LncRNA MCM3AP-AS1 on the apoptosis in HemECs. The results demonstrated that the apoptotic ratio of HemECs was significantly increased after knock-down of LncRNA MCM3AP-AS1 (**Figure 2B**). To examine whether LncRNA MCM3AP-AS1 was linked to cell cycle arrest in HemECs, we analyzed the effects of knock-down of LncRNA MCM3AP-AS1 on cell cycle of HemECs, and found that the percentage of cells in the G1 phase was significantly increased (**Figure 2C**). The above results demonstrated that knockdown of LncRNA MCM3AP-AS1 inhibited proliferation, induced apoptosis of HemECs, and arrested hemangioma cells in the G1phase of cell cycle.

LncRNA MCM3AP-AS1 Directly Targeted miR-138-5p

To explore which miRNAs functioned as the sponge of LncRNA MCM3AP-AS1 to co-regulate the expression of downstream genes, we searched the starBase v3.0 (http://

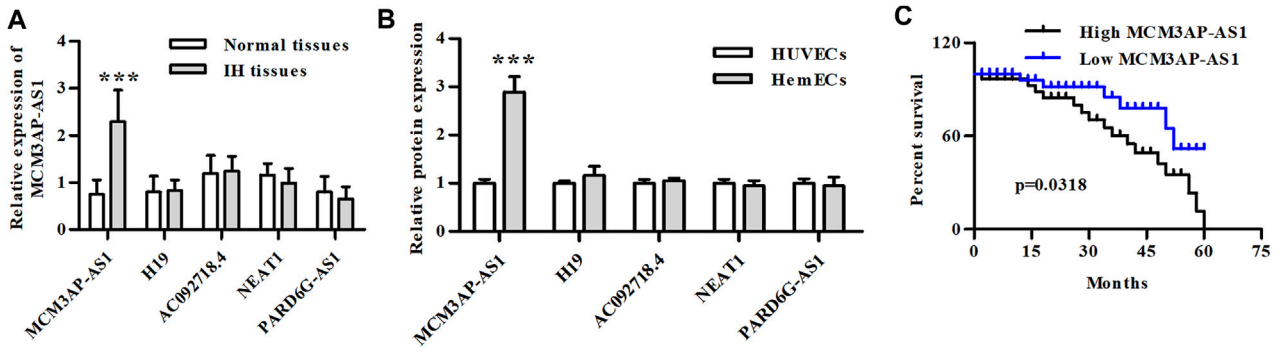

FIGURE 1 | The relative mRNA expression of LncRNAs in IH clinical samples and IH cells. **(A)** The relative mRNA expression of LncRNAs in IH patients (***$p < 0.001$, compared with the Normal tissue group). **(B)** The relative mRNA expression of LncRNAs in HemECs and HUVECs cell lines (***$p < 0.001$, compared with the HUVECs group). **(C)** Kaplan-Meier analysis of OS compared high- and low-expression of LncRNA MCM3AP-AS1 in IH patients.

starbase.sysu.edu.cn/index.php) and found that LncRNA MCM3AP-AS1 harbored a putative binding site for miR-138-5p (**Figure 3A**). To further evaluate this conjecture, we construct the LncRNA MCM3AP-AS1-WT or LncRNA MCM3AP-AS1-Mut luciferase reporter and transfected these reporters into HemECs together with miR-138-5p mimic or its NC mimic. Dual-luciferase reporter assays showed that miR-138-5p mimic significantly reduced the luciferase activity of LncRNA MCM3AP-AS1-WT reporter, whereas exhibited modest effects on the activity of LncRNA MCM3AP-AS1-MUT reporter (**Figure 3B**). qPCR results showed that miR-138-5p mimics significantly reduced the expression of LncRNA MCM3AP-AS1 (**Figure 3C**). Then we detected the expression of miR-138-5p in HemECs and IH clinical tissues. As expected, the expression of miR-138-5p was significantly decreased in both IH cells and clinical samples compared with control groups (**Figures 3D,E**). These results demonstrated that LncRNA MCM3AP-AS1 directly targeted miR-138-5p.

MiR-138-5p Targeted HIF-1α Directly

We then predicted the downstream target genes of miR-138-5p using the three databases and Venn analysis showed two overlapping genes (**Figure 4A**). Through further binding site analysis, we found that the downstream regulatory gene of miR-138-5p was the hypoxia-inducible factor-1alpha (HIF-1α) (**Figure 4B**). HIF-1α-WT and HIF-1α--Mut luciferase reporters were constructed and transfected into HemECs together with miR-138-5p mimic or its NC mimic. Dual-luciferase reporter assays showed that miR-138-5p mimic significantly reduced the luciferase activity of HIF-1α-WT reporter, whereas exhibited no significant effects on the activity of HIF-1α-MUT reporter (**Figure 4C**). qRT-PCR results showed that miR-138-5p mimics significantly reduced the expression of HIF-1α (**Figure 4D**). Further analysis of clinical patient information from the database demonstrated that patients with low expression of HIF-1α had significantly better overall survival (**Figure 4E**).

The Process of Glycolysis in IH was Mediated by LncRNA MCM3AP-AS1 via Regulating miR-138-5p/HIF-1α Axis

Previous studies have shown that the abnormally elevated glycolysis level of tumor cells was reversed by inhibiting the expression of HIF-1α, which forced tumor cells to return to the metabolic mode of glucose oxidative phosphorylation, increased the energy consumption of tumor cells, and induced the death of tumor cells. Therefore, we examined the effect of HIF-1α on glycolysis in IH. Our results showed that LncRNA MCM3AP-AS1 significantly increased glucose consumption of HemECs, but this effect was partially reversed by adding HIF-1α inhibitor (DPT) (**Figure 5A**). Since the abnormally increased glycolysis of tumor cells was mainly manifested as increased pyruvate production and lactic acid production, we also tested the effect of HIF-1α on lactic acid production in IH. Results revealed that LncRNA MCM3AP-AS1 significantly increased lactic acid production of HemECs, but this effect was partially reversed by adding HIF-1α inhibitor (DPT) (**Figure 5B**). We also examined the expression of several key genes involved in glycolysis. The qPCR results showed that LncRNA MCM3AP-AS1 largely increased the expression of GLUT1, LDH and HK2, while HIF-1α inhibitor (DPT) partially reverse the enhancement of these genes expression induced by LncRNA MCM3AP-AS1 on IH (**Figure 5C**).

We further evaluated whether LncRNA MCM3AP-AS1 exerted regulatory roles via miR-138-5p/HIF-1α pathway in HemECs. CCK-8 analysis demonstrated that LncRNA MCM3AP-AS1 knockdown alone decreased the number of HemECs, while miR-138-5p inhibitor alone or siHIF-1α significantly attenuated the proliferation-inhibiting effects of siLncRNA MCM3AP-AS1 on HemECs (**Figure 6A**). Similarly, the FACS analysis results demonstrated that the apoptotic ratio of HemECs was significantly increased after knock-down of LncRNA MCM3AP-AS1. However, miR-138-5p inhibitor alone or siHIF-1α significantly reversed the apoptosis-inducing effects of siLncRNA MCM3AP-AS1 on HemECs (**Figure 6B**). The cell cycle analysis revealed that most HemECs were arrested at G0/G1phase of the cell cycle in cells with LncRNA MCM3AP-AS1 knock-down. Interestingly, miR-138-5p inhibitor alone or siHIF-1α partially reversed the effect induced by siLncRNA

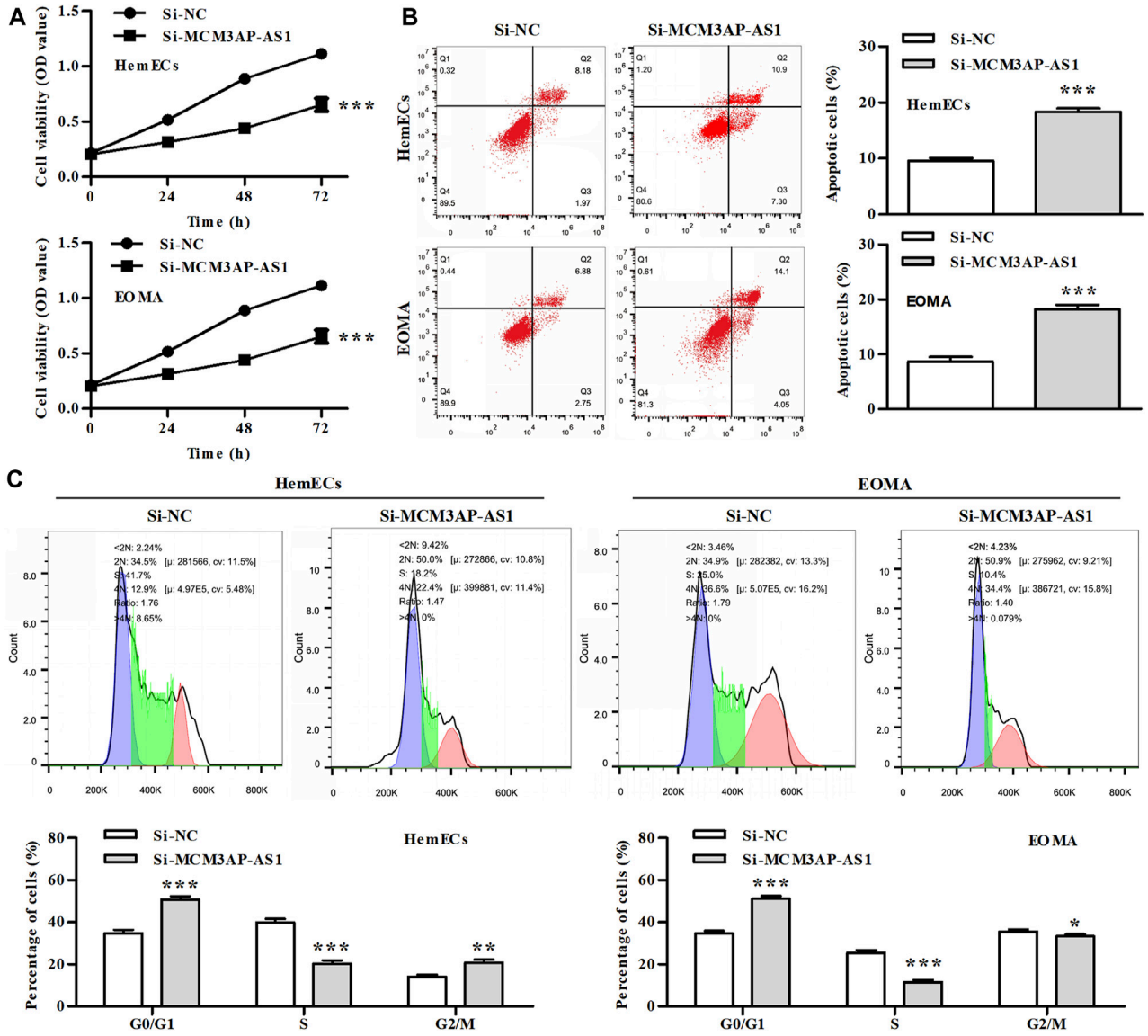

FIGURE 2 | The effect of silencing LncRNA MCM3AP-AS1 on proliferation of IH cells. **(A)** In CCK-8 assay, cell viability was presented by OD value after HemECs cells were transfected with siNC mimics or si-MCM3AP-AS1 24, 48 and 72 h. **(B)** FACS analysis showing the apoptosis induced by siNC mimics or siMCM3AP-AS1 in HemECs. **(C)** Cell cycle analysis showing siMCM3AP-AS1 induced HemECs cell cycle arrest at the G1 phase.*$p < 0.05$, **$p < 0.01$, ***$p < 0.001$, compared with the si-NC group.

MCM3AP-AS1 on HemECs (**Figure 6C**). Further analysis showed that knock-down of LncRNA MCM3AP-AS1 significantly decreased the glucose consumption and lactate production while miR-138-5p inhibitor alone or siHIF-1α significantly reversed these effects of siLncRNA MCM3AP-AS1 on HemECs (**Figures 6D,E**).

LncRNA MCM3AP-AS1, miR-138-5p and HIF-1α Expressed in IH Tissues

Previous results have demonstrated that LncRNA MCM3AP-AS1 and miR-138-5p played an opposite role in the progression of IH disease, and miR-138-5p negatively regulates HIF-1α expression. Therefore, we examined the expression of these three genes in clinical tissues. IHC was employed to evaluate the expression of LncRNA MCM3AP-AS1 on the same ISH which was used for the evaluation of miR-138-5p expression. We found that both of LncRNA MCM3AP-AS1 and miR-138-5p were expressed in three clinical tissues. The same analysis strategy was used to examine the expression of miR-138-5p and HIF-1α (**Figures 7A-C**). The above analysis demonstrated that the expression of LncRNA MCM3AP-AS1 is negatively correlated with miR-138-5p, and miR-138-5p negatively correlated with HIF-1α in IH tissues.

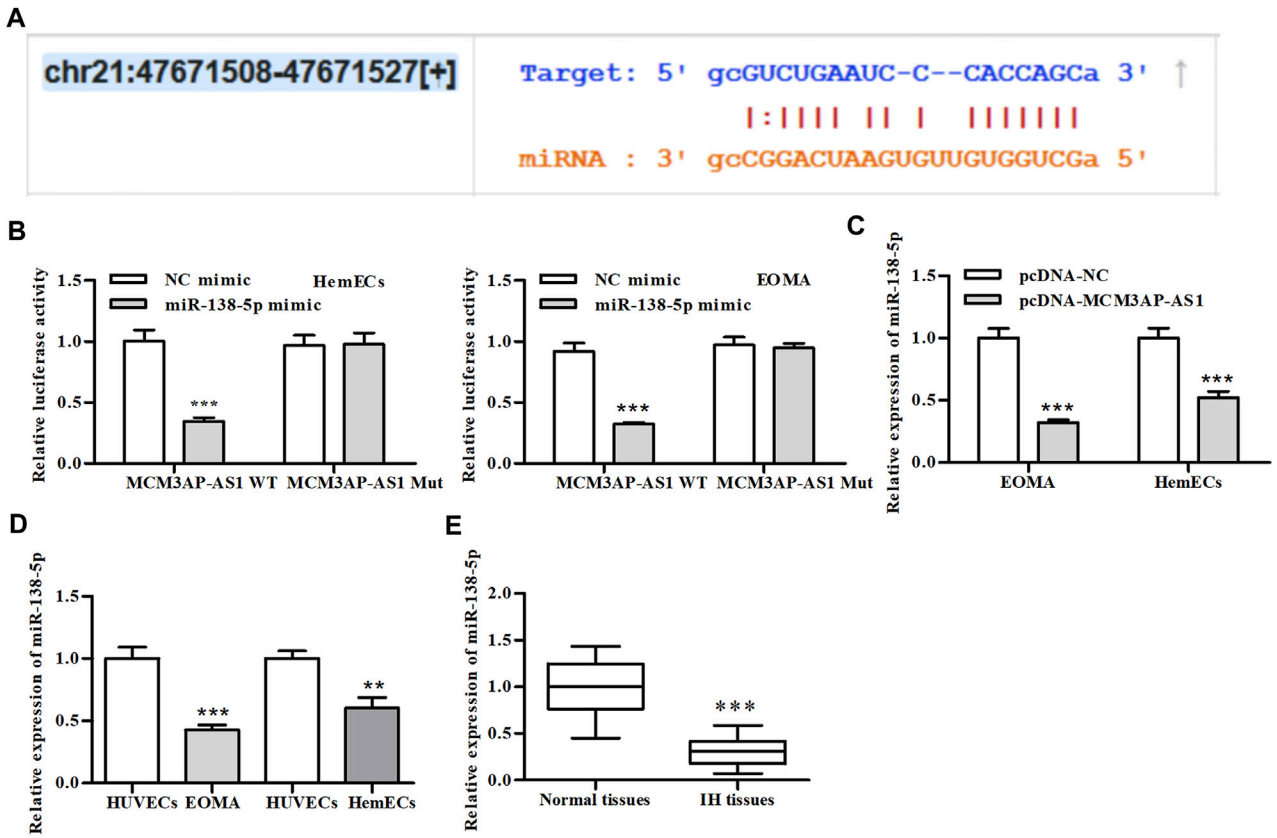

FIGURE 3 | LncRNA-MCM3AP-AS1 directly binds to miR-138-5p. **(A)** The putative LncRNA-MCM3AP-AS1 binding sequence of miR-138-5p. **(B)** Luciferase activity of a luciferase reporter plasmid containing MCM3AP-AS1-WT or MUT co-transfected with miR-138-5p mimics or NC mimics by the dual luciferase reporter assay (***$p < 0.001$, compared with the NC mimic group). **(C)** The expression of miR-138-5p in MCM3AP-AS1-transfected HemECs cells (***$p < 0.001$, compared with the pcDNA-NC group, $n = 3$). **(D)** The expression of miR-138-5p compared between HemECs cell and HUVECs (**$p < 0.01$, ***$p < 0.001$, compared with the HUVECs group, $n = 3$). **(E)** The expression of miR-138-5p compared between IH patient tissue and normal skin tissue (***$p < 0.001$, compared with the Normal tissues group, $n = 3$).

DISCUSSION

Infantile hemangioma is the most common childhood tumor, generally affecting the head and neck region. The tumor may grow rapidly and cause obstruction in normal anatomical structures, leading to severe damage. As a class of non-coding RNAs that has attracted a lot of attention in recent years, LncRNA plays important roles in the process of tumor development, proliferation and metastasis (Gu et al., 2018). MCM3AP-AS1 is the antisense LncRNA of MCM3AP, which is associated with the malignant progression of various tumors such as thyroid cancer and liver cancer (Liang et al., 2019; Zhang et al., 2019). Wang et al. (2019c) found that high expression of MCM3AP AS1 was positively correlated with large tumor volume, high tumor grade, advanced tumor stage and poor prognosis of HCC patients. Yang et al. (2019) indicated that silencing of MCM3AP-AS1 inhibited the proliferation of pancreatic cancer cells. In addition, previous studies have reported that LncRNAs displayed crucial roles during IH progression. Liu et al. (2019a) demonstrated that knock down of LncRNA LINC00342 inhibited the proliferation of infantile hemangioma by sponging miR-3619-5p. Zhang and Zhang (2019) and his colleagues found that LncRNA UCA1 was highly expressed in IH, and LncRNA UCA1 promoted proliferation, migration and invasion via regulating miR-200c in hemangioma cells. In this study, we found that MCM3AP-AS1 was highly expressed in IH cell lines and clinical specimens from IH patients. Moreover, IH patients with highly expressed MCM3AP-AS1 had a worse survival rate.

In this study, we confirmed that LncRNA MCM3AP-AS1 was highly expressed in IH clinical tissue samples and IH cells, and patients with high expression of LncRNA MCM3AP-AS1 had a worse survival rate. Importantly, knock down of LncRNA MCM3AP-AS1 significantly inhibited the proliferation of IH cells, and arrested the cell cycle at G1 phase. Furthermore, by bioinformatic and experimental analysis, we found that LncRNA MCM3AP-AS1 bound to miR-138-5p, and the downstream target gene of miR-138-5p was HIF-1α. In addition, we observed that the process of glycolysis in IH was mediated by LncRNA MCM3AP-AS1 via regulating miR-138-5p/HIF-1α axis, and confirmed this phenomenon through the rescue experiment. At last, we found that LncRNA MCM3AP-AS1 negatively

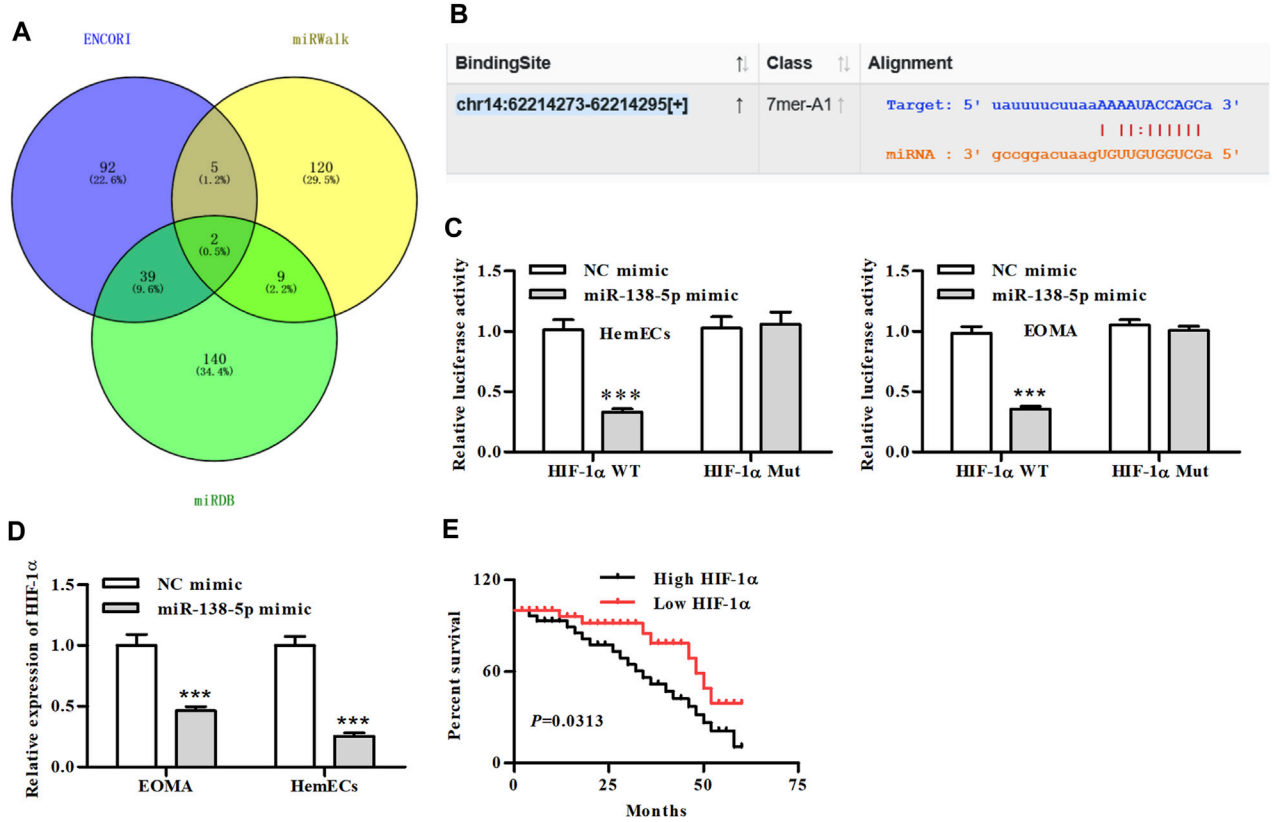

FIGURE 4 | MiR-138-5p directly binds to HIF-1α. **(A)** Venn diagram of predicted genes screened from the three database **(B)** The putative miR-138-5p binding sequence of HIF-1α. **(C)** Luciferase activity of a luciferase reporter plasmid containing HIF-1α-WT or MUT co-transfected with miR-138-5p mimics or NC mimics by the dual luciferase reporter assay (***$p < 0.001$, compared with the NC mimic group). **(D)** The expression of HIF-1α in miR-138-5p-transfected HemECs cells (***$p < 0.001$, compared with the NC mimic group). **(E)** Kaplan-Meier analysis of OS compared high- and low-expression of HIF-1α in IH patients.

correlated with miR-138-5p, and miR-138-5p negatively correlated with HIF-1α in IH patients. Based on the above results, we demonstrated that knock down of LncRNA-MCM3AP-AS1 inhibits the progression of hemangioma by decreasing glycolysis via regulating miR-138-5p/HIF-1α axis, which laid a foundation for exploring the molecular mechanism of IH treatment.

MicroRNA-138-5p is one of the important tumor suppressor regulators, and has been found in breast cancer (Xun et al., 2021), gastric cancer (Fan et al., 2021), renal cell carcinoma (Xue et al., 2021), pancreatic cancer (Han et al., 2021), and other tumors. In recent studies on breast cancer (Xun et al., 2021), it has been found that miR-138-5p mimics can be transfected to up-regulate miR-138-5p which reduced the expression of KDM6B and thus inhibited M1 polarization and promoted M2 polarization of macrophages in breast cancer. Fan et al. found that miRNA was expressed at low level in patients with gastric cancer (Fan et al., 2021), and knock down of Circ-CORO1C inhibited the proliferation of gastric cancer by sponging miR-138-5p. More importantly, the down-regulation of miR-138-5p was of special significance for lymph node metastasis and local infiltration of gastric cancer. In the study of pancreatic cancer (Han et al., 2021), it was found that miR-138-5p was down-regulated in PANC-1 cells, and silencing of miR-138-5p induced the increase of CCAT1 and HMGA1 expression. CCAT1 competitively bound to miR-138-5p to regulate downstream HMGA1 expression, and ultimately affected the progression of pancreatic cancer. However, to the best of our knowledge, there is no existing research on how miR-138-5p affected the proliferation, apoptosis of IH cells and survival rates of IH patients. In this study, by bioinformatics analysis, we found that LncRNAs MCM3AP AS1 bound to miR-138-5p, and the binding was verified by dual luciferase reporter assay and qPCR. More importantly, our results showed that miR-138-5p inhibited the proliferation of IH cells by targeting HIF-1α.

Hypoxia is one of the characteristics of most tumors. Hypoxic microenvironment exists in the vast majority of tumors, including liver cancer (Ma et al., 2021a) and IH (Wu et al., 2021). The hypoxic microenvironment promotes the metastasis of tumor cells (Yu et al., 2021), enhances the tolerance of tumor cells to radiotherapy and chemotherapy (Sun et al., 2021), and also changes the gene expression of tumor cells. HIF-1α is an important transcription factor in hypoxic microenvironment. It is strictly regulated by oxygen concentration and is abnormally

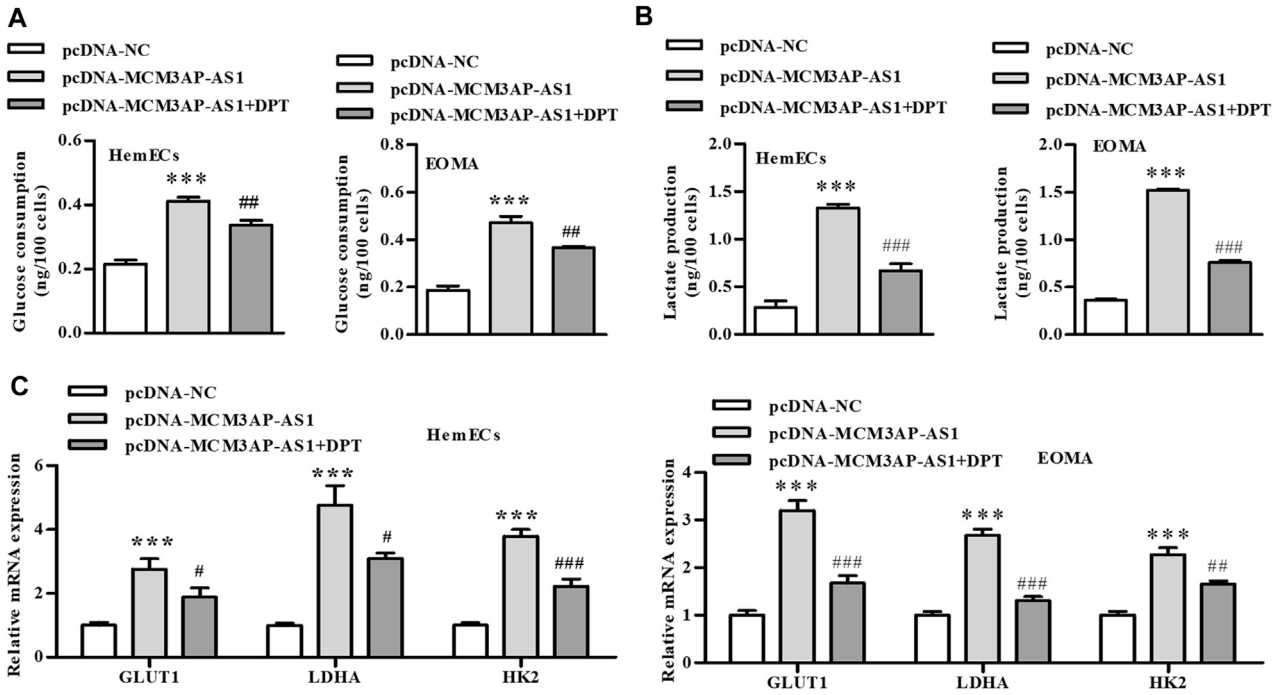

FIGURE 5 | LncRNA-MCM3AP-AS1 mediates glycolysis in IH disease by regulating HIF-1α. **(A)** Glucose consumption test demonstrated that LncRNA MCM3AP-AS1 significantly increased glucose consumption of HemECs, and this elevated effect was partially reversed by adding HIF-1α inhibitor (DPT) (***$p < 0.001$ compared with the pcDNA-NC group; ##$p < 0.01$ compared with the pcDNA-MCM3AP-AS1 group). **(B)** Lactate production test showed LncRNA MCM3AP-AS1 significantly increased lactate production of HemECs, and this elevated effect was partially reversed by adding HIF-1α inhibitor (DPT) (***$p < 0.001$ compared with the pcDNA-NC group; ###$p < 0.001$ compared with the pcDNA-MCM3AP-AS1 group). **(C)** The expression of key genes involved in glycolysis. LncRNA MCM3AP-AS1 significantly increased the expression of GLUT1, LDHA and HK2, and this elevated effect was partially reversed by adding HIF-1α inhibitor (DPT) (***$p < 0.001$ compared with the pcDNA-NC group; #$p < 0.05$, ##$p < 0.01$, ###$p < 0.001$ compared with the pcDNA-MCM3AP-AS1 group).

overexpressed in hypoxic tissues (Chappell et al., 2019). HIF-1α plays a regulatory role of hypoxia on tumor cell genes and promotes the survival of tumor cells in hypoxic microenvironment (Gonzalez et al., 2018). In the present study, we not only found that miR-138-5p mimics reduced the expression of HIF-1α in IH disease, but also that IH patients with low expression of HIF-1α had a better survival rate, suggesting that HIF-1α promotes the progression of IH, and these findings are consistent with the results of previous studies.

Previous studies have shown that one common phenomena in the development of tumors is hypoxia (Li et al., 2021; Liu et al., 2021; Zhu et al., 2021). In the process of tumor growth, due to the active growth of tumor cells, the degree of proliferation exceeds the speed of angiogenesis, resulting in local tissue hypoxia (Liu et al., 2021). Therefore, the adaptation of cells to hypoxia is a key step in tumor pathogenesis, and its main mechanisms are glucose transportation, glycolysis, and tumor angiogenesis (Ma et al., 2021b). Under hypoxic condition, the expression of HIF-1α increase exponentially (Peng et al., 2014). HIF-1α is up-regulated in almost all types of tumors and is involved in initiating transcription of several genes involved in tumor growth adaptation to anoxic environment. There are more than 60 target genes of HIF-1α (Hepp et al., 2021; Quiroga et al., 2021), such as erythropoietin (EPO), glucose transport protein-1 (Glut-1), vascular endothelial growth factor (VEGF), tyrosine hydroxylase, glycolysis related enzymes and more. HIF-1α induces the expression of these factors and enzymes and induces a series of hypoxia adaptation responses in the body. We confirmed that upregulation of LncRNA MCM3AP AS1 leads to increased glucose consumption and lactic acid production in IH patients, which is manifested by increased glycolytic levels in IH patients. We also demonstrated that inhibition of HIF-1α in IH patients can partially reverse this elevated effect caused by upregulated LncRNAs MCM3AP AS1.

It was known that LncRNAs play important roles in tumors by targeting and regulating mRNA through competitive binding to miRNAs (Chou et al., 2016). For example, MCM3AP-AS1 promotes the progression of papillary thyroid carcinoma by regulating the miR-211-5p/SPARC axis (Liang et al., 2019). In liver cancer, LINC-RORs up-regulate the expression of FOXMI by adsorbing miR-876-5p, thereby promoting the proliferation and metastasis of tumor cells (Zhi et al., 2019). In CRC, LncRNA GAS5 inhibits the proliferation of cancer cells and promotes apoptosis by targeting miR-222-3p (Liu et al., 2019b). In this study, we proved that the process of glycolysis in IH was mediated by LncRNA MCM3AP-AS1 via regulating miR-138-5p/HIF-1α axis. Further analysis on clinical specimens demonstrated that the expression of LncRNA MCM3AP-AS1 was negatively correlated

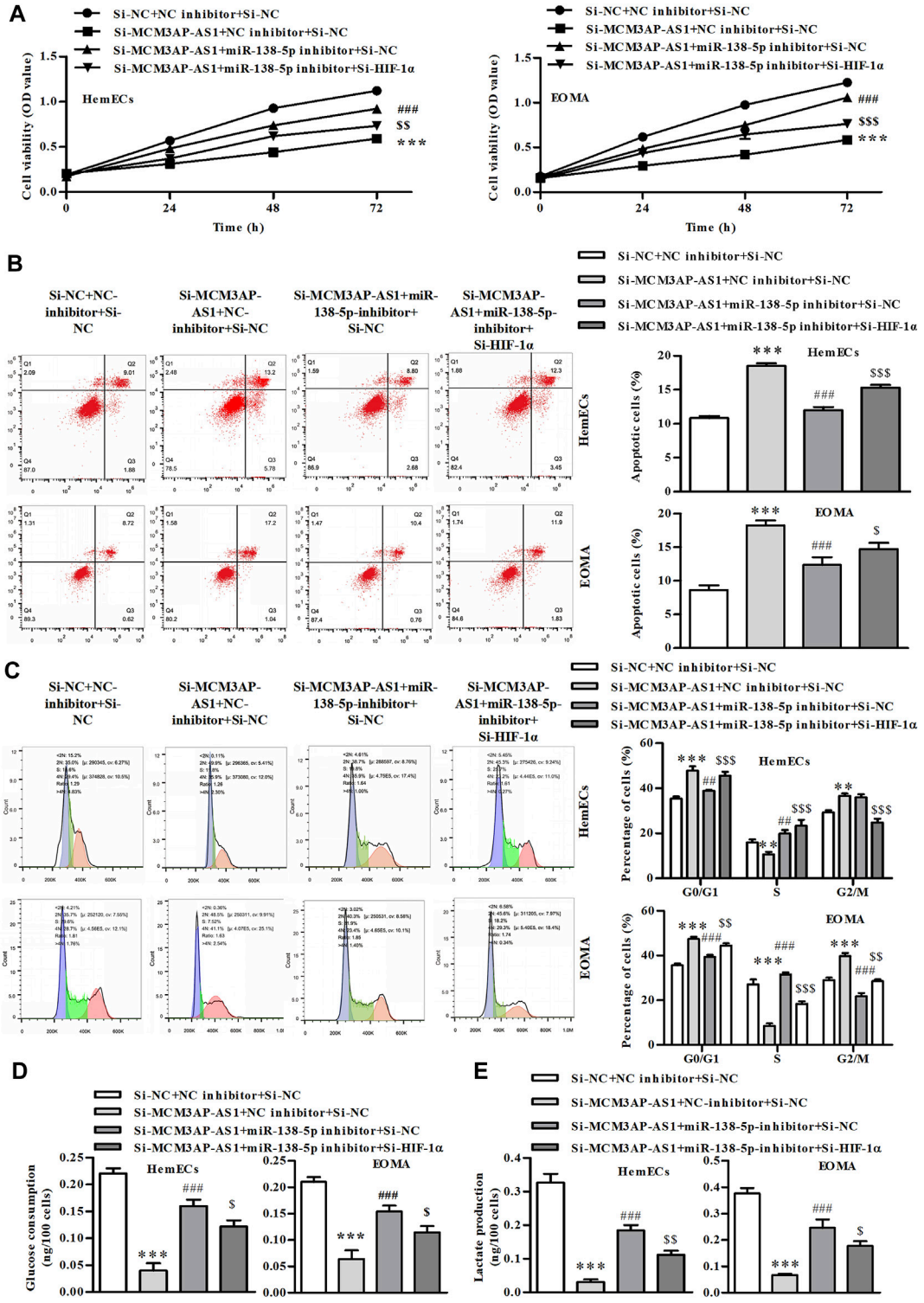

FIGURE 6 | The process of glycolysis in IH is mediated by LncRNA MCM3AP-AS1 via regulating miR-138-5p/HIF-1α axis. **(A)** In CCK-8 assay on HemECs treated with NC mimics, si-MCM3AP-AS1, miR-138-5p, or si-HIF-1α 24, 48 and 72 h. **(B)** FACS analysis showing the apoptosis induced by NCmimics, siMCM3AP-AS1, miR-138-5p or siHIF-1α 48 h in HemECs. **(C)** Cell cycle analysis indicating cell cycle arrested by NCmimics, siMCM3AP-AS1, miR-138-5p or siHIF-1α in HemECs. **(D)** Glucose consumption test demonstrated that the effects of NCmimics, siMCM3AP-AS1, miR-138-5p or siHIF-1α on the HemECs. **(E)** Lactate production test demonstrated that the effects of NCmimics, siMCM3AP-AS1, miR-138-5p or siHIF-1α on the HemECs (**$p < 0.01$, ***$p < 0.001$ compared with the si-NC + NC inhibitor + si-NC group; $^{\#\#}p < 0.01$, $^{\#\#\#}p < 0.001$ compared with the si-MCM3AP-AS1 + NC inhibitor + si-NC group; $^{\$}p < 0.05$, $^{\$\$}p < 0.01$, $^{\$\$\$}p < 0.001$ compared with the si-MCM3AP-AS1 + miR-138-5p inhibitor + si-NC group).

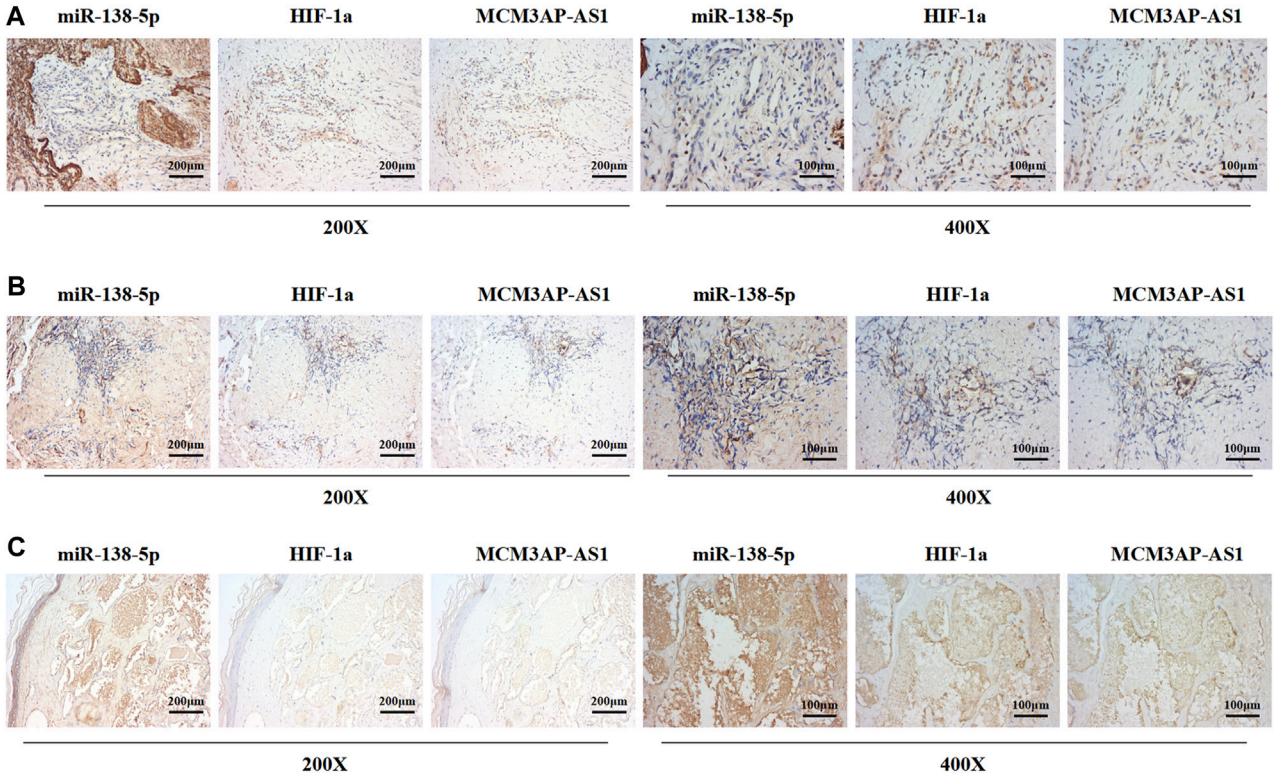

FIGURE 7 | The expression of LncRNA MCM3AP-AS1 is negatively correlated with miR-138-5p, and miR-138-5p negatively correlated with HIF-1α in IH tissues. **(A–C)** ISH and IHC result from three IH clinical tissues. The ISH score of miR-1306-3p is negatively correlated with LncRNA MCM3AP-AS1 in the IH tissue. The ISH score of miR-1306-3p is negatively correlated with the IHC scores of HIF-1α in the IH tissues.

with miR-138-5p, and miR-138-5p negatively correlated with HIF-1α in IH patients.

In summary, this study demonstrated that LncRNA-MCM3AP-AS1 promotes the progression of hemangioma by regulating miR-138-5p/HIF-1α axis and glycolysis. This study suggested the potential value of LncRNA-MCM3AP-AS1/miR-138-5p as a treatment strategy for hemangioma.

MATERIALS AND METHODS

Clinical Samples

Twenty-two infantile hemangioma specimens including normal subcutaneous tissues and infantile hemangioma tissues in the involuting stage (four males and eight females; median age, 7 months) and proliferating stage (two males and eight females; median age, 6 months), were collected in the plastic surgery department of our hospital from October 2019 to October 2020. All the samples were immediately frozen at −80°C for further analysis. The informed consent was obtained from the parents of patients. The experiments were approved by the Ethics Committee for Experiment of Nantong University.

HemECs were isolated from IH tissues in the proliferating phase as previously described (Khan et al., 2006). HemECs were cultured in human endothelial-serum free medium (Gibco; Thermo Fisher Scientific, Inc.) containing 10% FBS (Gibco; Thermo Fisher Scientific, Inc.) with 5% CO_2 at 37°C.

RNA Extraction and Quantitative Real-Time PCR

All the specimens were detached quickly and immersed in lysis solution (4305895, Thermo Scientific) at the ratio of 1:6, then the samples were homogenized using an ultrasound homogenizer. Total RNA extraction was performed as the supplier's protocol (AM 1912, Thermo Scientific). NanoDrop ND-1000 spectrophotometer (Thermo Scientific) was used to evaluate the quantity and purity of RNA. Complementary DNAs were obtained by the reverse transcription reaction with a reverse transcription kit (RR037A, Takara) and applied as templates to determine the expression of target genes by PCR. All the primers were designed by Primer Premier 5.0 software, and synthesized by Sangon Biotech (Shanghai, China). The primers were designed and synthesized as follows: hsa-miR-138-5p, 5′-gtcgtatccagtgca gggtccgaggtattcgcactggatacgaccggcct-3′; LncRNA-MCM3AP-AS1, forward: 5′-GCTGCTAATGGCAACACTGA-3′ and reverse: 5′-AGGTGCTGTCTG GTGGAGAT-3′. GAPDH, forward: 5′-CAG GAGGCATTGCTGATGAT-3′ and reverse: 5′-GAAGGCTGGGGCTCATTT-3′. LncRNA H19 forward: 5′-ACCACTGCACTACCTGACTC-3′, and reverse: 5′-CCGCAG

GGGGTGGCCATGAA-3′; LncRNA AC092718.4 forward: 5′-GCAACTCCTAGATTCGATAC-3′, and reverse: 5′-CACGCG TATGGTAACATGCT-3′; LncRNA NEAT1 forward: 5′-TTCCGTGCT TCCTCTTCTGT-3′ and reverse: 5′-CAGGGT GTCCTCCACCTTTA-3′; LncRNA PARD6G-AS1, forward: 5′-ATGCTGCAACTTGTAACT-3′ and reverse: 5′-ACTTGC GACTTGACACTTAGATT-3′;

Cell Counting Kit-8 Assay

CCK-8 assay was used to assess the cell viability of HemECs and EoMA cells. Briefly, HemECs and EoMA cells (about 10,000 per well) were seeded into 96-well plates. After 24, 48, and 72 h, CCK-8 solution (10 μL) was added into each well and incubated with HemECs and EoMA cells at 37 °C for 3 h. Then the light absorbance was measured at the wavelength of 450 nm to assess the cell viability of HemECs and EoMA cells.

Flow Cytometric Analysis of Cell Cycle Distribution and Apoptosis

The cells were seeded into 6-well plates. For cell cycle analysis, the cells were transfected with the different plasmids for 48 h. Then, the cells were washed by PBS (4°C), and collected with cold 70% ethanol (4°C) followed by washing with PBS. After the above operations, the cells were incubated with 1 ml of 20 mg/ml propidium iodide (PI) which contained RNase (1 mg/ml) in PBS for 30 min followed by fluorescence-activated cell sorting (FACS) assay. For the apoptosis assay, the cells were collected after treatment with the different plasmids for 48 h. The cells were washed with cold (4°C) PBS, followed by incubation with PI and Annexin V-EGFP according to the procedures specified in the kit (KeyGen Biotech Co. Ltd., Nanjing, China). Then, the processed cells were inspected using FACS assay.

Dual-Luciferase Reporter Assay

For the luciferase reporter assay, a dual luciferase reporter assay system (Promega corporation) was used to detect the binding between miR-138-5p and LncRNA MCM3AP-AS1 or 3′-UTR of HIF-1α according to the manufacturer's protocols. HemECs were seeded onto a 6-well plate and cultured for 24 h, cells were co-transfected with pGL3-MCM3AP-AS1 WT, or pGL3-MCM3AP-AS1 Mut (pGL3-HIF-1α 3′UTR WT or pGL3-HIF-1α 3′UTR Mut) and miR-138-5p mimic/NC mimic. After 48 h, luciferase activity was detected using the Dual-Luciferase Reporter Assay System (Promega, Madison, WI, United States).

In situ Hybridization

The paraffin-embedded tissues were cut into 4 μm thick sections and sections heated at 56°C for 5 min. After that, xylene and ethanol were used for deparaffinization. The sections were sealed with 3% H_2O_2 for 10 min, hybridized with 20 μl pre hybridizing solution in 42°C incubators for 3.5 h, and hybridized with 20 μl probe (The corresponding probe for detecting genes) solution (synthesized by Sangon Biotech Co., Ltd., Shanghai, China) in 40°C incubators for 20 h. The hybridization was coated with 3% BSA for 2 h in 37°C, washed and sealed. Biotinylated secondary anti-digoxin, streptavidin-biotin peroxidase complex ABC and DAB were added in turn according to the instructions of the ISH kit. Finally, the samples were observed under a light microscope.

Immunohistochemical Analysis

As for immunohistochemical analysis, paraffin-embedded tissue sections were deparaffinized by xylene and hydrated with gradient ethanol. Then, the sections were treated with citrate buffer (pH = 6) for 20 min and immersed in 3% H_2O_2 for 10 min in a humidified chamber. After washing with PBS 5 min 3 times and blocked for 30 min with 10% goat serum, sections were incubated with rabbit HIF-1α antibody (1:400 Abcam, Cambridge, MA, United States) in a humidified chamber at 4°C overnight with a two-step protocol. Five randomly selected fields were captured under high-power magnification (×200) using a bright-field microscope (Olympus, Tokyo, Japan) and analyzed using Image-Pro Plus v6.2 software (Media Cybernetics, Silver Spring, MD).

Binding Sites Prediction

The ENCORI database (http://starbase.sysu.edu.cn/), miRWalk database (http://mirwalk.umm.uni-heidelberg.de/) and miRDB database (http://www.mirdb.org) are powerful databases to study non-coding RNAs, such as LncRNAs, miRNAs and circRNAs. These databases were used to predict the binding sites between LncRNA MCM3AP-AS1 and miR-138-5p or miR-138-5p and the 3′-UTR of HIF-1α.

Statistical Analysis

All the experiments were repeated at least three times independently. Data were analyzed using SPSS (SPSS 12.0, SPSS (IBM) Inc., Illinois, United States). The categorical variants were assigned a numerical value. Data were presented as mean ± standard deviation. Unpaired Student's t tests or one-way ANOVA was used for data comparison (SPSS 12.0, SPSS (IBM) Inc., Illinois, United States). Statistical significance was determined at defined $p < 0.05$.

DATA AVAILABILITY STATEMENT

The original contributions presented in the study are included in the article/Supplementary Materials, further inquiries can be directed to the corresponding author.

ETHICS STATEMENT

The studies involving human participants were reviewed and approved by The Ethics Committee for Experiment of Nantong University. The patients/participants provided their written informed consent to participate in this study.

AUTHOR CONTRIBUTIONS

JK conceived and designed the study. HM and HX performed the literature search and data extraction. HM and HX drafted the manuscript. All authors read and approved the final manuscript.

REFERENCES

Baselga, E., Roe, E., Coulie, J., Muñoz, F. Z., Boon, L. M., McCuaig, C., et al. (2016). Risk Factors for Degree and Type of Sequelae after Involution of Untreated Hemangiomas of Infancy.[J]. *JAMA Dermatol.* 152 (11), 1239–1243. doi:10.1001/jamadermatol.2016.2905

Caussé, S., Aubert, H., Saint-Jean, M., Puzenat, E., Bursztejn, A. C., Eschard, C., et al. (2013). Propranolol-resistant Infantile haemangiomas.[J]. *Br. J. Dermatol.* 169 (1), 125–129. doi:10.1111/bjd.12417

Chamli, A., Aggarwal, P., and Jamil, R. T. (2021). Hemangioma.[Z]. *StatPearls*. 18 July 2021

Chang, L. C., Haggstrom, A. N., and Drolet, B. A. (2008). Growth Characteristics of Infantile Hemangiomas: Implications for management.[J]. *Pediatrics* 122 (2), 360–367. doi:10.1542/peds.2007-2767

Chappell, J. C., Payne, L. B., and Rathmell, W. K. (2019). Hypoxia, Angiogenesis, and Metabolism in the Hereditary Kidney cancers.[J]. *J. Clin. Invest.* 129 (2), 442–451. doi:10.1172/jci120855

Cheng, C. E., and Friedlander, S. F. (2016). Infantile Hemangiomas, Complications and treatments.[J]. *Semin. Cutan. Med. Surg.* 35 (3), 108–116. doi:10.12788/j.sder.2016.050

Chou, J., Wang, B., Zheng, T., Li, X., Zheng, L., Hu, J., et al. (2016). MALAT1 Induced Migration and Invasion of Human Breast Cancer Cells by competitively.[J]. *Biochem. biophysical Res. Commun.* 472 (1), 262–269. doi:10.1016/j.bbrc.2016.02.102

Darrow, D. H., Greene, A. K., Mancini, A. J., and Nopper, A. J. (2015). Diagnosis and Management of Infantile Hemangioma.[J]. *Pediatrics* 136 (4), e1060–e1104. doi:10.1542/peds.2015-2485

Dong, H., Lei, J., Ding, L., Wen, Y., Ju, H., and Zhang, X. (2013). MicroRNA: Function, Detection, and bioanalysis.[J]. *Chem. Rev.* 113 (8), 6207–6233. doi:10.1021/cr300362f

Fan, Y., Liu, M., Liu, A., Cui, N., Chen, Z., Yang, Q., et al. (2021). Depletion of Circular RNA circ_CORO1C Suppresses Gastric Cancer Development by.[J]. *Cancer Manag. Res.* 13, 3789–3801. doi:10.2147/cmar.s290629

Gonzalez, F. J., Xie, C., and Jiang, C. (2018). The Role of Hypoxia-Inducible Factors in Metabolic diseases.[J]. *Nat. Rev. Endocrinol.* 15 (1), 21–32. doi:10.1038/s41574-018-0096-z

Gu, J., Wang, Y., Wang, X., Zhou, D., Wang, X., Zhou, M., et al. (2018). Effect of the LncRNA GAS5-MiR-23a-ATG3 Axis in Regulating Autophagy in Patients with Breast Cancer.[J]. *Cell Physiol. Biochem. : Int. J. Exp. Cell. Physiol. Biochem. Pharmacol.* 48 (1), 194–207. doi:10.1159/000491718

Hagman, Z., Larne, O., Edsjö, A., Bjartell, A., Ehrnström, R. A., Ulmert, D., et al. (2010). miR-34c Is Downregulated in Prostate Cancer and Exerts Tumor Suppressive functions.[J]. *Int. J. Cancer* 127 (12), 2768–2776. doi:10.1002/ijc.25269

Han, W., Sulidankazha, Q., Nie, X., Yilidan, R., and Len, K. (2021). Pancreatic Cancer Cells-Derived Exosomal Long Non-coding RNA [J]. *Life Sci.* 278, 119495. doi:10.1016/j.lfs.2021.119495

Hepp, M., Werion, A., De Greef, A., de Ville de Goyet, C., de Bournonville, M., Behets, C., et al. (2021). Oxidative Stress-Induced Sirtuin1 Downregulation Correlates to HIF-1α, GLUT-1, and [J]. *Int. J. Mol. Sci.* 22 (8), 3806. doi:10.3390/ijms22083806

Khan, Z. A., Melero-Martin, J. M., Wu, X., Paruchuri, S., Boscolo, E., Mulliken, J. B., et al. (2006). Endothelial Progenitor Cells from Infantile Hemangioma and Umbilical Cord Blood Display Unique Cellular Responses to endostatin.[J]. *Blood* 108 (3), 915–921. doi:10.1182/blood-2006-03-006478

Li, B., Wang, X., Hong, S., Wang, Q., Li, L., Eltayeb, O., et al. (2021). MnO 2 Nanosheets Anchored with Polypyrrole Nanoparticles as a Multifunctional Platform for Combined Photothermal/photodynamic Therapy of TumorsMnO(2) nanosheets anchored with polypyrrole nanoparticles as a multifunctional [J]. *Food Funct.* 2 (14), 6334–6347. doi:10.1039/d1fo00032b

Liang, M., Jia, J., Chen, L., Wei, B., Guan, Q., Ding, Z., et al. (2019). LncRNA MCM3AP-AS1 Promotes Proliferation and Invasion through Regulating miR-211-5p/SPARC axis in Papillary Thyroid cancer.[J]. *Endocrine* 65 (2), 318–326. doi:10.1007/s12020-019-01939-4

Liu, L., Wang, H., Meng, T., Lei, C., Yang, X. H., Wang, Q. S., et al. (2019). lncRNA GAS5 Inhibits Cell Migration and Invasion and Promotes Autophagy by Targeting miR-222-3p via the GAS5/PTEN-Signaling Pathway in CRC.[J]. *Mol. Ther. Nucleic Acids* 17, 644–656. doi:10.1016/j.omtn.2019.06.009

Liu, R., Feng, Y., Deng, Y., Zou, Z., Ye, J., Cai, Z., et al. (2021). A HIF1α-GPD1 Feedforward Loop Inhibits the Progression of Renal clear Cell Carcinoma [J]. *J. Exp. Clin. Cancer Res.* 40 (1), 188. doi:10.1186/s13046-021-01996-6

Liu, Z., Kang, Z., Dai, Y., Zheng, H., and Wang, Y. (2019). Long Noncoding RNA LINC00342 Promotes Growth of Infantile Hemangioma by Sponging miR-3619-5p from HDGF.[J]. *Am. J. Physiol. Heart circulatory Physiol.* 317 (4), H830–H839. doi:10.1152/ajpheart.00188.2019

Ma, L., Craig, A. J., and Heinrich, S. (2021). Hypoxia Is a Key Regulator in Liver Cancer progression.[Z]. *J. Hepatol.* 75 (3), 736–737. doi:10.1016/j.jhep.2021.05.032

Ma, L., Craig, A. J., and Heinrich, S. (2021). Hypoxia Is a Key Regulator in Liver Cancer progression.[Z]. *J. Hepatol.* 75 (3), P736–P737. doi:10.1016/j.jhep.2021.05.032

Nyga, A., Hart, A., and Tetley, T. D. (2019). Molecular Analysis of HIF Activation as a Potential Biomarker for Adverse Reaction to Metal Debris (ARMD) in Tissue and Blood samples.[Z]. *J. Biomed. Mater. Res. B Appl. Biomater.* 107, 1352–1362. doi:10.1002/jbm.b.34227

Ørom, U. A., and Shiekhattar, R. (2011). Long Non-coding RNAs and enhancers.[J]. *Curr. Opin. Genet. Dev.* 21 (2), 194–198. doi:10.1016/j.gde.2011.01.020

Peng, Y., Yuan, G., Khan, S., Nanduri, J., Makarenko, V. V., Reddy, V. D., et al. (2014). Regulation of Hypoxia-Inducible Factor-α Isoforms and Redox State by Carotid Body [J]. *J. Physiol.* 592 (17), 3841–3858. doi:10.1113/jphysiol.2014.273789

Quiroga, J., Alarcón, P., Manosalva, C., Teuber, S., Taubert, A., Hermosilla, C., et al. (2021). Metabolic Reprogramming and Inflammatory Response Induced by D-Lactate in Bovine.[J]. *Front. Vet. Sci.* 8, 625347. doi:10.3389/fvets.2021.625347

Sarkar, N., and Kumar, A. (2021). microRNAs: New-Age Panacea in Cancer Therapeutics.[J]. *Indian J. Surg. Oncol.* 12 (Suppl. 1), 52–56. doi:10.1007/s13193-020-01110-w

Sun, C., Gao, S., Tan, Y., Zhang, Z., and Xu, H. (2021). Side-Chain Selenium-Grafted Polymers Combining Antiangiogenesis Treatment with [J]. *ACS Biomater. Sci. Eng.* 7 (7), 3201–3208. doi:10.1021/acsbiomaterials.1c00254

Wan, W., Peng, K., Li, M., Qin, L., Tong, Z., Yan, J., et al. (2017). Histone Demethylase JMJD1A Promotes Urinary Bladder Cancer Progression by Enhancing Glycolysis through Coactivation of Hypoxia Inducible Factor 1α.[J]. *Oncogene* 36 (27), 3868–3877. doi:10.1038/onc.2017.13

Wang, Y., Bai, C., Ruan, Y., Liu, M., Chu, Q., Qiu, L., et al. (2019). Coordinative Metabolism of Glutamine Carbon and Nitrogen in Proliferating Cancer Cells under hypoxia.[J]. *Nat. Commun.* 10 (1), 201. doi:10.1038/s41467-018-08033-9

Wang, Y., Yang, L., Chen, T., Liu, X., Guo, Y., Zhu, Q., et al. (2019). A Novel lncRNA MCM3AP-AS1 Promotes the Growth of Hepatocellular Carcinoma by Targeting miR-194-5p/FOXA1 axis.[J]. *Mol. Cancer* 18 (1), 28. doi:10.1186/s12943-019-0957-7

Wang, Y., Yang, L., Chen, T., and Nopper, A. J. (2019). A Novel lncRNA MCM3AP-AS1 Promotes the Growth of Hepatocellular Carcinoma by Targeting miR-194-5p/FOXA1 axis.[J]. *Mol. Cancer* 18 (1), 28. doi:10.1186/s12943-019-0957-7

Wu, P., Xu, H., Li, N., Huo, R., Shen, B., Lin, X., et al. (2021). Hypoxia-Induced Cyr61/CCN1 Production in Infantile Hemangioma.[J]. *Plast. Reconstr. Surg.* 147 (3), 412e–423e. doi:10.1097/prs.0000000000007672

Xu, J., Liao, X., Lu, N., Liu, W., and Wong, C. W. (2011). Chromatin-modifying Drugs Induce miRNA-153 Expression to Suppress Irs-2 in Glioblastoma Cell lines.[J]. *Int. J. Cancer* 129 (10), 2527–2531. doi:10.1002/ijc.25917

Xue, L., Tao, Y., Yuan, Y., Qu, W., and Wang, W. (2021). Curcumin Suppresses Renal Carcinoma Tumorigenesis by Regulating [J]. *Anti-cancer drugs* 32 (7), 734–744. doi:10.1097/CAD.0000000000001063

Xun, J., Du, L., Gao, R., Shen, L., Wang, D., Kang, L., et al. (2021). Cancer-derived Exosomal miR-138-5p Modulates Polarization of tumor-associated.[J]. *Theranostics* 11 (14), 6847–6859. doi:10.7150/thno.51864

Yang, C., Zheng, J., Xue, Y., Yu, H., Liu, X., Ma, J., et al. (2017). The Effect of MCM3AP-AS1/miR-211/KLF5/AGGF1 Axis Regulating Glioblastoma Angiogenesis.[J]. *Front. Mol. Neurosci.* 10, 437. doi:10.3389/fnmol.2017.00437

Yang, M., Sun, S., Guo, Y., and QinLiu, J. G. (2019). Long Non-coding RNA MCM3AP-AS1 Promotes Growth and Migration through Modulating FOXK1 by Sponging miR-138-5p in Pancreatic cancer.[J]. *Mol. Med. (Cambridge, Mass.)* 25 (1), 55. doi:10.1186/s10020-019-0121-2

Yoon, D. J., Kaur, R., Gallegos, A., West, K., Yang, H., Schaefer, S., et al. (2021). Repurposing Ophthalmologic Timolol for Dermatologic Use: Caveats and Historical [J]. *Am. J. Clin. Dermatol.* 22 (1), 89–99. doi:10.1007/s40257-020-00567-3

Yu, F., Liang, M., Huang, Y., Wu, W., Zheng, B., Chen, C., et al. (2021). Hypoxic Tumor-Derived Exosomal miR-31-5p Promotes Lung Adenocarcinoma Metastasis by [J]. *J. Exp. Clin. Cancer Res. : CR* 40 (1), 179. doi:10.1186/s13046-021-01979-7

Zhang, H., Luo, C., and Zhang, G. (2019). LncRNA MCM3AP-AS1 Regulates Epidermal Growth Factor Receptor and Autophagy to Promote Hepatocellular Carcinoma Metastasis by Interacting with miR-455.[J]. *DNA Cel. Biol.* 38 (8), 857–864. doi:10.1089/dna.2019.4770

Zhang, J., and Zhang, C. (2019). Silence of Long Non-coding RNA UCA1 Inhibits Hemangioma Cells Growth, Migration and Invasion by Up-Regulation of miR-200c.[J]. *Life Sci.* 226, 33–46. doi:10.1016/j.lfs.2019.03.038

Zhang, J., Zhang, Y., Mo, F., Patel, G., Butterworth, K., Shao, C., et al. (2021). The Roles of HIF-1α in Radiosensitivity and Radiation-Induced Bystander Effects [J]. *Front. Cel. Dev. Biol.* 9, 637454. doi:10.3389/fcell.2021.637454

Zhang, Y., Ren, Y., Guo, L., Ji, C., Hu, J., Zhang, H., et al. (2017). Nucleus Accumbens-Associated Protein-1 Promotes Glycolysis and Survival of Hypoxic Tumor Cells via the HDAC4-HIF-1α axis.[J]. *Oncogene* 36 (29), 4171–4181. doi:10.1038/onc.2017.51

Zhi, Y., Abudoureyimu, M., Zhou, H., Wang, T., Feng, B., Wang, R., et al. (2019). FOXM1-Mediated LINC-ROR Regulates the Proliferation and Sensitivity to Sorafenib in Hepatocellular Carcinoma.[J]. *Mol. Ther. Nucleic Acids* 16, 576–588. doi:10.1016/j.omtn.2019.04.008

Zhu, T., Yu, Q., Feng, Z., Zhao, W., Liu, S., Huang, W., et al. (2021). Photothermal Responsive Singlet Oxygen Nanocarriers for Hypoxic Cancer Cell.[J]. *Chembiochem : a Eur. J. Chem. Biol.* 22 (15), 2546–2552. doi:10.1002/cbic.202100098

Conflict of Interest: The authors declare that the research was conducted in the absence of any commercial or financial relationships that could be construed as a potential conflict of interest.

Publisher's Note: All claims expressed in this article are solely those of the authors and do not necessarily represent those of their affiliated organizations, or those of the publisher, the editors and the reviewers. Any product that may be evaluated in this article, or claim that may be made by its manufacturer, is not guaranteed or endorsed by the publisher.

frontiers in Molecular Biosciences

REVIEW
published: 25 November 2021
doi: 10.3389/fmolb.2021.763902

Recent Metabolomics Analysis in Tumor Metabolism Reprogramming

Jingjing Han[1], *Qian Li*[1], *Yu Chen*[1]* *and Yonglin Yang*[2]*

[1]Department of Anesthesiology, First Affiliated Hospital of Nanjing Medical University, Nanjing, China, [2]Division of Infectious Diseases, Taizhou Clinical Medical School of Nanjing Medical University (Taizhou People's Hospital), Taizhou, China

Metabolic reprogramming has been suggested as a hallmark of cancer progression. Metabolomic analysis of various metabolic profiles represents a powerful and technically feasible method to monitor dynamic changes in tumor metabolism and response to treatment over the course of the disease. To date, numerous original studies have highlighted the application of metabolomics to various aspects of tumor metabolic reprogramming research. In this review, we summarize how metabolomics techniques can help understand the effects that changes in the metabolic profile of the tumor microenvironment on the three major metabolic pathways of tumors. Various non-invasive biofluids are available that produce accurate and useful clinical information on tumor metabolism to identify early biomarkers of tumor development. Similarly, metabolomics can predict individual metabolic differences in response to tumor drugs, assess drug efficacy, and monitor drug resistance. On this basis, we also discuss the application of stable isotope tracer technology as a method for the study of tumor metabolism, which enables the tracking of metabolite activity in the body and deep metabolic pathways. We summarize the multifaceted application of metabolomics in cancer metabolic reprogramming to reveal its important role in cancer development and treatment.

Keywords: metabolomics, metabolic reprogramming, biomarkers, stable isotope resolved metabolomics, drug resistance

OPEN ACCESS

Edited by:
Haishi Qiao,
China Pharmaceutical University, China

Reviewed by:
Stefana Cacciatore,
International Centre for Genetic Engineering and Biotechnology (ICGEB), South Africa
Christos K. Kontos,
National and Kapodistrian University of Athens, Greece
Xiawei Cheng,
East China University of Science and Technology, China
Yujie Su,
Washington State University, United States
Jinghui Sun,
Chengdu Medical College, China

***Correspondence:**
Yu Chen
chenyu_njmu@126.com
Yonglin Yang
easing@163.com

Specialty section:
This article was submitted to Molecular Diagnostics and Therapeutics, a section of the journal Frontiers in Molecular Biosciences

Received: *24 August 2021*
Accepted: *08 November 2021*
Published: *25 November 2021*

Citation:
Han J, Li Q, Chen Y and Yang Y (2021) Recent Metabolomics Analysis in Tumor Metabolism Reprogramming. Front. Mol. Biosci. 8:763902. doi: 10.3389/fmolb.2021.763902

INTRODUCTION

In recent years, metabolism, as an important link between environmental factors, metabolic small molecules, host genes and diseases, has gained increasing interest regarding its relationship with tumors. Under environmental selection pressures induced by microenvironmental and genetic factors, the inside of the tumor undergoes evolution. Simultaneously, under the control of genotypes, metabolic characteristics of the tumor undergo adaptive changes; this is termed metabolic reprogramming (Zhao et al., 2019). Studies have shown that the tumor microenvironment is often nutritionally deficient; thus, tumor cells reprogram their metabolism and that of the microenvironment to maintain their proliferative ability (Wu and Dai, 2017; Ringel et al., 2020).

Metabolic reprogramming of the tumor microenvironment is considered one of the markers of cancer and an important direction of tumor research (Hanahan and Weinberg, 2011). Continuous developments in high-throughput sequencing and bioinformatics technology have enabled wide use of the combined analysis of metabolomics (Kaushik and DeBerardinis, 2018), genomics (Horn et al., 2019), transcriptomics (Finotello and Trajanoski, 2018), and proteomics (Kim et al., 2019) to determine the etiology and pathogenesis of diseases. Metabolomics is regarded as the final node of

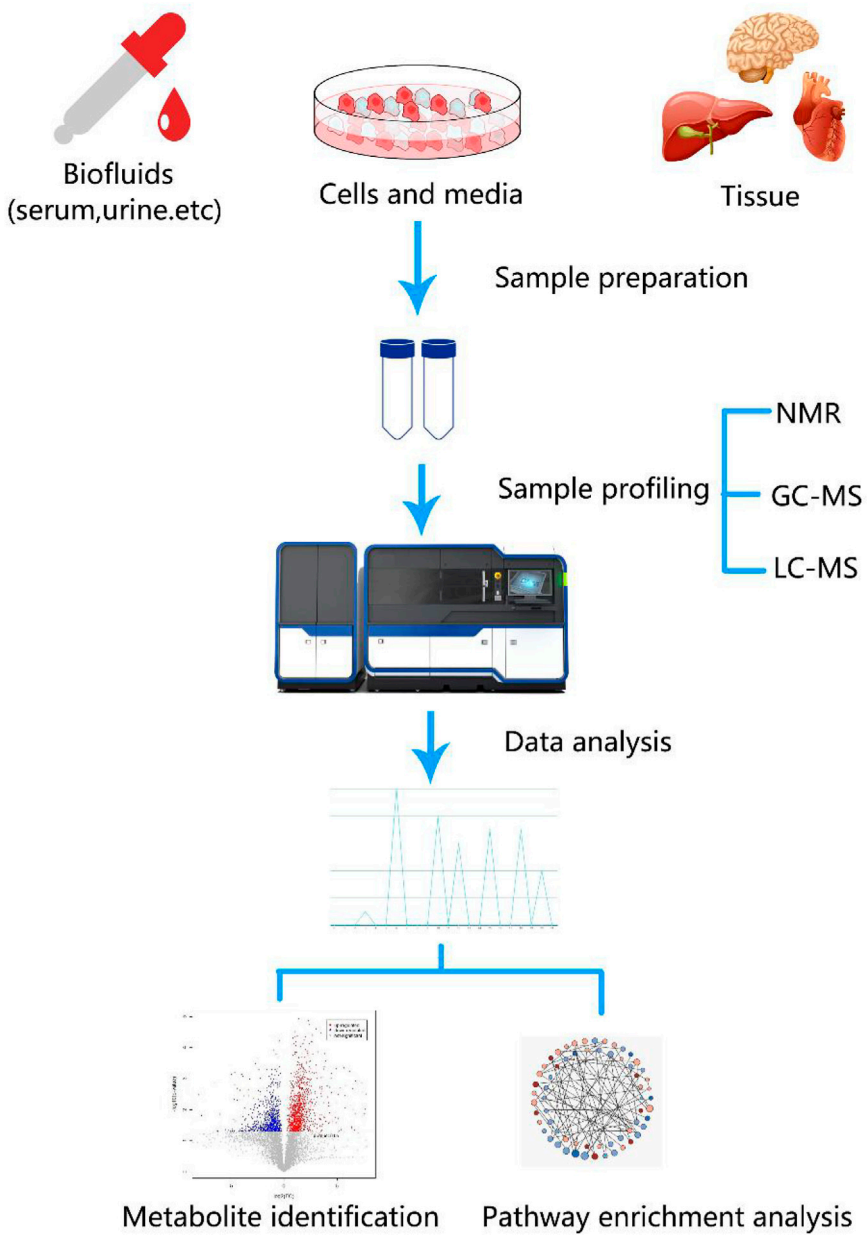

FIGURE 1 | (A) Analytical workflow of metabolomics studies. A typical metabolomics study includes experimental design, sample collection, sample profiling, data analysis, and functional interpretation stages. Metabolites from biological fluids, cells, and tissues that differ between tumor and control groups can be detected using metabolomics [e.g., nuclear magnetic resonance (NMR), liquid chromatography-mass spectrometry (LC-MS), and gas chromatography-mass spectrometry (GC-MS)] and data analyses. Discovery of metabolic biomarkers and pathways that are specific to certain cancers benefit cancer research.

various molecular pathways and is considered the ultimate goal of omics research. The rise of metabolomics has allowed considerable progress to be made in understanding the relationship between metabolic regulation and cancer.

Metabolomics techniques are defined as the measurement of the dynamic multiparameter metabolic response of biological systems to various stimuli and genetic changes in specified quantities (Johnson et al., 2016). They primarily involve analyses of metabolites in bodily fluids, cells, and tissues and are usually applied as a valuable means to identify biomarkers (Zampieri et al., 2017). The basic research approach involves measuring metabolites using high-throughput and high-resolution detection technology, acquiring massive datasets, obtaining different metabolites via data analysis, finding metabolic pathways, and explaining their biological significance (Toledo et al., 2017). Metabolomics techniques usually include nuclear magnetic resonance (NMR), liquid chromatography-mass spectrometry (LC-MS), and gas

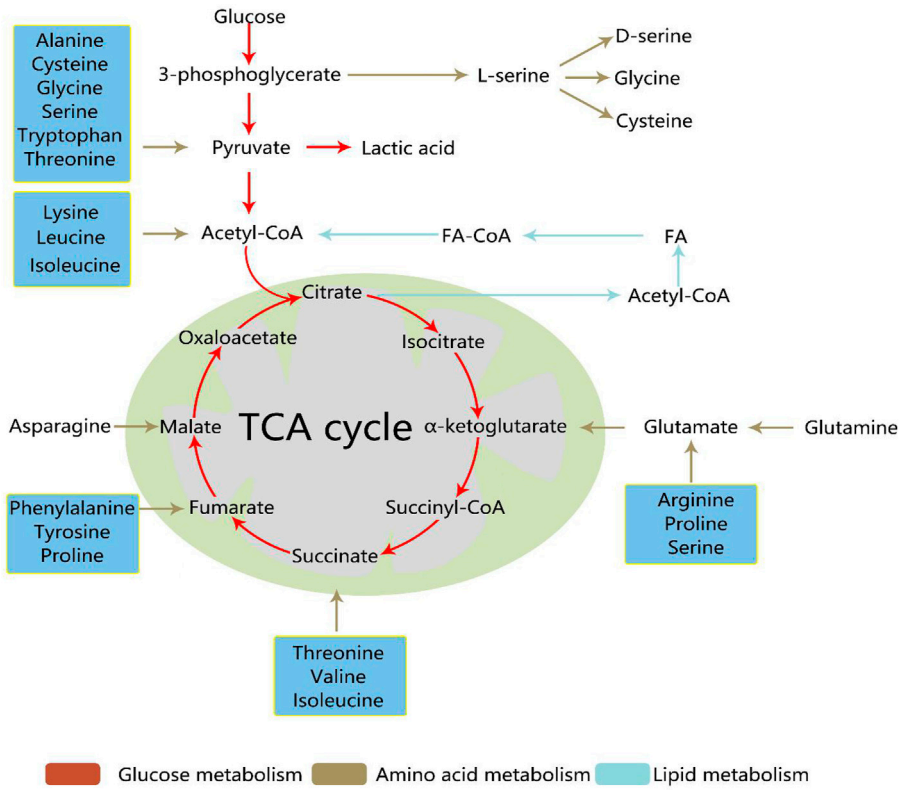

FIGURE 2 | The regulation of the three pathways of cancer cells and their crossover. During cancer development, metabolic reprogramming provides cancer cells the ability to survive and proliferate. Glucose, amino acid, and lipid metabolism are inseparable. Activated glycolysis and impaired aerobic respiration shape the altered glucose metabolism. In addition, deregulated anabolism/catabolism of fatty and amino acids, especially glutamine, serine, and glycine, have been identified to function as metabolic regulators in supporting cancer cell growth. TCA, tricarboxylic acid; FA, fatty acid; acetyl-CoA, acetyl coenzyme A; FA-CoA, fatty acetyl coenzyme A.

chromatography-mass spectrometry (GC-MS) (Fiehn, 2016; Lane et al., 2019). In addition, the accuracy of qualitative metabolite analyses depends not only on the detection and resolution ability of the mass spectrometer but also on the corresponding metabolite database (Wishart et al., 2013; Johnson et al., 2016). **Figure 1** illustrates the basic workflow of metabolomics techniques.

Mass spectrometry-based technology has become the mainstream technology for the analysis of targeted metabolomics pathways. Numerous studies have revealed that differences in small molecular metabolites, such as serum, tissues, urine, and saliva, and changes in corresponding metabolic pathways are closely related to tumor risk, tumor type, and the sensitivity and efficacy of chemotherapy drugs as well as potential drug targets (Wishart 2019). Metabolomics technology could bring a new dimension to tumor metabolism. Several excellent reviews of metabolomics applications in cancer research have been published, which have focused primarily on the search for metabolic biomarkers and investigations on metabolic mechanisms underlying various tumors (Zhang et al., 2014; Xiao and Zhou, 2017). In this review, we first summarize the applications of metabolomics to the three major metabolism pathways of cancers. We then focus on biofluid markers for the early prediction of tumors, metabolomics in cancer drug treatments, and applications of resistance mechanisms. Finally, we introduce the applications of stable isotope tracer technology to the field of metabolomics and offer future directions.

METABOLOMICS ANALYSIS OF THE THREE MAJOR METABOLIC PATHWAYS OF TUMOR

During cancer development, metabolic reprogramming provides cancer cells the ability to survive and proliferate. The most famous is the Warburg effect, which suggests that the aerobic glycolysis pathway is closely related to the occurrence of cancer. In addition, deregulated anabolism/catabolism of fatty (FAs) and amino acids, especially glutamine, serine, and glycine, have been shown to function as metabolic regulators in supporting cancer cell growth. The occurrence and development of cancer cells are closely related to the three metabolic pathways. **Figure 2** shows the regulation of the three pathways of cancer cells and how they crossover. Metabolomics techniques can be used to supplement tumor metabolism by analyzing the metabolic profiles of different tumors.

Glucose Metabolism Reprogramming in Cancer Progression

Owing to the need for malignant proliferation, tumor cells exhibit a rapid glycolysis phenomenon in various environments called the Warburg effect. Tumor cells have a high ability to proliferate and a high demand for energy, which often leads to hypoxia in the local tissue microenvironment (Warburg, 1956; Williams et al., 2016). Although glycolysis is not as efficient as aerobic respiration in terms of energy supply, it is 100 times faster than aerobic respiration and provides the amino acids and intermediate metabolites of pentose phosphate essential for highly proliferating cancer cells (Cacciatore and Loda, 2015). Thus, cancer cells weaken or even cease using the mitochondrial aerobic oxidation pathway in favor of the glucose glycolysis pathway for energy, which produces large amounts of lactic acid (Chen et al., 2014). Aerobic glycolysis is a key metabolic feature of the Warburg phenotype and is caused by active metabolic reprogramming that is required to support sustained cancer cell proliferation and malignant progression (Kishton et al., 2016). Glucose metabolism includes not only glycolysis but also other pathways that require glucose. These pathways include pentose phosphate pathway (PPP), hexosamine pathway, glycogenesis. They are all reprogrammed in cancer cells, and this reprogramming can be used to selectively target cancer cells.

High-throughput omics screening has shown that the tumor microenvironment and various cancer-promoting signaling pathways significantly up-regulate the glycolysis process, which results in the Warburg effect. Recent investigations of renal carcinoma cells and tissues from xenografted mice and patients using metabolomics, proteomics, and transcriptomics have unambiguously confirmed that this phenomenon is a key component of metabolic reprogramming (Perroud et al., 2009). As an example of Warburg metabolism, levels of enzymes involved in glycolysis, such as hexokinase-1 pyruvate kinase, and lactate dehydrogenase A were significantly increased in renal carcinoma cells and tissues (Perroud et al., 2006). In a breast cancer study (Dai et al., 2017), researchers cultured MCF-7 and T47D breast cancer cells with different glucose concentrations and found that low glucose concentration significantly inhibited the proliferation of breast cancer cells. Moreover, signal pathway enrichment analysis showed that the Hippo-Yap cell signaling pathway in MCF-7 breast cancer cells was downregulated when the glucose concentration in the culture environment was reduced, whereas the expression of NRF2 pathway-related genes in T47D breast cancer cells was significantly increased (Maldonado et al., 2021). In a recent lung cancer study, researchers found that glucose metabolism disorders may be closely associated with the carcinogenesis of lung cancer, which suggests that glucose metabolism may be a potential therapeutic target for lung cancer (Ding et al., 2019).

Essentially, the Warburg effect in tumor cells is caused by the increased expression of metabolic enzymes related to the glycolysis pathway. In recent years, the regulation of glycolytic metabolic enzymes, especially rate-limiting enzymes, has attracted considerable attention in the field of oncology (Chen et al., 2016). Through metabolomics analysis, researchers confirmed that KRAS gene's effect on tumor metabolism can be realized through transcriptional regulation of glucose transporters and glycolysis enzymes. And the KRAS activating mutations copy gain creates unique metabolic dependences that can be exploited to selectively target these aggressive mutant KRAS tumors (Kerr et al., 2016). Wong et al. showed that protein arginine N-methyltransferase 6 (PRMT6) regulates aerobic glycolysis in human hepatocellular carcinoma (HCC) through nuclear relocalization of pyruvate kinase M2 isoform (PKM2), a key regulator of the Warburg effect. This research provides a mechanistic link between tumorigenicity of tumors and glucose metabolism (Wong et al., 2020). The tumor microenvironment and various cancer-promoting signaling pathways have been found to significantly upregulate the glycolysis process and thus, providing a variety of potential targets for inhibiting glycolysis in tumor therapy. This has been confirmed in a variety of tumor settings and is associated with poor tumor outcomes (Li et al., 2018; Zhang et al., 2020).

Lipid Metabolic Reprogramming in Cancer Cells

Tumor cells exhibit metabolic plasticity, which provides a selective advantage for the survival and proliferation of tumor cells in harsh microenvironments, such as hypoxia, acidosis, and malnutrition (Hanahan and Weinberg, 2011). Significant characteristics of lipid metabolism in tumor cells include increased adipogenesis rate and an upregulated mitochondrial fatty acid β-oxidation level (Currie et al., 2013). A variety of tumors have shown similar trends, and various metabolites involved in lipid metabolism have exhibited typical changes. In such microenvironments, tumor cell lipid synthesis is increased (Peng et al., 2018). Lipids provide a large amount of energy for the proliferation of tumor cells to maintain membrane synthesis and other related functions during tumor cell growth. Systemic metabolic alterations associated with increased consumption of saturated fat and obesity are linked with increased risk of prostate cancer progression and mortality. Studies have shown that in primary prostate cancer, dietary saturated fat intake contributes to tumor progression by mimicking MYC over expression, setting the stage for therapeutic approaches involving changes to the diet (Labbé et al., 2019). Lipid metabolomics techniques provide information on lipid changes in various tumor cells (Poczobutt et al., 2016).

Lipid metabolism presents as a network of pathways with flexible feedback loops and crosstalk to meet the increased metabolic needs of cancer cells. Based on multi-omics data of pan-cancer, researchers have found extensive alterations in FAs, arachidonic acid, cholesterol metabolism, and peroxisome proliferator-activated receptor (PPAR)-signaling in different tumors, and lipid metabolism features are shared among tumors with similar tissue origin tumors. Moreover, possible causes of metabolic disorders have been correlated with lipids in tumors from several perspectives, which include somatic mutation, DNA methylation abnormality, and regulation of

transcription factors (Hao et al., 2019). For example, hexadecenoic acid, docosahexaenoic acid, heptanoic acid, and β-hydroxybutyrate, are significantly greater in gastric cancer than they are in benign tissue (Stuart et al., 2014). Untargeted metabolomic studies of kidney cancers have shown increased use of FAs by cancer cells (Ganti et al., 2012). Consistent with this finding, FA oxidation inhibitors, such as the PPAR α antagonist GW6471, have been tested in several models of renal clear cell cancer and have been shown to inhibit the growth of related tumor cells (Abu Aboud et al., 2015).

Lipid metabolism can not only affect the growth of tumor cells by metabolic recombination of fatty acids and other molecules, but also regulate the cross-talk between tumor cells and tumor associated stromal cells to modulate the high metabolic needs of the tumor. It has been reported that the liver X receptor (LXR), a lipid activated transcription factor, plays an important role in modulating the TME. Apoptotic tumor cells containing oxysterols activate LXR in macrophages causing suppression of dendritic cell migration and recruitment of neutrophils in tumors resulting in tolerance and immunosuppression (Traversari et al., 2014). Cancer stem cells (CSCs) or tumor-initiating cells (TICs) represent a small group of cancer cells with self-renewing, tumor-initiating, and unique metabolic properties. Unlike most tumor cells, CSCs and TICs are conventionally treated refractory tumors that are the cause of recurrence in cancer patients. Recent advances in metabolomic detection have shown that lipid uptake of new fat to form lipid droplets and induce changes in lipid desaturation and FA oxidation are related to the regulation of CSCs (Brandi et al., 2017). Changes in lipid metabolism not only meet the energy requirements and biomass production of CSCs but also activate several important carcinogenic signaling pathways, including Wnt/β-catenin and Hippo/YAP signaling pathways (Wang et al., 2016; Yi et al., 2018). It has been suggested that lipid metabolism in tumor cells and its role in tumor progression and metastasis have attracted more and more attention.

Amino Acid Metabolism Reprogramming in Tumor Growth

Cancer cells' need for amino acids increases in order to sustain their rapid proliferation. In addition to their use in protein synthesis, amino acids are increasingly being studied as metabolites and regulators that support cancer cell growth (Wen et al., 2018). Multiple amino acids have been confirmed to be valuable in the identification of potential biomarkers and understanding the pathogenesis of various malignant tumors. Among these, the study of glutamine, serine, and glycine has been a primary focus (Jung et al., 2014; Yip-Schneider et al., 2019). Amino acid uptake, steady-state levels, and catabolism are all elevated in the leukemia stem cell (LSC) population (Jones et al., 2018). Changes in the amino acid metabolic spectrum are correlated with the occurrence of gastric cancer, and the amino acid metabolic pathway is abnormal in gastric cancer patients, as shown by the significant correlation between the levels of alanine and arginine and cancer T stage (Chen et al., 2010).

Increased glutamine metabolism is a commonly observed metabolic change in cancer, and glutamine is second only to glucose in importance as a nutrient in cancer. As the most abundant free amino acid, glutamine is involved in a series of energy generation, macromolecular synthesis, and signal transmission pathways of cancer cells by providing nitrogen and carbon atoms (Coloff et al., 2016; Kappler et al., 2017). Glutamine can synthesize a variety of other amino acids to participate in the tricarboxylic acid (TCA) cycle. Moreover, glutamine-derived fumarate, malate, and citrate increase significantly when glucose is deprived, which suggests that glutamine drives the glucose-independent TCA cycle (Spinelli et al., 2017). Increasing glutamine for mitochondrial-dependent bioenergy production and cell biosynthesis is a key feature of many tumor cells (Wang et al., 2019). In a study that analyzed differences in metabolic profiles between gastric cancer (GC) and gastric ulcer (GU), researchers used LC-MS-based plasma metabolic analysis and found that plasma ornithine levels were higher, and plasma glutamine, histidine, arginine, and tryptophan levels were lower in GC patients than in GU patients (Jing et al., 2018). Several independent studies have also shown higher utilization of glutamine in renal clear cell carcinoma compared with that in normal renal tissue (Wettersten et al., 2015; Hakimi et al., 2016).

Other amino acids, such as aspartic acid and arginine, are involved in the reprogramming of amino acid metabolism in cancer. In a study that investigated significant metabolomic changes in plasma in the early and late stages of 4T1 metastatic breast cancer in mice, the plasma arginine concentration was higher during the early stage of metastasis but gradually decreased, and the urine-arginine/arginine ratio increased in the late stages (Kus et al., 2018). This is consistent with the activation of the arginine metabolic pathway in cancer. Xie et al. used a combined liquid and gas chromatography technology to compare and the plasma metabolic spectrum in breast cancer patients and found that aspartic acid concentration was significantly negatively correlated with the risk of breast cancer (Xie et al., 2015). In addition, low serum aspartic acid concentrations were found to be unique in breast cancer patients, and no significant changes were observed for the serum aspartic acid levels of other malignant tumors, such as gastric and colorectal cancer (Zhang et al., 2020). Aspartic acid is a major neurotransmitter that is known to inhibit tumor cell proliferation, and it may induce tumor cell death through the Akt pathway (Chen et al., 2020). Antimetabolites that interrupt amino acid synthesis have also been developed and are undergoing clinical trials as cancer therapeutics (Tabe et al., 2019).

METABOLOMIC MARKERS IN CANCER PROGRESSION

With the comprehensive development of modern molecular biology, many new tumor markers carry important clinical value for the early diagnosis and screening of malignant tumors; however, current routine tumor markers lack sensitivity and specificity for the early diagnosis of tumors. As

TABLE 1 | Metabolites in biofluid samples of cancer and non-cancer groups.

Year	Sample types	Tumor types	Patients/animal models	Method	Discriminant metabolites or findings	Related metabolic pathways	Ref
2016	plasma	Papillary thyroid microcarcinoma	patients with cancer (n = 26) from healthy controls (n = 17)	NMR	Elevated levels of glucose, mannose, pyruvate and 3-hydroxybutyrate in plasma, are involved in the metabolic alterations in papillary thyroid microcarcinoma	Glycolysis, amino acid	Lu et al. (2016)
2016	plasma	Lung and liver cancer	lung (n = 50) and liver cancer patients (n = 50)	LC-MS	two values was discovered to identify lung and liver cancer, which were the product of the plasma concentration of putrescine and spermidine; and the ratio of the urine concentration of S-adenosyl-l-methionine and N-acetylspermidine	The pathways of polyamines metabolome	Xu et al. (2016)
2020	plasma	Pancreatic cancer	patients with pancreatic cancer (n = 60) from healthy controls (n = 60)	LC-MS	The top 10 ranked differential metabolites were precisely aligned as glycocholic acid, agmatine, melatonin, beta-sitosterol, sphinganine, hypoxanthine, spermidine, hippuric acid, creatine and inosine.new metabolite biomarkers in plasma (creatine, inosine, beta-sitosterol, sphinganine and glycocholic acid) can be used to readily diagnose pancreatic cancer in a clinical setting	purine metabolism, glycine and serine metabolism, arginine and proline metabolism, steroid biosynthesis, sphingolipid metabolism and bile metabolism	Luo et al. (2020)
2019	plasma	Pancreatic cancer	patients with pancreatic cancer (n = 22) from healthy controls (n = 40)	LC-MS	About 270 lipids belonging to 20 lipid species were found significantly dysregulated. LysoPC 22:0, PC (P-14:0/22:2) and PE (16:0/18:1) are all associated with tumor stage, CA19-9, CA242 and tumor diameter. What's more, PE (16:0/18:1) is also found to be significantly correlated with the patient's overall survival	lipids	Tao et al. (2019)
2014	plasma	Oral squamous cell carcinoma	Patients with locally advanced OSCC(n = 105)	GC-MS	Chemotherapy leads to up-regulation of fatty acids, steroids, and antioxidant substances. Lactate, glucose, glutamate, aspartate, leucine, and glycerol are associated with efficacy of induction chemotherapy. Lactate, glutamate, and aspartate can precisely predict the suitability and efficacy of induction chemotherapy	Glycolysis, amino acid, fatty acid	Ye et al. (2014)
2019	plasma	Breast cancer	1,624 first primary incident invasive breast cancer cases and 1,624 matched controls	LC-MS	There were significant differences in lysoPCs in breast cancer patients. LysoPC aaC18:0 was negatively associated with the risk of breast cancer, while higher concentrations of phosphatidylcholine PC ae C30:0 were associated with an increased risk of breast cancer	lysoPCs	His et al. (2019)

(Continued on following page)

TABLE 1 | (*Continued*) Metabolites in biofluid samples of cancer and non-cancer groups.

Year	Sample types	Tumor types	Patients/animal models	Method	Discriminant metabolites or findings	Related metabolic pathways	Ref
2018	plasma	Pancreatic cancer	pancreatic ductal adenocarcinoma (n = 271), chronic pancreatitis (n = 282), liver cirrhosis (n = 100) or healthy as well as non-pancreatic disease controls (n = 261)	GC-MS	Proline, Sphingomyelin (d18:2, C17:0), Phosphatidylcholine, Isocitrate (C18:0, C22:6), Sphinganine-1-phosphate (d18:0), Histidine, Pyruvate, Ceramide (d18:1, C24:0), Sphingomyelin (d17:1, C18:0) and CA19-9 formed a biomarker signature. The biomarker signature could be identified as a differential diagnosis between pancreatic ductal adenocarcinoma (PDAC) and chronic pancreatitis (CP)	complex lipids, fatty acids and related metabolites	Mayerle et al. (2018)
2017	Urine	Prostate cancer	64 prostate cancer patients and 51 individuals diagnosed with benign prostate hyperplasia	NMR	Branchedchain amino acids, glutamate, pseudouridine, glycine, P = 0.015; dimethylglycine, fumarate and 4-imidazole- acetate were able to distinguish between prostate cancer and benign prostate hyperplasia (BPH)	TCA cycle of glucose metabolism	Pérez-Rambla et al. (2017)
2012	Urine	Kidney cancer	(Group A: 29 cancer patients, 33 controls; Group B: 6 cancers,6 controls)	GC-MS	Results showed differential urinary concentrations of several acylcarnitines as a function of both cancer status and kidney cancer grade, with most acylcarnitines being increased in the urine of cancer patients and in those patients with high cancer grades	acylcarnitines	Ganti et al. (2012)
2011	Urine	Bladder cancer	27 bladder cancer (BC) patients and 32 healthy controls	LC-MS	Cancer patients have elevated levels of acetyl carnitine and adipate in their urine. Carnitine C9:1 and component I, were combined as a biomarker pattern	Fatty acid and carnitine metabolism	Huang et al. (2011)
2020	Urine	Breast cancer	patients with breast cancer (n = 56) and benign breast tumors (n = 22), as well as from healthy females (n = 20)	GC-MS	1-methyl adenosine (1-MA), 1-methylguanosine (1-MG) and 8-hydroxy-2′-deoxyguanosine (8-OHdG) levels were significantly elevated in the early stages of breast cancer, but no significant differences were observed between the benign tumor group and the healthy group	nucleoside metabolomes	Omran et al. (2020)
2013	Urine	Ovarian cancer	40 preoperative epithelial ovarian cancer (EOC) patients, 62 benign ovarian tumor (BOT) patients, and 54 healthy controls	LC-MS	The concentrations of some urinary metabolites of 18 postoperative EOC patients among the 40 EOC patients changed significantly compared with those of their preoperative condition, and four of them suggested recovery tendency toward normal level after surgical operation, including N4-acetylcytidine, pseudouridine, urate-3-ribonucleoside, and succinic acid	nucleotide metabolism, histidine metabolism, tryptophan metabolism, mucin metabolism	Zhang et al. (2013)

(Continued on following page)

TABLE 1 | (*Continued*) Metabolites in biofluid samples of cancer and non-cancer groups.

Year	Sample types	Tumor types	Patients/animal models	Method	Discriminant metabolites or findings	Related metabolic pathways	Ref
2019	Urine	Lung cancer	lung cancer (n = 32) and healthy controls (n = 29)	GC–MS	Six metabolites were altered in urine (l-glycine, phosphoric acid, isocitric acid, inositol, palmitic acid and stearic acid) and four metabolites (l-glycine, phosphoric acid, isocitric acid and inositol) were decreased from patients with cancer, indicating a strong, unified marker of lung cancer pathology	Fatty acid and glucose metabolism	Callejón-Leblic et al. (2019)
2010	Saliva	Oral, breast and pancreatic cancer	69 oral, 18 pancreatic and 30 breast cancer patients, 11 periodontal disease patients and 87 healthy controls	CE-TOFMS	They identified 57 principal metabolites that can be used to accurately predict the probability of being affected by each individual disease. Patients with oral cancer had significantly higher levels of salivary polyamines compared to the control group, and taurine and piperidin were identified as oral cancer-specific metabolites, providing promising markers for oral cancer screening	Polyamines and amino acid metabolism	Soini et al. (2010)
2016	Saliva	Oral cancer	patients with oral cancer (n = 24) and healthy controls (n = 44)	CE-TOFMS	In total, 85 metabolites in tumor and 45 metabolites in saliva were identified to be significantly different between oral cancer and controls, and the combination of S-adenosylmethionine and pipecolate can discriminate oral cancers from controls	metabolites in the urea cycle and one carbon cycle	Ishikawa et al. (2016)
2017	Saliva	Oral squamous cell carcinoma	22 patients with oral squamous cell carcinoma (OSCC) and 21 healthy controls	CE-TOFMS	A total of 25 metabolites were revealed as potential markers to discriminate between patients with OSCC and healthy controls	Choline and metabolites of the BCAA cycle	Ohshima et al. (2017)
2019	Saliva	Breast cancer	101 patients with invasive carcinoma of the breast, 23 patients with ductal carcinoma *in situ*, and 42 healthy controls	LC-MS	The levels of polyamines in the saliva of breast cancer patients were significantly increased. In addition, polyamines and their acetylated forms were elevated invasive carcinoma of the breast only	Polyamine metabolism	Murata et al. (2019)
2018	Saliva	Pancreatic cancer	patients with PC (n = 39), those with chronic pancreatitis (CP, n = 14), and controls (C, n = 26)	CE-TOFMS	Polyamines, such as spermine, N_1-acetylspermidine, and N_1-acetylspermine, showed a significant difference between patients with PC and those with C, and the combination of four metabolites including N_1-acetylspermidine showed high accuracy in discriminating PC from the other two groups	Polyamine metabolism	Asai et al. (2018)
2012	CSF	Malignant gliomas	10 patients presenting malignant gliomas and seven control patients that did not present malignancy	LC-MS	One subtype contained metabolites rich in citric acid cycle components that distinguished the metabolic characteristics of patients with malignant glioma from those in the control group. Newly diagnosed patients were classified into different subtypes and showed low levels of metabolites involved in tryptophan metabolism, which may indicate a loss of inflammatory features	Metabolites from the citric acid cycle, gluconeogenesis, and pyrimidine metabolism, urea cycle	Locasale et al. (2012)

(Continued on following page)

TABLE 1 | (*Continued*) Metabolites in biofluid samples of cancer and non-cancer groups.

Year	Sample types	Tumor types	Patients/animal models	Method	Discriminant metabolites or findings	Related metabolic pathways	Ref
2013	CSF	Glioma	32 patients with histologically confirmed	GC–MS	The citric and isocitric acid levels were significantly higher in the glioblastoma (GBM) samples than in the grades I-II and grade III glioma samples. In addition, the lactic and 2-aminopimelic acid levels were relatively higher in the GBM samples than in the grades I-II glioma samples. The CSF levels of the citric, isocitric, and lactic acids were significantly higher in grade I-III gliomas with mutant isocitrate dehydrogenase (IDH) than in those with wild-type IDH.	Metabolites from the aerobic glycolysis	Nakamizo et al. (2013)
2020	CSF	Medullo-blastoma (MB)	8 patients diagnosed with recurrent MB and 7 healthy controls	LC-MS	The up-regulation of tryptophan, methionine, serine and lysine, which have all been described to be induced upon hypoxia in CSF. While cyclooxygenase products were hardly detectable, the epoxygenase product and beta-oxidation promoting lipid hormone 12,13-DiHOME was found to be strongly up-regulated	Lipid and amino acid metabolism	Reichl et al. (2020)
2020	CSF	different types of brain tumors	A cohort of 163 histologically-proven patients with brain disorders	LC-MS	A total of 508 ion features were detected by the LC-Q/TOF-MS analysis, of which 27 metabolites were selected as diagnostic markers to discriminate different brain tumor types	Amino acids and citrate metabolism	Wang et al. (2020)

NMR, nuclear magnetic resonance; GC-MS, gas chromatography-mass spectrometry; LC-MS, liquid chromatography-mass spectrometry; CE-TOFMS, capillary electrophoresis time-of-flight mass spectrometry; CSF, cerebrospinal fluid.

an emerging omics technology, metabolomics mainly involves the study of small molecular metabolites (i.e., those less than 1,500 Da) and reflects a series of small changes in the body at the level of metabolites, which is suitable for the diagnosis of diseases. Many scholars have used a variety of detection techniques to conduct research on the early diagnosis and treatment prediction of tumors (Srivastava and Creek, 2019). Metabolomics approaches are used to identify and validate metabolic biomarkers that accurately and sensitively diagnose tumor field progression and metastasis in a clinical setting. Furthermore, such efforts can be left to clinicians with appropriate time frames to promote early and effective therapeutic interventions, which will significantly improve the 5-years survival rate of tumor patients. We summarize the major findings of previous tumor blood metabolome studies (**Table 1**).

Blood Biomarkers

Because blood is a readily available biological specimen, blood biomarker studies account for the majority of metabolomics and tumor studies. The application of metabolomics technology has led to significant breakthroughs in the discovery of biomarkers for a variety of tumors, which include pancreatic, liver, lung, and breast cancers (Ye et al., 2014; Xu et al., 2016; His et al., 2019). For instance, Lu et al. used NMR spectroscopy to screen metabolic changes in thyroid tissues and plasma from papillary thyroid microcarcinoma patients respectively. The results revealed reduced levels of fatty acids and elevated levels of several amino acids in thyroid tissues (Lu et al., 2016). This work illustrates that the metabolomics approach is capable of providing more sensitive diagnostic results and more systematic therapeutic information for all kinds of tumor.

In the case of pancreatic cancer, researchers have identified five new metabolic biomarkers (creatine, inosine, beta-sitosterol, sphinganine and glycocholic acid) that can be used for the clinical diagnosis of pancreatic cancer by comparing plasma metabolomics between patients with pancreatic cancer (n = 60) and healthy controls (n = 60) (Luo et al., 2020). Subsequently, a large prospective study comparing the lipid metabolomics of serum exosomes between pancreatic cancer patients and healthy controls showed that approximately 270 lipids were significantly dysregulated. Further analysis of the correlation between these abnormal lipids and other phosphatidylcholine (PC)-related factors showed that LysoPC 22:0, PC (14:0/22:2), and PE (16:0/18:1) were correlated with

tumor stage, CA19-9, CA242, and tumor diameter. In addition, PE (16:0/18:1) was significantly associated with overall survival (Tao et al., 2019). Currently, non-invasive diagnostic tests can only distinguish pancreatic ductal adenocarcinoma (PDAC) from chronic pancreatitis (CP) in approximately two-thirds of patients. Using untargeted metabolomics techniques, Mayerle demonstrated that a biomarker signature (nine metabolites and an additional CA19-9) could be identified as differential diagnoses of PDAC and CP (Mayerle et al., 2018). In addition, inflammatory metabolites identified by serum metabolomics can also stratify tumor and improve diagnosis of patients with aggressive tumor (Cacciatore et al., 2021). The discovery of metabolomics for tumor blood biomarkers can be extended to various aspects, which include the discovery of significantly different metabolites, changes in the tumor metabolic spectrum, and direct identification of tumors and inflammation.

Urine Biomarkers

The non-invasive nature of urine biomarkers makes them particularly suitable for a wide range of screening purposes, especially for measuring urine from asymptomatic high-risk groups to distinguish between those who may and may not be carrying a disease. Accurate and effective analyses of urine metabolites offer promise for their applications to provide a deeper understanding of tumor pathology and eventually, clinical transformations (Pérez-Rambla et al., 2017; Dinges et al., 2019).

In urological tumors, Ganti used GC-MS to measure carnitine in two different laboratories (Laboratory A: 29 cancer patients and 33 controls; Laboratory B: 6 cancer patients and 6 controls) and showed that differences in urinary concentrations of several acylcarnitines were a function of cancer status and renal cancer grade. Most cancer patients and those with high-grade cancers have increased acylcarnitine in their urine (Ganti et al., 2012). In a bladder cancer study, researchers reported elevated levels of acetylcarnitine and adipate in the urine of cancer patients, which suggested dysregulation of FA metabolism. Changes in the mitochondrial TCA cycle and energy metabolism or the excessive production of acetyl-coenzyme A (acetyl-CoA) lead to changes in acetylcarnitine levels (Huang et al., 2011). Under normal physiological conditions, lipid in urine is limited; thus, the increase in lipid markers in urine is a clear indication of tumorigenesis, especially in the urinary system. Moreover, in non-urinary tumors, such as liver, stomach, cervical, and breast cancers, differential metabolites in urine distinguish cancer patients from healthy controls (Dinges, Hohm et al., 2019). Omran used GC-MS to detect urine metabolites from breast cancer patients and compared these with samples from patients with benign breast tumors and healthy women. Results suggested that 1-methyl adenosine (1-MA), 1-methylguanosine (1-MG), and 8-hydroxy-2′-deoxyguanosine (8-OHdG) levels were significantly elevated in the early stages of breast cancer; however, no significant differences were observed between the benign tumor group and the healthy group (Omran et al., 2020). Urine also plays a role in the uniqueness of biomarkers for specific cancer types (Zhang et al., 2013; Callejón-Leblic et al., 2019).

Salivary Biomarkers

In addition to blood and urine, other biological fluid biomarkers are available for the early diagnosis of specific cancers. Saliva is a biological fluid made up of more than 99% water and less than 1% of proteins, electrolytes, and other low-molecular-weight components (Soini et al., 2010). Saliva plays a key role in lubrication, chewing, swallowing, and digestion. It protects the integrity of oral tissue and also provides clues for local and systemic diseases and conditions (Abraham et al., 2012). In 2010, using capillary electrophoresis time-of-flight mass spectrometry (CE-TOFMS), Sugimoto found that saliva metabolites were embedded with cancer-specific signals. They performed a comprehensive metabolite analysis of saliva samples from patients with oral cancer and periodontal disease and healthy controls. Patients with oral cancer had significantly higher levels of salivary polyamines compared with the control group, and taurine and piperidine were identified as oral cancer-specific metabolites, which may be promising markers for oral cancer screening (Sugimoto et al., 2010). To explore applications of salivary metabolite biomarkers in oral cancer screening, hydrophilic metabolites in the saliva and tumor tissues of patients with oral cancer were analyzed using CE-TOFMS. In total, 85 metabolites in tumors and 45 metabolites in saliva were identified to be significantly different between oral cancer patients and controls, and the combination of S-adenosylmethionine and pipecolate discriminated oral cancer patients from controls (Ishikawa et al., 2016).

Since then, several studies have shown that the combination of saliva and tumor metabolomics is beneficial for the identification of salivary metabolite biomarkers and the screening of noninvasive oral cancers (Ohshima et al., 2017). In addition to salivary metabolomics of oral cancer, metabolite profiles of saliva in other cancers and diseases have been analyzed (Murata et al., 2019). Great progress has been made in the clinical application of salivary biomarkers. Several biomarkers for systematic cancer detection have been identified and validated at preclinical levels (Asai et al., 2018). The discovery of saliva biomarkers also has special significance for noninvasive identification and recognition of tumors.

Cerebrospinal Fluid Biomarkers

Cerebrospinal fluid (CSF) is a biological fluid that is most likely to be affected by central nervous system dysfunction, and its analysis can better reflect inherent neurological and biochemical changes (Crews et al., 2009). In 2012, Locasale et, al. first analyzed the metabolic profiles of 10 patients with malignant glioma and seven control patients with non-malignant glioma using a targeted mass spectrometry metabolomics platform and reported a significant association between CSF metabolites and glioma malignancy (Locasale et al., 2012). The study also provided the first global assessment of the polar metabolic composition of CSF associated with malignancies and demonstrated that data acquired using mass spectrometry technology may have sufficient predictive power for the identification of biomarkers and classification of neurological diseases.

In recent years, several studies have also confirmed that the use of untargeted metabolomics techniques to analyze metabolic

characteristics of different brain tumors in clinical CSF samples enables reliable identification of significant metabolic differences between different brain tumors, which offers significant promise for diagnoses of brain tumors (Nakamizo et al., 2013; Reichl et al., 2020; Wang et al., 2020). More metabolites, including tricarboxylic acid cycle products, tryptophan and methionine, were also found in the cerebrospinal fluid of gliomas and metastatic tumors (Ballester et al., 2018). Brain tumors are often associated with ischemic necrosis and inflammatory responses. Inflammation-related markers can be detected in the cerebrospinal fluid, which may aid the diagnosis of CNS tumors. Elevated levels of inflammatory markers, such as interleukin-10 and soluble interleukin-receptor, were found in the cerebrospinal fluid of primary CNS lymphoma (Geng et al., 2021). Specific cerebrospinal fluid biomarkers could help avoid high-risk biopsy operations and unnecessary craniotomy, and even guide preoperative surgical planning.

METABOLOMICS AND ONCOLOGY DRUGS

Application of Metabolomics in the Evaluation of Tumor Drug Efficacy

The main purpose of drug therapy of tumors is to control the growth of the tumor and improve the quality of life of patients. Selecting the most effective anti-tumor drugs has become a top priority. In clinical practice, metabolomics can be used to detect body or cell metabolites that reflect the effects of anti-tumor drugs on the body or cells to improve the efficacy of drugs and reduce avoidable adverse reactions.

Kim et al. used NMR to investigate metabolic alterations following adriamycin (ADR) treatment for gastric adenocarcinoma. After human gastric adenocarcinomas were implanted into mice, ADR was intraperitoneally administered for 5 days, and urine was collected on days 2 and 5. Results showed that the levels of trimethylamine oxide, hippurate, and taurine decreased in the tumor model and increased following ADR treatment. In addition, the levels of 2-oxoglutarate, 3-indoxylsulfate, trigonelline, and citrate, which all increased in the tumor model, significantly decreased to those of normal controls following ADR treatment (Kim et al., 2013). In a plasma metabolomics study of 54 patients with colorectal cancer who received capecitabine before and after treatment, it was found that the content of low-density lipoprotein-derived lipids was positively correlated with drug toxicity during treatment (Backshall et al., 2011).

Furthermore, using untargeted lipidomics and quantitative polymerase chain reaction, Zhang et al. identified distinct features of lipid metabolism in imidazole ketone erastin (IKE)-induced ferroptosis and demonstrated that IKE slows tumor growth (Zhang et al., 2019). Once drugs act on the body, changes in genes and/or proteins can impact changes in terminal metabolites, which can be reflected at the metabolic level. Therefore, the early efficacy of drugs can be assessed using metabolomics, which enables medication regimens to be adjusted.

Application of Metabolomics in the Evaluation of Drug Resistance in Cancer

The metabolic pattern of tumor cells changes following the development of drug resistance. The same drug can produce different metabolic changes in sensitive and drug-resistant cells (Zhang et al., 2016). Therefore, metabolomics can be used to detect metabolic changes in cells and their response to drugs to determine whether tumor cells are resistant to drugs and monitor drug resistance as early as possible. As a fast, simple, and effective method, metabolomics uses a multivariable and dynamic method to evaluate metabolic results across a variety of physiological and pathological states, which allows the prediction and assessment of patients' sensitivity and drug resistance to chemotherapy.

Metabolomics can be used to distinguish between platinum resistance and metabolite levels. Poschner et al. used LC-MS to characterize the levels of steroids, active estrogen, and sulfated or aldehyde glucose during the development of platinum resistance in ovarian cancer and found that these metabolites are highly expressed in carboplatin-sensitive cells (Poschner et al., 2020). In a study of non-small cell lung cancer (NSCLC), cisplatin-resistant cells were more sensitive to nutrient deprivation than were sensitive cells, and adding glutamine to cisplatin-resistant cells restored cell death due to nutrient deprivation by increasing the intracellular nucleotide concentration. Therefore, cisplatin-resistant patients can improve efficacy by combining drugs, such as 5-fluorocrail, that target nucleoside metabolism (Obrist et al., 2018). The metabolic pattern analysis of cancer patients can also find the metabolic differences between drug-resistant patients and drug-sensitive patients, so as to monitor the drug resistance of patients as early as possible and carry out follow-up treatment (Jiye et al., 2010). Metabolomics has made great strides in the study of drug resistance genes in tumors.

METABOLIC FLUX ANALYSIS AND FLUXOMICS IN CANCER METABOLISM EXPLORATIONS

Quantitative analysis of metabolism has improved our understanding of metabolic features including metabolite concentrations, fluxes, and free energies. With the development of nuclear magnetic resonance, mass spectrometry, and other technologies, the application of stable isotope tracer technology to the field of metabolomics has become an important aspect of biological research (Bruntz et al., 2017). Stable isotope-resolved metabolomics (SIRM) is a method that extrapolates metabolic pathways and fluxes via the analysis of changes in stable isotope tracer precursor substances to substances. SIRM works primarily by injecting isotopically-enriched precursors, such as [^{13}C6]-Glc, into biological systems and detecting subsequent metabolic transformations. Incorporating stable isotopes, such as 2H, 13C, or 15N, into biological precursors has long been used to trace their metabolism in living systems. . Biological samples can be studied using NMR, mass spectrometry, and other detection platforms (Fan et al., 2012) (**Figure 3**).

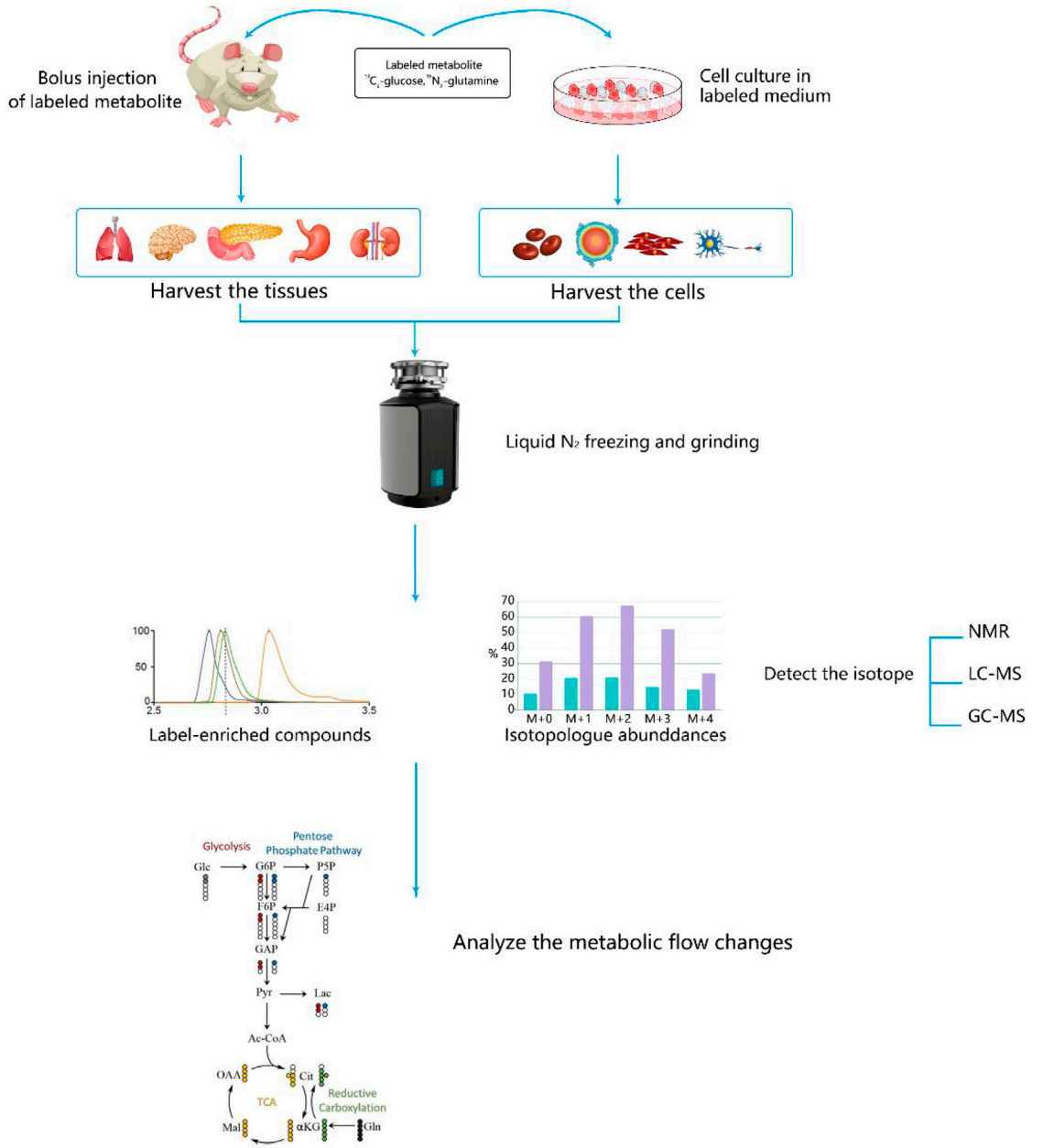

FIGURE 3 | Steps for studying cancer metabolism using stable isotope-resolved metabolomics (SIRM). Stable isotope tracers, such as uniformly ^{13}C-labeled glucose ($^{13}C_6$-Glc) or uniformly ^{13}C,^{15}N-labeled glutamine ($^{13}C_5$,$^{15}N_2$-Gln), are administered via addition to the culture medium for cells or via intravenous injection into whole organisms. Metabolites are then extracted, labeled by tracers, and subjected to various NMR and MS analyses to probe metabolic activity.

Glucose plays a vital role in important glucose catabolic pathways, such as the glycolysis and TCA cycles; thus, ^{13}C-labeled glucose is commonly used as a tracer. Metabolic differences derived from SIRM have shown that energy and anabolism are increased in cultured lung cancer cells and NSCLC compared with those in the normal lung (Lane et al., 2011). Moreover, a study using SIRM found that the proliferation of cancer cells can be reduced by inhibiting the glycolysis pathway in cancer cells (Gu et al., 2016). Researchers used ^{13}C-labeled glucose to track the glycolysis pathway in lung cancer patients and animal models (Hu et al., 2019) and revealed that lactic acid contributes more to the Krebs cycle than does glucose. This result suggests that lactic acid is the end metabolic waste of the Warburg effect and provides new opportunities for the diagnosis and treatment of cancer (Hui et al., 2017). Proliferating cells shunt glucose into pathways other than the glycolysis and Krebs cycle pathways, and SIRM has confirmed that an increase of glucose flux into these pathways occurs. For example, enhanced non-oxidative and oxidative pentose phosphate pathway activity has been reported in pancreatic and renal cancers, respectively, using

a (^{13}C2-1, 2)-glucose tracer (Boros et al., 2005; Yang et al., 2013). In addition, many clinically successful drugs and promising candidates for drug targeting tumor therapy may benefit from SIRM analyses to gain insights into their molecular mechanisms. For example, SIRM and microarray experiments have demonstrated that selenium agents perturb Krebs cycle activity and attenuate lipid biosynthesis in lung cancer cells, and these alterations are related to the activation of the AMP-activated protein kinase pathway. Anti-cancer target discovery is one of the most promising translational applications for SIRM, and inhibitors of several targets have been developed and are showing promise in preclinical models (Svensson et al., 2016).

In recent years, Dynamic nuclear polarization enhanced magnetic resonance imaging based on isotope tracer have become dependable imaging tools for the diagnosis and treatment assessment in cancer. Based on preclinical studies that have demonstrated the use of hyperpolarized (1–13C) -pyruvate imaging tools for prostate cancer, Researchers have investigated the *in vivo* pharmacokinetics and pharmacodynamics of hyperpolarized (1–13 C)-pyruvate in order to apply as a tool for imaging liver cancer (Salamanca-Cardona and Keshari, 2015). Applications of probes other than pyruvate are still in the early stages, but molecular imaging of real-time metabolic events could be a valuable tool to elucidate hitherto undiscovered metabolic fluxes that play a role in cancer development and treatment (Perkons et al., 2021).

By gaining insights into metabolic dysfunction due to cancer development or drug interventions, Metabolic flux analysis and fluxomics can be integrated with genomic and proteomic information to achieve systems biochemical insights in both model systems and individual human patients.

SUMMARY AND FUTURE DIRECTIONS

Metabolomics has been used across many aspects of cancer research, which include cancer pathophysiology, biomarker discovery, and therapeutic response. Metabolic reprogramming is a hallmark of malignancy, and changes in metabolic profiles strongly influence cancer development, progression, and response to treatment. Metabolomics techniques can be used to monitor the dynamics of tumor metabolism and response to treatment over the course of the disease. Moreover, another area of increasing importance is the identification of biomarkers for personalized treatment strategies. At the same time, metabolomic analysis may also yield more accurate and useful clinical information about the metabolic needs of the tumor, as well as the identification of new pharmacodynamic biomarkers and the monitoring of drug resistance of the tumor. On this basis, the applications of stable isotope tracer technology to the field of metabolomics have become an important part of biological research to track the activity of metabolites in the body and trace deep metabolic pathways.

However, there are still several limitations in the study of metabolic reprogramming in tumors using metabolomics. Methodologically, absolute homogeneity across different batches of biological samples cannot be achieved, and the techniques and methods used should be optimized to establish a set of highly sensitive routine procedures that apply to metabolites of varying polarity across different samples. Secondly, most existing studies focus on the metabolomics of biological fluids or extracellular metabolites; however, it is also of importance to study the metabolic characteristics of intracellular metabolites and cancer cells. Thirdly, the mechanisms underlying metabolic changes need to be clarified. This can be achieved by integrating transcriptomic and/or proteomic analyses to identify genes or proteins that cause or are associated with metabolomic changes, which may be potential targets for tumor therapy. Analyzing metabolic changes in tumor cells in response to drugs and revealing the metabolic mechanism underlying tumor drug resistance may provide opportunities to overcome tumor chemotherapy resistance or reverse tumor sensitivity via metabolic regulation. Metabolomics provides a novel approach to study the metabolic reprogramming of tumors and will continue to be widely used in the diagnosis and treatment of different tumors in the future.

AUTHOR CONTRIBUTIONS

JH designed this review, searched literature and wrote the initial manuscript. QL made the table and figures. YC and YY supervised and provided critical comments on the manuscript. JH, QL, YC and YY read, amended, and discussed the article.

REFERENCES

Abraham, J. E., Maranian, M. J., Spiteri, I., Russell, R., Ingle, S., Luccarini, C., et al. (2012). Saliva Samples Are a Viable Alternative to Blood Samples as a Source of DNA for High Throughput Genotyping. *BMC Med. Genomics* 5, 19. doi:10.1186/1755-8794-5-19

Abu Aboud, O., Donohoe, D., Bultman, S., Fitch, M., Riiff, T., Hellerstein, M., et al. (2015). PPARα Inhibition Modulates Multiple Reprogrammed Metabolic Pathways in Kidney Cancer and Attenuates Tumor Growth. *Am. J. Physiology-Cell Physiol.* 308 (11), C890–C898. doi:10.1152/ajpcell.00322.2014

Asai, Y., Itoi, T., Sugimoto, M., Sofuni, A., Tsuchiya, T., Tanaka, R., et al. (2018). Elevated Polyamines in Saliva of Pancreatic Cancer. *Cancers* 10 (2), 43. doi:10.3390/cancers10020043

Backshall, A., Sharma, R., Clarke, S. J., and Keun, H. C. (2011). Pharmacometabonomic Profiling as a Predictor of Toxicity in Patients with Inoperable Colorectal Cancer Treated with Capecitabine. *Clin. Cancer Res.* 17 (9), 3019–3028. doi:10.1158/1078-0432.Ccr-10-2474

Ballester, L. Y., Lu, G., Zorofchian, S., Vantaku, V., Putluri, V., Yan, Y., et al. (2018). Analysis of Cerebrospinal Fluid Metabolites in Patients with Primary or Metastatic central Nervous System Tumors. *Acta Neuropathol. Commun.* 6 (1), 85. doi:10.1186/s40478-018-0588-z

Boros, L. s. G., Lerner, M. R., Morgan, D. L., Taylor, S. L., Smith, B. J., Postier, R. G., et al. (2005). [1,2-13C2]-D-glucose Profiles of the Serum, Liver, Pancreas, and DMBA-Induced Pancreatic Tumors of Rats. *Pancreas* 31 (4), 337–343. doi:10.1097/01.mpa.0000186524.53253.fb

Brandi, J., Dando, I., Pozza, E. D., Biondani, G., Jenkins, R., Elliott, V., et al. (2017). Proteomic Analysis of Pancreatic Cancer Stem Cells: Functional Role of Fatty

Acid Synthesis and Mevalonate Pathways. *J. Proteomics* 150, 310–322. doi:10.1016/j.jprot.2016.10.002

Bruntz, R. C., Lane, A. N., Higashi, R. M., and Fan, T. W.-M. (2017). Exploring Cancer Metabolism Using Stable Isotope-Resolved Metabolomics (SIRM). *J. Biol. Chem.* 292 (28), 11601–11609. doi:10.1074/jbc.R117.776054

Cacciatore, S., and Loda, M. (2015). Innovation in Metabolomics to Improve Personalized Healthcare. *Ann. N.Y. Acad. Sci.* 1346 (1), 57–62. doi:10.1111/nyas.12775

Cacciatore, S., Wium, M., Licari, C., Ajayi-Smith, A., Masieri, L., Anderson, C., et al. (2021). Inflammatory Metabolic Profile of South African Patients with Prostate Cancer. *Cancer Metab.* 9 (1), 29. doi:10.1186/s40170-021-00265-6

Callejón-Leblic, B., García-Barrera, T., Pereira-Vega, A., and Gómez-Ariza, J. L. (2019). Metabolomic Study of Serum, Urine and Bronchoalveolar Lavage Fluid Based on Gas Chromatography Mass Spectrometry to Delve into the Pathology of Lung Cancer. *J. Pharm. Biomed. Anal.* 163, 122–129. doi:10.1016/j.jpba.2018.09.055

Chen, J.-L., Tang, H. Q., Hu, J. D., Fan, J., Hong, J., and Gu, J. Z. (2010). Metabolomics of Gastric Cancer Metastasis Detected by Gas Chromatography and Mass Spectrometry. *Wjg* 16 (46), 5874–5880. doi:10.3748/wjg.v16.i46.5874

Chen, W.-L., Wang, J.-H., Zhao, A.-H., Xu, X., Wang, Y.-H., Chen, T.-L., et al. (2014). A Distinct Glucose Metabolism Signature of Acute Myeloid Leukemia with Prognostic Value. *Blood* 124 (10), 1645–1654. doi:10.1182/blood-2014-02-554204

Chen, Y.-J., Mahieu, N. G., Huang, X., Singh, M., Crawford, P. A., Johnson, S. L., et al. (2016). Lactate Metabolism Is Associated with Mammalian Mitochondria. *Nat. Chem. Biol.* 12 (11), 937–943. doi:10.1038/nchembio.2172

Chen, Y., Wang, K., Liu, T., Chen, J., Lv, W., Yang, W., et al. (2020). Decreased Glucose Bioavailability and Elevated Aspartate Metabolism in Prostate Cancer Cells Undergoing Epithelial-mesenchymal Transition. *J. Cel Physiol* 235 (7-8), 5602–5612. doi:10.1002/jcp.29490

Coloff, J. L., Murphy, J. P., Braun, C. R., Harris, I. S., Shelton, L. M., Kami, K., et al. (2016). Differential Glutamate Metabolism in Proliferating and Quiescent Mammary Epithelial Cells. *Cel Metab.* 23 (5), 867–880. doi:10.1016/j.cmet.2016.03.016

Crews, B., Wikoff, W. R., Patti, G. J., Woo, H.-K., Kalisiak, E., Heideker, J., et al. (2009). Variability Analysis of Human Plasma and Cerebral Spinal Fluid Reveals Statistical Significance of Changes in Mass Spectrometry-Based Metabolomics Data. *Anal. Chem.* 81 (20), 8538–8544. doi:10.1021/ac9014947

Currie, E., Schulze, A., Zechner, R., Walther, T. C., and Farese, R. V., Jr. (2013). Cellular Fatty Acid Metabolism and Cancer. *Cel Metab.* 18 (2), 153–161. doi:10.1016/j.cmet.2013.05.017

Dai, X., Cheng, H., Bai, Z., and Li, J. (2017). Breast Cancer Cell Line Classification and its Relevance with Breast Tumor Subtyping. *J. Cancer* 8 (16), 3131–3141. doi:10.7150/jca.18457

Ding, M., Li, F., Wang, B., Chi, G., and Liu, H. (2019). A Comprehensive Analysis of WGCNA and Serum Metabolomics Manifests the Lung Cancer-associated Disordered Glucose Metabolism. *J. Cel Biochem* 120 (6), 10855–10863. doi:10.1002/jcb.28377

Dinges, S. S., Hohm, A., Vandergrift, L. A., Nowak, J., Habbel, P., Kaltashov, I. A., et al. (2019). Cancer Metabolomic Markers in Urine: Evidence, Techniques and Recommendations. *Nat. Rev. Urol.* 16 (6), 339–362. doi:10.1038/s41585-019-0185-3

Fan, T. W.-M., Lorkiewicz, P. K., Sellers, K., Moseley, H. N. B., Higashi, R. M., and Lane, A. N. (2012). Stable Isotope-Resolved Metabolomics and Applications for Drug Development. *Pharmacol. Ther.* 133 (3), 366–391. doi:10.1016/j.pharmthera.2011.12.007

Fiehn, O. (2016). Metabolomics by Gas Chromatography-Mass Spectrometry: Combined Targeted and Untargeted Profiling. *Curr. Protoc. Mol. Biol.* 114, 30. doi:10.1002/0471142727.mb3004s114

Finotello, F., and Trajanoski, Z. (2018). Quantifying Tumor-Infiltrating Immune Cells from Transcriptomics Data. *Cancer Immunol. Immunother.* 67 (7), 1031–1040. doi:10.1007/s00262-018-2150-z

Ganti, S., Taylor, S. L., Abu Aboud, O., Yang, J., Evans, C., Osier, M. V., et al. (2012). Kidney Tumor Biomarkers Revealed by Simultaneous Multiple Matrix Metabolomics Analysis. *Cancer Res.* 72 (14), 3471–3479. doi:10.1158/0008-5472.Can-11-3105

Ganti, S., Taylor, S. L., Kim, K., Hoppel, C. L., Guo, L., Yang, J., et al. (2012). Urinary Acylcarnitines Are Altered in Human Kidney Cancer. *Int. J. Cancer* 130 (12), 2791–2800. doi:10.1002/ijc.26274

Geng, M., Song, Y., Xiao, H., Wu, Z., Deng, X., Chen, C., et al. (2021). Clinical Significance of Interleukin-10 C-oncentration in the C-erebrospinal F-luid of P-atients with P-rimary central N-ervous S-ystem L-ymphoma. *Oncol. Lett.* 21 (1), 1. doi:10.3892/ol.2020.12263

Gu, J., Hu, X., Shao, W., Ji, T., Yang, W., Zhuo, H., et al. (2016). Metabolomic Analysis Reveals Altered Metabolic Pathways in a Rat Model of Gastric Carcinogenesis. *Oncotarget* 7 (37), 60053–60073. doi:10.18632/oncotarget.11049

Hakimi, A. A., Reznik, E., Lee, C.-H., Creighton, C. J., Brannon, A. R., Luna, A., et al. (2016). An Integrated Metabolic Atlas of Clear Cell Renal Cell Carcinoma. *Cancer Cell* 29 (1), 104–116. doi:10.1016/j.ccell.2015.12.004

Hanahan, D., and Weinberg, R. A. (2011). Hallmarks of Cancer: the Next Generation. *Cell* 144 (5), 646–674. doi:10.1016/j.cell.2011.02.013

Hao, Y., Li, D., Xu, Y., Ouyang, J., Wang, Y., Zhang, Y., et al. (2019). Investigation of Lipid Metabolism Dysregulation and the Effects on Immune Microenvironments in Pan-Cancer Using Multiple Omics Data. *BMC Bioinformatics* 20 (Suppl. 7), 195. doi:10.1186/s12859-019-2734-4

His, M., Viallon, V., Dossus, L., Gicquiau, A., Achaintre, D., Scalbert, A., et al. (2019). Prospective Analysis of Circulating Metabolites and Breast Cancer in EPIC. *BMC Med.* 17 (1), 178. doi:10.1186/s12916-019-1408-4

Horn, L., Whisenant, J. G., Wakelee, H., Reckamp, K. L., Qiao, H., Leal, T. A., et al. (2019). Monitoring Therapeutic Response and Resistance: Analysis of Circulating Tumor DNA in Patients with ALK+ Lung Cancer. *J. Thorac. Oncol.* 14 (11), 1901–1911. doi:10.1016/j.jtho.2019.08.003

Hu, L., Zeng, Z., Xia, Q., Liu, Z., Feng, X., Chen, J., et al. (2019). Metformin Attenuates Hepatoma Cell Proliferation by Decreasing Glycolytic Flux through the HIF-1α/PFKFB3/PFK1 Pathway. *Life Sci.* 239, 116966. doi:10.1016/j.lfs.2019.116966

Huang, Z., Lin, L., Gao, Y., Chen, Y., Yan, X., Xing, J., et al. (2011). Bladder Cancer Determination via Two Urinary Metabolites: a Biomarker Pattern Approach. *Mol. Cell Proteomics* 10 (10), M111. doi:10.1074/mcp.M111.007922

Hui, S., Ghergurovich, J. M., Morscher, R. J., Jang, C., Teng, X., Lu, W., et al. (2017). Glucose Feeds the TCA Cycle via Circulating Lactate. *Nature* 551 (7678), 115–118. doi:10.1038/nature24057

Ishikawa, S., Sugimoto, M., Kitabatake, K., Sugano, A., Nakamura, M., Kaneko, M., et al. (2016). Identification of Salivary Metabolomic Biomarkers for Oral Cancer Screening. *Sci. Rep.* 6, 31520. doi:10.1038/srep31520

Jing, F., Hu, X., Cao, Y., Xu, M., Wang, Y., Jing, Y., et al. (2018). Discriminating Gastric Cancer and Gastric Ulcer Using Human Plasma Amino Acid Metabolic Profile. *IUBMB Life* 70 (6), 553–562. doi:10.1002/iub.1748

Jiye, A., Qian, S., Wang, G., Yan, B., Zhang, S., Huang, Q., et al. (2010). Chronic Myeloid Leukemia Patients Sensitive and Resistant to Imatinib Treatment Show Different Metabolic Responses. *PLoS One* 5 (10), e13186. doi:10.1371/journal.pone.0013186

Johnson, C. H., Ivanisevic, J., and Siuzdak, G. (2016). Metabolomics: beyond Biomarkers and towards Mechanisms. *Nat. Rev. Mol. Cel Biol* 17 (7), 451–459. doi:10.1038/nrm.2016.25

Johnson, L. A., Zuloaga, K. L., Kugelman, T. L., Mader, K. S., Morré, J. T., Zuloaga, D. G., et al. (2016). Amelioration of Metabolic Syndrome-Associated Cognitive Impairments in Mice via a Reduction in Dietary Fat Content or Infusion of Non-diabetic Plasma. *EBioMedicine* 3, 26–42. doi:10.1016/j.ebiom.2015.12.008

Jones, C. L., Stevens, B. M., D'Alessandro, A., Reisz, J. A., Culp-Hill, R., Nemkov, T., et al. (2018). Inhibition of Amino Acid Metabolism Selectively Targets Human Leukemia Stem Cells. *Cancer Cell* 34 (5), 724–740. doi:10.1016/j.ccell.2018.10.005

Jung, J., Jung, Y., Bang, E. J., Cho, S.-i., Jang, Y.-J., Kwak, J.-M., et al. (2014). Noninvasive Diagnosis and Evaluation of Curative Surgery for Gastric Cancer by Using NMR-Based Metabolomic Profiling. *Ann. Surg. Oncol.* 21 (Suppl. 4), 736–742. doi:10.1245/s10434-014-3886-0

Kappler, M., Pabst, U., Rot, S., Taubert, H., Wichmann, H., Schubert, J., et al. (2017). Normoxic Accumulation of HIF1α Is Associated with Glutaminolysis. *Clin. Oral Invest.* 21 (1), 211–224. doi:10.1007/s00784-016-1780-9

Kaushik, A. K., and DeBerardinis, R. J. (2018). Applications of Metabolomics to Study Cancer Metabolism. *Biochim. Biophys. Acta (Bba) - Rev. Cancer* 1870 (1), 2–14. doi:10.1016/j.bbcan.2018.04.009

Kerr, E. M., Gaude, E., Turrell, F. K., Frezza, C., and Martins, C. P. (2016). Mutant Kras Copy Number Defines Metabolic Reprogramming and Therapeutic Susceptibilities. *Nature* 531 (7592), 110–113. doi:10.1038/nature16967

Kim, E.-K., Song, M.-J., Jung, Y., Lee, W.-S., and Jang, H. H. (2019). Proteomic Analysis of Primary Colon Cancer and Synchronous Solitary Liver Metastasis. *Cancer Genomics Proteomics* 16 (6), 583–592. doi:10.21873/cgp.20161

Kim, K.-B., Yang, J.-Y., Kwack, S. J., Kim, H. S., Ryu, D. H., Kim, Y.-J., et al. (2012). Potential Metabolomic Biomarkers for Evaluation of Adriamycin Efficacy Using a Urinary 1H-NMR Spectroscopy. *J. Appl. Toxicol.* 33 (11), 1251–1259. doi:10.1002/jat.2778

Kishton, R. J., Barnes, C. E., Nichols, A. G., Cohen, S., Gerriets, V. A., Siska, P. J., et al. (2016). AMPK Is Essential to Balance Glycolysis and Mitochondrial Metabolism to Control T-ALL Cell Stress and Survival. *Cel Metab.* 23 (4), 649–662. doi:10.1016/j.cmet.2016.03.008

Kus, K., Kij, A., Zakrzewska, A., Jasztal, A., Stojak, M., Walczak, M., et al. (2018). Alterations in Arginine and Energy Metabolism, Structural and Signalling Lipids in Metastatic Breast Cancer in Mice Detected in Plasma by Targeted Metabolomics and Lipidomics. *Breast Cancer Res.* 20 (1), 148. doi:10.1186/s13058-018-1075-y

Labbé, D. P., Zadra, G., Yang, M., Reyes, J. M., Lin, C. Y., Cacciatore, S., et al. (2019). High-fat Diet Fuels Prostate Cancer Progression by Rewiring the Metabolome and Amplifying the MYC Program. *Nat. Commun.* 10 (1), 4358. doi:10.1038/s41467-019-12298-z

Lane, A. N., Fan, T. W.-M., Bousamra, M., 2nd, Higashi, R. M., Yan, J., and Miller, D. M. (2011). Stable Isotope-Resolved Metabolomics (SIRM) in Cancer Research with Clinical Application to Nonsmall Cell Lung Cancer. *OMICS: A J. Integr. Biol.* 15 (3), 173–182. doi:10.1089/omi.2010.0088

Lane, A. N., Higashi, R. M., and Fan, T. W.-M. (2019). NMR and MS-based Stable Isotope-Resolved Metabolomics and Applications in Cancer Metabolism. *Trac Trends Anal. Chem.* 120, 115322. doi:10.1016/j.trac.2018.11.020

Li, G., Su, Q., Liu, H., Wang, D., Zhang, W., Lu, Z., et al. (2018). Frizzled7 Promotes Epithelial-To-Mesenchymal Transition and Stemness via Activating Canonical Wnt/β-Catenin Pathway in Gastric Cancer. *Int. J. Biol. Sci.* 14 (3), 280–293. doi:10.7150/ijbs.23756

Locasale, J. W., Melman, T., Song, S., Yang, X., Swanson, K. D., Cantley, L. C., et al. (2012). Metabolomics of Human Cerebrospinal Fluid Identifies Signatures of Malignant Glioma. *Mol. Cell Proteomics* 11 (6), M111. doi:10.1074/mcp.M111.014688

Lu, J., Hu, S., Miccoli, P., Zeng, Q., Liu, S., Ran, L., et al. (2016). Non-invasive Diagnosis of Papillary Thyroid Microcarcinoma: a NMR-Based Metabolomics Approach. *Oncotarget* 7 (49), 81768–81777. doi:10.18632/oncotarget.13178

Luo, X., Liu, J., Wang, H., and Lu, H. (2020). Metabolomics Identified New Biomarkers for the Precise Diagnosis of Pancreatic Cancer and Associated Tissue Metastasis. *Pharmacol. Res.* 156, 104805. doi:10.1016/j.phrs.2020.104805

Maldonado, R., Talana, C., Song, C., Dixon, A., Uehara, K., and Weichhaus, M. (2021). B-hydroxybutyrate D-oes N-ot A-lter the E-ffects of G-lucose D-eprivation on B-reast C-ancer C-ells. *Oncol. Lett.* 21 (1), 65. doi:10.3892/ol.2020.12326

Mayerle, J., Kalthoff, H., Reszka, R., Kamlage, B., Peter, E., Schniewind, B., et al. (2018). Metabolic Biomarker Signature to Differentiate Pancreatic Ductal Adenocarcinoma from Chronic Pancreatitis. *Gut* 67 (1), 128–137. doi:10.1136/gutjnl-2016-312432

Murata, T., Yanagisawa, T., Kurihara, T., Kaneko, M., Ota, S., Enomoto, A., et al. (2019). Salivary Metabolomics with Alternative Decision Tree-Based Machine Learning Methods for Breast Cancer Discrimination. *Breast Cancer Res. Treat.* 177 (3), 591–601. doi:10.1007/s10549-019-05330-9

Nakamizo, S., Sasayama, T., Shinohara, M., Irino, Y., Nishiumi, S., Nishihara, M., et al. (2013). GC/MS-based Metabolomic Analysis of Cerebrospinal Fluid (CSF) from Glioma Patients. *J. Neurooncol.* 113 (1), 65–74. doi:10.1007/s11060-013-1090-x

Obrist, F., Michels, J., Durand, S., Chery, A., Pol, J., Levesque, S., et al. (2018). Metabolic Vulnerability of Cisplatin-resistant Cancers. *Embo j* 37 (14). doi:10.15252/embj.201798597

Ohshima, M., Sugahara, K., Kasahara, K., and Katakura, A. (2017). Metabolomic Analysis of the Saliva of Japanese Patients with Oral Squamous Cell Carcinoma. *Oncol. Rep.* 37 (5), 2727–2734. doi:10.3892/or.2017.5561

Omran, M. M., Rashed, R. E., Darwish, H., Belal, A. A., and Mohamed, F. Z. (2020). Development of a Gas Chromatography-Mass Spectrometry Method for Breast Cancer Diagnosis Based on Nucleoside Metabolomes 1-methyl Adenosine, 1-methylguanosine and 8-hydroxy-2′-deoxyguanosine. *Biomed. Chromatogr.* 34 (1), e4713. doi:10.1002/bmc.4713

Peng, X., Chen, Z., Farshidfar, F., Xu, X., Lorenzi, P. L., Wang, Y., et al. (2018). Molecular Characterization and Clinical Relevance of Metabolic Expression Subtypes in Human Cancers. *Cell Rep* 23 (1), 255–e4. doi:10.1016/j.celrep.2018.03.077

Pérez-Rambla, C., Puchades-Carrasco, L., García-Flores, M., Rubio-Briones, J., López-Guerrero, J. A., and Pineda-Lucena, A. (2017). Non-invasive Urinary Metabolomic Profiling Discriminates Prostate Cancer from Benign Prostatic Hyperplasia. *Metabolomics* 13 (5), 52. doi:10.1007/s11306-017-1194-y

Perkons, N. R., Johnson, O., Pilla, G., and Gade, T. P. F. (2021). Pharmacodynamics and Pharmacokinetics of Hyperpolarized [1- 13 C]-pyruvate in a Translational Oncologic Model. *NMR Biomed.* 34 (6), e4502. doi:10.1002/nbm.4502

Perroud, B., Ishimaru, T., Borowsky, A. D., and Weiss, R. H. (2009). Grade-dependent Proteomics Characterization of Kidney Cancer. *Mol. Cell Proteomics* 8 (5), 971–985. doi:10.1074/mcp.M800252-MCP200

Perroud, B., Lee, J., Valkova, N., Dhirapong, A., Lin, P.-Y., Fiehn, O., et al. (2006). Pathway Analysis of Kidney Cancer Using Proteomics and Metabolic Profiling. *Mol. Cancer* 5, 64. doi:10.1186/1476-4598-5-64

Poczobutt, J. M., Nguyen, T. T., Hanson, D., Li, H., Sippel, T. R., Weiser-Evans, M. C. M., et al. (2016). Deletion of 5-Lipoxygenase in the Tumor Microenvironment Promotes Lung Cancer Progression and Metastasis through Regulating T Cell Recruitment. *J.I.* 196 (2), 891–901. doi:10.4049/jimmunol.1501648

Poschner, S., Wackerlig, J., Castillo-Tong, D. C., Wolf, A., von der Decken, I., Rižner, T. L., et al. (2020). Metabolism of Estrogens: Turnover Differs between Platinum-Sensitive and -Resistant High-Grade Serous Ovarian Cancer Cells. *Cancers* 12 (2), 279. doi:10.3390/cancers12020279

Reichl, B., Niederstaetter, L., Boegl, T., Neuditschko, B., Bileck, A., Gojo, J., et al. (2020). Determination of a Tumor-Promoting Microenvironment in Recurrent Medulloblastoma: A Multi-Omics Study of Cerebrospinal Fluid. *Cancers* 12 (6), 1350. doi:10.3390/cancers12061350

Ringel, A. E., Drijvers, J. M., Baker, G. J., Catozzi, A., García-Cañaveras, J. C., Gassaway, B. M., et al. (2020). Obesity Shapes Metabolism in the Tumor Microenvironment to Suppress Anti-tumor Immunity. *Cell* 183 (7), 1848–1866. doi:10.1016/j.cell.2020.11.009

Salamanca-Cardona, L., and Keshari, K. R. (2015). 13C-labeled Biochemical Probes for the Study of Cancer Metabolism with Dynamic Nuclear Polarization-Enhanced Magnetic Resonance Imaging. *Cancer Metab.* 3, 9. doi:10.1186/s40170-015-0136-2

Soini, H. A., Klouckova, I., Wiesler, D., Oberzaucher, E., Grammer, K., Dixon, S. J., et al. (2010). Analysis of Volatile Organic Compounds in Human Saliva by a Static Sorptive Extraction Method and Gas Chromatography-Mass Spectrometry. *J. Chem. Ecol.* 36 (9), 1035–1042. doi:10.1007/s10886-010-9846-7

Spinelli, J. B., Yoon, H., Ringel, A. E., Jeanfavre, S., Clish, C. B., and Haigis, M. C. (2017). Metabolic Recycling of Ammonia via Glutamate Dehydrogenase Supports Breast Cancer Biomass. *Science* 358 (6365), 941–946. doi:10.1126/science.aam9305

Srivastava, A., and Creek, D. J. (2019). Discovery and Validation of Clinical Biomarkers of Cancer: A Review Combining Metabolomics and Proteomics. *Proteomics* 19 (10), 1700448. doi:10.1002/pmic.201700448

Stuart, E., Buchert, M., Putoczki, T., Thiem, S., Farid, R., Elzer, J., et al. (2014). Therapeutic Inhibition of Jak Activity Inhibits Progression of Gastrointestinal Tumors in Mice. *Mol. Cancer Ther.* 13 (2), 468–474. doi:10.1158/1535-7163.Mct-13-0583-t

Sugimoto, M., Wong, D. T., Hirayama, A., Soga, T., and Tomita, M. (2010). Capillary Electrophoresis Mass Spectrometry-Based Saliva Metabolomics Identified Oral, Breast and Pancreatic Cancer-specific Profiles. *Metabolomics* 6 (1), 78–95. doi:10.1007/s11306-009-0178-y

Svensson, R. U., Parker, S. J., Eichner, L. J., Kolar, M. J., Wallace, M., Brun, S. N., et al. (2016). Inhibition of Acetyl-CoA Carboxylase Suppresses Fatty Acid Synthesis and Tumor Growth of Non-small-cell Lung Cancer in Preclinical Models. *Nat. Med.* 22 (10), 1108–1119. doi:10.1038/nm.4181

Tabe, Y., Lorenzi, P. L., and Konopleva, M. (2019). Amino Acid Metabolism in Hematologic Malignancies and the Era of Targeted Therapy. *Blood* 134 (13), 1014–1023. doi:10.1182/blood.2019001034

Tao, L., Zhou, J., Yuan, C., Zhang, L., Li, D., Si, D., et al. (2019). Metabolomics Identifies Serum and Exosomes Metabolite Markers of Pancreatic Cancer. *Metabolomics* 15 (6), 86. doi:10.1007/s11306-019-1550-1

Toledo, J. B., Arnold, M., Kastenmüller, G., Chang, R., Baillie, R. A., Han, X., et al. (2017). Metabolic Network Failures in Alzheimer's Disease: A Biochemical Road Map. *Alzheimer's Demen.* 13 (9), 965–984. doi:10.1016/j.jalz.2017.01.020

Traversari, C., Sozzani, S., Steffensen, K. R., and Russo, V. (2014). LXR-dependent and -independent Effects of Oxysterols on Immunity and Tumor Growth. *Eur. J. Immunol.* 44 (7), 1896–1903. doi:10.1002/eji.201344292

Wang, F.-X., Chen, K., Huang, F.-Q., Alolga, R. N., Ma, J., Wu, Z.-X., et al. (2020). Cerebrospinal Fluid-Based Metabolomics to Characterize Different Types of Brain Tumors. *J. Neurol.* 267 (4), 984–993. doi:10.1007/s00415-019-09665-7

Wang, H., Xi, Q., and Wu, G. (2016). Fatty Acid Synthase Regulates Invasion and Metastasis of Colorectal Cancer via Wnt Signaling Pathway. *Cancer Med.* 5 (7), 1599–1606. doi:10.1002/cam4.711

Wang, Y., Bai, C., Ruan, Y., Liu, M., Chu, Q., Qiu, L., et al. (2019). Coordinative Metabolism of Glutamine Carbon and Nitrogen in Proliferating Cancer Cells under Hypoxia. *Nat. Commun.* 10 (1), 201. doi:10.1038/s41467-018-08033-9

Warburg, O. (1956). On Respiratory Impairment in Cancer Cells. *Science* 124 (3215), 269–270. doi:10.1126/science.124.3215.269

Wen, L. Y., Zhang, Y. S., Zhou, X., Li, G., Hu, C. Y., Li, Y., et al. (2018). Effect of Branched Chain Amino Acids on Perioperative Temperature, Glucose Level and Fat Metabolism in Patients with Gastrointestinal Tumors. *J. Biol. Regul. Homeost Agents* 32 (2), 357–363.

Wettersten, H. I., Hakimi, A. A., Morin, D., Bianchi, C., Johnstone, M. E., Donohoe, D. R., et al. (2015). Grade-Dependent Metabolic Reprogramming in Kidney Cancer Revealed by Combined Proteomics and Metabolomics Analysis. *Cancer Res.* 75 (12), 2541–2552. doi:10.1158/0008-5472.Can-14-1703

Williams, M. J., Werner, B., Barnes, C. P., Graham, T. A., and Sottoriva, A. (2016). Identification of Neutral Tumor Evolution across Cancer Types. *Nat. Genet.* 48 (3), 238–244. doi:10.1038/ng.3489

Wishart, D. S., Jewison, T., Guo, A. C., Wilson, M., Knox, C., Liu, Y., et al. (2013). HMDB 3.0-The Human Metabolome Database in 2013. *Nucleic Acids Res.* 41 (Database issue), D801–D807. doi:10.1093/nar/gks1065

Wishart, D. S. (2019). Metabolomics for Investigating Physiological and Pathophysiological Processes. *Physiol. Rev.* 99 (4), 1819–1875. doi:10.1152/physrev.00035.2018

Wong, T. L., Ng, K. Y., Tan, K. V., Chan, L. H., Zhou, L., Che, N., et al. (2020). CRAF Methylation by PRMT6 Regulates Aerobic Glycolysis-Driven Hepatocarcinogenesis via ERK-Dependent PKM2 Nuclear Relocalization and Activation. *Hepatology* 71 (4), 1279–1296. doi:10.1002/hep.30923

Wu, T., and Dai, Y. (2017). Tumor Microenvironment and Therapeutic Response. *Cancer Lett.* 387, 61–68. doi:10.1016/j.canlet.2016.01.043

Xiao, S., and Zhou, L. (2017). Gastric Cancer: Metabolic and Metabolomics Perspectives (Review). *Int. J. Oncol.* 51 (1), 5–17. doi:10.3892/ijo.2017.4000

Xie, G., Zhou, B., Zhao, A., Qiu, Y., Zhao, X., Garmire, L., et al. (2015). Lowered Circulating Aspartate Is a Metabolic Feature of Human Breast Cancer. *Oncotarget* 6 (32), 33369–33381. doi:10.18632/oncotarget.5409

Xu, H., Liu, R., He, B., Bi, C., Bi, K., and Li, Q. (2016). Polyamine Metabolites Profiling for Characterization of Lung and Liver Cancer Using an LC-Tandem MS Method with Multiple Statistical Data Mining Strategies: Discovering Potential Cancer Biomarkers in Human Plasma and Urine. *Molecules* 21 (8), 1040. doi:10.3390/molecules21081040

Yang, Y., Lane, A. N., Ricketts, C. J., Sourbier, C., Wei, M.-H., Shuch, B., et al. (2013). Metabolic Reprogramming for Producing Energy and Reducing Power in Fumarate Hydratase Null Cells from Hereditary Leiomyomatosis Renal Cell Carcinoma. *PLoS One* 8 (8), e72179. doi:10.1371/journal.pone.0072179

Ye, G., Liu, Y., Yin, P., Zeng, Z., Huang, Q., Kong, H., et al. (2014). Study of Induction Chemotherapy Efficacy in Oral Squamous Cell Carcinoma Using Pseudotargeted Metabolomics. *J. Proteome Res.* 13 (4), 1994–2004. doi:10.1021/pr4011298

Yi, M., Li, J., Chen, S., Cai, J., Ban, Y., Peng, Q., et al. (2018). Emerging Role of Lipid Metabolism Alterations in Cancer Stem Cells. *J. Exp. Clin. Cancer Res.* 37 (1), 118. doi:10.1186/s13046-018-0784-5

Yip-Schneider, M. T., Simpson, R., Carr, R. A., Wu, H., Fan, H., Liu, Z., et al. (2019). Circulating Leptin and Branched Chain Amino Acids-Correlation with Intraductal Papillary Mucinous Neoplasm Dysplastic Grade. *J. Gastrointest. Surg.* 23 (5), 966–974. doi:10.1007/s11605-018-3963-y

Zampieri, M., Sekar, K., Zamboni, N., and Sauer, U. (2017). Frontiers of High-Throughput Metabolomics. *Curr. Opin. Chem. Biol.* 36, 15–23. doi:10.1016/j.cbpa.2016.12.006

Zhang, A., Yan, G., Han, Y., and Wang, X. (2014). Metabolomics Approaches and Applications in Prostate Cancer Research. *Appl. Biochem. Biotechnol.* 174 (1), 6–12. doi:10.1007/s12010-014-0955-6

Zhang, T., Wu, X., Ke, C., Yin, M., Li, Z., Fan, L., et al. (2013). Identification of Potential Biomarkers for Ovarian Cancer by Urinary Metabolomic Profiling. *J. Proteome Res.* 12 (1), 505–512. doi:10.1021/pr3009572

Zhang, W., Borcherding, N., and Kolb, R. (2020). IL-1 Signaling in Tumor Microenvironment. *Adv. Exp. Med. Biol.* 1240, 1–23. doi:10.1007/978-3-030-38315-2_1

Zhang, Y., Gao, Y., Li, Y., Zhang, X., and Xie, H. (2020). Characterization of the Relationship between the Expression of Aspartate β-Hydroxylase and the Pathological Characteristics of Breast Cancer. *Med. Sci. Monit.* 26, e926752. doi:10.12659/msm.926752

Zhang, Y., Tan, H., Daniels, J. D., Zandkarimi, F., Liu, H., Brown, L. M., et al. (2019). Imidazole Ketone Erastin Induces Ferroptosis and Slows Tumor Growth in a Mouse Lymphoma Model. *Cel Chem. Biol.* 26 (5), 623–633. doi:10.1016/j.chembiol.2019.01.008

Zhang, X., Chen, Y., Hao, L., Hou, A., Chen, X., Li, Y., et al. (2016). Macrophages induce resistance to 5-fluorouracil chemotherapy in colorectal cancer through the release of putrescine. *Cancer Lett.* 381 (2), 305–313. doi:10.1016/j.canlet.2016.08.004

Zhao, S., Ren, S., Jiang, T., Zhu, B., Li, X., Zhao, C., et al. (2019). Low-Dose Apatinib Optimizes Tumor Microenvironment and Potentiates Antitumor Effect of PD-1/pd-L1 Blockade in Lung Cancer. *Cancer Immunol. Res.* 7 (4), 0640–643. doi:10.1158/2326-6066.Cir-17-0640

Conflict of Interest: The authors declare that the research was conducted in the absence of any commercial or financial relationships that could be construed as a potential conflict of interest.

Publisher's Note: All claims expressed in this article are solely those of the authors and do not necessarily represent those of their affiliated organizations, or those of the publisher, the editors and the reviewers. Any product that may be evaluated in this article, or claim that may be made by its manufacturer, is not guaranteed or endorsed by the publisher.

frontiers in Molecular Biosciences

ORIGINAL RESEARCH
published: 25 November 2021
doi: 10.3389/fmolb.2021.759173

Computational Identification of Immune- and Ferroptosis-Related LncRNA Signature for Prognosis of Hepatocellular Carcinoma

Anmin Huang[1,2], *Ting Li*[2], *Xueting Xie*[2] *and Jinglin Xia*[1,3]*

[1]Key Laboratory of Diagnosis and Treatment of Severe Hepato-Pancreatic Diseases of Zhejiang Province, The First Affiliated Hospital of Wenzhou Medical University, Wenzhou, China, [2]School of the First Clinical Medical Sciences, Wenzhou Medical University, Wenzhou, China, [3]Liver Cancer Institute, Zhongshan Hospital of Fudan University, Shanghai, China

Long non-coding RNAs (lncRNAs), which were implicated in many pathophysiological processes including cancer, were frequently dysregulated in hepatocellular carcinoma (HCC). Studies have demonstrated that ferroptosis and immunity can regulate the biological behaviors of tumors. Therefore, biomarkers that combined ferroptosis, immunity, and lncRNA can be a promising candidate bioindicator in clinical therapy of cancers. Many bioinformatics methods, including Pearson correlation analysis, univariate Cox proportional hazard regression analysis, least absolute shrinkage and selection operator (LASSO) analysis, and multivariate Cox proportional hazard regression analysis were applied to develop a prognostic risk signature of immune- and ferroptosis-related lncRNA (IFLSig). Finally, eight immune- and ferroptosis-related lncRNAs (IFLncRNA) were identified to develop and IFLSig of HCC patients. We found the prognosis of patients with high IFLSig will be worse, while the prognosis of patients with low IFLSig will be better. The results provide an efficient method of uniting critical clinical information with immunological characteristics, enabling estimation of the overall survival (OS). Such an integrative prognostic model with high predictive power would have a notable impact and utility in prognosis prediction and individualized treatment strategies.

Keywords: ferroptosis, immune, long non-coding RNA (lncRNA), hepatocellular carcinoma, prognosis

OPEN ACCESS

Edited by:
Zhe-Sheng Chen,
St. John's University, United States

Reviewed by:
Yi Qin,
Cancer Institute, Fudan University, China
Jiaping Li,
The First Affiliated Hospital of Sun Yat-sen University, China

***Correspondence:**
Jinglin Xia
xiajinglin@wzhospital.cn

Specialty section:
This article was submitted to Molecular Diagnostics and Therapeutics, a section of the journal Frontiers in Molecular Biosciences

Received: *16 August 2021*
Accepted: *29 October 2021*
Published: *25 November 2021*

Citation:
Huang A, Li T, Xie X and Xia J (2021) Computational Identification of Immune- and Ferroptosis-Related LncRNA Signature for Prognosis of Hepatocellular Carcinoma. Front. Mol. Biosci. 8:759173. doi: 10.3389/fmolb.2021.759173

INTRODUCTION

As one of the top five leading causes of cancer-related deaths worldwide and the fifth most frequent in China, liver cancer still has an estimated number of 392,868 new cases and 368,960 cancer-related deaths in 2018 (Feng et al., 2019). The symptoms of HCC are not obvious in the early stage, but are perceptible in the late stage, which can easily lead to delayed diagnosis and poor treatment effects (Bray et al., 2018). Therefore, individual treatment and prognosis determination of liver cancer are still major challenges.

LncRNA with transcripts longer than 200 nt is initially considered to be a meaningless plate in transcription (Chew et al., 2018). With the large-scale use of massively parallel signature sequencing technology, lncRNAs instead have shown a high correlation with liver cancer, mainly in their regulatory roles during liver carcinogenesis (Wang et al., 2015; Wang et al., 2016). These cancer-related lncRNAs participate in numerous biological processes, including epigenetic regulation, signal transduction, and cell cycle control (Yuan et al., 2017; Wu et al., 2019; Xu et al., 2019).

Ferroptosis is a recently recognized cell death modality that is intimately associated with the development of tumor-immunosuppressive microenvironment, and the existence of ferroptosis-related intercourse was evidenced between tumor cells and immune cells (Jiang et al., 2021; Xu et al., 2021). A plethora of research on the relationship between ferroptosis and immunity have given a new outlook on our understanding of the pathogenesis of liver cancer, and the intervention of ferroptosis can effectively improve immunosuppression (Gao et al., 2015; Ou et al., 2016; Sun et al., 2016; Wang et al., 2021). In the tumor microenvironment, ferroptosis can be regulated by many molecular factors, and abundant protein interactions also participate in this progress. Ferroptosis can expose the antigens in tumor cells, thereby increasing the immunogenicity of the tumor immune microenvironment and improving the availability of immunotherapy (Tang et al., 2020). In addition, several factors such as the tumor microenvironment, tumor immune-infiltrating cells, and response to immunotherapy provide a certain association with the clinical outcome of cancer (Vitale et al., 2019; Zheng et al., 2020). These theories are the cornerstone of tumor immunotherapy in the future.

A novel lncRNA prognostic risk model, combining ferroptosis and immunity, was constructed for clinical practice in this study. First of all, to provide a better strategy to orchestrate the immune system in eradicating cancers, we comprehensively analyzed the lncRNA profiles, combining ferroptosis and immunity profiles, as well as determined their clinical significance to construct a prognostic algorithm. Following this, we provide evidence of the scale of immune profile and the potential effectiveness of immunotherapy use in our prognostic risk model. We conclude with suggestions for providing an opportunity to further optimize the modeling tool for the prognosis and therapy responses of HCC.

MATERIALS AND METHODS

Data Collection

The RNA sequencing (RNA-seq) data and corresponding clinical information of 421 cases in total (including 363 cancer samples and 58 normal samples) were obtained from The Cancer Genome Atlas database (TCGA, http://portal.gdc.cancer.gov/), and the missing and abnormal values were processed with multiple imputation by utilizing SPSS ver. 25.0 (IBM United States). Ferroptosis-related genes were obtained from the FerrDb database (http://www.zhounan.org/ferrdb/), and immune-related genes were obtained from the ImmPort database (https://www.immport.org).

The Construction and Validation of Prognostic Risk Model

Differential expression of lncRNA genes (DEGs) was performed between cancer samples and normal samples with R package "Dseq2," and the cut-off was set at log2foldchange (logFC) <−2, p-value <0.05, and adjusted p-value <0.01. The relevance between DEGs and ferroptosis-related genes and immune-related genes was explored by Pearson correlation analysis. Then, univariate Cox proportional regression analysis and least absolute shrinkage and selection operator (LASSO) Cox proportional regression were performed to identify candidate immune- and ferroptosis-related lncRNAs (IFLncRNA). A total of 363 HCC patients were randomized into the training cohort or test cohort for the construction and validation of risk score at the ratio of 6:4 (218 in the training cohort and 145 in the test cohort). For the training cohort, our prognostic risk signature of immune- and ferroptosis-related lncRNA (IFLSig) was structured by applying the linear combination of the expression values of each prognostic IFLncRNA, weighted by their estimated regression coefficients through the multivariate Cox proportional hazard regression analysis as follows:

$$\text{Risk score}\,(\text{patients}) = \sum \text{coefficient}\,(\text{lncRNA}) * \text{expression}\,(\text{lncRNA})$$

Risk score (patients) is a latent prediction risk score for patients, and IFLSig is a prediction risk score based on IFLncRNA. The expression (lncRNA) is the expression value of IFLncRNA of HCC. The meaning of coefficient (lncRNA) is the contribution of IFLncRNA that was derived from the coefficient of multivariate Cox regression in the training cohort. The median of IFLSig in the training cohort and test cohort was used as a cut-off to sort patients into the high-risk group and the low-risk group. The Kaplan–Meier (K-M) survival curves and receiver operating characteristic (ROC) curves were used to estimate the predictive power of overall survival (OS). A principal component analysis (PCA) was applied to estimate the expression difference of IFLncRNA in HCC patients. Univariate Cox proportional hazard regression and multivariate Cox proportional hazard regression analyses for OS were performed on the independent prognostic factor of the risk score. Moreover, a nomogram was constructed with IFLSig and other clinical factors.

Functional Enrichment Analysis

Gene Set Enrichment Analysis (GSEA) (ver. 4.1.0, http://www.gsea-msigdb.org/gsea/index.jsp) was performed to identify signal pathways and functional categories associated with IFLSig in the enrichment of Kyoto Encyclopedia of Genes and Genomes (KEGG) and Gene Ontology (GO).

Clinical Therapy Response With IFLSig for HCC Patients

To estimate the prediction accuracy of IFLSig with immunotherapy response for clinical practice, the algorithm from CIBERSORT (https://cibersort.stanford.edu/) was used to estimate the profile of immune cell subtypes in HCC patients. The correlation between IFLSig and immune checkpoints was analyzed to confirm the potential of IFLSig as a biomarker for immune checkpoint inhibitor (ICI) treatments. The sensitivity and resistance chemotherapeutic drugs were identified by using the R package "pRRophetic."

Statistical Analysis

All statistical analyses were applied by R software ver. 3.6.3 and SPSS ver. 25.0. Pearson correlation analysis was performed with R

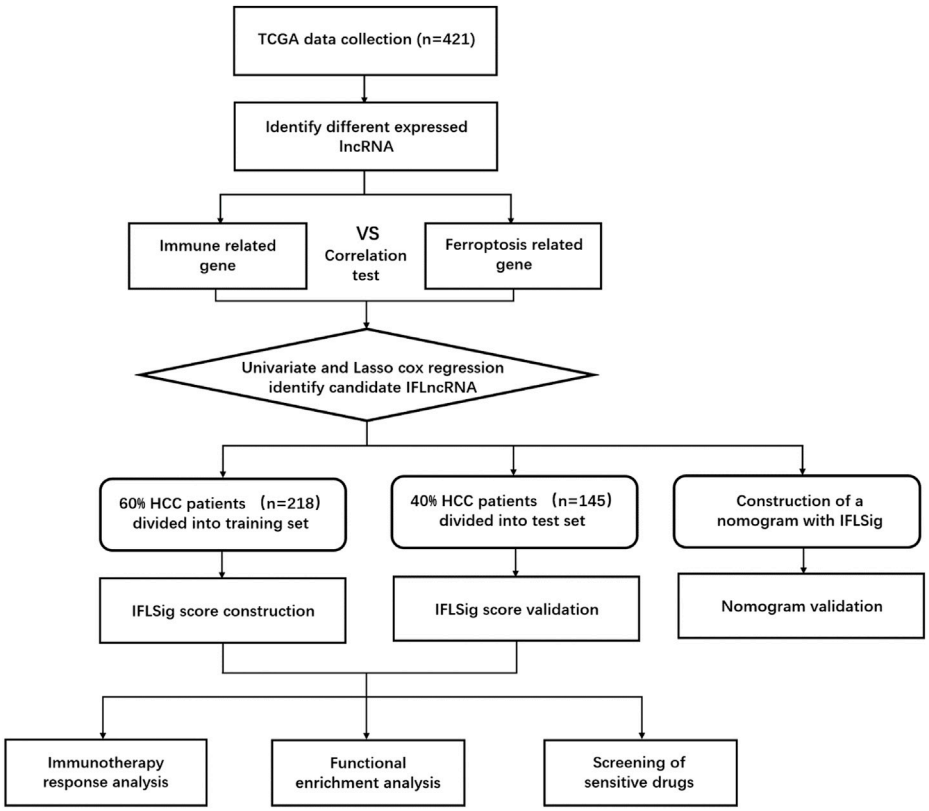

FIGURE 1 | Flow chart of whole design thought.

package "stats." Univariate Cox proportional hazard regression analysis, multivariate Cox proportional hazard regression analysis, and nomogram were performed with R package "survival" and "survminer." A log-rank test was used for calculating the statistical difference in OS between the low-risk group and high-risk group. LASSO Cox proportional regression was performed with R package "glmnet." ROC curve was performed with R package "survivalROC." Harrell's index of concordance (*C*-index) was performed to estimate the prognostic power of the nomogram.

RESULTS

Data Processing

A total of 15,095 lncRNA RNA-seq were obtained from the TCGA database, and 681 downregulated DEGs were preliminary screened (**Figure 1A**). We extracted 248 ferroptosis-related genes from the FerrDb database and 453 immune-related genes from the ImmPort database. Pearson correlation analysis was performed between the lncRNAs and ferroptosis-related genes and immune-related genes (with a Correlation coefficient >0.4 and $p < 0.01$). Univariate Cox proportional regression analysis was performed to estimate the prognostic power of lncRNAs. A total of 26 lncRNAs ($p < 0.05$) were identified in the TCGA series. The LASSO Cox regression kept 17 candidate IFLncRNAs after filtration: AC009005.1, AC016773.1, AC090164.2, AC092119.2, AC099850.3, AL021807.1, AL356234.2, AL359510.2, CASC9, DUXAP8, GDNF-AS1, LINC01224, LINC01436, LINC02202, LUCAT1, PTGES2-AS1, and ZFPM2-AS1. LASSO coefficient profiles and optimal penalty parameter lambda are shown in **Supplementary Figures S1A,B**. The predictive performance of candidate IFLncRNA would be determined in the training cohort to construct a prognostic risk model.

Construction and Validation of Prognosis Risk Model for HCC

In the training set, the predictive performance of IFLncRNA was determined by multivariate Cox regression. As a result, the total risk score is determined by the following equation:

$$\begin{aligned}\text{Risk score}(\text{patients}) = {} & (0.671{*}\text{AC009005.1}) \\ & + (-2.555{*}\text{AC092119.2}) + (0.820{*}\text{AC099850.3}) \\ & + (-0.941{*}\text{AL356234.2}) + (-0.301{*}\text{GDNF}-\text{AS1}) \\ & + (0.373{*}\text{LINC01224}) + (0.218{*}\text{LUCAT1}) \\ & + (0.114{*}\text{ZFPM2}-\text{AS1})\end{aligned}$$

Based on the median value of the risk score, all patients were categorized into the high-risk group or low-risk group in the

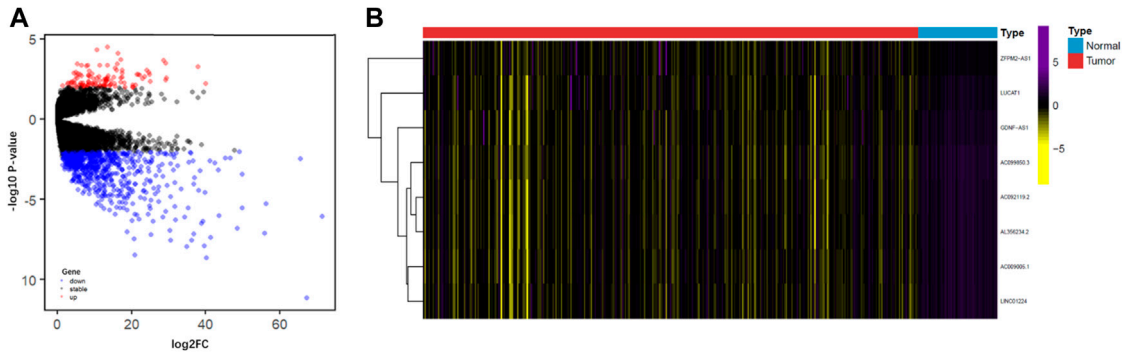

FIGURE 2 | (A) Volcano diagram showing the DEGs between cancer and normal samples. The red, black, and blue dots represent the upregulated genes, no difference, and downregulated genes, respectively. **(B)** Heatmap of the expression value of eight IFLncRNAs, differential expression of lncRNA genes; IFLncRNAs, immune- and ferroptosis-related lncRNAs.

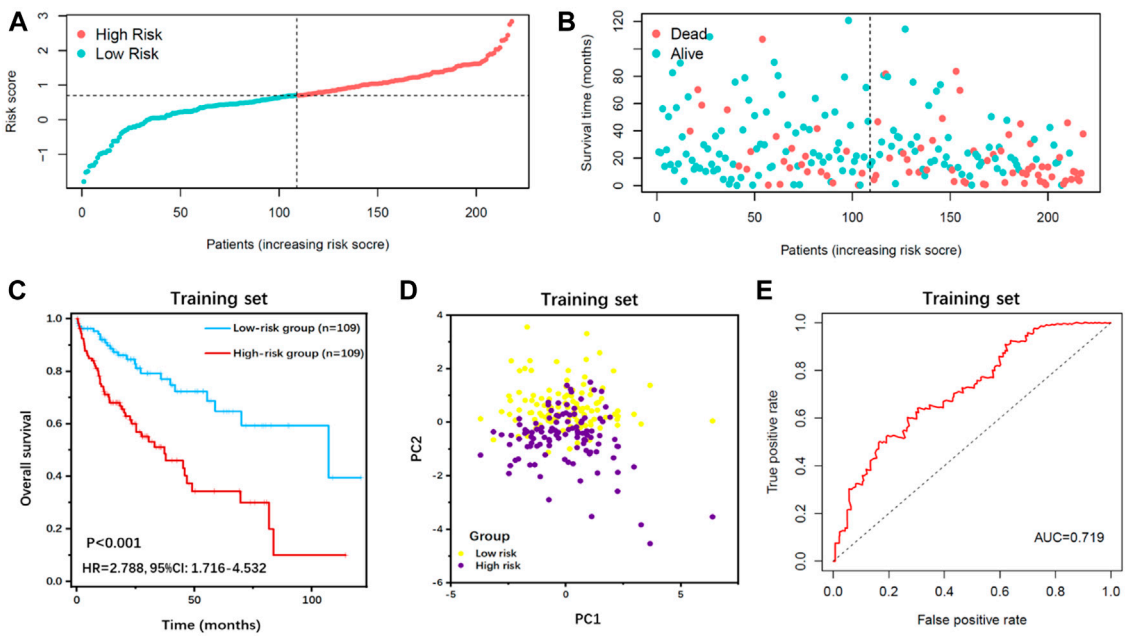

FIGURE 3 | Survival analysis of IFLSig in the training cohort. **(A)** Distribution of IFLSig of HCC cases, which were categorized into two groups based on the median of risk score. **(B)** Distribution of survival time of HCC cases. The positions of the dots reveal the association between the IFLSig and survival time. **(C)** K-M curve for IFLSig relative to the overall survival of the training cohort. **(D)** PCA plot of the training cohort. **(E)** ROC curve of the sensitivity and specificity of survival time on the risk scoreIFLSig, prognostic risk signature of immune- and ferroptosis-related lncRNA; HCC, hepatocellular carcinoma; K-M, Kaplan-Meier; PCA, principal component analysis; ROC, receiver operating characteristic.

training cohort (**Figures 3A,B**) and test cohort (**Figures 4A,B**). The expression values of eight IFLncRNAs are shown in **Figure 2B**. In the training cohort, the OS was significantly different between the high-risk group and the low-risk group [**Figure 3C**, $p < 0.001$, hazard ratio (HR): 2.788, 95% confidence interval (CI): 1.716–4.532]. The same significant difference with the OS was repeated in both groups of the test cohort (**Figure 4C**, $p = 0.002$, HR: 2.447, 95% CI: 1.386–4.323). As shown in the results, the patients with low risk scores had a better clinical prognosis than the patients with high risk scores, which is a consistent similar outcome for both groups of each cohort. The results of PCA verified the differential expression of IFLncRNA in HCC patients (**Figures 3D**, **4D**). Time-dependent ROC curves of 36 months were applied for the assessment capability of IFLSig with survival time. The area under the curve (AUC) value was 0.719 in the training cohort

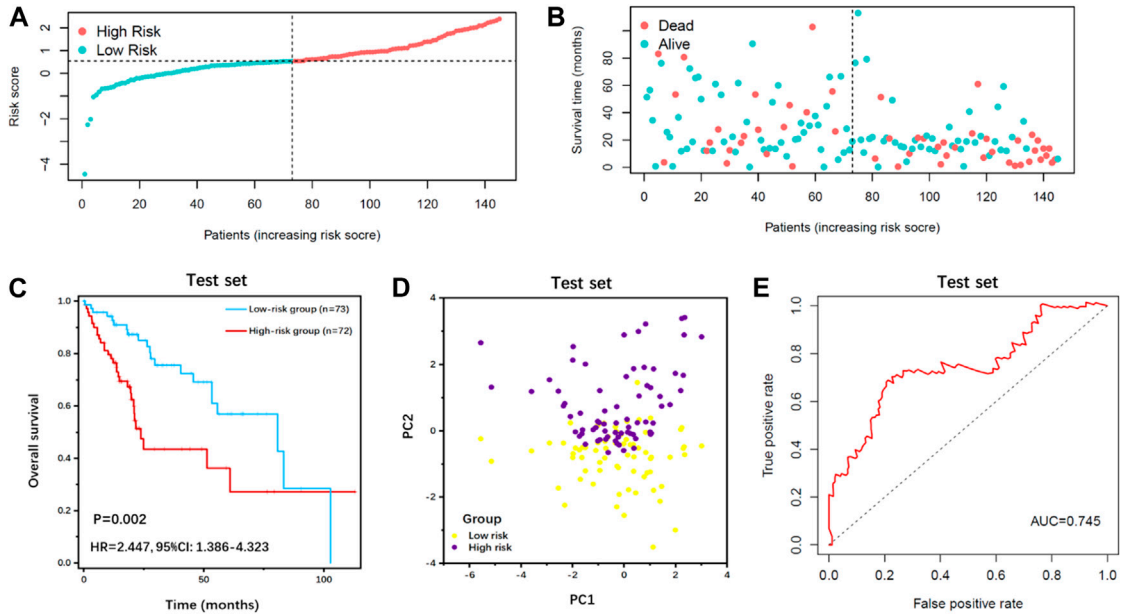

FIGURE 4 | Survival analysis of IFLSig in the test cohort. **(A)** Distribution of IFLSig of HCC cases, which were categorized into two groups based on the median of risk score. **(B)** Distribution of survival time of HCC cases. The positions of the dots reveal the association between the IFLSig and survival time. **(C)** K-M curve for IFLSig relative to the overall survival of the test cohort. **(D)** PCA plot of the test cohort. **(E)** ROC curve of the sensitivity and specificity of survival time on the risk score.

TABLE 1 | Univariate and multivariate Cox regression analyses in each data set.

Variables	Univariate analysis			Multivariate analysis		
	HR	95% CI of HR	*p*-value	HR	95% CI of HR	*p*-value
			Training set			
Risk score	2.718	1.995–3.703	<0.001	2.358	1.710–3.251	<0.001
Gender (male/female)	0.822	0.518–1.307	0.408	0.885	0.554–1.412	0.608
Stage (I/II/III/IV)	1.979	1.569–2.497	<0.001	1.706	1.345–2.163	<0.001
Age (<75/≥75)	2.067	1.188–3.597	0.010	1.812	1.036–3.170	0.037
			Test set			
Risk score	2.475	1.690–3.626	<0.001	2.590	1.735–3.865	<0.001
Gender (male/female)	0.851	0.481–1.506	0.580	0.882	0.485–1.601	0.679
Stage (I/II/III/IV)	1.254	0.911–1.727	0.164	1.296	0.930–1.807	0.126
Age (<75/≥75)	1.749	0.839–3.644	0.136	1.398	0.658–2.974	0.384

(**Figure 3E**) and 0.745 in the test cohort (**Figure 4E**). All the results suggested that IFLSig might have an accurate predictive ability for OS.

IFLSig as an Individual Prognostic Variable

To confirm that the IFLSig was an independent prognostic factor of other clinical characteristics, univariate and multivariate Cox regression analyses were performed (**Table 1**). For the training set, the results of univariate Cox regression analysis ($p < 0.001$, HR: 2.718, 95% CI: 1.995–3.703) and multivariate Cox regression analysis ($p < 0.001$, HR: 2.358, 95% CI: 1.710–3.251) revealed that a high level of IFLSig was significantly associated with shorter survival, and the HR was significantly higher than other factors, whereas patients with a low level of IFLSig were associated with better clinical outcomes. With the same scoring model and risk split point method from the test set, the IFLSig was used to categorize patients into two distinct subgroups. We subjected IFLSig and other clinicopathological features to univariate Cox regression ($p < 0.001$, HR: 2.475, 95% CI: 1.690–3.626) and multivariate Cox regression ($p < 0.001$, HR: 2.590, 95% CI: 1.735–3.865), and IFLSig was still an independent prognostic element for other confounding factors in the test set.

Functional Enrichment Analysis

We further performed GO and KEGG pathway enrichment analyses using the GSEA to identify the functional categories and biological pathways of IFLSig. The KEGG pathway

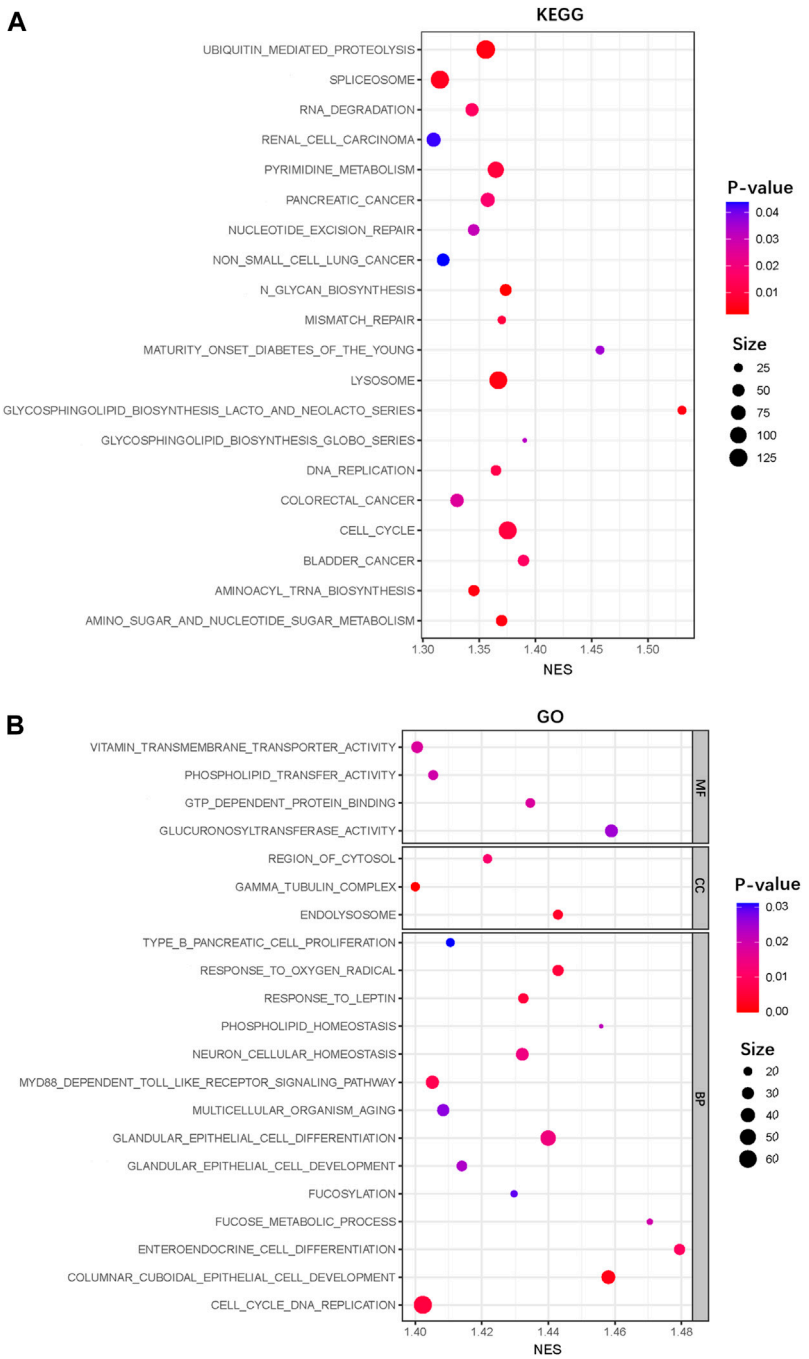

FIGURE 5 | GSEA functional enrichment analysis. **(A)** KEGG enrichment analysis of the IFLSig in the TCGA cohort. **(B)** GO enrichment analysis of the IFLSig in the TCGA cohort. GSEA, Gene Set Enrichment Analysis; KEGG, Kyoto Encyclopedia of Genes and Genomes; TCGA, The Cancer Genome Atlas.

analysis revealed main enrichment in cell cycle, spliceosome, lysosome, and ubiquitin-mediated proteolysis (**Figure 5A**). The results of GO enrichment analyses are shown in **Figure 5B**. The enriched biological process was mainly involved in the cell cycle DNA replication, glandular epithelial cell differentiation, and columnar cuboidal epithelial cell development. The enriched cellular components were mainly in the region of cytosol, gamma-tubulin complex, and endolysosome. The molecular functions mainly included vitamin transmembrane transporter activity and glucuronosyltransferase activity. We found that most of the enriched functional categories and biological pathways are related to nucleic acid, cell growth, and cell development. This suggested that IFLncRNA may participate in nucleic acid metabolism to regulate cell proliferation, migration, and death to affect the progress of HCC.

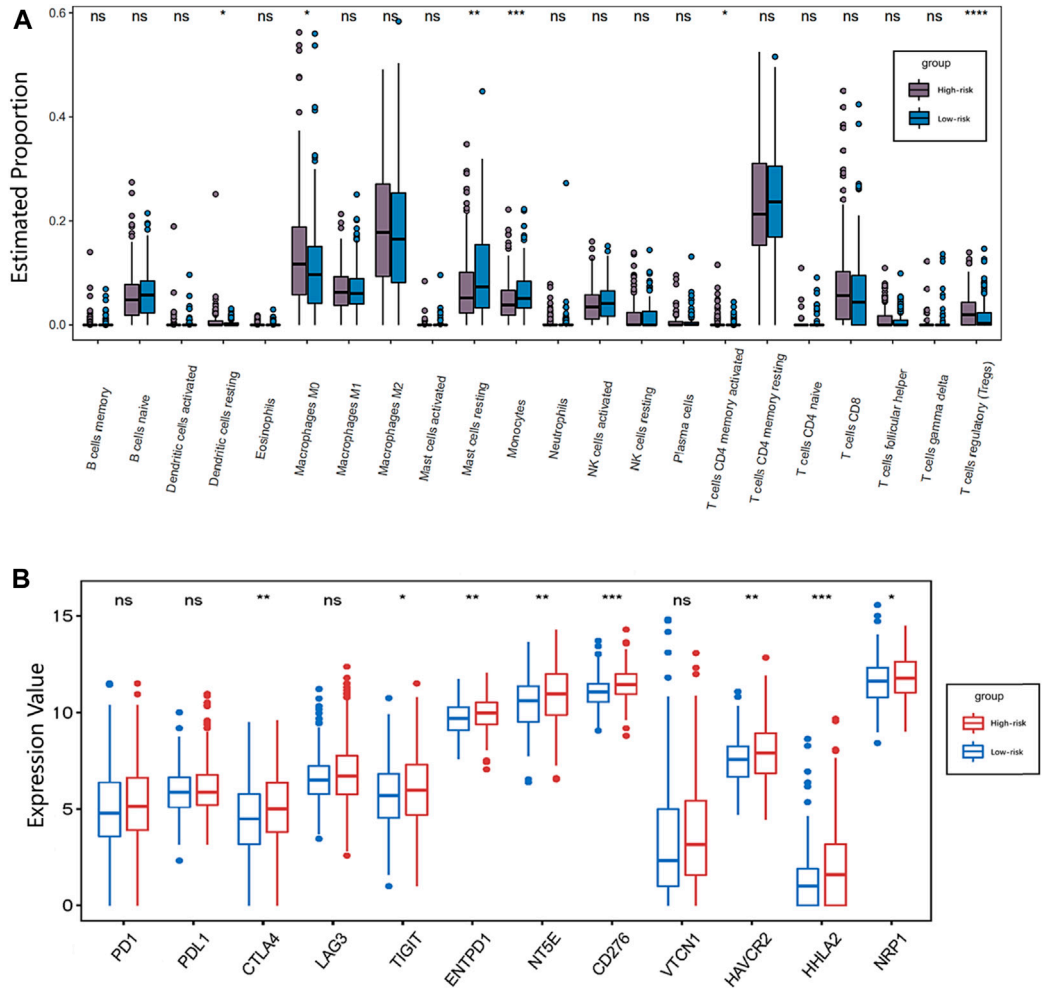

FIGURE 6 | Immunotherapy response analysis. **(A)** Boxplot showing the association between IFLSig and immune cell lines; ANOVA was used as the significance test, *$p < 0.05$, **$p < 0.01$, ***$p < 0.001$, and ****$p < 0.0001$. **(B)** Boxplot showing the association between IFLSig and immune checkpoints; ANOVA was used as the significance test, *$p < 0.05$, **$p < 0.01$, ***$p < 0.001$, and ****$p < 0.0001$. GSEA, Gene Set Enrichment Analysis; KEGG, Kyoto Encyclopedia of Genes and Genomes; TCGA, The Cancer Genome Atlas.

The Potential of IFLSig for Immunotherapy With HCC

To better investigate the complex crosstalk between IFLSig and immune characteristics, we evaluated the immune infiltration profiles of 22 immune infiltration cells in HCC samples by using the CIBERSORT. The proportion of immune profiles and correlation heatmap are shown in **Supplementary Figures S2A,B**. We further compared the association between immune infiltration cells and IFLSig, and the immune infiltration of most immune cell subtypes was visibly decreased in the high-risk group. Notably, dendritic cells in resting ($p < 0.05$), macrophages in M0 ($p < 0.05$), activated CD4 memory T cells ($p < 0.05$), mast cells in resting ($p < 0.01$), monocytes ($p < 0.001$), and regulatory T cells (Tregs, $p < 0.0001$) increased significantly in HCC patients in the high-risk group (**Figure 6A**). It is consistent with previous observations linking higher expression of Tregs and macrophages to tumor progression and immunosuppression. Tumor immune infiltration can be adjusted by the immune checkpoints, so we compared the expression value of 12 immune checkpoints and IFLSig. As shown in **Figure 6B**, the difference in the expressions of CTLA-4 ($p < 0.01$), TIGIT ($p < 0.05$), NRP1 ($p < 0.05$), ENTPD1 ($p < 0.01$), NT5E ($p < 0.01$), HAVCR2 ($p < 0.01$), CD276 ($p < 0.001$), and HHLA2 ($p < 0.001$) was statistically significant. These results indicate that IFLncRNA might be a potential predictive biomarker of response to ICI immunotherapy for HCC.

Heterogeneous Drug Resistance and Sensitivity With IFLSig

Drug resistance to many chemotherapeutic drugs often occurs during the process of cancer treatment, which leads to poor drug

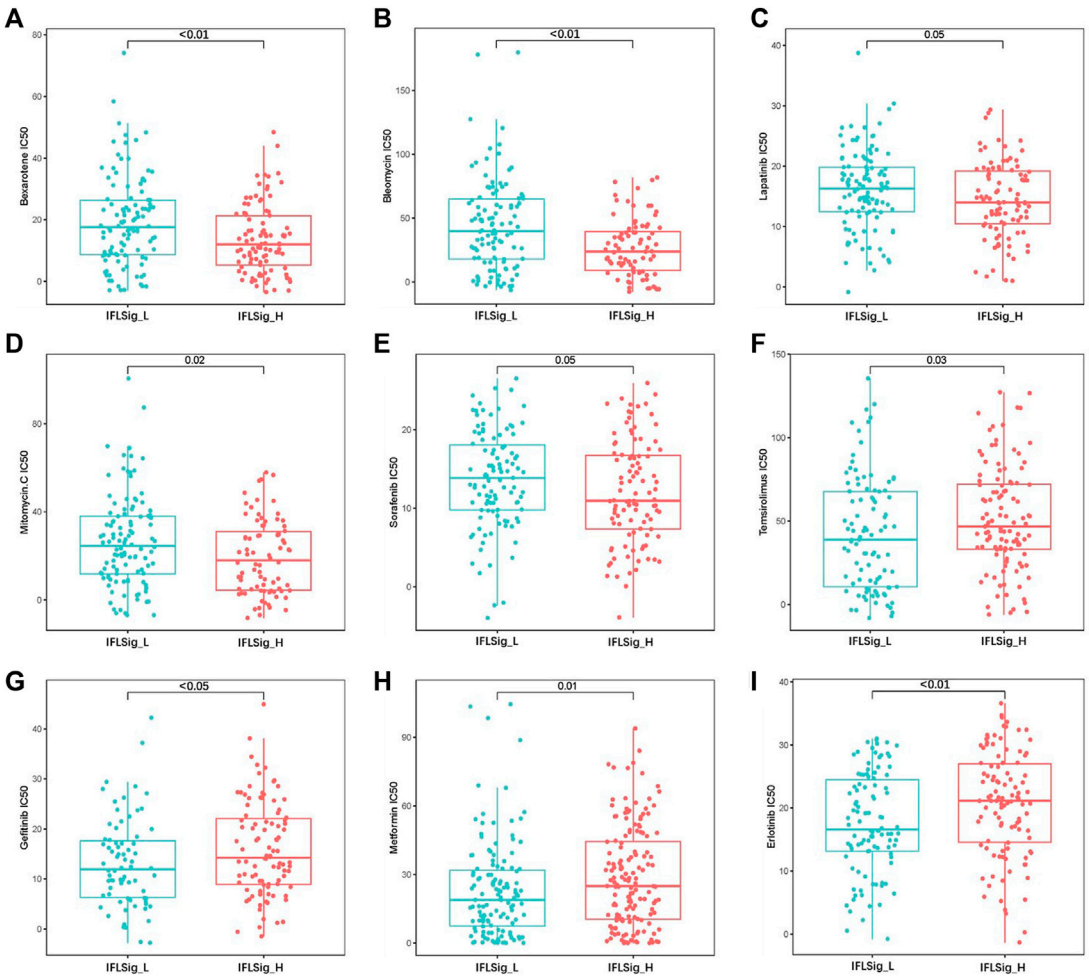

FIGURE 7 | Drug resistance and sensitivity analysis in the low-risk and high-risk groups.

efficacy in liver cancer and worse clinical outcomes. To verify the application of IFLSig in chemotherapy, we compared the half-maximal inhibitory concentration (IC50) and IFLSig. IC50 can help to quantify the therapeutic capacity of a drug to induce cancer apoptosis, which is inversely related to the sensitivity of chemotherapeutics. We evaluated the chemotherapeutic effects of 30 anti-tumor drugs on patients with HCC, and those with $p >$ 0.05 were removed. As shown in **Figure 7**, the IC50 of gefitinib ($p < 0.05$), mitomycin ($p = 0.02$), temsirolimus ($p = 0.03$), and erlotinib ($p < 0.01$) was significantly higher in the high-risk group than in the low-risk group, which means that patients with high IFLSig may not benefit from these drugs. The IC50 of bexarotene ($p < 0.01$), metformin ($p = 0.01$), sorafenib ($p = 0.05$), bleomycin ($p < 0.01$), and lapatinib ($p = 0.05$) was significantly lower in the high-risk group, and therefore, these chemotherapeutic drugs may have a greater effect on patients with high IFLSig. It showed that IFLSig can not only segregate individuals into different risk groups but can also assist in selecting chemotherapeutic drug pools based on the sensitivity values corresponding to the HCC patients under clinical observation.

Identification and Validation of a Nomogram

The nomogram is a reliable tool to estimate individualized risk score in cancer patients. In this study, we constructed a nomogram based on the entire TCGA set by using the multivariate Cox regression analysis of the IFLSig and other clinicopathological covariables (**Figure 8A**), and it was internally validated in the training cohort and test cohort by using the *C*-index. The *C*-index of the nomogram was 0.675 (95% CI: 0.623–0.727) in the entire TCGA set, 0.7108 (95% CI: 0.653–0.769) in the training cohort, and 0.633 (95% CI: 0.539–0.726) in the test cohort. The AUC of the nomogram were 0.761, 0.704, and 0.715 for 1, 3, and 5 years, respectively, showing that the nomogram had a good level of specificity and sensitivity for OS (**Figure 8B**). The calibration plot is in agreement with the diagonal line, and it confirmed the predictive value of the prognostic nomogram for OS at 1, 3, and 5 years (**Figure 8C**). All the results demonstrated that the nomogram constructed by IFLSig had good prognostic power in HCC patients.

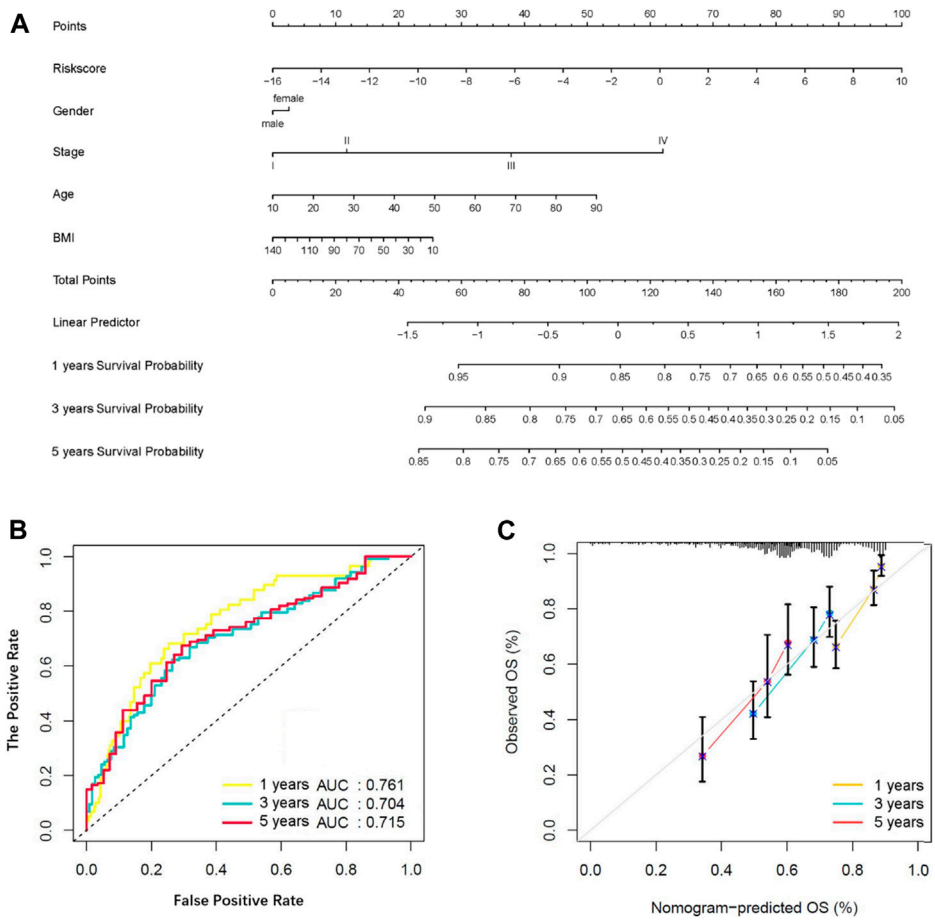

FIGURE 8 | Construction and verification of a nomogram. **(A)** Survival nomogram based on total TCGA cohort. **(B)** The ROC curve compared the prognostic power of the nomogram at 1, 3, and 5 years in the TCGA cohort. **(C)** The calibration curve for predicting HCC patient survival at 1, 3, and 5 years in the TCGA cohort.

DISCUSSION

Recently, lncRNA has been suggested to play an important role in the oncogenesis and progression of HCC (Ding et al., 2018; Guo et al., 2020). Multiple lncRNAs have been suggested to possess aberrant expression and participate in cancerous phenotypes through their binding with hereditary substances, encoding proteins or other small molecule peptides (Wong et al., 2018; Pan et al., 2019; Peng et al., 2020). Simultaneously, clinical management places emphasis on the importance of early and effective disease detection and prediction of prognosis. This requires finding the right types of components, biomarkers, and detection methods that could be applied to tumor detection and treatment. Historically, some prognostic models have been constructed for clinical practice, but the accuracy, safety, and effectiveness should be evaluated over a long period of time. Therefore, we developed a lncRNA prognostic risk model combined with ferroptosis and immunity to provide new insights into HCC pathogenesis and an effective tool for predicting the treatment efficacy of HCC, which may help bring about additional therapeutic and prognostic benefits. Research suggests that immunity is suppressed in the process of hepatocarcinogenesis, so we selected downregulated immune genes to develop the prognostic model linked to previous studies (Sun et al., 2020; Zhou et al., 2021). In this study, cancer samples were allocated into IFLSig high-risk group and low-risk group. IFLSig was the dominant factor in the prognostic risk model and nomogram. Our results achieved a satisfactory association with clinical outcomes, which suggested that IFLSig is an excellent prediction risk factor. We analyzed the resistance and sensitivity of chemotherapeutic drugs to verify the predictive potential of IFLSig to determine therapeutic efficacy. In summary, we have developed an IFLSig index that was closely associated with the prognosis of HCC, and it combines immunological characteristics to better estimate OS and can predict clinical therapy response for HCC. Our IFLSig model would hopefully provide new insights into HCC pathogenesis and novel tools to improve prognosis prediction and determination of treatment efficacy in patients with HCC.

IFLncRNA has been confirmed to exert a pivotal function in the proliferation, differentiation, invasion, and metastasis of liver tumors through different pathways in tumors progression and pathogenesis. Presently, it has been confirmed that ZFPM2-AS1, LINC01224, and LUCAT1 possess differing expression levels in liver cancer tissues and are involved in multiple processes promoting hepatocarcinogenesis, including enhancing proliferation of tumor cells, anti-apoptosis, improving the migration ability of cancer cells, and strengthening the invasiveness of cancer cells (He et al., 2020; Liu et al., 2020). LINC01224 can specifically upregulate the anti-apoptotic protein CHEK1 to influence the cancer cells (Gong et al., 2020). LUCAT1 can activate the metalloproteinase protein, regulating the expression of DLC1, and enhance the malignant phenotype of hepatoma cells (Lou et al., 2019; Wu et al., 2020). GDNF-AS1 is a natural antisense transcript that can increase the expression of site-specific gene GDNF after its knockout (Modarresi et al., 2012). GDNF can significantly activate hepatic stellate fibroblasts and promote liver fibrosis, participate in the microenvironment of liver cancer, affect the metabolism of extracellular matrix, and is closely related to the occurrence and progression of primary liver cancer (Tao et al., 2019; Barry et al., 2020).

In the tumor microenvironment, cancer cells and immune cells exert a great number of chemokines and cytokines to regulate tumor pathogenesis and progression. In this study, we found that the increase in regulatory T cells was particularly significant. The robust immunosuppressive microenvironment in cancer represents a crucial challenge for cancer treatment. Tregs and tumor-associated macrophages can directly decrease the proliferation of T cells in the immune microenvironment (Peterson et al., 2018; Ohue and Nishikawa, 2019). It can also influence tumor aggressiveness by affecting lactate metabolism (Wang et al., 2020). Our study suggested that IFLncRNA of HCC patients might be related to immune escape. However, the mechanism between IFLncRNA and Tregs remains obscure, and further research will be required to resolve this question. We further evaluated the expression level of these immunosuppressive checkpoint inhibitors, and IFLSig showed great relativity with CTLA-4, TIGIT, NRP1, ENTPD1, NT5E, HAVCR2, CD276, and HHLA2. In addition, the immunotherapy of anti-CTLA4 has been widely used in the treatment of liver cancer (Agdashian et al., 2019; Lai et al., 2021; Martini et al., 2021). Based on GSEA, we found that IFLSig was enriched in ubiquitin-mediated proteolysis, RNA degradation, lysosome, and cell cycle, which can strongly influence the metabolism of PD1 and PDL1. Although there is no significant difference between IFLSig and PD1 or PDL1, IFLSig may influence PD1 and PDL1 by affecting the above-listed molecular mechanisms (Burr et al., 2017; Gou et al., 2020; Kalbasi and Ribas, 2020; Zhong et al., 2021). In summary, we believe the results show that IFLSig has the potential in predicting the effectiveness of immunotherapy.

There are some shortcomings in this study. The prediction capacity of the motioned prognostic signature failed to be authenticated in the GEO cohort and ICGC cohort because none of the cases included the expression array of IFLncRNA. We were also concerned about whether the plain correlation test can accurately calculate the correlation between lncRNA, ferroptosis, and immunity. It should be noted that this study is a retrospective analysis based on bioinformatics data without yet the validation of a prospective analysis. Therefore, more experimental and clinical data are needed for verification.

CONCLUSION

In conclusion, we developed an IFLSig prognostic index based on eight IFLncRNAs, which are related to the clinical outcomes of HCC, by performing many bioinformatics statistical analyses. The IFLSig can be considered an independent prognostic signature that may be able to estimate the OS and clinical therapy response in HCC patients. This study provides a new understanding of IFLncRNA in the development and progression of HCC.

DATA AVAILABILITY STATEMENT

The original contributions presented in the study are included in the article/**Supplementary Material**, further inquiries can be directed to the corresponding author.

AUTHOR CONTRIBUTIONS

AH and JX conceived the structure of the manuscript. AH, TL, and XX drafted and revised the manuscript. AH, TL, and XX made the figures and tables. All authors contributed to the article and approved the submitted version.

ACKNOWLEDGMENTS

The datasets and recourse for this study can be found in TCGA, CIBERSORT, GSEA, ImmPort, and FerrDb public databases. Therefore, we are very grateful to all the employees of these databases for providing such excellent platforms.

SUPPLEMENTARY MATERIAL

The Supplementary Material for this article can be found online at: https://www.frontiersin.org/articles/10.3389/fmolb.2021.759173/full#supplementary-material

REFERENCES

Agdashian, D., ElGindi, M., Xie, C., Sandhu, M., Pratt, D., Kleiner, D. E., et al. (2019). The Effect of Anti-CTLA4 Treatment on Peripheral and Intra-tumoral T Cells in Patients with Hepatocellular Carcinoma. *Cancer Immunol. Immunother.* 68 (4), 599–608. doi:10.1007/s00262-019-02299-8

Barry, A. E., Baldeosingh, R., Lamm, R., Patel, K., Zhang, K., Dominguez, D. A., et al. (2020). Hepatic Stellate Cells and Hepatocarcinogenesis. *Front. Cel Dev. Biol.* 8, 709. doi:10.3389/fcell.2020.00709

Bray, F., Ferlay, J., Soerjomataram, I., Siegel, R. L., Torre, L. A., and Jemal, A. (2018). Global Cancer Statistics 2018: GLOBOCAN Estimates of Incidence and Mortality Worldwide for 36 Cancers in 185 Countries. *Ca: A. Cancer J. Clin.* 68 (6), 394–424. doi:10.3322/caac.21492

Burr, M. L., Sparbier, C. E., Chan, Y.-C., Williamson, J. C., Woods, K., Beavis, P. A., et al. (2017). CMTM6 Maintains the Expression of PD-L1 and Regulates Anti-tumour Immunity. *Nature* 549 (7670), 101–105. doi:10.1038/nature23643

Chew, C. L., Conos, S. A., Unal, B., and Tergaonkar, V. (2018). Noncoding RNAs: Master Regulators of Inflammatory Signaling. *Trends Mol. Med.* 24 (1), 66–84. doi:10.1016/j.molmed.2017.11.003

Ding, B., Lou, W., Xu, L., and Fan, W. (2018). Non-coding RNA in Drug Resistance of Hepatocellular Carcinoma. *Biosci. Rep.* 38 (5), BSR20180915. doi:10.1042/bsr20180915

Feng, R.-M., Zong, Y.-N., Cao, S.-M., and Xu, R.-H. (2019). Current Cancer Situation in China: Good or Bad News from the 2018 Global Cancer Statistics? *Cancer Commun.* 39 (1), 22. doi:10.1186/s40880-019-0368-6

Gao, M., Monian, P., Quadri, N., Ramasamy, R., and Jiang, X. (2015). Glutaminolysis and Transferrin Regulate Ferroptosis. *Mol. Cel.* 59 (2), 298–308. doi:10.1016/j.molcel.2015.06.011

Gong, D., Feng, P.-C., Ke, X.-F., Kuang, H.-L., Pan, L.-L., Ye, Q., et al. (2020). Silencing Long Non-coding RNA LINC01224 Inhibits Hepatocellular Carcinoma Progression via MicroRNA-330-5p-Induced Inhibition of CHEK1. *Mol. Ther. Nucleic Acids* 19, 482–497. doi:10.1016/j.omtn.2019.10.007

Gou, Q., Dong, C., Xu, H., Khan, B., Jin, J., Liu, Q., et al. (2020). PD-L1 Degradation Pathway and Immunotherapy for Cancer. *Cell Death Dis.* 11 (11), 955. doi:10.1038/s41419-020-03140-2

Guo, T., Gong, C., Wu, P., Battaglia-Hsu, S.-F., Feng, J., Liu, P., et al. (2020). LINC00662 Promotes Hepatocellular Carcinoma Progression via Altering Genomic Methylation Profiles. *Cell Death Differ.* 27 (7), 2191–2205. doi:10.1038/s41418-020-0494-3

He, H., Wang, Y., Ye, P., Yi, D., Cheng, Y., Tang, H., et al. (2020). Long Noncoding RNA ZFPM2-AS1 Acts as a miRNA Sponge and Promotes Cell Invasion through Regulation of miR-139/GDF10 in Hepatocellular Carcinoma. *J. Exp. Clin. Cancer Res.* 39 (1), 159. doi:10.1186/s13046-020-01664-1

Jiang, X., Stockwell, B. R., and Conrad, M. (2021). Ferroptosis: Mechanisms, Biology and Role in Disease. *Nat. Rev. Mol. Cel Biol.* 22 (4), 266–282. doi:10.1038/s41580-020-00324-8

Kalbasi, A., and Ribas, A. (2020). Tumour-intrinsic Resistance to Immune Checkpoint Blockade. *Nat. Rev. Immunol.* 20 (1), 25–39. doi:10.1038/s41577-019-0218-4

Lai, E., Astara, G., Ziranu, P., Pretta, A., Migliari, M., Dubois, M., et al. (2021). Introducing Immunotherapy for Advanced Hepatocellular Carcinoma Patients: Too Early or Too Fast? *Crit. Rev. Oncol. Hematol.* 157, 103167. doi:10.1016/j.critrevonc.2020.103167

Liu, W., Zhang, G. Q., Zhu, D. Y., Wang, L. J., Li, G. T., Xu, J. G., et al. (2020). Long Noncoding RNA ZFPM2-AS1 Regulates ITGB1 by miR-1226-3p to Promote Cell Proliferation and Invasion in Hepatocellular Carcinoma. *Eur. Rev. Med. Pharmacol. Sci.* 24 (14), 7612–7620. doi:10.26355/eurrev_202007_22259

Lou, Y., Yu, Y., Xu, X., Zhou, S., Shen, H., Fan, T., et al. (2019). Long Non-coding RNA LUCAT1 Promotes Tumourigenesis by Inhibiting ANXA2 Phosphorylation in Hepatocellular Carcinoma. *J. Cel Mol. Med.* 23 (3), 1873–1884. doi:10.1111/jcmm.14088

Martini, G., Ciardiello, D., Paragliola, F., Nacca, V., Santaniello, W., Urraro, F., et al. (2021). How Immunotherapy Has Changed the Continuum of Care in Hepatocellular Carcinoma. *Cancers* 13 (18), 4719. doi:10.3390/cancers13184719

Modarresi, F., Faghihi, M. A., Lopez-Toledano, M. A., Fatemi, R. P., Magistri, M., Brothers, S. P., et al. (2012). Inhibition of Natural Antisense Transcripts *In Vivo* Results in Gene-specific Transcriptional Upregulation. *Nat. Biotechnol.* 30 (5), 453–459. doi:10.1038/nbt.2158

Ohue, Y., and Nishikawa, H. (2019). Regulatory T (Treg) Cells in Cancer: Can Treg Cells Be a New Therapeutic Target? *Cancer Sci.* 110 (7), 2080–2089. doi:10.1111/cas.14069

Ou, Y., Wang, S.-J., Li, D., Chu, B., and Gu, W. (2016). Activation of SAT1 Engages Polyamine Metabolism with P53-Mediated Ferroptotic Responses. *Proc. Natl. Acad. Sci. USA* 113 (44), E6806–E6812. doi:10.1073/pnas.1607152113

Pan, W., Li, W., Zhao, J., Huang, Z., Zhao, J., Chen, S., et al. (2019). Lnc RNA - PDPK 2P Promotes Hepatocellular Carcinoma Progression through the PDK 1/AKT/Caspase 3 Pathway. *Mol. Oncol.* 13 (10), 2246–2258. doi:10.1002/1878-0261.12553

Peng, L., Chen, Y., Ou, Q., Wang, X., and Tang, N. (2020). LncRNA MIAT Correlates with Immune Infiltrates and Drug Reactions in Hepatocellular Carcinoma. *Int. Immunopharmacol.* 89 (Pt A), 107071. doi:10.1016/j.intimp.2020.107071

Peterson, L. B., Bell, C. J. M., Howlett, S. K., Pekalski, M. L., Brady, K., Hinton, H., et al. (2018). A Long-Lived IL-2 Mutein that Selectively Activates and Expands Regulatory T Cells as a Therapy for Autoimmune Disease. *J. Autoimmun.* 95, 1–14. doi:10.1016/j.jaut.2018.10.017

Sun, J., Zhang, Z., Bao, S., Yan, C., Hou, P., Wu, N., et al. (2020). Identification of Tumor Immune Infiltration-Associated lncRNAs for Improving Prognosis and Immunotherapy Response of Patients with Non-small Cell Lung Cancer. *J. Immunother. Cancer* 8 (1), e000110. doi:10.1136/jitc-2019-000110

Sun, X., Niu, X., Chen, R., He, W., Chen, D., Kang, R., et al. (2016). Metallothionein-1G Facilitates Sorafenib Resistance through Inhibition of Ferroptosis. *Hepatology* 64 (2), 488–500. doi:10.1002/hep.28574

Tang, R., Xu, J., Zhang, B., Liu, J., Liang, C., Hua, J., et al. (2020). Ferroptosis, Necroptosis, and Pyroptosis in Anticancer Immunity. *J. Hematol. Oncol.* 13 (1), 110. doi:10.1186/s13045-020-00946-7

Tao, L., Ma, W., Wu, L., Xu, M., Yang, Y., Zhang, W., et al. (2019). Glial Cell Line-Derived Neurotrophic Factor (GDNF) Mediates Hepatic Stellate Cell Activation via ALK5/Smad Signalling. *Gut* 68 (12), 2214–2227. doi:10.1136/gutjnl-2018-317872

Vitale, I., Manic, G., Coussens, L. M., Kroemer, G., and Galluzzi, L. (2019). Macrophages and Metabolism in the Tumor Microenvironment. *Cel Metab.* 30 (1), 36–50. doi:10.1016/j.cmet.2019.06.001

Wang, G., Xie, L., Li, B., Sang, W., Yan, J., Li, J., et al. (2021). A Nanounit Strategy Reverses Immune Suppression of Exosomal PD-L1 and Is Associated with Enhanced Ferroptosis. *Nat. Commun.* 12 (1), 5733. doi:10.1038/s41467-021-25990-w

Wang, H., Franco, F., Tsui, Y.-C., Xie, X., Trefny, M. P., Zappasodi, R., et al. (2020). CD36-mediated Metabolic Adaptation Supports Regulatory T Cell Survival and Function in Tumors. *Nat. Immunol.* 21 (3), 298–308. doi:10.1038/s41590-019-0589-5

Wang, X., Sun, W., Shen, W., Xia, M., Chen, C., Xiang, D., et al. (2016). Long Non-coding RNA DILC Regulates Liver Cancer Stem Cells via IL-6/STAT3 axis. *J. Hepatol.* 64 (6), 1283–1294. doi:10.1016/j.jhep.2016.01.019

Wang, Y., He, L., Du, Y., Zhu, P., Huang, G., Luo, J., et al. (2015). The Long Noncoding RNA lncTCF7 Promotes Self-Renewal of Human Liver Cancer Stem Cells through Activation of Wnt Signaling. *Cell Stem Cell* 16 (4), 413–425. doi:10.1016/j.stem.2015.03.003

Wong, C.-M., Tsang, F. H.-C., and Ng, I. O.-L. (2018). Non-coding RNAs in Hepatocellular Carcinoma: Molecular Functions and Pathological Implications. *Nat. Rev. Gastroenterol. Hepatol.* 15 (3), 137–151. doi:10.1038/nrgastro.2017.169

Wu, H., Liu, T., Qi, J., Qin, C., and Zhu, Q. (2020). Four Autophagy-Related lncRNAs Predict the Prognosis of HCC through Coexpression and ceRNA Mechanism. *Biomed. Res. Int.* 2020, 1–19. doi:10.1155/2020/3801748

Wu, J., Zhu, P., Lu, T., Du, Y., Wang, Y., He, L., et al. (2019). The Long Non-coding RNA LncHDAC2 Drives the Self-Renewal of Liver Cancer Stem Cells via Activation of Hedgehog Signaling. *J. Hepatol.* 70 (5), 918–929. doi:10.1016/j.jhep.2018.12.015

Xu, H., Ye, D., Ren, M., Zhang, H., and Bi, F. (2021). Ferroptosis in the Tumor Microenvironment: Perspectives for Immunotherapy. *Trends Mol. Med.* 27 (9), 856–867. doi:10.1016/j.molmed.2021.06.014

Xu, X., Gu, J., Ding, X., Ge, G., Zang, X., Ji, R., et al. (2019). LINC00978 Promotes the Progression of Hepatocellular Carcinoma by Regulating EZH2-Mediated Silencing of P21 and E-Cadherin Expression. *Cel Death Dis.* 10 (10), 752. doi:10.1038/s41419-019-1990-6

Yuan, J.-h., Liu, X.-n., Wang, T.-t., Pan, W., Tao, Q.-f., Zhou, W.-p., et al. (2017). The MBNL3 Splicing Factor Promotes Hepatocellular Carcinoma by Increasing PXN Expression through the Alternative Splicing of lncRNA-PXN-AS1. *Nat. Cel Biol.* 19 (7), 820–832. doi:10.1038/ncb3538

Zheng, S., Zou, Y., Liang, J. y., Xiao, W., Yang, A., Meng, T., et al. (2020). Identification and Validation of a Combined Hypoxia and Immune index for Triple-negative Breast Cancer. *Mol. Oncol.* 14 (11), 2814–2833. doi:10.1002/1878-0261.12747

Zhong, R., Zhang, Y., Chen, D., Cao, S., Han, B., and Zhong, H. (2021). Single-cell RNA Sequencing Reveals Cellular and Molecular Immune Profile in a Pembrolizumab-Responsive PD-L1-Negative Lung Cancer Patient. *Cancer Immunol. Immunother.* 70 (8), 2261–2274. doi:10.1007/s00262-021-02848-0

Zhou, M., Zhang, Z., Bao, S., Hou, P., Yan, C., Su, J., et al. (2021). Computational Recognition of lncRNA Signature of Tumor-Infiltrating B Lymphocytes with Potential Implications in Prognosis and Immunotherapy of Bladder Cancer. *Brief Bioinform.* 22 (3), bbaa047. doi:10.1093/bib/bbaa047

Conflict of Interest: The authors declare that the research was conducted in the absence of any commercial or financial relationships that could be construed as a potential conflict of interest.

Publisher's Note: All claims expressed in this article are solely those of the authors and do not necessarily represent those of their affiliated organizations, or those of the publisher, the editors, and the reviewers. Any product that may be evaluated in this article, or claim that may be made by its manufacturer, is not guaranteed or endorsed by the publisher.

frontiers in Molecular Biosciences

REVIEW
published: 05 January 2022
doi: 10.3389/fmolb.2021.791927

Metabolic Reprogramming Underlying Brain Metastasis of Breast Cancer

Baoyi Liu[1] *and Xin Zhang*[1,2,3]*

[1]Clinical Experimental Center, Jiangmen Key Laboratory of Clinical Biobanks and Translational Research, Jiangmen Central Hospital, Jiangmen, China, [2]Dongguan Key Laboratory of Medical Bioactive Molecular Developmental and Translational Research, Guangdong Provincial Key Laboratory of Medical Molecular Diagnostics, Guangdong Medical University, Dongguan, China, [3]Collaborative Innovation Center for Antitumor Active Substance Research and Development, Guangdong Medical University, Zhanjiang, China

The development of brain metastasis is a major cause of death in patients with breast cancer, characterized by rapid progression of the disease and poor prognosis, and lack of effective treatment has existed as an unresolved issue clinically. Extensive research has shown that a variety of metabolic changes associated with cellular metastasis exist in primary breast cancer or brain metastases, therefore to elucidate metabolic characteristics at each step of the metastasis cascade will provide important clues to the efficient treatment. In this review, we discuss the changes in metabolic patterns of breast cancer cells at every step of metastasis for exploring the potential therapeutic target based on metabolic reprogramming, and provide new insights on the design and development of drugs for breast cancer brain metastasis.

Keywords: metabolic reprogramming, breast cancer, brain metastasis, metastatic cascade, drug targets

OPEN ACCESS

Edited by:
Wei Zhao,
City University of Hong Kong, Hong Kong SAR, China

Reviewed by:
Xue-Yan He,
Cold Spring Harbor Laboratory, United States
Xiawei Cheng,
East China University of Science and Technology, China

***Correspondence:**
Xin Zhang
zhangx45@mail3.sysu.edu.cn

Specialty section:
This article was submitted to Molecular Diagnostics and Therapeutics, a section of the journal Frontiers in Molecular Biosciences

Received: *09 October 2021*
Accepted: *08 December 2021*
Published: *05 January 2022*

Citation:
Liu B and Zhang X (2022) Metabolic Reprogramming Underlying Brain Metastasis of Breast Cancer. Front. Mol. Biosci. 8:791927. doi: 10.3389/fmolb.2021.791927

INTRODUCTION

In the process of cancer development, about 20% patients with cancer will develop brain metastasis, whose common primary tumors are lung cancer, breast cancer, colorectal cancer and melanoma. Breast cancer is second frequently to metastasize to the brain, whose incidence is estimated to be 5–20% (Achrol et al., 2019). In fact, it's supposed to have a higher incidence since those patients without neurological symptoms were not recommend to receive brain MRI screening (Ramakrishna et al., 2014). Multiple studies have demonstrated that the prevalence of brain metastases of breast cancer is increasing, and the patients have rapid progression of the disease and poor prognosis (Martin et al., 2017; Kuksis et al., 2021). To date, lack of effective drugs for brain metastasis has existed as a major challenge. There are two contributing factors mainly responsible for the difficulties of treatment in brain metastases: the limitation of access of systemic drugs by several barriers in the central nervous system (CNS), and the differences of molecular characteristics as well as microenvironment between brain metastases and primary lesions. Consequently, research on the pathogenesis of brain metastasis is of great significance for finding drug targets.

Metastasis establishment is a dynamic process, referred to as invasion-metastatic cascade. As a first step, cancer cells invade locally then intravasate into nearby blood and lymphatic vessels, followed by transit through the lymphatic and hematogenous systems, and finally cancer cells in the circulation manage to extravasate from vessels then grow into metastatic lesions (Chaffer and Weinberg, 2011; Valastyan and Weinberg, 2011). Actually, brain metastatic cells differ from primary breast cancer cells in a number of important ways. Brain metastatic cells need to acquire certain metastatic trails to escape from apoptosis, migrate to the brain, break through the blood-brain barrier and able to survive and grow in the brain, therefore metabolic changes have a pivotal role in

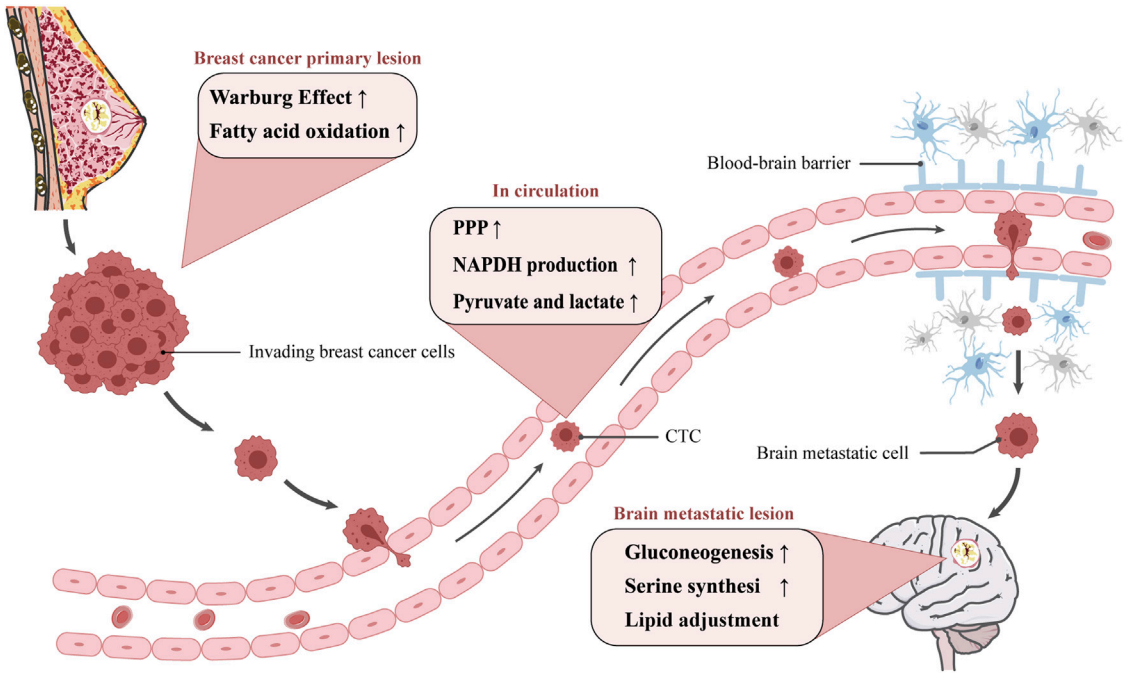

FIGURE 1 | The metabolism adjustment of breast cancer cells migrating to brain. Diagram depicting potential mechanism of cellular metabolic reprogramming during different step of metastatic cascade. The metastatic route is simplified to be in the primary lesion, in circulation, and in the brain metastatic lesion. The possible metabolic reprogramming of breast cancer cells at various stages is outlined in the pink boxes.

metastasis formation (Bergers and Fendt, 2021). This review set out to mainly discuss metabolic traits during different step of metastatic cascade (**Figure 1**) and explore potential metabolism-based therapeutic strategies.

METABOLIC REPROGRAMMING IN BREAST CANCER WITH BRAIN METASTASIS

Metabolic Reprogramming in Invading Breast Cancer Cells

The first step of metastatic cascade is invasion of nearby tissues by cancer cells. Cancer cells of primary lesion probably go through epithelial-mesenchymal transition (EMT) to become motile and invasive. Although no definite pattern of metabolic changes has been identified that discriminates invasive from noninvasive cancer, several studied have shown that breast cancer cells undergoing EMT display enhanced glycolysis and lipid metabolism, and this metabolic change may help tumor cells to obtain local invasion ability.

Warburg Effect May Induce EMT to Promote Tumor Metastasis

The energy metabolism of most tumor cells shows notable differences compared with normal cells. Normal cells utilize the capacity of mitochondrial oxidative phosphorylation, while most tumor cells utilize aerobic glycolysis, which has been termed the Warburg effect (Warburg et al., 1927). The change of energy pattern is linked to the metastasis of breast cancer. On the one hand, abnormal expression of glucose metabolism enzymes like hexokinase (HK) and Pyruvate kinase M2 (PKM2) was found in primary breast cancer tissues. When their expressions are down-regulated, the glycolytic activity and lactate expression will be decreased, thereby preventing tumor growth and development (Zhang et al., 2019; Yu et al., 2020). Moreover, Fructose-1,6-bisphosphatases (FBP) has been found to be inhibited by Snail-G9a-Dnmt1 complex in basal-like breast cancer (BLBC), and Snail is critical for E-cadherin promoter silencing (Dong et al., 2013).

On the other hand, there is evidence that certain metabolites of aerobic glycolysis enable cancer cells migration by participating in modulating activity of signaling pathways, for example, increased pyruvate and lactate metabolism directly stimulate the invasion and migration potential of cancer cells. The acidification of the microenvironment caused by the increased lactate, an end-product of glycolysis, entered the endothelial cells through lactate transporters such as MCT1 which activated transcription factor NF-κB to promote cancer cell migration. NF-κB is involved in the degradation of extracellular matrix (ECM) and angiogenesis, and related to the inducement of EMT (Payen et al., 2016; Payen et al., 2017). In addition, the formation of methylglyoxal, through aerobic glycolysis, resulted in elevated nuclear YAP (Nokin et al., 2016), which is a key transcriptional co-activator for regulating tumor growth and invasion (Lundo et al., 2020). Thus, presumably enhanced aerobic glycolysis directly or indirectly contribute to promote tumor invasion and migration by driving ECM degradation and EMT program.

Asparagine and Glutamine Metabolism Co-Regulate Tumor Cell Metastasis

Asparagine and glutamine are likely to work in concert to drive tumor growth and metastasis by regulating cell survival, growth, and EMT regulatory pathways (Luo et al., 2018). In a mouse model of breast cancer, the asparagine content in the protein driving the EMT is selectively increased, suggesting that the asparagine in part governs metastasis by modulating the EMT program. Of note, aspartic acid can be converted into asparagine by asparagine synthetase (ASNS), and reduction of asparagine by knockdown of ASNS or treatment with bacterial L-asparaginase reduces breast cancer invasion, circulating tumor cells (CTC), and metastasis without affecting primary tumor growth (Knott et al., 2018).

Both glutamine and glucose are crucial fuel for cancer cells and generate biosynthetic intermediates for the synthesis of macromolecules (Vander Heiden and DeBerardinis, 2017). A study has revealed that the conversion of glutamine to glutamate in invasive breast cancer cells activated up-regulation of MT1-MMP, leading to basement membrane disruption and cell invasiveness (Dornier et al., 2017). It was surprising that as extracellular glutamine levels declined, tumor cells became asparagine-dependent for proliferation and protein synthesis (Pavlova et al., 2018).

Together, the studies described above support the notion that asparagine and glutamine jointly regulate the survival, growth, and metastasis of tumor cells, but it remains elusive as to how they affect the EMT-related protein during the invasion stage.

Fatty Acid Metabolism Provides Energy for Tumor Cell Invasion

To some extent, lipid metabolic adjustment is correlated with the occurrence and metastasis of breast cancer. For example, fatty acids probably can be oxidized to fuel for tumor cell invasion. Previous studied has documented compared with the adipocytes cultured alone, the fatty acid oxidation of breast cancer cells was significantly increased when cocultured with adipocytes (Wang et al., 2017). If co-cultivated cells were injected into mice from their tail vein, the metastasis ability of these cancer cells in mice was significantly enhanced (Dirat et al., 2011). Besides, breast cancer cells down-regulated the mitochondrial protein LACTB by ZEB1, resulting in increased phospholipid metabolism, cancer cell proliferation, and EMT inducement (Keckesova et al., 2017). Intriguingly, the overexpression of human epidermal growth factor receptor 2 (HER2) was observed to indirectly activated ZEB1 to promote cell migration (Zeng et al., 2019).

Although the potential mechanistic link between fatty acid metabolism and metastasis formation has not been disclosed, studies have confirmed that CD36, which is highly expressed in a variety of metastatic cancer cells, regulates fatty acid metabolism and plays an important role in the invasion and metastasis of various types of tumors (Pascual et al., 2017). CD36 is a transmembrane protein that promotes fatty acid entry into cells. The secretion of breast-associated adipocytes induced CD36 expression, thereby enhancing the ability of breast cancer cells to uptake fatty acid and their invasiveness *in vitro*. In line with this, inhibition of CD36 reduced lipid droplet accumulation and weakened the aggressiveness of breast cancer cell lines (Zaoui et al., 2019). Thus, CD36 may serve as an important regulatory factor mediating reprogramming of fatty acid metabolism in breast cancer cells.

As a precursor of lipid synthesis and the end product of fatty acid β-oxidation, changes in acetyl-CoA levels can also affect lipid anabolism in tumor cells. Phenotypically, increased invasiveness of breast cancer cells was induced by the upregulation of acetyl-CoA (Schug et al., 2015). Mechanistically, leptin and TGF-β1 inhibited the lipogenic enzyme acetyl-CoA carboxylase (ACC) 1 via TAK-AMPK pathway, resulting in the accumulation of acetyl-CoA, which activated the EMT program through Smad2 transcription factor acetylation, then induced breast cancer cell invasion (Rios Garcia et al., 2017). Taken together, these findings indicated that fatty acid and acetate are used as alternative nutritional source by metastasizing cancer cells.

Metabolic Reprogramming in Circulating Breast Cancer Cells

After the tumor cells detach from the primary focus, they infiltrate into the blood vessels and migrate along with the blood circulation system. On account of exposure to various stresses in new environments, such as increased oxidative stress and attack by immune cells, most CTC undergo apoptosis or phagocytosis in circulation, and only a few cells manage to escape and develop into metastatic tumor, which referred to as anoikis (Frisch and Francis, 1994). Therefore, cancer cells need to strengthen their antioxidant defense in the circulation through certain mechanisms such as metabolic remodeling to avoid cell death result from matrix detachment. Several studies have shown that the protection of CTC from oxidative damage mainly depends on nicotinamide adenine dinucleotide phosphate (NADPH) produced by pentose phosphate pathway (PPP) to avoid the hazard of reactive oxygen species (ROS).

Upregulation of PPP Support the Survival of Detached Metastasizing Cells

Once tumor cells enter the circulatory system, they will produce reduction products NADPH and glutathione (GSH) through PPP pathway, endowing cells with stronger antioxidant capacity and eliminating ROS, thus reducing cell anoikis (Schafer et al., 2009). In the circulatory system, cells may induce metabolic changes through corresponding gene changes. For instance, a study has reported that the glucose uptake and ATP production in normal mammary epithelial cells separated from ECM were significantly reduced. Interestingly, when the ErbB2 signal was activated, it could restore glucose uptake and ATP production. Additionally, over-expression of ErbB2 also activated the PPP, which increased NADPH production to protect CTC from oxidative stress (Schafer et al., 2009).

Pyruvate and Lactate Metabolism Protect CTC Against Oxidative Damage

The metabolism of pyruvate and lactate is conducive to the resistance of matrix detachment-induced cells death. There was supporting evidence that serum pyruvate concentration in

patients with advanced metastatic breast cancer was higher than that in patients with localized early breast cancer (Jobard et al., 2014). When pyruvate carboxylase (PC) transcription was down-regulated, the acetone-to-oxaloacetic acid pathway was blocked, resulted in a decreased ratio of NADPH/NADP+ and GSH/GSSG, leading to increased oxidative stress (Wilmanski et al., 2017). The high concentration of pyruvate and lactate in the blood possibly promoted the hypoxic response and maintain the activity of CTC and cell clusters through the hypoxia-inducible factor 1α (HIF-1α) (Vande Voorde et al., 2019). The studies described above suggested that pyruvate can act as an extracellular antioxidant to facilitate cells survive by enhancing the resistance of CTC to oxidative stress, and lactate drives the PPP pathway to produce NADPH(Ying et al., 2021). In conclusion, antioxidant defense is essential to avoid tumor cell death in circulation. Treatment based on metabolic reprogramming in CTC, in combination with surgical treatment of the primary tumor, may better reduce the recurrence and metastasis of cancer.

Metabolic Reprogramming in Metastatic Breast Cancer Cells During Brain Colonization

Although upregulation of expression level of the key glycolytic enzyme HK2 gene and glucose transporter 3 was found in brain metastases (Palmieri et al., 2009; Kuo et al., 2019), increased glycolytic activity does not appear to be a metabolic feature of brain metastases from breast cancer. This was exemplified in a metabolic study of breast cancer brain metastases, which has found that the metastatic cells can rely on gluconeogenesis and the oxidation of glutamine and branched chain amino acids to satisfy energy requirements, thus evolving their ability to survive and proliferate independent of glucose (Chen et al., 2015).

Enhancement of FBP-Dependent Gluconeogenesis Found in Brain Metastases

FBP is one of the key enzymes in the gluconeogenesis pathway. Expression levels of FBP and glycogen were elevated in brain metastases compared to primary breast tumors in patients. In BLBC, silencing FBP could induce glycolysis, leading to an increase in glucose uptake and a decrease in the activity of metastatic cells. It could also suppress oxygen consumption by inhibiting mitochondrial complex I to activate oxidation products (Chen et al., 2015). In contrast, FBP was inhibited in invading breast cancer cells (Dong et al., 2013). Nevertheless, FBPS and glycogen are indispensable substances for normal metabolism of the human, thereby they may be difficult to serve as drug targets in brain metastases.

Upregulation of Serine Induced by PHGDH in Brain Metastases

Serine is a kind of non-essential amino acid. In addition to food supply, serine can be produced by cells *in vivo* via the serine synthesis pathway. A functional genomics study revealed that SSP is essential for the development of breast cancer (Possemato et al., 2011). The Phosphoglycerate dehydrogenase-catalyzed process is the first step in the serine biosynthesis pathway. Up-regulation of phosphoglycerate dehydrogenase (PHGDH) protein expression may occur in approximately 70% of ER-negative breast cancer tissues (Possemato et al., 2011). The expression of PHGDH in breast cancer brain metastases was significantly higher than other metastatic colonization such as lung, liver, and ovary. After suppression of PHGDH by genetic silencing or inhibitor such as PH-755, metastatic capacity of cancer cells was impaired and overall survival of the mice was improved due to a decrease in serine content in the brain, yet the growth of extracranial tumors (metastases such as lung and liver) was not affected (Ngo et al., 2020).

Breast Cancer Cells Display GABAergic Properties in the Brain Microenvironment

A study in brain metastasis has shown that breast-to-brain metastatic tissue and cells displayed a GABAergic phenotype similar to that of neuronal cells. By using γ-aminobutyric acid (GABA) as an oncometabolite, brain metastases catabolize GABA into succinate to promote the tricarboxylic acid (TCA) cycle, thus indirectly increasing cell proliferation (Neman et al., 2014). What's more, brain interstitial space contains high levels of glutamine, which is an important precursor of the neurotransmitters glutamate and GABA (Chen et al., 2015). Above evidence suggested that glutamine serve as energy substrates in the brain microenvironment, but it cannot be used as a therapeutic target due to little is known about the concrete mechanism of utilization.

Lipid Adjustment Is Important for Brain Colonization

Jin et al. pointed out that adjustment in lipid metabolism were necessary in breast cancer brain metastasis, and treatment on lipid metabolism of breast cancer cells might be beneficial to curb brain metastasis development (Jin et al., 2020). Fatty acid binding protein (FABP 7) is a brain-specific intracellular lipid-binding protein, and its overexpression was shown to coincide with the low survival rate of patients with HER2-enriched breast cancer and the increased incidence of brain metastasis. FABP7 is involved in the metabolic reprogramming of cancer cells, supporting the glycolytic phenotype and the storage of lipid droplets, thus enabling them to grow in the unique environment of the brain. What was surprising was that up-regulation of FABP7 was not detected in the primary breast cancer, which supported the potential function of FABP7 on the brain viability of breast cancer cells (Cordero et al., 2019).

Fatty acid synthase (FASN) is likely to be another potential target for inhibiting brain metastasis of breast cancer (Menendez and Lupu, 2017). FASN is the key enzyme in fatty acid biosynthesis, and its expression is necessary for lipid synthesis and maintenance of palmitate level, especially in the environment of exogenous lipid deficiency, such as the brain. Additionally, the genetic and pharmacological effects of FASN abolished the growth of brain metastases, further demonstrating that fatty acid synthesis is crucial for the growth of metastatic tumor in the brain (Ferraro et al., 2021).

Brain metastases could also use acetate as a compensatory source of carbon to support *de novo* lipid synthesis (Mashimo

et al., 2014). Acetate oxidation has been verified in primary and metastatic mouse brain tumors and patients with brain metastases, and this process could be performed simultaneously with glucose oxidation. Of interest, glucose contributed less than 50% of the acetyl-CoA pool (Maher et al., 2012), suggesting that tumors utilized additional substrates, thus glucose may be a minor source of acetyl-CoA in the TCA cycle (Mashimo et al., 2014).

TARGETING METABOLISM TO TREAT BREAST CANCER WITH BRAIN METASTASIS

The existence of human blood-brain barrier greatly hinders the killing effect of chemotherapeutic drugs on brain tumors. Therefore, surgery and radiotherapy remain the main treatment for brain metastases. Over the past decades, molecular targeted drugs against a variety of key enzymes of glycolysis, tricarboxylic acid cycle, lipid metabolism, amino acid metabolism and other metabolic pathways are being developing, and some of the drugs have involved in clinical trials, showing good clinical application prospects. Metastatic breast cancer cells display metabolic flexibility, that is, cancer cells can use different metabolites to meet the different metabolic requirements in specific steps of the metastasis cascade, so targeting metabolism reprogramming tend to be one of the effective strategies for the treatment of brain metastases from breast cancer.

Targeting Metabolic Enzyme of Brain Metastatic Cancer Cell

The Warburg effect endows breast cancer cells with the ability to invade by inducing EMT, thereby targeting glycolysis metabolism probably is a promising therapeutic strategy. For example, the HK2 inhibitor, 2- deoxy -D- glucose (2-DG), inhibited tumor metastasis by inducing a change in the metabolic pattern of oxidative phosphorylation and reducing the production of lactate. Yet, it showed no obvious therapeutic effect on mouse xenografts and patients (Zhang et al., 2019).

Altering the acidic environment presumably is another extremely effective strategy to block metastasis. There is abundant evidence that accumulation of the metabolic byproduct lactate and extracellular acidification exacerbates tumor cell proliferation, metastasis, and angiogenesis. The acidic environment created by lactate accumulation promotes the degradation of ECM, mainly due to PH decline could stimulate the secretion and activation of hydrolases, including cathepsins and MMP-9 (Payen et al., 2016). MMP-2 and MMP-9 are also correlated with the development of breast cancer metastasis (Li et al., 2017). Furthermore, extracellular acidification mediates immunosuppression and reinforces tumor immune escape. Brown et al. observed that breast cancer cell-derived lactic acid activated G-protein-coupled receptor (GPR) 81 in dendritic cells and prevented the presentation of tumor-specific antigens to other immune cells (Brown et al., 2020). Chen et al. reported that lactate activates macrophage GPR132 and thus promotes lung metastasis of breast cancer (Chen et al., 2017).

What's more, enzymes involved in lipid metabolism may also be suitable targets for preventing the formation of brain metastases, such as FASN, which is a promising target for the treatment of brain metastasis originated from breast cancer (Kingwell, 2021). Moreover, PHGDH inhibitors that interfere with serine synthesis in the brain may also contribute to the treatment of brain metastases (Ngo et al., 2020).

Blocking Signaling Pathways for Metabolic Regulation of Brain Metastases

Existing research recognized the critical role played by Notch signaling in regulating metabolism during brain metastasis of breast. High expression of IL-1β in brain metastases activated the expression of peripheral astrocyte JAG1, and the subsequent their interaction leaded to the activation of Notch pathway and promotes the growth of brain metastasis of breast cancer stem cell-like cells. On the contrary, the inhibition of Notch signal significantly prevents the occurrence of brain metastasis (McGowan et al., 2011; Xing et al., 2013).

PI3K/AKT/mTOR pathway is an intracellular signaling pathway significant for cell metabolism involved in cancer metastasis. EGFR signal activated PI3K/AKT/mTOR pathway, and up-regulated HIF-1α-mediated enhancement of glucose uptake and glycolysis-related gene expression, which may be driven by or in synergy with c-MYC to promote tumor proliferation (Masui et al., 2014). Several studies have documented that immune checkpoint inhibitors such as PD-1 could decrease mTOR activity and thus inhibited the Warburg effect (Chang et al., 2015). And it has been reported that the mTOR inhibitor rapamycin could reduce the expression of FASN in breast cancer cells (Yan et al., 2014).

According to these data, we can infer that Notch signaling and mTOR signaling axis are key players in modulating cellular metabolism and tumor growth during brain metastasis. But since the signaling pathways are interrelated with each other, it may be necessary to target multiple pathways simultaneously to obtain effective antitumor activity.

CONCLUSION

In recent years, attention has been drawn to the fact that energy metabolism reprogramming is crucial for primary tumor growth, invasion and metastasis, however, the metabolic interaction has not been elucidated. Molecular subtypes may be one of the factors affecting metabolic energy supply. Gene expression analysis has identified different molecular subtypes of breast cancer, including Luminal A, Luminal B, HER2-enriched and the basal-like subtype (largely overlaps with triple negative breast cancers, TNBC), and each subtype of breast cancer has a unique metastasis pattern. In particular, patients with HER2-enriched and TNBC are the most likely to develop brain metastasis (Kennecke et al., 2010; Kuksis et al., 2021). Luminal subtypes are found to exhibit reverse-

Warburg/null phenotypes, in contrast, TNBC preferentially utilize the glycolysis energy (Choi et al., 2013). Nonetheless, it remains unclear whether different subtypes of cancer cells affect the selection of metastasis sites by adopting diverse metabolic strategies (Gandhi and Das, 2019). Another contributing factor of metabolic differences is tumor microenvironment. Tumor metabolism is environmentally dependent, and the availability of nutrients in the environment indirectly affects metabolic changes in cancer cells. The breast is mainly composed of breast and fat, of which fat accounts for about 90%. By contrast, the brain contains high levels of glutamine and branched chain amino acids, which can serve as alternative energy substrates to power metastasizing cells colonized in the brain.

Although tremendous progress has been made in the research on the mechanism of metabolic therapy, the main challenge faced by drug development are as followed. First, due to pharmacokinetic constraints of blood-brain barrier, most of the existing targeted drugs cannot reach the brain metastases successfully. Second, those drugs targeting metabolic pathways show significant side effects, which presumably on account of the metabolic heterogeneity in tumors and metabolic compensation pathways. Therefore, cancer metabolism research should take into consideration genetic factors, the cell interaction in the micro-environment, the influence of diet and microorganisms on tumor metabolism preference. Last but not least, there still lack of effective biomarkers for the prediction of metastatic risk and the evaluation of metabolic therapies, making it difficult to determine the optimal therapeutic window for drugs in patients. In summary, energy metabolism reprogramming is a key feature in the occurrence and development of tumors. With the deepening understanding on tumor metabolic mechanisms, it will better help people to discover metabolism-based drug to treat breast cancer with brain metastasis.

AUTHOR CONTRIBUTIONS

XZ contributed to conception and edited the manuscript. BL contributed to the manuscript writing and the figure design.

FUNDING

This study was supported by the grants from the National Natural Science Foundation of China (81802918), the China Postdoctoral Science Foundation Grant (2019M660206), the Science and Technology Project of Guangdong Province (2019A1515011565, 2018A030310007), and the Science and Technology Project of Jiangmen (202003010314000897 8, 2019030102430012905).

REFERENCES

Achrol, A. S., Rennert, R. C., Anders, C., Soffietti, R., Ahluwalia, M. S., Nayak, L., et al. (2019). Brain Metastases. *Nat. Rev. Dis. Primers* 5 (1), 5. doi:10.1038/s41572-018-0055-y

Bergers, G., and Fendt, S.-M. (2021). The Metabolism of Cancer Cells during Metastasis. *Nat. Rev. Cancer* 21 (3), 162–180. doi:10.1038/s41568-020-00320-2

Brown, T. P., Bhattacharjee, P., Ramachandran, S., Sivaprakasam, S., Ristic, B., Sikder, M. O. F., et al. (2020). The Lactate Receptor GPR81 Promotes Breast Cancer Growth via a Paracrine Mechanism Involving Antigen-Presenting Cells in the Tumor Microenvironment. *Oncogene* 39 (16), 3292–3304. doi:10.1038/s41388-020-1216-5

Chaffer, C. L., and Weinberg, R. A. (2011). A Perspective on Cancer Cell Metastasis. *Science* 331 (6024), 1559–1564. doi:10.1126/science.1203543

Chang, C.-H., Qiu, J., O'Sullivan, D., Buck, M. D., Noguchi, T., Curtis, J. D., et al. (2015). Metabolic Competition in the Tumor Microenvironment Is a Driver of Cancer Progression. *Cell* 162 (6), 1229–1241. doi:10.1016/j.cell.2015.08.016

Chen, J., Lee, H.-J., Wu, X., Huo, L., Kim, S.-J., Xu, L., et al. (2015). Gain of Glucose-independent Growth upon Metastasis of Breast Cancer Cells to the Brain. *Cancer Res.* 75 (3), 554–565. doi:10.1158/0008-5472.CAN-14-2268

Chen, P., Zuo, H., Xiong, H., Kolar, M. J., Chu, Q., Saghatelian, A., et al. (2017). Gpr132 Sensing of Lactate Mediates Tumor-Macrophage Interplay to Promote Breast Cancer Metastasis. *Proc. Natl. Acad. Sci. USA* 114 (3), 580–585. doi:10.1073/pnas.1614035114

Choi, J., Kim, D. H., Jung, W. H., and Koo, J. S. (2013). Metabolic Interaction between Cancer Cells and Stromal Cells According to Breast Cancer Molecular Subtype. *Breast Cancer Res.* 15 (5), R78. doi:10.1186/bcr3472

Cordero, A., Kanojia, D., Miska, J., Panek, W. K., Xiao, A., Han, Y., et al. (2019). FABP7 Is a Key Metabolic Regulator in HER2+ Breast Cancer Brain Metastasis. *Oncogene* 38 (37), 6445–6460. doi:10.1038/s41388-019-0893-4

Dirat, B., Bochet, L., Dabek, M., Daviaud, D., Dauvillier, S., Majed, B., et al. (2011). Cancer-associated Adipocytes Exhibit an Activated Phenotype and Contribute to Breast Cancer Invasion. *Cancer Res.* 71 (7), 2455–2465. doi:10.1158/0008-5472.CAN-10-3323

Dong, C., Yuan, T., Wu, Y., Wang, Y., Fan, T. W. M., Miriyala, S., et al. (2013). Loss of FBP1 by Snail-Mediated Repression Provides Metabolic Advantages in Basal-like Breast Cancer. *Cancer Cell* 23 (3), 316–331. doi:10.1016/j.ccr.2013.01.022

Dornier, E., Rabas, N., Mitchell, L., Novo, D., Dhayade, S., Marco, S., et al. (2017). Glutaminolysis Drives Membrane Trafficking to Promote Invasiveness of Breast Cancer Cells. *Nat. Commun.* 8 (1), 2255. doi:10.1038/s41467-017-02101-2

Ferraro, G. B., Ali, A., Luengo, A., Kodack, D. P., Deik, A., Abbott, K. L., et al. (2021). Fatty Acid Synthesis Is Required for Breast Cancer Brain Metastasis. *Nat. Cancer* 2 (4), 414–428. doi:10.1038/s43018-021-00183-y

Frisch, S., and Francis, H. (1994). Disruption of Epithelial Cell-Matrix Interactions Induces Apoptosis. *J. Cel Biol.* 124 (4), 619–626. doi:10.1083/jcb.124.4.619

Gandhi, N., and Das, G. (2019). Metabolic Reprogramming in Breast Cancer and its Therapeutic Implications. *Cells* 8 (2), 89. doi:10.3390/cells8020089

Jin, X., Demere, Z., Nair, K., Ali, A., Ferraro, G. B., Natoli, T., et al. (2020). A Metastasis Map of Human Cancer Cell Lines. *Nature* 588 (7837), 331–336. doi:10.1038/s41586-020-2969-2

Jobard, E., Pontoizeau, C., Blaise, B. J., Bachelot, T., Elena-Herrmann, B., and Trédan, O. (2014). A Serum Nuclear Magnetic Resonance-Based Metabolomic Signature of Advanced Metastatic Human Breast Cancer. *Cancer Lett.* 343 (1), 33–41. doi:10.1016/j.canlet.2013.09.011

Keckesova, Z., Donaher, J. L., De Cock, J., Freinkman, E., Lingrell, S., Bachovchin, D. A., et al. (2017). LACTB Is a Tumour Suppressor that Modulates Lipid Metabolism and Cell State. *Nature* 543 (7647), 681–686. doi:10.1038/nature21408

Kennecke, H., Yerushalmi, R., Woods, R., Cheang, M. C. U., Voduc, D., Speers, C. H., et al. (2010). Metastatic Behavior of Breast Cancer Subtypes. *Jco* 28 (20), 3271–3277. doi:10.1200/JCO.2009.25.9820

Kingwell, K. (2021). Metabolic Target for Brain Metastasis. *Nat. Rev. Drug Discov.* 20 (6), 426. doi:10.1038/d41573-021-00073-z

Knott, S. R. V., Wagenblast, E., Khan, S., Kim, S. Y., Soto, M., Wagner, M., et al. (2018). Asparagine Bioavailability Governs Metastasis in a Model of Breast Cancer. *Nature* 554 (7692), 378–381. doi:10.1038/nature25465

Kuksis, M., Gao, Y., Tran, W., Hoey, C., Kiss, A., Komorowski, A. S., et al. (2021). The Incidence of Brain Metastases Among Patients with Metastatic Breast Cancer: a Systematic Review and Meta-Analysis. *Neuro Oncol.* 23 (6), 894–904. doi:10.1093/neuonc/noaa285

Kuo, M.-H., Chang, W.-W., Yeh, B.-W., Chu, Y.-S., Lee, Y.-C., and Lee, H.-T. (2019). Glucose Transporter 3 Is Essential for the Survival of Breast Cancer Cells in the Brain. *Cells* 8 (12), 1568. doi:10.3390/cells8121568

Li, H., Qiu, Z., Li, F., and Wang, C. (2017). The Relationship between MMP-2 and MMP-9 Expression Levels with Breast Cancer Incidence and Prognosis. *Oncol. Lett.* 14 (5), 5865–5870. doi:10.3892/ol.2017.6924

Lundø, K., Trauelsen, M., Pedersen, S. F., and Schwartz, T. W. (2020). Why Warburg Works: Lactate Controls Immune Evasion through GPR81. *Cel Metab.* 31 (4), 666–668. doi:10.1016/j.cmet.2020.03.001

Luo, M., Brooks, M., and Wicha, M. S. (2018). Asparagine and Glutamine: Co-conspirators Fueling Metastasis. *Cel Metab.* 27 (5), 947–949. doi:10.1016/j.cmet.2018.04.012

Maher, E. A., Marin-Valencia, I., Bachoo, R. M., Mashimo, T., Raisanen, J., Hatanpaa, K. J., et al. (2012). Metabolism of [U-13 C]glucose in Human Brain Tumors *In Vivo*. *NMR Biomed.* 25 (11), 1234–1244. doi:10.1002/nbm.2794

Martin, A. M., Cagney, D. N., Catalano, P. J., Warren, L. E., Bellon, J. R., Punglia, R. S., et al. (2017). Brain Metastases in Newly Diagnosed Breast Cancer. *JAMA Oncol.* 3 (8), 1069–1077. doi:10.1001/jamaoncol.2017.0001

Mashimo, T., Pichumani, K., Vemireddy, V., Hatanpaa, K. J., Singh, D. K., Sirasanagandla, S., et al. (2014). Acetate Is a Bioenergetic Substrate for Human Glioblastoma and Brain Metastases. *Cell* 159 (7), 1603–1614. doi:10.1016/j.cell.2014.11.025

Masui, K., Cavenee, W. K., and Mischel, P. S. (2014). mTORC2 in the center of Cancer Metabolic Reprogramming. *Trends Endocrinol. Metab.* 25 (7), 364–373. doi:10.1016/j.tem.2014.04.002

McGowan, P. M., Simedrea, C., Ribot, E. J., Foster, P. J., Palmieri, D., Steeg, P. S., et al. (2011). Notch1 Inhibition Alters the CD44hi/CD24lo Population and Reduces the Formation of Brain Metastases from Breast Cancer. *Mol. Cancer Res.* 9 (7), 834–844. doi:10.1158/1541-7786.MCR-10-0457

Menendez, J. A., and Lupu, R. (2017). Fatty Acid Synthase (FASN) as a Therapeutic Target in Breast Cancer. *Expert Opin. Ther. Targets* 21 (11), 1001–1016. doi:10.1080/14728222.2017.1381087

Neman, J., Termini, J., Wilczynski, S., Vaidehi, N., Choy, C., Kowolik, C. M., et al. (2014). Human Breast Cancer Metastases to the Brain Display GABAergic Properties in the Neural Niche. *Proc. Natl. Acad. Sci.* 111 (3), 984–989. doi:10.1073/pnas.1322098111

Ngo, B., Kim, E., Osorio-Vasquez, V., Doll, S., Bustraan, S., Liang, R. J., et al. (2020). Limited Environmental Serine and Glycine Confer Brain Metastasis Sensitivity to PHGDH Inhibition. *Cancer Discov.* 10 (9), 1352–1373. doi:10.1158/2159-8290.CD-19-1228

Nokin, M.-J., Durieux, F., Peixoto, P., Chiavarina, B., Peulen, O., Blomme, A., et al. (2016). Methylglyoxal, a Glycolysis Side-Product, Induces Hsp90 Glycation and YAP-Mediated Tumor Growth and Metastasis. *Elife* 5. doi:10.7554/eLife.19375

Palmieri, D., Fitzgerald, D., Shreeve, S. M., Hua, E., Bronder, J. L., Weil, R. J., et al. (2009). Analyses of Resected Human Brain Metastases of Breast Cancer Reveal the Association between Up-Regulation of Hexokinase 2 and Poor Prognosis. *Mol. Cancer Res.* 7 (9), 1438–1445. doi:10.1158/1541-7786.MCR-09-0234

Pascual, G., Avgustinova, A., Mejetta, S., Martín, M., Castellanos, A., Attolini, C. S.-O., et al. (2017). Targeting Metastasis-Initiating Cells through the Fatty Acid Receptor CD36. *Nature* 541 (7635), 41–45. doi:10.1038/nature20791

Pavlova, N. N., Hui, S., Ghergurovich, J. M., Fan, J., Intlekofer, A. M., White, R. M., et al. (2018). As Extracellular Glutamine Levels Decline, Asparagine Becomes an Essential Amino Acid. *Cel Metab.* 27 (2), 428–438. doi:10.1016/j.cmet.2017.12.006

Payen, V. L., Hsu, M. Y., Rädecke, K. S., Wyart, E., Vazeille, T., Bouzin, C., et al. (2017). Monocarboxylate Transporter MCT1 Promotes Tumor Metastasis Independently of its Activity as a Lactate Transporter. *Cancer Res.* 77 (20), 5591–5601. doi:10.1158/0008-5472.CAN-17-0764

Payen, V. L., Porporato, P. E., Baselet, B., and Sonveaux, P. (2016). Metabolic Changes Associated with Tumor Metastasis, Part 1: Tumor pH, Glycolysis and the Pentose Phosphate Pathway. *Cell. Mol. Life Sci.* 73 (7), 1333–1348. doi:10.1007/s00018-015-2098-5

Possemato, R., Marks, K. M., Shaul, Y. D., Pacold, M. E., Kim, D., Birsoy, K., et al. (2011). Functional Genomics Reveal that the Serine Synthesis Pathway Is Essential in Breast Cancer. *Nature* 476 (7360), 346–350. doi:10.1038/nature10350

Ramakrishna, N., Temin, S., Chandarlapaty, S., Crews, J. R., Davidson, N. E., Esteva, F. J., et al. (2014). Recommendations on Disease Management for Patients with Advanced Human Epidermal Growth Factor Receptor 2-positive Breast Cancer and Brain Metastases: American Society of Clinical Oncology Clinical Practice Guideline. *Jco* 32 (19), 2100–2108. doi:10.1200/JCO.2013.54.0955

Rios Garcia, M., Steinbauer, B., Srivastava, K., Singhal, M., Mattijssen, F., Maida, A., et al. (2017). Acetyl-CoA Carboxylase 1-Dependent Protein Acetylation Controls Breast Cancer Metastasis and Recurrence. *Cel Metab.* 26 (6), 842–855. doi:10.1016/j.cmet.2017.09.018

Schafer, Z. T., Grassian, A. R., Song, L., Jiang, Z., Gerhart-Hines, Z., Irie, H. Y., et al. (2009). Antioxidant and Oncogene rescue of Metabolic Defects Caused by Loss of Matrix Attachment. *Nature* 461 (7260), 109–113. doi:10.1038/nature08268

Schug, Z. T., Peck, B., Jones, D. T., Zhang, Q., Grosskurth, S., Alam, I. S., et al. (2015). Acetyl-CoA Synthetase 2 Promotes Acetate Utilization and Maintains Cancer Cell Growth under Metabolic Stress. *Cancer Cell* 27 (1), 57–71. doi:10.1016/j.ccell.2014.12.002

Valastyan, S., and Weinberg, R. A. (2011). Tumor Metastasis: Molecular Insights and Evolving Paradigms. *Cell* 147 (2), 275–292. doi:10.1016/j.cell.2011.09.024

Vande Voorde, J., Ackermann, T., Pfetzer, N., Sumpton, D., Mackay, G., Kalna, G., et al. (2019). Improving the Metabolic Fidelity of Cancer Models with a Physiological Cell Culture Medium. *Sci. Adv.* 5 (1), eaau7314. doi:10.1126/sciadv.aau7314

Vander Heiden, M. G., and DeBerardinis, R. J. (2017). Understanding the Intersections between Metabolism and Cancer Biology. *Cell* 168 (4), 657–669. doi:10.1016/j.cell.2016.12.039

Wang, Y. Y., Attané, C., Milhas, D., Dirat, B., Dauvillier, S., Guerard, A., et al. (2017). Mammary Adipocytes Stimulate Breast Cancer Invasion through Metabolic Remodeling of Tumor Cells. *JCI Insight* 2 (4), e87489. doi:10.1172/jci.insight.87489

Warburg, O., Wind, F., and Negelein, E. (1927). The Metabolism of Tumors in the Body. *J. Gen. Physiol.* 8 (6), 519–530. doi:10.1085/jgp.8.6.519

Wilmanski, T., Zhou, X., Zheng, W., Shinde, A., Donkin, S. S., Wendt, M., et al. (2017). Inhibition of Pyruvate Carboxylase by 1α,25-Dihydroxyvitamin D Promotes Oxidative Stress in Early Breast Cancer Progression. *Cancer Lett.* 411, 171–181. doi:10.1016/j.canlet.2017.09.045

Xing, F., Kobayashi, A., Okuda, H., Watabe, M., Pai, S. K., Pandey, P. R., et al. (2013). Reactive Astrocytes Promote the Metastatic Growth of Breast Cancer Stem-like Cells by Activating Notch Signalling in Brain. *EMBO Mol. Med.* 5 (3), 384–396. doi:10.1002/emmm.201201623

Yan, C., Wei, H., Minjuan, Z., Yan, X., Jingyue, Y., Wenchao, L., et al. (2014). The mTOR Inhibitor Rapamycin Synergizes with a Fatty Acid Synthase Inhibitor to Induce Cytotoxicity in ER/HER2-positive Breast Cancer Cells. *PLoS One* 9 (5), e97697. doi:10.1371/journal.pone.0097697

Ying, M., You, D., Zhu, X., Cai, L., Zeng, S., and Hu, X. (2021). Lactate and Glutamine Support NADPH Generation in Cancer Cells under Glucose Deprived Conditions. *Redox Biol.* 46, 102065. doi:10.1016/j.redox.2021.102065

Yu, P., Li, A.-x., Chen, X.-s., Tian, M., Wang, H.-y., Wang, X.-l., et al. (2020). PKM2-c-Myc-Survivin Cascade Regulates the Cell Proliferation, Migration, and Tamoxifen Resistance in Breast Cancer. *Front. Pharmacol.* 11, 550469. doi:10.3389/fphar.2020.550469

Zaoui, M., Morel, M., Ferrand, N., Fellahi, S., Bastard, J.-P., Lamazière, A., et al. (2019). Breast-Associated Adipocytes Secretome Induce Fatty Acid Uptake and Invasiveness in Breast Cancer Cells via CD36 Independently of Body Mass Index, Menopausal Status and Mammary Density. *Cancers* 11 (12), 2012. doi:10.3390/cancers11122012

Zeng, P., Sun, S., Li, R., Xiao, Z.-X., and Chen, H. (2019). HER2 Upregulates ATF4 to Promote Cell Migration via Activation of ZEB1 and Downregulation of E-Cadherin. *Ijms* 20 (9), 2223. doi:10.3390/ijms20092223

Zhang, T., Zhu, X., Wu, H., Jiang, K., Zhao, G., Shaukat, A., et al. (2019). Targeting the ROS/PI3K/AKT/HIF-1α/HK2 axis of Breast Cancer Cells: Combined Administration of Polydatin and 2-Deoxy-d-glucose. *J. Cel Mol Med.* 23 (5), 3711–3723. doi:10.1111/jcmm.14276

Conflict of Interest: The authors declare that the research was conducted in the absence of any commercial or financial relationships that could be construed as a potential conflict of interest.

Publisher's Note: All claims expressed in this article are solely those of the authors and do not necessarily represent those of their affiliated organizations, or those of the publisher, the editors and the reviewers. Any product that may be evaluated in this article, or claim that may be made by its manufacturer, is not guaranteed or endorsed by the publisher.

frontiers in Molecular Biosciences

ORIGINAL RESEARCH
published: 09 February 2022
doi: 10.3389/fmolb.2021.785922

Co-Overexpression of GRK5/ACTC1 Correlates With the Clinical Parameters and Poor Prognosis of Epithelial Ovarian Cancer

Longyang Liu[1,2†], Jin Lv[2,3†], Zhongqiu Lin[4], Yingxia Ning[5], Jing Li[1], Ping Liu[1]* and Chunlin Chen[1]**

[1]Department of Gynecology and Obstetrics, Nanfang Hospital, Southern Medical University, Guangzhou, China, [2]Cancer Center, Integrated Hospital of Traditional Chinese Medicine, Southern Medical University, Guangzhou, China, [3]Department of Obstetrics and Gynecology, Longgang Central Hospital of Shenzhen City, Shenzhen, China, [4]Department of Gynecology Oncology, The Memorial Hospital of Sun Yat-sen University, Guangzhou, China, [5]Department of Gynecology and Obstetrics, The First Affiliated Hospital of Guangzhou Medical University, Guangzhou, China

OPEN ACCESS

Edited by:
Zhe-Sheng Chen,
St. John's University, United States

Reviewed by:
Khushboo Jani,
RAPT Therapeutics, United States
Yiyi Liu,
Guangzhou Medical University, China

***Correspondence:**
Jing Li
lijing7405@126.com
Ping Liu
lpivy@126.com
Chunlin Chen
jieru@163.com

†These authors share first authorship

Specialty section:
This article was submitted to Molecular Diagnostics and Therapeutics, a section of the journal Frontiers in Molecular Biosciences

Received: 29 September 2021
Accepted: 06 December 2021
Published: 09 February 2022

Citation:
Liu L, Lv J, Lin Z, Ning Y, Li J, Liu P and Chen C (2022) Co-Overexpression of GRK5/ACTC1 Correlates With the Clinical Parameters and Poor Prognosis of Epithelial Ovarian Cancer. Front. Mol. Biosci. 8:785922. doi: 10.3389/fmolb.2021.785922

Background: The prognosis of epithelial ovarian cancer (EOC) is poor, and the present prognostic predictors of EOC are neither sensitive nor specific.

Objective: The aim of this study was to search the prognostic biomarkers of EOC and to investigate the expression of G protein-coupled receptor kinase 5 (GRK5) and actin alpha cardiac muscle 1 (ACTC1) in EOC tissues (both paraffin-embedded and fresh-frozen tissues) and to explore their association with clinicopathological parameters and prognostic value in patients with EOC.

Methods: A total of 172 paraffin-embedded cancer tissues of EOC patients diagnosed and operated at the memorial hospital of Sun Yat-sen University between December 2009 and March 2017 and 41 paratumor tissues were collected and the expression of GRK5 and ACTC1 was examined using immunohistochemistry. Furthermore, 16 fresh-frozen EOC tissues and their matched paratumor tissues were collected from the Integrated Hospital of Traditional Chinese Medicine, Southern Medical University, between August 2013 and November 2019 and subjected to reverse-transcription quantitative PCR analysis to detect the mRNA expression of GRK5 and ACTC1.

Results: The expression of GRK5 and ACTC1 was both higher in cancer tissues than in paratumor tissues. GRK5 expression was positively correlated with ACTC1 expression. In addition, GRK5, ACTC1, and GRK5/ACTC1 expression was associated with the recurrence-free survival and overall survival of EOC patients. Furthermore, multivariate logistic regression analysis indicated that GRK5+/ACTC1+ co-expression, intestinal metastasis, postoperative chemotherapy, platinum resistance, and hyperthermic intraperitoneal chemotherapy were independent prognostic factors of EOC.

Conclusion: GRK5 and ACTC1 are both upregulated in EOC compared with those in paratumor tissues. The co-expression of GRK5+/ACTC1+ rather than GRK5 or ACTC1 is an independent prognostic biomarker of EOC.

Keywords: GRK5, ACTC1, epithelial ovarian cancer, prognosis, expression

INTRODUCTION

Ovarian cancer (OC) is the main cause of mortality in female reproductive malignant cancers in China (Chen et al., 2016), and it is the second most common cause of gynecologic cancer-related death in women worldwide (Lheureux et al., 2019). Globally, there are 239,000 new cases and 152,000 deaths every year, making OC the seventh most common cancer and the second most common cause of gynecologic cancer-related mortality (Lheureux et al., 2019). The most common type of OC is epithelial ovarian cancer (EOC). Cytoreduction and combination chemotherapies were performed to treat OC, but the prognosis remains poor (Liu et al., 2019a; Yao et al., 2019; Liu et al., 2020). Recently, tumor biomarkers have been used to monitor the progression and predict the prognosis of EOC, but these biomarkers are not very accurate (Liu et al., 2019a; Yao et al., 2019; Liu et al., 2020).

In our previous study, we found that non-muscle myosin heavy chain B (MYH10) is an independent prognostic biomarker of EOC (in print). Furthermore, we used the Biogrid website to predict the candidate interacting proteins of MYH10, and we found some candidate proteins that may closely correlate with MYH10, such as MYL9 (Deng et al., 2021), MACF1 (Liu et al., 2021), MYH9 (Liu et al., 2019b), and so on. In the further study, we found that the co-expression of GRK5 (G protein-coupled receptor kinase 5) and ACTC1 (actin alpha cardiac muscle 1) is indeed independent prognostic biomarkers, which indicates their important role in EOC. GRK5 is one of the G protein-coupled receptor kinase (GRK) family members (Gambardella et al., 2016; Jiang et al., 2018; Zhao et al., 2019a; Lagman et al., 2019; Sommer et al., 2019), which is a candidate interacting protein of MYH10. GRK5 can regulate GPCR signaling, which correlates with various diseases like cardiac dysfunction, diabetes, hypertension, Alzheimer's disease, and cancers (Kim et al., 2012; Komolov et al., 2017; Jiang et al., 2018; Alshabi et al., 2019; Zhao et al., 2019b). GRK5 functions as oncogenes in glioblastoma (GBM) (Yang et al., 2018), prostate (Kim et al., 2012), pancreas (Tseng and Zhang, 2000), non-small-cell lung (Jiang et al., 2018), and breast (Sommer et al., 2019) cancers. However, to the best of our knowledge, the role of GRK5 in EOC has not been reported.

Similar to GRK5, ACTC1 is also a cardiac-related gene (Kondrashov et al., 2018), and both of them are the candidate interacting proteins of MYH10. ACTC1 encodes cardiac actin, and a mutation at c.G301A causes hypertrophic cardiomyopathy and, in some cases, sudden cardiac death (Frank et al., 2019). Recently, some reports (Kim et al., 2019; da Rocha et al., 2019; Wanibuchi et al., 2018; Cheung et al., 2017; Li et al., 2017; Ohtaki et al., 2017; Zaravinos et al., 2011) have demonstrated that ACTC1 plays an important role in human colon cancer, oral squamous cell carcinoma, GBM, and so on. However, the role of ACTC1 in EOC has not been reported, and the relationship of GRK5 and ACTC1 and EOC has not been explored yet.

The present study identified that GRK5 and ACTC1 were both upregulated in EOC. More importantly, GRK5+/ACTC1+ co-expression was an independent prognostic factor. The GRK5+/ACTC1+ co-expression could predict the development, metastasis, and prognosis of EOC.

MATERIALS AND METHODS

Paraffin-Embedded Tissue Sections

Between December 2009 and March 2017, a total of 172 paraffin-embedded EOC tissues and 41 matched paraffin-embedded paratumor tissues (the distance away from the margin of the cancer tissue is more than 1.0 cm) that had been pathologically confirmed at the memorial hospital of Sun Yat-sen University were collected for the present study. The survival duration was calculated from the date of surgery to November 1, 2018 (last follow-up). The approval of the present study was obtained from the Ethics Committee of the memorial hospital of Sun Yat-sen University. All of the patients provided written informed consent prior to the operation.

Fresh Tissue Specimens

Between August 2013 and June 2019, 16 fresh EOC tissues and their matched fresh paratumor tissues were collected from the Integrated Hospital of Traditional Chinese Medicine, Southern Medical University, at the time of diagnosis after surgery. All fresh samples were immediately preserved in liquid nitrogen. Approval was obtained from the Ethics Committee of the Integrated Hospital of Traditional Chinese Medicine, Southern Medical University. All of the patients provided written informed consent prior to surgery.

Immunohistochemistry

The expression of GRK5 and ACTC1 in paraffin-embedded EOC and paired paratumor tissues was detected by IHC staining. First, 4-μm paraffin-embedded sections were baked at 65°C for 2 h, deparaffinized with xylene, and rehydrated; high tension was used for antigen retrieval, and the specimens were treated with 3% hydrogen peroxide in methanol, followed by incubation with 1% bovine serum albumin to block non-specific binding. Subsequently, the samples were incubated with anti-rabbit GRK5 polyclonal (1:150 dilution; Cat. 17032-1-AP; Proteintech) or ACTC1 antibodies (1:200 dilution; Cat. 66125-1-IG; Proteintech) at 4°C overnight. Next, the samples were treated with secondary antibody (OriGene, Rockville, MD, USA) and then incubated with streptavidin horseradish peroxidase complex (OriGene, Rockville, MD, USA), immersed in 3-amino-9-ethyl carbazole. The sections were then counterstained with 10% Mayer's hematoxylin, dehydrated, and mounted in Crystal Mount. Two pathologists evaluated the score of immunostaining for each section. The score was based on the proportion of positively stained cancer cells and the staining intensity. The percentage was scored as follows: samples with <10% positive cancer cells were scored as 0; 10–50% were scored as 1, 50–75% were scored as 2, and >75% were scored as 3. Furthermore, the tissues were classified into four grades based on

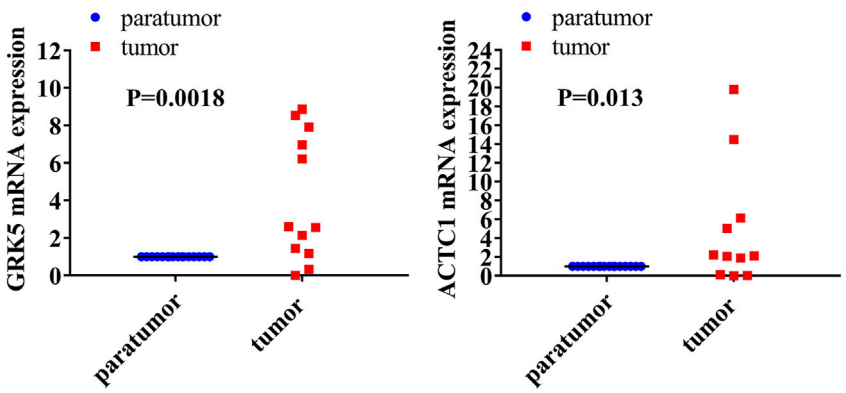

FIGURE 1 | Both GRK5 and ACTC1 were significantly upregulated in EOC tissues compared with that in paratumor tissues using RT-qPCR analysis.

TABLE 1 | Both GRK5 and ACTC1 were significantly upregulated in EOC tissues compared with that in paratumor tissues.

Group	GRK5 mRNA expression	ACTC1 mRNA expression
All of paratumor tissues (total of 16 cases)	1.00 ± 0.00	1.00 ± 0.00
Patient 1	6.218 ± 4.482	14.480 ± 5.654
Patient 2	6.963 ± 3.018	5.057 ± 3.370
Patient 3	8.547 ± 2.435	166.100 ± 105.700
Patient 4	8.865 ± 1.137	833.800 ± 584.800
Patient 5	2.610 ± 0.800	0.115 ± 0.075
Patient 6	2.149 ± 0.737	0.016 ± 0.004
Patient 7	1.442 ± 0.489	2.229 ± 0.837
Patient 8	29.440 ± 31.740	53.560 ± 20.970
Patient 9	0.002 ± 0.145	0.029 ± 0.010
Patient 10	96.510 ± 58.720	246.700 ± 29.080
Patient 11	2.564 ± 2.011	1.885 ± 0.405
Patient 12	0.326 ± 0.116	2.079 ± 0.790
Patient 13	1.173 ± 0.165	6.146 ± 1.582
Patient 14	7.917 ± 5.036	2.116 ± 0.705
Patient 15	22.360 ± 9.835	19.800 ± 2.400
Patient 16	148.300 ± 30.390	2,575.000 ± 312.400
Expression of all patients	21.590 ± 43.210**	245.600 ± 656.600*
p	**0.0018**	0.013

ACTC1, actin alpha cardiac muscle 1; GRK5, G protein-coupled receptor kinase 5. Bold value indicates the significant differences.

staining intensity: 0 indicated no staining, 1 indicated weak staining, 2 indicated moderate staining, and 3 indicated strong staining. The staining index (0–9) was calculated as the product of the proportion of positive cells multiplied by the staining intensity score. The best cutoff value was defined as follows: a staining score of ≥6 was considered to indicate high GRK5 or ATCT1 protein expression (also called GRK5+ or ACTC1+), and a staining score of ≤5 indicated low GRK5 or ATCT1 protein expression (also called GRK5- or ACTC1-) (Fu et al., 2017; Zhen et al., 2017; Zhao et al., 2018; Liang et al., 2019; Zou et al., 2019).

Real-Time Quantitative Polymerase Chain Reaction

The total RNA was extracted from the EOC tissues and paratumor tissues by using TRIzol (Takara Bio, Inc., Shiga, Japan). GAPDH mRNA was detected as the internal control (Liu et al., 2020). The expression levels of each matched fresh paratumor tissue sample were set as the control group (the expression levels of MYL9 in all of the paratumor tissues were 1.00 ± 0.00), and the relative expression is $2^{-\Delta\Delta Ct}$. The thermocycling conditions (Zhao et al., 2016; Liu et al., 2019c; Li et al., 2019; Lin et al., 2019; Xiao et al., 2019) were 95°C for 10 min to activate DNA polymerase, followed by 45 cycles of 95°C for 15 s, 60°C for 15 s, and 72°C for 10 s. The specificity of amplification products was confirmed by melting curve analysis. Independent experiments were performed in triplicate. The specific primer sequences were as follows: GRK5 forward, 5′-CCTCCGAAGGACCATAGACA-3′ and reverse, 5′-GACTGGGGACTTTGGAGTGA-3’; ACTC1 forward, 5′-GGTGATGAAGCCCAGAGCAA-3′ and reverse, 5′-GTGGTGACAAAGGAGTAGCC-3’; GAPDH forward, 5′-CCATCTTCCAGGAGCGAGAT-3′ and reverse, 5′-TGCTGATGATCTTGAGGCTG-3’.

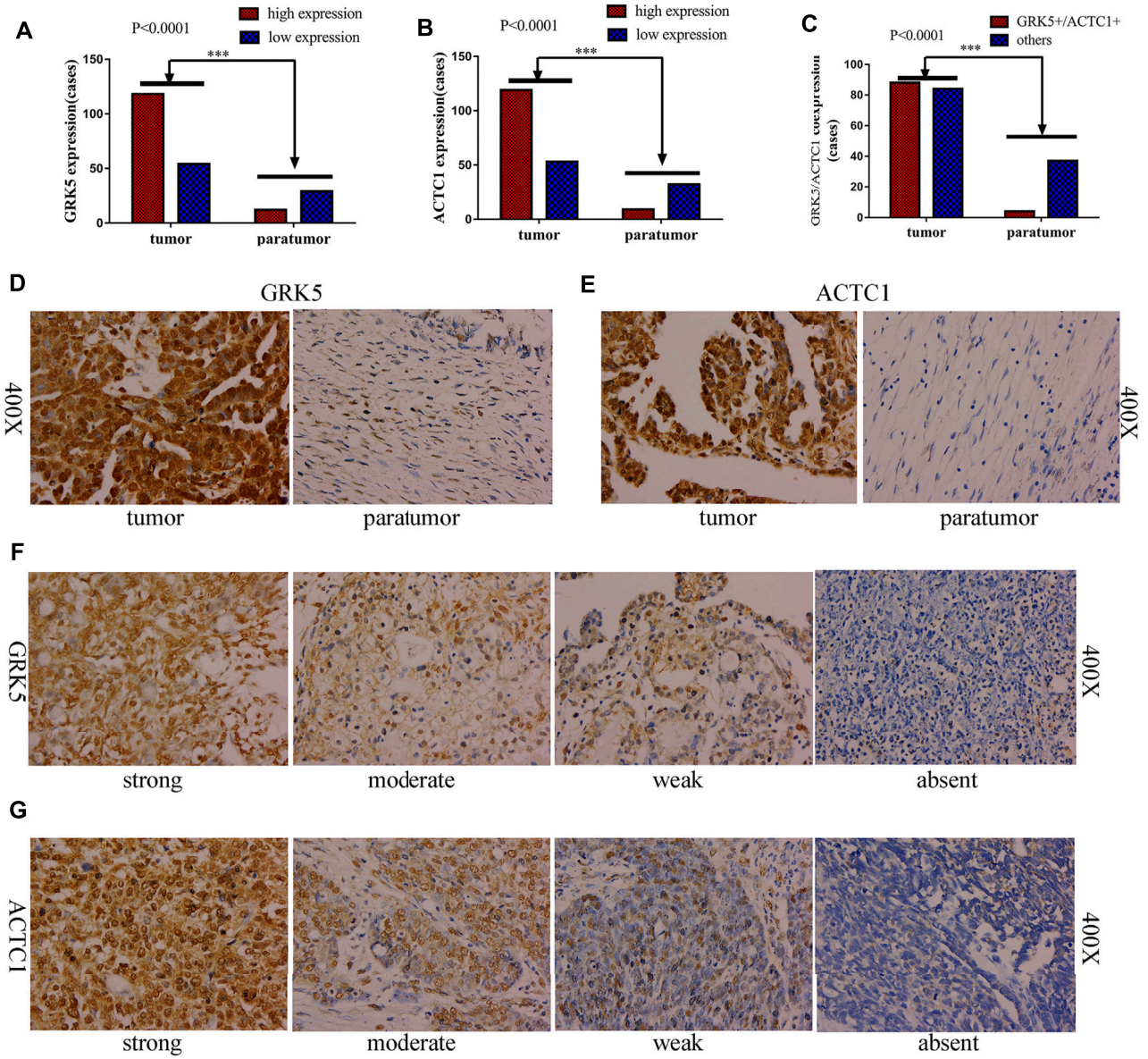

FIGURE 2 | GRK5 and ACTC1 were both upregulated in paraffin-embedded EOC. **(A)** GRK5 expression in EOC tissues and paratumor tissues ($p < 0.0001$); **(B)** ACTC1 expression in EOC tissues and paratumor tissues ($p < 0.0001$); **(C)** GRK5/ACTC1 co-expression in EOC tissues and paratumor tissues ($p < 0.0001$); **(D)** Comparison of EOC/paratumor tissues immunohistochemically stained for GRK5 (400X); **(E)** Comparison of EOC/paratumor tissues immunohistochemically stained for ACTC1 (400X); **(F)** the staining of GRK5 expression in EOC tissues (400X); **(G)** the staining of ACTC1 expression in EOC tissues (400X).

Statistical Analysis

All data analyses were performed using the statistical software package SPSS 21.0 (IBM Corp.) and GraphPad Prism 7 (GraphPad Software, Inc.). The mRNA expression of GRK5 or ACTC1 was expressed as the mean ± standard deviation. A two-tailed Student's t-test was used for comparisons between two independent groups (the expression of GRK5 or ACTC1 in paratumor tissues as the control group). The chi-square test or Fisher's exact test was used to analyze the association among GRK5 or ACTC1 or GRK5/ACTC1 co-expression (including GRK5+/ACTC1+, GRK5-/ACTC1+, GRK5+/ACTC1-, and GRK5-/ACTC1-) and clinicopathological parameters. Furthermore, the recurrence-free survival (RFS) and overall survival (OS) were analyzed by Kaplan–Meier analysis, and the differences were assessed using the log-rank test. Cox's proportional hazards regression model was used for univariate and multivariate analysis. Spearman or Pearson correlation was used for the correlation between GRK5 and ACTC1 expression. $p < 0.05$ was considered to indicate statistical significance.

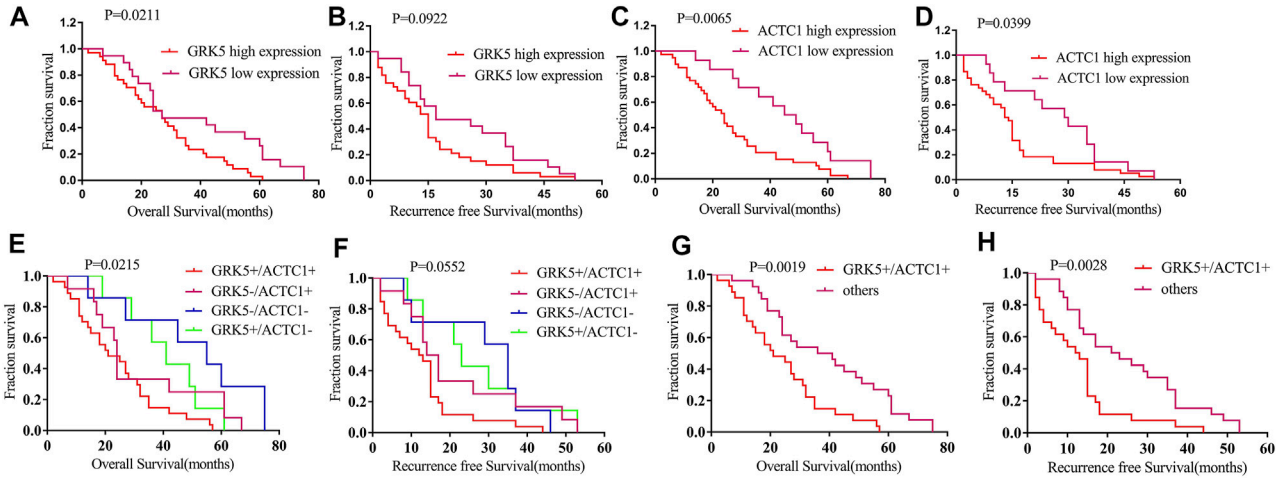

FIGURE 3 | Kaplan–Meier survival of RFS and OS among GRK5 and ACTC1 and co-expression of GRK5/ACTC1 in EOC patients: **(A)** Kaplan–Meier survival of OS between GRK5 expression and EOC patients; **(B)** Kaplan–Meier survival of RFS between GRK5 expression and EOC patients; **(C)** Kaplan–Meier survival of OS between ACTC1 expression and EOC patients; **(D)** Kaplan–Meier survival of RFS between ACTC1 expression and EOC patients; **(E,G)** Kaplan–Meier survival of OS between GRK5/ACTC1 co-expression and EOC patients; **(F,H)** Kaplan–Meier survival of RFS between GRK5/ACTC1 co-expression and EOC patients.

RESULTS

GRK5 and ACTC1 mRNA Were Both Upregulated in Fresh Epithelial Ovarian Cancer Tissues Compared With That in Paratumor Tissues

Reverse-transcription quantitative PCR (RT-qPCR) analysis was performed to detect the mRNA expression levels of both GRK5 and ACTC1 in 16 fresh EOC tissues and matched paratumor tissues (**Figure 1**). The expression of GRK5 or ACTC1 in all of the matched paratumor tissues was set as 1.00 ± 0.00, and the expression in each of the tumor tissues was compared with that in the matched paratumor tissues. The results indicated that the mean expression of GRK5 and ACTC1 in the 16 fresh EOC tissues was 21.590 and 245.600, respectively. There was a significant difference between EOC tissues and paratumor tissues ($p = 0.0018$; $p = 0.013$; **Table 1** and **Figure 1**).

GRK5 and ACTC1 Expression Were Both Assessed in Paraffin-Embedded Epithelial Ovarian Cancer Tissues and Paratumor Tissues by Immunohistochemistry

To further determine whether GRK5 or ACTC1 protein is upregulated in EOC, 172 paraffin-embedded EOC tissues and 41 matched paratumor tissues were subjected to the IHC analysis of GRK5 and ACTC1 expression. The results indicated that 54/172 (31.40%, GRK5) and 53/172 (30.81%, ACTC1) of the cancer samples had low/absent staining (rated as low expression) and 118/172 (68.60%, GRK5) and 119/172 (69.19%, ACTC1) had moderate/strong staining (rated as high expression), while the IHC analysis of the 41 paratumor tissues indicated that 29/41 (70.73%, GRK5) and 32/41 (78.05%, ACTC1) of the paratumor samples had low/absent staining and 12/41 (29.27%, GRK5) and 9/41 (21.95%, ACTC1) had moderate/strong staining. Moreover, the results indicated that 88/172 (51.16%, GRK5+/ACTC1+) of the cancer samples had moderate/strong staining and 84/172 (48.84%, others) had low/absent staining, while the IHC analysis of the 41 paratumor tissues indicated that 37/41 (90.24%, others) and low/absent staining and 4/41 (9.76%, GRK5+/ACTC1+) had moderate/strong staining. There was a significant difference on the GRK5, ACTC1, and GRK5/ACTC1 expression between the cancer and paratumor tissues ($p < 0.0001$, $p < 0.0001$, $p < 0.0001$; **Figures 2A–C**). Furthermore, it was observed that GRK5 and ACTC1 proteins were both located in the nucleus (**Figures 2D–G**).

GRK5 or ACTC1 or GRK5/ACTC1 Co-expression Was Associated With Recurrence-Free Survival and Overall Survival of Epithelial Ovarian Cancer Patients

In this study, patients with GRK5+ exhibited a median OS time of 27 months, while patients with GRK5- exhibited a median OS time of 27 months (HR = 1.81, 95% CI: 1.056–3.101). Patients with GRK5+ exhibited a median RFS time of only 15 months, while patients with GRK5- exhibited a median RFS time of 17 months (HR = 1.555, 95% CI: 0.9023–2.681). Moreover, patients with ACTC1+ exhibited a median OS time of only 24 months, while patients with ACTC1- exhibited a median OS time of 47 months (HR = 2.159, 95% CI: 1.255–3.716). Patients with ACTC1+ exhibited a median RFS time of only 14 months, while patients with ACTC1- exhibited a median RFS time of 29.5 months (HR = 1.784, 95% CI: 1.024–3.11). In addition, patients with GRK5+/ACTC1+ co-expression exhibited a median OS time of only 21.0 months, while patients with others co-expression exhibited a mean

TABLE 2 | GRK5, ACTC1 and GRK5/ACTC1 co-expression in association with clinical parameters of EOC.

Parameters		Total	GRK5			*ACTC1*			Co-expression of GRK5/ACTC1		
			Low	High	*p*-value (χ2 or Fisher's exact test)	Low	High	*p*-value (χ2 or Fisher's exact test)	GRK5+/ ACTC1+	Others	*p*-value (χ2 or Fisher's exact test)
Age (years)	≤50	75	27	48	0.2525	25	50	0.5292	33	42	0.0984
	>50	97	27	70		28	69		55	42	
Histology	Serous	110	29	81	0.0580	29	81	0.0729	65	45	**0.0095**
	Mucoid	10	6	4		5	5		2	8	
	Endometrial	22	10	12		7	15		7	15	
	Clear cell	12	5	7		7	5		4	8	
FIGO stage	I/II	48	24	24	**0.0011**	25	23	**0.0002**	11	37	**<0.0001**
	III/IV	124	30	94		28	96		77	47	
Lymph node metastasis	No	47	23	24	0.0832	24	23	**0.0266**	12	35	**0.0062**
	Yes	28	8	20		7	21		16	12	
Intraperitoneal metastasis	No	57	25	32	**0.0131**	29	28	**<0.0001**	16	41	**<0.0001**
	Yes	115	29	86		24	91		72	43	
Intestinal metastasis	No	93	44	49	**<0.0001**	39	54	**0.0006**	29	64	**<0.0001**
	Yes	79	10	69		14	65		59	20	
Vital status	Alive	60	24	36	0.6502	28	32	**0.0262**	19	41	**0.0374**
	Dead	53	19	34		14	39		27	26	
Intraperitoneal recurrence	No	122	38	84	0.8558	41	81	0.3497	60	62	0.5503
	Yes	46	15	31		12	34		25	21	
Distant recurrence	No	140	45	95	0.7105	47	93	0.2069	69	71	0.4478
	Yes	28	8	20		6	22		16	12	
Differentiation grade	G1/G2	58	26	32	**0.0029**	21	37	0.1418	22	36	**0.0046**
	G3	103	23	80		26	77		63	40	
Platinum resistance	No	164	50	114	0.1784	50	114	0.6438	84	80	0.6782
	Yes	5	3	2		2	3		2	3	
Ascites with tumor cells	No	45	22	23	**0.0077**	16	29	0.5082	16	29	**0.0153**
	Yes	35	7	28		10	25		22	13	
CA125 (U/ml)	≤35	22	7	15	0.8794	4	18	0.3150	13	9	0.4464
	>35	139	42	97		44	95		70	69	
CA72-4 (U/ml)	≤7	69	23	46	0.5078	22	47	0.6315	33	36	0.3135
	>7	71	20	51		20	51		40	31	
CA153 (U/ml)	≤25	11	5	6	0.3095	3	8	>0.9999	6	5	0.9267
	>25	41	12	29		10	31		23	18	
AFP (U/ml)	≤25	130	40	90	>0.9999	40	90	>0.9999	66	64	>0.9999
	>25	1	0	1		0	1		1	0	
CEA (U/ml)	≤5	117	35	82	0.8534	34	83	0.1893	61	56	0.5433
	>5	18	5	13		8	10		8	10	
HE4 (U/ml)	≤140	30	8	22	0.6835	9	21	0.5101	17	13	0.2746
	>140	65	20	45		24	41		29	36	

ACTC1, actin alpha cardiac muscle 1; FIGO, International Federation of Gynecology and Obstetrics; GRK5, G protein-coupled receptor kinase 5. Bold values indicate the significant differences.

OS time of 38.5 months (HR = 2.17, 95% CI: 1.22–3.858). Patients with GRK5+/ACTC1+ co-expression exhibited a median RFS time of only 12.5 months, while patients with other co-expressions exhibited a mean RFS time of 22 months (HR = 2.092, 95% CI: 1.17–3.739). Kaplan–Meier survival analysis demonstrated that there was a statistical significance on the OS and RFS between GRK5+/ACTC1+ and others co-expression (p = 0.0019 and p = 0.0028, respectively), and there was also a statistical significance on the OS and RFS between ACTC1+ and ACTC1- (p = 0.0065 and p = 0.0399, respectively). However, there was a significant difference between the GRK5+ and GRK5- on OS (p = 0.0211), but there was no significance on the RFS between GRK5+ and GRK5- (p = 0.0922) (**Figure 3**). A survival analysis showed that the cumulative OS and RFS rates of EOC patients increased with the increase in GRK5+/ACTC1+ co-expression (**Figure 3**).

TABLE 3 | Correlation between GRK5 and ACTC1 expression.

GRK5	ACTC1		Spearman's R	χ2	*p*
	High	Low			
high	88	30	0.173	5.122	0.0236
Low	31	23			

ACTC1, actin alpha cardiac muscle 1; GRK5, G protein-coupled receptor kinase 5

GRK5 and ACTC1 and GRK5/ACTC1 Co-expression Were Associated With the Clinicopathological Parameters of Epithelial Ovarian Cancer Patients

Subsequently, we evaluated their correlation with the clinicopathological parameters of EOC patients. The results of using χ2 or Fisher's exact test showed that there were significant relationships between GRK5 expression and clinicopathological parameters of EOC, such as the following factors: FIGO (International Federation of Gynecology and Obstetrics) stage, intraperitoneal metastasis, intestinal metastasis, differentiation grade, ascites with tumor cells, and so on (**Table 2**). There were significant relationships between ACTC1 expression and the clinicopathological parameters of EOC, such as the following factors: FIGO stage, lymph node metastasis, intraperitoneal metastasis, intestinal metastasis, vital status, and so on (**Table 2**). At last, we used χ2 or Fisher's exact test to explore the relationship between GRK5/ACTC1 co-expression and the clinicopathological parameters of EOC, and we found that there were significant differences in the following factors: histology, FIGO stage, lymph node metastasis, intraperitoneal metastasis, intestinal metastasis, vital status, differentiation grade, ascites with tumor cells, and so on (**Table 2**).

Correlation Between GRK5 and ACTC1 Expression

To explore the relationship between GRK5 and ACTC1, Spearman correlation and χ2 tests were used for analysis, and the results showed that there is a statistical significance between them ($p = 0.0236$) (**Table 3**).

GRK5 mRNA Was Positively Correlated With ACTC1 mRNA

Further, we assessed the correlation between GRK5 and ACTC1 mRNA expression. Using Pearson correlation analysis, we found that GRK5 was positively correlated with ACTC1 ($r = 0.8174$, $p = 0.0001$) (**Figure 4**).

Co-Expression of GRK5+/ACTC1+ Was a Useful Independent Prognostic Predictor of Epithelial Ovarian Cancer

Furthermore, we also assessed the prognostic value of GRK5, ACTC1, and GRK5/ACTC1 co-expression in EOC patients. In a univariate Cox model analysis, GRK5, ACTC1, and GRK5/ACTC1 co-expression; intestinal metastasis; postoperative chemotherapy; platinum resistance; and hyperthermic intraperitoneal chemotherapy (HIPEC) were significant prognostic factors (**Table 4**). Moreover, in a multivariate Cox regression model, we found that GRK5+/ACTC1+ co-expression, intestinal metastasis, postoperative chemotherapy, platinum resistance, and HIPEC were indeed independent prognostic factors of EOC (**Table 4**), but GRK5 expression and ACTC1 expression were no longer significant.

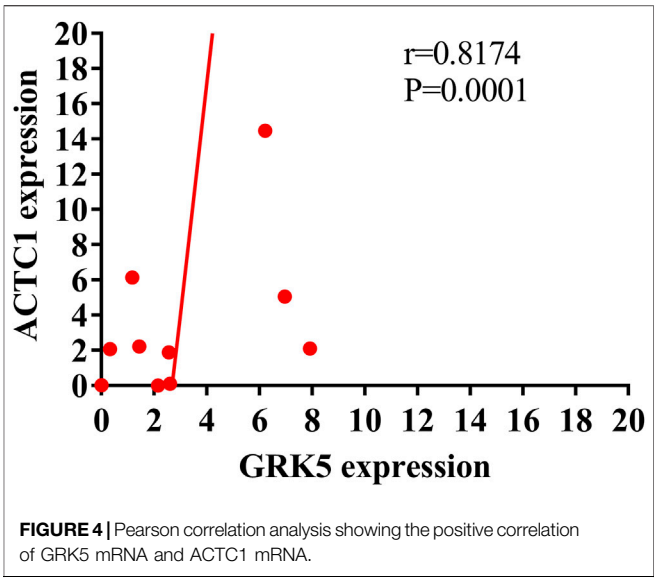

FIGURE 4 | Pearson correlation analysis showing the positive correlation of GRK5 mRNA and ACTC1 mRNA.

DISCUSSIONS

In our previous study, we found that MYH10 is an independent prognostic biomarker of EOC (in print). Furthermore, we used the Biogrid website to predict the candidate interacting proteins of MYH10, and we found some candidate proteins that may closely correlate with MYH10, such as MYL9 (Deng et al., 2021), MACF1 (Liu et al., 2021), MYH9 (Liu et al., 2019b), and so on. In the further study, we found that the co-expression of GRK5 and ACTC1 is indeed independent prognostic biomarkers, which indicates their important role in EOC. GRK5 plays oncogenic roles in GBM, prostate, pancreas, renal cell, non-small-cell lung, and breast cancers (Kim et al., 2012; Gambardella et al., 2016; Komolov et al., 2017; Jiang et al., 2018; Yang et al., 2018; Alshabi et al., 2019; Zhao et al., 2019a; Zhao et al., 2019b; Lagman et al., 2019; Sommer et al., 2019). It is clear (Gambardella et al., 2016) that when GRK5 is localized at the plasma membrane, it often exerts an anti-tumoral effect, attenuating growth-associated signaling pathways through its ability to desensitize GPCR and non-GPCR receptors. However, when GRK5 moves to cytosol or nucleus, it often promotes tumor growth acting on nonreceptor substrates. Consistent with previous findings (Kim et al., 2012; Jiang et al., 2018; Alshabi

TABLE 4 | Cox regression univariate and multivariate analyses of prognostic factors in EOC.

Variable	Univariate analysis				Multivariate analysis		
	Number of patients	*p*	Exp(B)/ OR	95% confidence interval	*p*	Hazard ratios	95% confidence interval
GRK5		0.026	1.427	1.044–1.951	0.967	-	-
High expression	118						
Low expression	54						
ACTC1		0.010	1.729	1.239–2.411	0.482	-	-
High expression	119						
Low expression	53						
Co-expression of GRK5/ACTC1		0.003	0.399	0.218–0.730	**0.011**	**0.425**	0.220–0.821
Others	84						
GRK5+/ACTC1+	88						
Intestinal metastasis		0.016	2.110	1.147–3.882	**0.010**	**2.515**	1.249–5.063
Yes	79						
No	93						
Postoperative chemotherapy		0.035	0.192	0.041–0.891	**0.006**	**0.095**	0.018–0.501
Yes	164						
No	6						
Platinum resistance		0.040	0.285	0.086–0.945	**0.001**	**0.021**	0.069–0.802
No	164						
Yes	5						
HIPEC		0.014	16.913	1.759–162.606	**0.021**	**84.504**	6.866–1,040.019
No	152						
Yes	19						

ACTC1, actin alpha cardiac muscle 1; GRK5, G protein-coupled receptor kinase 5; HIPEC, hyperthermic intraperitoneal chemotherapy. Bold values indicate the significant differences.

et al., 2019; Zhao et al., 2019a), in the present study, our results showed that GRK5 was upregulated in paraffin-embedded and fresh EOC tissues, and it is located mainly at the nucleus, which suggested that GRK5 may play a candidate oncogenic role in EOC. Further, Kaplan–Meier survival analysis showed that GRK5 high expression was associated with shorter OS, but not RFS, which is consistent with the previous reports (Jiang et al., 2018; Zhao et al., 2019a) that GRK5 high-expression NSCLC or renal cell carcinoma patients had a worse OS rate than the low-expression patients. Furthermore, GRK5 expression was associated with the following clinicopathological parameters, such as: FIGO stage, intraperitoneal metastasis, intestinal metastasis, differentiation grade, and ascites with tumor cells, which showed that GRK5 high expression was closely related with the development and metastasis of EOC.

Similar to GRK5, ACTC1 is also a cardiac-related gene (Kondrashov et al., 2018), and both of them are the candidate interacting proteins of MYH10. ACTC1 encodes the cardiac form of actin (Kondrashov et al., 2018). Ohtaki et al. reported (Ohtaki et al., 2017) that ACTC1 served as a clinical marker to detect migration and poor prognosis in GBM patients. In addition, our results also demonstrated that ACTC1 was upregulated in paraffin-embedded and fresh EOC tissues compared with that in paratumor tissues, which suggested that ACTC1 played a candidate oncogenic role in EOC. This is consistent with the role of ACTC1 (Kim et al., 2019; da Rocha et al., 2019; Wanibuchi et al., 2018; Cheung et al., 2017; Li et al., 2017; Ohtaki et al., 2017; Zaravinos et al., 2011) in GBM, colon, prostate, oral squamous cell and breast cancers. Further, Kaplan–Meier survival analysis showed that ACTC1 high expression was closely associated with shorter OS and RFS, which is consistent with the previous study of ACTC1 in GBM. Furthermore, ACTC1 expression was associated with clinicopathological parameters of EOC, such as: FIGO stage, lymph node metastasis, intraperitoneal metastasis, intestinal metastasis, and vital status, which showed that ACTC1 was also closely associated with the development and metastasis of EOC.

Importantly, ACTC1 and GRK5 are both cardiac-related genes. In this study, our results showed that ACTC1 mRNA and protein expression were both positively correlated with GRK5 mRNA and protein expression, and Kaplan–Meier survival analysis showed that GRK5+/ACTC1+ was closely associated with poor OS and RFS. Multivariate Cox regression analysis showed that GRK5+/ACTC1+ co-expression was an independent prognostic factor rather than GRK5 or ACTC1 alone. Moreover, GRK5-/ACTC1+ patients had a worse survival than GRK5+/ACTC1- patients, which suggested that ACTC1 was more closely correlated with survival than GRK5. In addition, GRK5/ACTC1 co-expression was associated with the following factors: histology, FIGO stage, lymph node metastasis, intraperitoneal metastasis, intestinal metastasis, vital status, differentiation grade, and ascites with tumor cells. All of these results suggested that the combination

of GRK5 and ACTC1 could predict the development, progression, metastasis, and prognosis of EOC more precisely. In future, we need more *in vivo* (such as the subcutaneous xenograft tumor studies and the lung xenograft tumor studies, and so on) and *in vitro* research to demonstrate its role and molecular mechanism in development, progression, metastasis, and prognosis of EOC.

CONCLUSION

Taken together, the results of the present study suggest that GRK5 and ACTC1 are both upregulated in EOC, and GRK5+/ACTC1+ co-expression could predict the development, metastasis, and prognosis of EOC. The co-expression of GRK5+/ACTC1+ can be recommended as prognostic-predicting biomarkers in EOC, and it may provide an important value in the clinical therapy and supervision of EOC.

DATA AVAILABILITY STATEMENT

The original contributions presented in the study are included in the article/Supplementary Material, further inquiries can be directed to the corresponding author.

ETHICS STATEMENT

The studies involving human participants were reviewed and approved by the Ethics Committee of the Integrated Hospital of Traditional Chinese Medicine, Southern Medical University. The patients/participants provided their written informed consent to participate in this study.

AUTHOR CONTRIBUTIONS

Conception: JL, PL and CC Interpretation or analysis of data: LL and JL Preparation of the manuscript: LL and JL Revision for important intellectual content: YN and ZL Supervision: CC.

FUNDING

This work was supported by the Guangdong Basic and Applied Basic Research Foundation (grant no. 2020A1515110030), the Natural Science Foundation of Guangdong Province (grant no. 2020A1515010284), the President funds of Integrated Hospital of Traditional Chinese Medicine, Southern Medical University (No. 1201902001; No. 1201901002), Guangzhou science and Technology Program (grant no. 202102080060).

REFERENCES

Alshabi, A. M., Vastrad, B., Shaikh, I. A., and Vastrad, C. (2019). Identification of Important Invasion and Proliferation Related Genes in Adrenocortical Carcinoma. *Med. Oncol.* 36, 73. doi:10.1007/s12032-019-1296-7

Chen, W., Zheng, R., Baade, P. D., Zhang, S., Zeng, H., Bray, F., et al. (2016). Cancer Statistics in China, 2015. *CA: A Cancer J. Clinicians* 66, 115–132. doi:10.3322/caac.21338

Cheung, A. S., de Rooy, C., Levinger, I., Rana, K., Clarke, M. V., How, J. M., et al. (2017). Actin Alpha Cardiac Muscle 1 Gene Expression Is Upregulated in the Skeletal Muscle of Men Undergoing Androgen Deprivation Therapy for Prostate Cancer. *J. Steroid Biochem. Mol. Biol.* 174, 56–64. doi:10.1016/j.jsbmb.2017.07.029

da Rocha, R. G., Santos, E. M. S., Santos, E. M., Gomes, E. S. B., Ramos, G. V., Aguiar, K. M., et al. (2019). Leptin Impairs the Therapeutic Effect of Ionizing Radiation in Oral Squamous Cell Carcinoma Cells. *J. Oral Pathol. Med.* 48, 17–23. doi:10.1111/jop.12786

Deng, Y., Liu, L., Feng, W., Lin, Z., Ning, Y., and Luo, X. (2021). High Expression of MYL9 Indicates Poor Clinical Prognosis of Epithelial Ovarian Cancer. *Pra* 16, 533–539. doi:10.2174/1574891X16666210706153740

Frank, D., Yusuf Rangrez, A., Friedrich, C., Dittmann, S., Stallmeyer, B., Yadav, P., et al. (2019). Cardiac α-Actin (ACTC1) Gene Mutation Causes Atrial-Septal Defects Associated with Late-Onset Dilated Cardiomyopathy. *Circ. Genom Precis Med.* 12, e002491. doi:10.1161/CIRCGEN.119.002491

Fu, Q., Song, X., Liu, Z., Deng, X., Luo, R., Ge, C., et al. (2017). miRomics and Proteomics Reveal a miR-296-3p/PRKCA/FAK/Ras/c-Myc Feedback Loop Modulated by HDGF/DDX5/β-catenin Complex in Lung Adenocarcinoma. *Clin. Cancer Res.* 23, 6336–6350. doi:10.1158/1078-0432.ccr-16-2813

Gambardella, J., Franco, A., Giudice, C. D., Fiordelisi, A., Cipolletta, E., Ciccarelli, M., et al. (2016). Dual Role of GRK5 in Cancer Development and Progression. *Transl Med. Unisa* 14, 28–37.

Jiang, L.-P., Fan, S.-Q., Xiong, Q.-X., Zhou, Y.-C., Yang, Z.-Z., Li, G.-F., et al. (2018). GRK5 Functions as an Oncogenic Factor in Non-small-cell Lung Cancer. *Cell Death Dis* 9, 295. doi:10.1038/s41419-018-0299-1

Kim, E.-K., Song, M.-J., Jung, Y., Lee, W.-S., and Jang, H. H. (2019). Proteomic Analysis of Primary Colon Cancer and Synchronous Solitary Liver Metastasis. *Cancer Genomics Proteomics* 16, 583–592. doi:10.21873/cgp.20161

Kim, J. I., Chakraborty, P., Wang, Z., and Daaka, Y. (2012). G-protein Coupled Receptor Kinase 5 Regulates Prostate Tumor Growth. *J. Urol.* 187, 322–329. doi:10.1016/j.juro.2011.09.049

Komolov, K. E., Du, Y., Duc, N. M., Betz, R. M., Rodrigues, J. P. G. L. M., Leib, R. D., et al. (2017). Structural and Functional Analysis of a β 2 -Adrenergic Receptor Complex with GRK5. *Cell* 169, 407–421. doi:10.1016/j.cell.2017.03.047

Kondrashov, A., Duc Hoang, M., Smith, J. G. W., Bhagwan, J. R., Duncan, G., Mosqueira, D., et al. (2018). Simplified Footprint-free Cas9/CRISPR Editing of Cardiac-Associated Genes in Human Pluripotent Stem Cells. *Stem Cell Dev.* 27, 391–404. doi:10.1089/scd.2017.0268

Lagman, J., Sayegh, P., Lee, C. S., Sulon, S. M., Jacinto, A. Z., Sok, V., et al. (2019). G Protein-Coupled Receptor Kinase 5 Modifies Cancer Cell Resistance to Paclitaxel. *Mol. Cell Biochem* 461, 103–118. doi:10.1007/s11010-019-03594-9

Lheureux, S., Braunstein, M., and Oza, A. M. (2019). Epithelial Ovarian Cancer: Evolution of Management in the Era of Precision Medicine. *CA. Cancer J. Clin.* 69, 280–304. doi:10.3322/caac.21559

Li, Y., Liu, X., Lin, X., Zhao, M., Xiao, Y., Liu, C., et al. (2019). Chemical Compound Cinobufotalin Potently Induces FOXO1-Stimulated Cisplatin Sensitivity by Antagonizing its Binding Partner MYH9. *Sig Transduct Target. Ther.* 4, 48. doi:10.1038/s41392-019-0084-3

Li, Y., Rong, G., and Kang, H. (2017). Taxotere-induced Elevated Expression of IL8 in Carcinoma-Associated Fibroblasts of Breast Invasive Ductal Cancer. *Oncol. Lett.* 13, 1856–1860. doi:10.3892/ol.2017.5612

Liang, Z., Liu, Z., Cheng, C., Wang, H., Deng, X., Liu, J., et al. (2019). VPS33B Interacts with NESG1 to Modulate EGFR/PI3K/AKT/c-Myc/P53/miR-133a-3p Signaling and Induce 5-fluorouracil Sensitivity in Nasopharyngeal Carcinoma. *Cell Death Dis* 10, 305. doi:10.1038/s41419-019-1457-9

Lin, X., Zuo, S., Luo, R., Li, Y., Yu, G., Zou, Y., et al. (2019). HBX-induced miR-5188 Impairs FOXO1 to Stimulate β-catenin Nuclear Translocation and Promotes Tumor Stemness in Hepatocellular Carcinoma. *Theranostics* 9, 7583–7598. doi:10.7150/thno.37717

Liu, L., Yi, J., Deng, X., Yuan, J., Zhou, B., Lin, Z., et al. (2019). MYH9 Overexpression Correlates with Clinicopathological Parameters and Poor

Prognosis of Epithelial Ovarian Cancer. *Oncol. Lett.* 18 (2), 1049–1056. doi:10.3892/ol.2019.10406

Liu, L., Hu, K., Zeng, Z., Xu, C., Lv, J., Lin, Z., et al. (2021). Expression and Clinical Significance of Microtubule-Actin Cross-Linking Factor 1 in Serous Ovarian Cancer. *Pra* 16 (1), 66–72. doi:10.2174/1574892816666210211091543

Liu, L., Ning, Y., Yi, J., Yuan, J., Fang, W., Lin, Z., et al. (2020). miR-6089/MYH9/β-catenin/c-Jun Negative Feedback Loop Inhibits Ovarian Cancer Carcinogenesis and Progression. *Biomed. Pharmacother.* 125, 109865. doi:10.1016/j.biopha.2020.109865

Liu, L., Zeng, Z., Yi, J., Zuo, L., Lv, J., Yuan, J., et al. (2019). Expression and Clinical Significance of Transcription Factor 4 (TCF4) in Epithelial Ovarian Cancer. *Cbm* 24, 213–221. doi:10.3233/cbm-181849

Liu, Y., Jiang, Q., Liu, X., Lin, X., Tang, Z., Liu, C., et al. (2019). Cinobufotalin Powerfully Reversed EBV-miR-BART22-Induced Cisplatin Resistance via Stimulating MAP2K4 to Antagonize Non-muscle Myosin Heavy Chain IIA/glycogen Synthase 3β/β-Catenin Signaling Pathway. *EBioMedicine* 48 (19), 386–404. doi:10.1016/j.ebiom.2019.08.040

Ohtaki, S., Wanibuchi, M., Kataoka-Sasaki, Y., Sasaki, M., Oka, S., Noshiro, S., et al. (2017). ACTC1 as an Invasion and Prognosis Marker in Glioma. *Jns* 126, 467–475. doi:10.3171/2016.1.jns152075

Sommer, A.-K., Falcenberg, M., Ljepoja, B., Fröhlich, T., Arnold, G. J., Wagner, E., et al. (2019). Downregulation of GRK5 Hampers the Migration of Breast Cancer Cells. *Sci. Rep.* 9, 15548. doi:10.1038/s41598-019-51923-1

Tseng, C.-C., and Zhang, X.-Y. (2000). Role of G Protein-Coupled Receptor Kinases in Glucose-dependent Insulinotropic Polypeptide Receptor Signaling*. *Endocrinology* 141, 947–952. doi:10.1210/endo.141.3.7365

Wanibuchi, M., Ohtaki, S., Ookawa, S., Kataoka-Sasaki, Y., Sasaki, M., Oka, S., et al. (2018). Actin, Alpha, Cardiac Muscle 1 (ACTC1) Knockdown Inhibits the Migration of Glioblastoma Cells *In Vitro*. *J. Neurol. Sci.* 392, 117–121. doi:10.1016/j.jns.2018.07.013

Xiao, Y. Y., Lin, L., Li, Y. H., Jiang, H. P., Zhu, L. T., Deng, Y. R., et al. (2019). ZEB1 Promotes Invasion and Metastasis of Endometrial Cancer by Interacting with HDGF and Inducing its Transcription. *Am. J. Cancer Res.* 9, 2314–2330.

Yang, Y., Wu, J. J., Cheng, C. D., Bao, D. J., Dong, Y. F., Li, D. X., et al. (2018). G-protein-coupled Receptor Kinase-5 Promotes Glioblastoma Progression by Targeting the Nuclear Factor Kappa B Pathway. *Am. J. Transl Res.* 10, 3370–3384.

Yao, Y., Liu, L., He, W., Lin, X., Zhang, X., Lin, Z., et al. (2019). Low Expression of KIF7 Indicates Poor Prognosis in Epithelial Ovarian Cancer. *Cbm* 26, 481–489. doi:10.3233/CBM-190328

Zaravinos, A., Lambrou, G. I., Boulalas, I., Delakas, D., and Spandidos, D. A. (2011). Identification of Common Differentially Expressed Genes in Urinary Bladder Cancer. *PLoS One* 6, e18135. doi:10.1371/journal.pone.0018135

Zhao, J., Li, X., Chen, X., Cai, Y., Wang, Y., Sun, W., et al. (2019). GRK5 Influences the Phosphorylation of Tau via GSK3β and Contributes to Alzheimer's Disease. *J. Cell Physiol* 234, 10411–10420. doi:10.1002/jcp.27709

Zhao, M., Luo, R., Liu, Y., Gao, L., Fu, Z., Fu, Q., et al. (2016). miR-3188 Regulates Nasopharyngeal Carcinoma Proliferation and Chemosensitivity through a FOXO1-Modulated Positive Feedback Loop with mTOR-P-Pi3k/akt-C-JUN. *Nat. Commun.* 7, 11309. doi:10.1038/ncomms11309

Zhao, M., Xu, P., Liu, Z., Zhen, Y., Chen, Y., Liu, Y., et al. (2018). RETRACTED ARTICLE: Dual Roles of miR-374a by Modulated C-Jun Respectively Targets CCND1-Inducing PI3K/AKT Signal and PTEN-Suppressing Wnt/β-Catenin Signaling in Non-small-cell Lung Cancer. *Cell Death Dis* 9, 78. doi:10.1038/s41419-017-0103-7

Zhao, T. L., Gan, X. X., Bao, Y., Wang, W. P., Liu, B., and Wang, L. H. (2019). GRK5 Promotes Tumor Progression in Renal Cell Carcinoma. *neo* 66, 261–270. doi:10.4149/neo_2018_180621n409

Zhen, Y., Fang, W., Zhao, M., Luo, R., Liu, Y., Fu, Q., et al. (2017). miR-374a-CCND1-pPI3K/AKT-c-JUN Feedback Loop Modulated by PDCD4 Suppresses Cell Growth, Metastasis, and Sensitizes Nasopharyngeal Carcinoma to Cisplatin. *Oncogene* 36, 275–285. doi:10.1038/onc.2016.201

Zou, Y., Lin, X., Bu, J., Lin, Z., Chen, Y., Qiu, Y., et al. (2019). Timeless-Stimulated miR-5188-Foxo1/β-Catenin-C-Jun Feedback Loop Promotes Stemness via Ubiquitination of β-Catenin in Breast Cancer. *Mol. Ther.* pii: S1525-0016 (19), 30398–30403.

Conflict of Interest: The reviewer YL declared a shared affiliation with one of the authors YN at time of review.

The remaining authors declare that the research was conducted in the absence of any commercial or financial relationships that could be construed as a potential conflict of interest.

Publisher's Note: All claims expressed in this article are solely those of the authors and do not necessarily represent those of their affiliated organizations, or those of the publisher, the editors and the reviewers. Any product that may be evaluated in this article, or claim that may be made by its manufacturer, is not guaranteed or endorsed by the publisher.

Advantages of publishing in Frontiers

OPEN ACCESS
Articles are free to read for greatest visibility and readership

FAST PUBLICATION
Around 90 days from submission to decision

HIGH QUALITY PEER-REVIEW
Rigorous, collaborative, and constructive peer-review

TRANSPARENT PEER-REVIEW
Editors and reviewers acknowledged by name on published articles

Frontiers
Avenue du Tribunal-Fédéral 34
1005 Lausanne | Switzerland

Visit us: www.frontiersin.org
Contact us: frontiersin.org/about/contact

REPRODUCIBILITY OF RESEARCH
Support open data and methods to enhance research reproducibility

DIGITAL PUBLISHING
Articles designed for optimal readership across devices

FOLLOW US
@frontiersin

IMPACT METRICS
Advanced article metrics track visibility across digital media

EXTENSIVE PROMOTION
Marketing and promotion of impactful research

LOOP RESEARCH NETWORK
Our network increases your article's readership